UNITED STATES DEPARTMENT OF COMMERCE
JESSE H. JONES, Secretary
NATIONAL BUREAU OF STANDARDS
Lyman J. Briggs, Director

✦

Journal of Research

of the

National Bureau of Standards

✦

Volume 25, Number 6
December 1940

[Published with approval of the Director of the Budget]

UNITED STATES
GOVERNMENT PRINTING OFFICE
WASHINGTON : 1940

For sale by the Superintendent of Documents, Washington, D. C. - - - - - - Price 35 cents
$3.50 per year on subscription

The prices of the separate Research Papers appearing in this JOURNAL are given on the front cover page. If 100 or more copies of any separate are ordered, a discount of 25 percent is allowed. Those who desire copies of separate Research Papers should send their orders and remittances without delay to the Superintendent of Documents, U. S. Government Printing Office, Washington, D. C. This will aid him to determine the number of copies to be printed for sale. Research Papers are not printed from electrotypes, and usually no more reprints can be had when the first and only printing is exhausted.

U. S. DEPARTMENT OF COMMERCE NATIONAL BUREAU OF STANDARDS

RESEARCH PAPER RP1346

Part of Journal of Research of the National Bureau of Standards, Volume 25, December 1940

MUTUAL INDUCTANCE OF TWO HELICES WHOSE AXES ARE PARALLEL

By Chester Snow

ABSTRACT

Formulas are obtained for the mutual inductance of two helical wires whose axes are parallel. The formulas are given as series in oblate spheroidal harmonics. The principal part is the inductance of the two corresponding current sheets, the correction terms being small when the coils are closely wound, so that the pitch is small compared to the diameter of the cylindrical form in each case.

CONTENTS

	Page
I. Introduction	619
II. Definitions and integral formulas for the mutual inductance of the two helices and of their current sheets	619
III. Difference between the formula for the mutual inductance of two helices and that of their current sheets	623
IV. Expansion of ω in a double Fourier's series of the azimuthal angles	634
V. Partial differential equations and boundary conditions satisfied by the function φ_{n_1, n_2}	641
VI. Expansion of φ_{n_1, n_2} in oblate spheroidal coordinates	646
VII. Expansion of ω_{n_1, n_2} in spheroidal coordinates	658
VIII. Corrections for diameter of the wires	670
IX. Summary	671

I. INTRODUCTION

The principal part of the mutual inductance between two helices whose axes are parallel is that between the two associated current sheets. This approximation may not be sufficient when the inductor is used for absolute electrical measurements of high precision. In this paper formulas are obtained which, in addition to the principal term, contain correction terms of the first and second order in the small quantities, such as the ratio of the pitch of the windings to their cylindrical radii.

The electromagnetic force between currents in the helices may be obtained by differentiation with respect to their relative coordinates. Such helices are not used as often as coaxial ones, although they do occur, for example, in the Ayrton-Jones type of current balance as used by the English National Physical Laboratory.

II. DEFINITIONS AND INTEGRAL FORMULAS FOR THE MUTUAL INDUCTANCE OF TWO HELICES AND OF THEIR CURRENT SHEETS

The two helices are shown in figure 1. The axis of the first, h_1, is the x-axis; that of the second, h_2, is the line in the xy plane parallel to the z-axis at a distance r from it, where $r \geqq 0$. If $r=0$, the helices are coaxial.

The cylindrical radius of the first is a_1; its pitch, $2\pi p_1$; and its axial length, $l_1=2\pi p_1 N_1$, where N_1, the "total number of turns," is not restricted to be an integer. The "number of turns per unit axial length" is $n_1=1/2\pi p_1$, not necessarily an integer. The initial planel

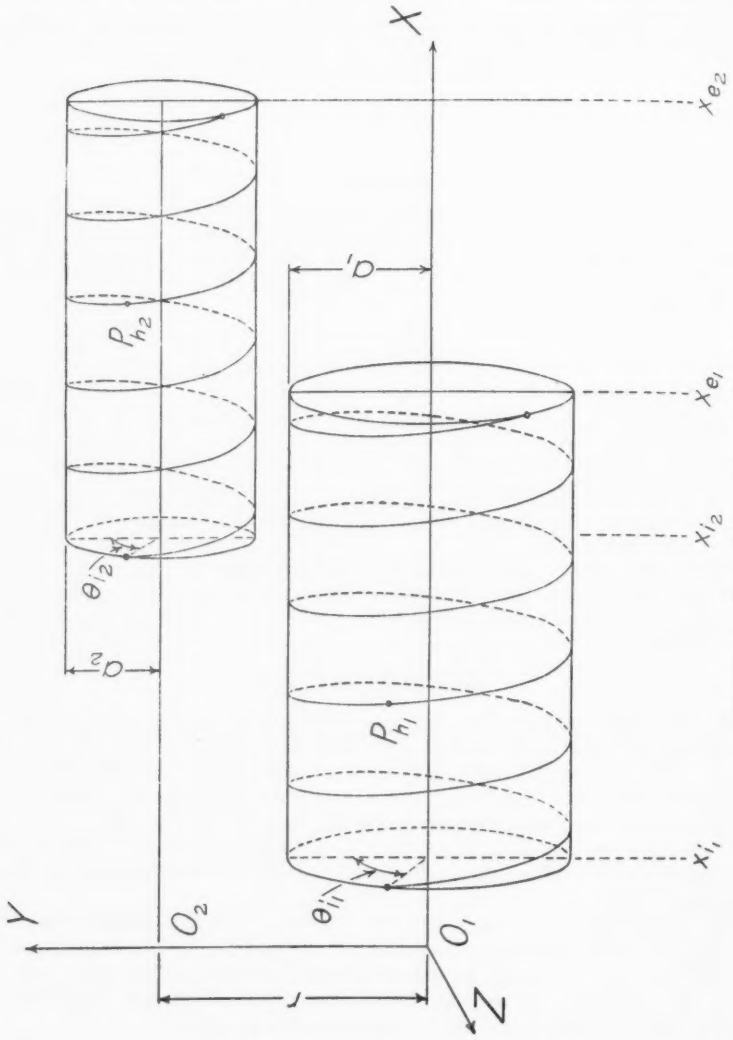

FIGURE 1.—*Two helices with parallel axes.*

$x=x_{i_1}$, contains its initial point, P_{i_1}, and the end plane, $x=x_{e_1}$ its end point, P_{e_1}, so that $l_1=2\pi p_1 N_1=x_{e_1}-x_{i_1}>0$. The current sheet, S_1, "associated with the helix, h_1," is the cylindrical surface (generated by rotating the helix about its axis through an angle 2π), upon which there is a surface current of unit strength (in electromagnetic cgs units), uniformly distributed, the direction of the current at any point being that of the helical filament passing through that point. This is equivalent to defining the current sheet as that part, included between

the terminal planes $x=x_i$ and $x=x_e$, of an endless cylinder which is completely covered by a helical tape winding of axial breadth equal to the pitch, so that no insulating space is left between successive windings. The angular current is $n_1=1/2\pi p_1$ per unit axial length. The axial current is $1/2\pi a_1$ per unit length along a circular arc for which x is constant.

If subscripts 2 refers to the second helix, h_2, or its sheet S_2, it follows from this definition that the mutual inductance, M_0, between the two current sheets is given by the double surface integral taken over the two sheets.

$$M_0=\frac{1}{4\pi^2 p_1 p_2}\int\int dS_1\int\int F(x_2-x_1,\theta_1,\theta_2)dS_2$$

$$=\frac{a_1a_2}{4\pi^2 p_1 p_2}\int_0^{2\pi}d\theta_1\int_{x_{i_1}}^{x_{e_1}}dx_1\int_0^{2\pi}d\theta_2\int_{x_{i_2}}^{x_{e_2}}dx_2F(x_2-x_1,\theta_1,\theta_2), \quad (1)$$

where

$$F(x_2-x_1,\theta_1,\theta_2)\equiv\frac{\cos(\theta_2-\theta_1)+p_1p_2/a_1a_2}{R_{12}(x_2-x_1,\theta_1,\theta_2)}, \quad (2)$$

and R_{12} is the distance from a point $P_1(x_1,y_1,z_1)$ on S_1 to $P_2(x_2,y_2,z_2)$ on S_2, so that

$$R_2(x_2-x_1,\theta_1,\theta_2)=(x_2-x_1)^2+a_1^2+a_2^2-2a_1a_2\cos(\theta_2-\theta_1)$$
$$+r^2+2r(a_2\cos\theta_2-a_1\cos\theta_1).] \quad (3)$$

The name "mutual inductance" is used here for the Neumann integral, so that when it refers to an unclosed circuit the implication is that the mutual inductance of the part (lead wires, etc.) which must be added to close the circuit must be evaluated by a Neumann's integral. With this understanding, it is evident that the term p_1p_2/a_1a_2 in the numerator of eq 2 gives rise in eq 1 to the mutual inductance of the axial currents in the two sheets, whereas the term "$\cos(\theta_2-\theta_1)$" gives rise to that due to their angular currents only.

In the integral (eq 1) the two independent variables, x_1, θ_1, are cylindrical coordinates referred to the axes of the first cylinder, and x_2, θ_2 are cylindrical coordinates referred to the axes of the second cylinder, so that the angles θ_1 and θ_2 each range over the interval from zero to 2π. If x_1, y_1, z_1 are the rectangular coordinates of any point P_1 on S_1, the position of P_1 may be specified by assigning the pair of cylindrical coordinates x_1 and θ_1 (with cylindrical radius a_1), or it may be specified by assigning the pair of semihelical coordinates θ_{i_1}, θ_1, the equations of transformation being

$$\left.\begin{matrix}x_1=x_{i_1}+p_1(\theta_1-\theta_{i_1})\\ y_1=a_1\cos\theta_1\\ z_1=a_1\sin\theta_1\end{matrix}\right\}, \text{ where } \left\{\begin{matrix}0\leq\theta_{i_1}<2\pi\\ \theta_{i_1}\leq\theta_1\leq\theta_{e_1}\equiv\theta_{i_1}+2\pi N_1\end{matrix}\right\}. \quad (4)$$

Considering the pair of variables θ_1 and θ_{i_1} for this range as two independent parameters which suffice to determine the position of P_1 on S_1, eq 4 are the parametric equations of the cylindrical surface S_1. The locus of the equation $\theta_{i_1}=$constant, is a helix, h_1, of pitch $2\pi p_1$ lying on S_1, while the locus of the equation $\theta_1=$constant is a straight line of length $2\pi p_1$ (or less) lying on S_1.

When the point $P_1(x_1y_1z_1)$ is also on the helix h_1, this may be designated by $P_{h_1}(x_{h_1}, y_{h_1}, z_{h_1})$, the x_{h_1}, y_{h_1}, and z_{h_1} being given as in eq 4 with the understanding that θ_{i_1} is a given constant and not a variable parameter.

The equations

$$\left.\begin{matrix} x_2 = x_{i_2} + p_2(\theta_2 - \theta_{i_2}) \\ y_2 = r + a_2 \cos \theta_2 \\ z_2 = a_2 \sin \theta_2 \end{matrix}\right\}, \text{ where } \left\{\begin{matrix} 0 \leqq \theta_{i_2} < 2\pi \\ \\ \theta_{i_2} \leqq \theta_2 \leqq \theta_{e_2} \equiv \theta_{i_2} + 2\pi N_2 \end{matrix}\right\} \tag{5}$$

are the parametric equations of the sheet S_2 when θ_2 and θ_{i_2} are both variables. The locus of the equation θ_{i_2}=constant is a helix h_2 of pitch $2\pi p_2$ lying on S_2.

The mutual inductance (Neumann's integral) of the helices, h_1 and h_2, is

$$M = \int_0^{s_1} ds_1 \int_0^{s_2} ds_2 \frac{\cos\ (ds_1, ds_2)}{R_{12}}$$

taken along both helices, where s_1 and s_2 denote total length of arc.

From eq 4 it is found that the element of length ds_1 has the magnitude

$$ds_1 = \sqrt{(a_1^2 + p_1^2)}\, d\theta_1 \tag{6}$$

and the direction cosines

$$\frac{dx_1}{ds_1} = \frac{p_1}{\sqrt{a_1^2 + p_1^2}}, \quad \frac{dy_1}{ds_1} = -\frac{a_1 \sin \theta_1}{\sqrt{a_1^2 + p_1^2}}, \quad \frac{dz_1}{ds_1} = \frac{a_1 \cos \theta_1}{\sqrt{a_1^2 + p_1^2}}. \tag{7}$$

The total length of the helix is s_1, where

$$s_1 = 2\pi N_1 \sqrt{a_1^2 + p_1^2} = \frac{l_1}{p_1} \sqrt{a_1^2 + p_1^2}, \tag{8}$$

where l_1 is its "axial length."

The same formulas, with change of subscript, refer to h_2, so that

$$ds_1, ds_2 \cos\ (ds_1, ds_2) = a_1 a_2 \left[\cos\ (\theta_2 - \theta_1) + \frac{p_1 p_2}{a_1 a_2}\right] d\theta_1 d\theta_2.$$

Hence the mutual inductance of the two helices is

$$M = a_1 a_2 \int_{\theta_{i_1}}^{\theta_{e_1}} d\theta_1 \int_{\theta_{i_2}}^{\theta_{e_2}} d\theta_2 \frac{\cos\ (\theta_2 - \theta_1) + p_1 p_2 / a_1 a_2}{R_{12}(x_{h_2} - x_{h_1}, \theta_1, \theta_2)} =$$

$$= a_1 a_2 \int_{\theta_{i_1}}^{\theta_{e_1}} d\theta_1 \int_{2}^{\theta_{e_2}} d\theta_2 F(x_{h_2} - x_{h_1}, \theta_1, \theta_2), \tag{9}$$

where x_{h_1} is a function of θ_1 only and x_{h_2} of θ_2 only, given by eq 4 and 5, the θ_{i_1} and θ_{i_2} being constants.

In the general case of helices whose axes are merely parallel, not necessarily coaxial, and whose terminal planes are arbitrary, eq 1 for the current sheets is sufficiently complicated, but eq 9 for the helices is even more troublesome. So far as we are aware, neither of these integrals may be evaluated in finite terms in general, although the

former may (in the case of coaxial current sheets) be so evaluated in terms of the three complete elliptic integrals. This is Jones' formula.[1]

The present paper is limited to what may, for brevity, be called the practical case, in which the two current sheets do not cut or touch each other, in fact they do not lie at any points close to each other. More precisely, considering the pitches $2\pi p_1$ and $2\pi p_2$ as infinitesimals of the first order compared to finite lengths like a_1, a_2, then the distance, R_{12} of a point P_1 on S_1 from a point P_2 on S_2, is, for all points, P_1 and P_2, finite (not a small quantity of the order of the pitch). The various expansions in infinite series to be obtained below for the current sheet are not subject to this limitation but cover the "impractical" cases also. The restriction is necessary, however, in order to obtain a practicable quantitative expression for the relatively small difference between the mutual inductance of the two helices and that of their associated current sheets.

If $f(x,\theta)$ is a continuous and single-valued function of position on a cylindrical sheet S, it must be a periodic function of θ with period 2π, and the line average of f along a helix on S is obviously very nearly the same as its surface average over S, provided that the pitch is small.

In the following section the two are compared, and an expression for their difference is obtained to the second order of small quantities inclusive, and application is made to the problem in hand, because, with closely wound coils, the precision of electrical measurements at present attainable requires formulas valid to the second order.

The general case of coaxial helices has been treated in an earlier paper,[2] so the emphasis here is upon the noncoaxial case.

III. DIFFERENCE BETWEEN THE FORMULA FOR THE MUTUAL INDUCTANCE OF TWO HELICES AND THAT OF THEIR CURRENT SHEETS

Certain problems relating to the helix could be treated more elegantly by the use of semihelical coordinates or by orthogonal helical ones. A plane rectangle ruled with two mutually orthogonal families of straight lines could be wrapped around a cylindrical surface, and the parameters defining these families would be orthogonal helical coordinates. However, it has been found by trial that the comparison of a line integral along a helix with a surface integral over its sheet may be made most simply by the use of ordinary cylindrical coordinates (x, θ) because the x limits and θ limits of the surface integral are independent of each other.

As the preliminary formulation applies to either helix h_1 or h_2, the subscripts may be omitted. In figure 2, with x as abscissa and $a\theta$ as ordinate, the rectangle represents the development of the cylindrical sheet S. The helix h is the system of parallel lines whose separation in the x-direction is $\Delta x \equiv 2\pi p =$ the pitch of the helix. The slope of these straight lines in figure 2 is p/a.

The variable θ lies between zero and 2π, and the initial azimuth. θ_i, also lies in that interval, but the end azimuth, θ_e, as defined in eq 4 or 5, does not, since $\theta_e = \theta_i + 2\pi N$. We, therefore, (for the moment) dis-

[1] J. V. Jones, Proc. Roy. Soc. (London) [A] **63**, 198 (1898).
[2] Chester Snow, *Mutual inductance and force between two coaxial helical wires*, J. Research NBS **22**, 269 (1939) RP 1178.

tinguish between θ_e and $\bar{\theta}_e$, where $\bar{\theta}_e \equiv \theta_e - 2\pi N' = \theta_i + 2\pi\ (N-N')$, where N' is the largest positive integer which is less than or equal to $\theta_e/2\pi$. When $\bar{\theta}_e$ is thus chosen, it lies in the interval, $0 \leqq \bar{\theta}_e \leqq 2\pi$, as

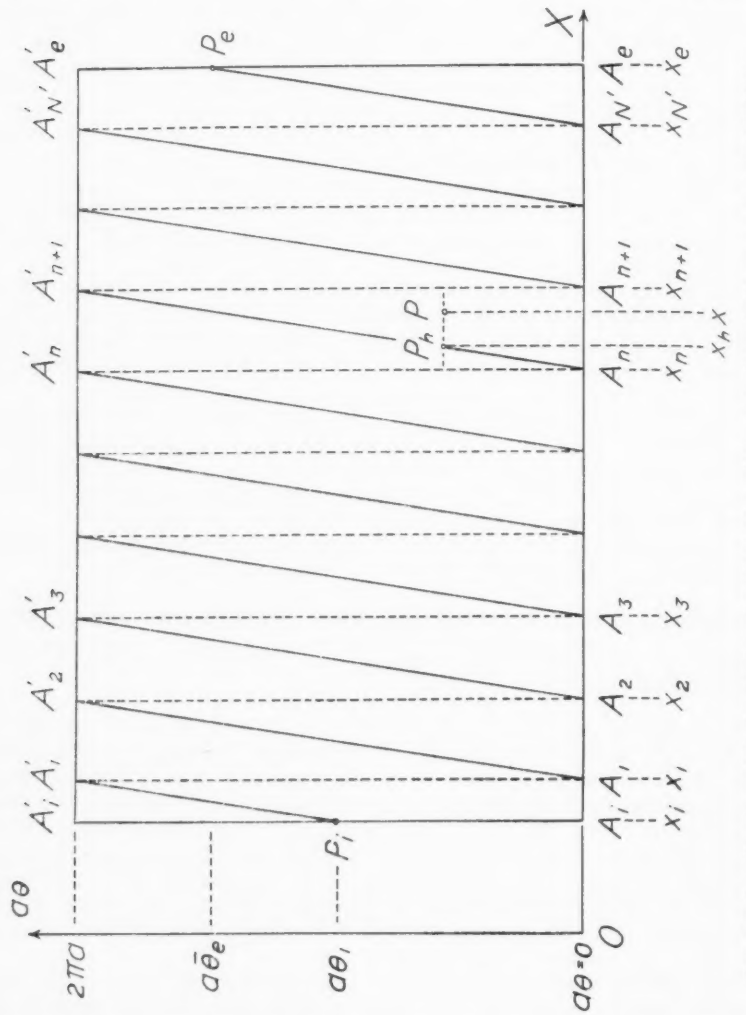

FIGURE 2.—*Development of cylindrical surface on a plane, showing a helix as a set of parallel lines.*

indicated in figure 2. The points A_1, A_2, ... $A_{N'}$ have abscissa x_n, where

$$x_n = x_i - p\theta_i + n\Delta x \text{ for } n = 1,2,3, \ldots . N'.$$

Hence the equation of the helix for figure 2 is

$x_h = x_i + p(\theta - \theta_i)$ when $x_i \leqq x < x_1$ and $\theta_i \leqq \theta < 2\pi$

$= x_n + p\theta$ when $x_n \leqq x < x_{n+1}$ and $0 \leqq \theta < 2\pi$ for $n = 1,2,3, \ldots . N'-1$

$= x_e + p(\theta - \bar{\theta}_e)$ when $x_{N'} \leqq x < x_e$ and $0 \leqq \theta < \bar{\theta}_e$.

Let $f(x,\theta)$ be a finite, continuous, and single-valued function of position on S. It is, therefore a periodic function of its second argument θ, with period 2π. The same character is assumed for $f'(x,\theta)$ and $f''(x,\theta)$, where primes denote partial derivatives with respect to the x-argument.

Hence, by eq 6, the line integral along a helix of $f(x,\theta)(a^2+p^2)^{-\frac{1}{2}}$ is

$$\sqrt{\frac{1}{a_2+p_2}}\int_0^s f(x,\theta)ds=\int_{\theta_i}^{\theta_e} f(x_h,\theta)d\theta=$$

$$=\int_{\theta_i}^{2\pi} f(x_i+p[\theta-\theta_i],\theta)d\theta+\int_0^{2\pi}d\theta\sum_{n=1}^{N'-1}f(x_n+p\theta,\theta)$$

$$+\int_0^{\bar{\theta}_e} f(x_e+p[\theta-\theta_e],\theta)d\theta.$$

The terms in the summation represent the principal part, the first and last integrals being relatively small (of the first order). Hence in them the integrand may be expanded by Taylor's theorem as a function of its x-argument, about the terminal values of x, so that

$$\frac{a}{\sqrt{a^2+p^2}}\int_0^s f(x,\theta)ds=a\int_0^{2\pi}d\theta\sum_{n=1}^{N'-1}f(x_n+p\theta,\theta)$$

$$+a\int_0^{\bar{\theta}_e}d\theta[f(x_e,\theta)+p(\theta-\bar{\theta}_e)f'(x_e,\theta)]$$

$$+a\int_{\theta_i}^{2\pi}d\theta[f(x_i,\theta)+p(\theta-\theta_i)f'(x_i,\theta)]. \tag{10}$$

To transform the summation, consider the following integral taken with respect to x, holding θ constant,

$$\int_{x1}^{x_{N'}} f(x,\theta)dx=\sum_{n=1}^{N'-1}\int_{x_n}^{x_n+\Delta x} f(x,\theta)dx, \tag{11}$$

where the integral is taken along the horizontal dotted line passing through P_h and P in figure 2, the latter point P being the general point of integration with abscissa $x=x_h+(x-x_h)$, so that expanding f as a function of x (with θ constant) about the point P_h on the helix in this n^h strip, we find

$$\int_{x_n}^{x_n+\Delta x} f(x,\theta)dx=\int_{x_n}^{x_n+\Delta x} f(x_h+[x-x_h],\theta)dx$$

$$=\int_{x_n}^{x_n+2\pi p}dx\left[f(x_h,\theta)+(x-x_h)f'(x_h,\theta)+\frac{(x-x_h)^2}{2}f''(x_h,\theta)\right].$$

On performing the integration with respect to x (θ and x_h being constant), these become, after placing $x_h=x_n+p\theta$,

$$\int_{x_n}^{x_n+\Delta x} f(x,\theta)dx=$$

$$=2\pi p\left\{f(x_n+p\theta,\theta)+p(\pi-\theta)f'(x_n+p\theta,\theta)+\frac{p^2}{2}\left[(\pi-\theta)^2+\frac{\pi^2}{3}\right]f''(x_n+p\theta,\theta)\right\},$$

so that eq 11 becomes

$$\int_{x_1}^{x_{N'}} f(x,\theta)dx = 2\pi p \sum_{n=1}^{N'-1} \left\{ f(x_n+p\theta,\theta)+p(\pi-\theta)f'(x_n+p\theta,\theta)+\frac{p^2}{2}\left[(\pi-\theta)^2+\frac{\pi^2}{3}\right]f''(x_n+p\theta,\theta)\right\}. \quad (12)$$

Applying the same formula to $f'(x,\theta)$ gives, after multiplying by $p(\pi-\theta)$,

$$p(\pi-\theta)\int_{x_1}^{x_{N'}} f'(x,\theta)dx = 2\pi p \sum_{n=1}^{N'-1}\left\{ p(\pi-\theta)f'(x_n+p\theta,\theta)+p^2(\pi-\theta)^2 f''(x_n+p\theta,\theta)\right\}, \quad (12')$$

which carries the approximation to the same order as in eq 12. Also, by eq 12, we may write to the same approximation

$$p^2\int_{x_1}^{x_{N'}} f''(x,\theta)dx = 2\pi p \sum_{n=1}^{N'-1} p^2 f(x_n+p\theta,\theta). \quad (12'')$$

Subtracting eq 12′ from eq 12, and making use of eq 12″, gives

$$\sum_{n=1}^{N'-1} f(x_n+p\theta,\theta) = \int_{x_1}^{x_{N'}} dx\left\{\frac{(fx,\theta)}{2\pi p}+\left(\frac{\theta-\pi}{2\pi}\right)f'(x,\theta)+\frac{p}{4\pi}\left[(\theta-\pi)^2-\frac{\pi^2}{3}\right]f''(x,\theta)\right\}$$

On integrating the second and third terms, this becomes

$$\sum_{n=1}^{N'-1} f(x_n+p\theta,\theta) = \frac{1}{2\pi p}\int_{x_i}^{x_e} f(x,\theta)dx - \frac{1}{2\pi p}\left[\int_{x_i}^{x_1} f(x,\theta)dx+\int_{x_{N'}}^{x_e} f(x,\theta)dx\right]\cdot$$
$$+\left(\frac{\theta-\pi}{2\pi}\right)[f(x_{N'},\theta)-f(x_1,\theta)]$$
$$+\frac{p}{4\pi}\left[(\theta-\pi^2-\frac{\pi^2}{3}\right][f'(x_{N'},\theta)-f'(x_1,\theta)]. \quad (13)$$

In the terms of smallest order we may place $f'(x_{N'},\theta)=f'(x_e,\theta)$ and $f'(x_1,\theta)=f'(x_i,\theta)$. In the terms involving $f(x_{N'},\theta)$ and $f(x_1,\theta)$, which relative to the principal term, are of first order, we may place

$$f(x_{N'},\theta)=f(x_e-p\bar{\theta}_e,\theta)=f(x_e,\theta)-p\bar{\theta}_e f'(x_e,\theta)$$
$$f(x_1,\theta)=f(x_i+p[2\pi-\theta_i],\theta)=f(x_i,\theta)+p(2\pi-\theta_i)f'(x_i,\theta).$$

Also

$$\frac{-1}{2\pi p}\int_{x_i}^{x_1} f(x,\theta)dx = \frac{-1}{2\pi p}\int_{x_i}^{x_i+p(2\pi-\theta_i)} dx\left\{f(x_i,\theta)+(x-x_i)f'(x_i,\theta)\right\}$$
$$=-\left(\frac{2\pi-\theta_i}{2\pi}\right)\left[f(x_i,\theta)+\frac{p}{2}(2\pi-\theta_i)f'(x_i,\theta)\right].$$

Similarly,

$$\frac{-1}{2\pi p}\int_{xN'} f(x,\theta)dx = \frac{-1}{2\pi p}\int_{x_e-p\bar{\theta}_e} dx \left\{ f(x_e,\theta)+(x-x_e)f'(x_e,\theta)\right\}$$

$$= -\frac{\bar{\theta}_e}{2\pi}\left[f(x_e,\theta) - \frac{p\bar{\theta}_e}{2} f'(x_e,\theta)\right].$$

By use of these expansions, eq 13 becomes

$$\sum_{n=1}^{N'-1} f(x_n+p\theta,\theta) = \frac{1}{2\pi p}\int_{x_i}^{x_e} f(x,\theta)dx$$

$$+\left(\frac{\theta-\bar{\theta}_e-\pi}{2\pi}\right)f(x_e,\theta)+\frac{p}{\pi}\left(\left[\frac{\theta-\bar{\theta}_e-\pi}{2}\right]^2-\frac{\pi^2}{12}\right]f'(x_e,\theta)$$

$$-\left(\frac{\theta-\theta_i+\pi}{2\pi}\right)f(x_i,\theta)-\frac{p}{\pi}\left[\left(\frac{\theta-\theta_i+\pi}{2}\right)^2-\frac{\pi^2}{12}\right]f'(x_i,\theta).$$

The series on the right side of eq 10 is found by multiplying this by $a d\theta$ and integrating from $\theta=0$ to $\theta=2\pi$. Equation 10 then becomes

$$\frac{a}{\sqrt{a^2+p^2}}\int_0^s f(x,\theta)ds = \frac{a}{2\pi p}\int_0^{2\pi} d\theta \int_{x_i}^{x_e} dx f(x,\theta)$$

$$+\frac{a}{\pi}\int_0^{\bar{\theta}_e} d\theta\left\{\left[\frac{\pi-(\bar{\theta}_e-\theta)}{2}\right]f(x_e,\theta)+p\left(\left[\frac{\pi-(\bar{\theta}_e-\theta)}{2}\right]^2-\frac{\pi^2}{12}\right)f'(x_e,\theta)\right\}$$

$$+\frac{a}{\pi}\int_{\bar{\theta}_e}^{2\pi} d\theta\left\{\left[\frac{\theta-\bar{\theta}_e-\pi}{2}\right]f(x_e,\theta)+p\left(\left[\frac{\theta-\bar{\theta}_e-\pi}{2}\right]-\frac{\pi^2}{12}\right)f'(x_e,\theta)\right\}$$

$$-\frac{a}{\pi}\int_0^{\theta_i} d\theta\left\{\left[\frac{\pi-(\theta_i-\theta)}{2}\right]f(x_i,\theta)+p\left(\left[\frac{\pi-(\theta_i-\theta)}{2}\right]^2-\frac{\pi^2}{12}\right)f'(x_i,\theta)\right\}$$

$$-\frac{a}{\pi}\int_{\theta_i}^{2\pi} d\theta\left\{\left[\frac{\theta-\theta_i-\pi}{2}\right]f(x_i,\theta)+p\left(\left[\frac{\theta-\theta_i-\pi}{2}\right]^2-\frac{\pi^2}{12}\right)f(x_i,\theta)\right\}. \qquad (14)$$

To reduce eq 14 to a more convenient form, consider the function $\Theta(\theta_i-\theta)$, which is an odd periodic function of its argument with period 2π, having a finite discontinuity when its argument is zero or $2\pi n$. It is defined for all other values of its argument by the series

$$\Theta(\theta_i-\theta) = \sum_{n=1}^{\infty}\frac{\sin n(\theta_i-\theta)}{n}, \qquad (15a)$$

so that

$$\left.\begin{aligned}\Theta(\theta_i-\theta) &= \frac{\pi}{2}-\left(\frac{\theta_i-\theta}{2}\right), \text{ when } 0<\theta_i-\theta<2\pi \\ &= -\frac{\pi}{2}-\left(\frac{\theta_i-\theta}{2}\right), \text{ when } -2\pi<\theta_i-\theta<0.\end{aligned}\right\} \qquad (15b)$$

Equation 14 may therefore be written

$$\frac{a}{\sqrt{a^2+p^2}}\int_0^s f(x,\theta)ds=\frac{1}{2\pi p}\Big(\int\int_s f(x,\theta)dS+$$

$$+2a\int_0^{2\pi}d\theta\Big\{p\Theta(\theta_e-\theta)f(x_e,\theta)+\Big[p^2\Theta^2(\theta_e-\theta)-\frac{\pi^2p^2}{12}\Big]f'(x_e,\theta)\Big\}$$

$$-2a\int_0^{2\pi}d\theta\Big\{p\Theta(\theta_i-\theta)f(x_i,\theta)+\Big[p^2\Theta^2(\theta_i-\theta)-\frac{\pi^2p^2}{12}\Big]f'(x_i,\theta)\Big\}\Big), \quad (16)$$

where $\bar{\theta}_e$ has been replaced by θ_e, the distinction between the two being now no longer material, since θ_e appears only in Θ $(\theta_e-\theta)$, which is a periodic function of its argument with period 2π.

The parenthesis on the right of eq 16, which has the factor $1/2\pi p$, contains three orders of magnitudes. The first, or finite term, is the surface integral of f taken over the sheet S.

If eq 16 be divided by $2\pi Na$, the first member becomes $1/s\int_0^s fds=$ the line average of f taken along the helix. The principal term on the right becomes $1/S\int\int fdS$, which is the surface average of f taken over S. Equation 16 is therefore the required relation giving the difference of these two averages as a relatively small quantity in which two orders of magnitude have been retained.

By two successive applications of the transformation represented in eq 16 we may convert the two successive line integrals along the two helices (which represent their mutual inductance, M) into two successive surface integrals over their equivalent sheets plus small correction terms. To begin this, eq 9 may be written

$$M=\frac{a_2}{\sqrt{a_2^2+p_2^2}}\int_0^{s_1}ds_2f(x_2,\theta_2) \quad (17)$$

the integration being along the second helix,

$$f(x_2,\theta_2)=\frac{a_1}{\sqrt{a_1^2+p_1^2}}\int_0^{s_1}ds_1F(x_2-x_1,\theta_1,\theta_2),$$

the latter integration being taken along the first helix.

By use of eq 16

$$f(x_2,\theta_2)=\frac{1}{2\pi p_1}\Big(\int\int_{s_1}dS_1F(x_2-x_1,\theta_1,\theta_2)$$

$$+2a_1\int_0^{2\pi}d\theta_1\Big\{p_1\Theta(\theta_{e_1}-\theta_1)F(x_2-x_{e_1},\theta_1,\theta_2)$$

$$-\Big[p_1^2\Theta^2(\theta_{e_1}-\theta_1)-\frac{\pi^2p_1^2}{12}\Big]F'(x_2-x_{e_1},\theta_1,\theta_2)\Big\}$$

$$-2a_1\int_0^{2\pi}d\theta_1\Big\{p_1\Theta(\theta_{i_1}-\theta_1)F(x_2-x_{i_1},\theta_1,\theta_2)$$

$$-\Big[p_1^2\Theta^2(\theta_{i_1}-\theta_1)-\frac{\pi^2p_1^2}{12}\Big]F'(x_2-x_{i_1},\theta_1,\theta_2)\Big\}\Big). \quad (18)$$

Applying the theorem (eq 16) to eq 17 gives

$$M=\frac{1}{2\pi p_2}\Big(\int\int_{S_2} dS_2 f(x_2,\theta_2)$$

$$+2a_2\int_0^{2\pi} d\theta_2\Big\{p_2\Theta(\theta_{e_2}-\theta_2)f(x_{e_2},\theta_2)+\Big[p_2^2\Theta^2(\theta_{e_2}-\theta_2)-\frac{\pi^2p_2^2}{12}\Big]f'(x_{e_2},\theta_2)\Big\}$$

$$-2a_2\int_0^{2\pi} d\theta_2\Big\{p_2\Theta(\theta_{i_2}-\theta_2)f(x_{i_2},\theta_2)+\Big[p_2^2\Theta^2(\theta_{i_2}-\theta_2)-\frac{\pi^2p_2^2}{12}\Big]f'(x_{i_2},\theta_2)\Big\}. \quad (19)$$

We may now introduce into the various integrals of eq 19 the expressions for $f(x_2,\theta_2)$, $f(x_{e_2},\theta_2)$, $f(x_{i_2},\theta_2)$, $f'(x_{e_2},\theta_2)$, and $f'(x_{i_2},\theta_2)$ obtained from eq 18. We retain only three orders of magnitude.

Since f' occurs only in the second-order terms of eq 19, we need only the principal part of f′, which is the x_2- derivative of the principal term in eq 18 so that we place

$$'(x_2,\theta_2)=\frac{a_1}{2\pi p_1}\int_0^{2\pi} d\theta_1\int_{x_{i_1}}^{x_{e_1}} dx_1 F'(x_2-x_1,\theta_1,\theta_2)$$

$$=\frac{-a_1}{2\pi p_1}\int_0^{2\pi} d\theta_1\Big\{F(x_2-x_{e_1},\theta_1,\theta_2)-F(x_2-x_{i_1},\theta_1,\theta_2)\Big\}.$$

This is required only for the constant values $x_2=x_{e_2}$ and $x_2=x_{i_2}$. On making these substitutions and taking account of eq 1, it is found that

$$M=M_0+\frac{1}{4\pi^2p_1p_2}\Big\{W_{12}+W_{21}+$$

$$+\omega_2(x_{e_2t_1},\theta_{i_1},\theta_{e_2})-\omega_2(x_{e_2e_1},\theta_{e_1},\theta_{e_2})$$

$$+\omega_2(x_{i_2e_1},\theta_{e_1},\theta_{i_2})-\omega_2(x_{i_2i_1},\theta_{i_1},\theta_{i_2})\Big\}, \quad (20)$$

where

$$\omega_2(x_{t_2t_1},\theta_{t_1},\theta_{t_2})\equiv$$

$$2a_1a_2\int_0^{2\pi} d\theta_1\int_0^{2\pi} d\theta_2\Big\{\Big[p_2\Theta(\theta_{t_2}-\theta_2)-p_1\Theta(\theta_{t_1}-\theta_1)\Big]^2-\frac{\pi^2(p_1^2+p_2^2)}{12}\Big\}F(x_{t_2t_1},\theta_1,\theta_2) \quad (21)$$

and

$$x_{t_2t_1}\equiv x_{t_2}-x_{t_1}, \quad (22)$$

where the subscript t suggests "terminal," so that x_{t2t1} is any one of the four possible distances between terminal planes, one of which is a terminal plane for the first sheet, the other for the second sheet.

Each of the four x-differences represented by $x_{t_2t_1}$, namely,

$$x_{e_2t_1}=x_{e_2}-x_{t_1},\ x_{e_2e_1}=x_{e_2}-x_{e_1},\ x_{i_2e_1}=x_{i_2}-x_{e_1},\ x_{i_2t_1}=x_{i_2}-x_{t_1} \quad (22')$$

may be positive or negative. The notation θ_{t_1} indicates which terminal azimuth of No. 1, and θ_{t_2} which terminal azimuth of No. 2 is associated with a specified x-difference.

The second-order term, ω_2, is an even function of its x-argument, but the other terms are not so simple for

$$W_{12} \equiv \int\int_{S_1} dS_1 2a_2 \int_0^{2\pi} d\theta_2 \left[p_2\Theta(\theta_{e_2}-\theta_2)F(x_{e_2}-x_1,\theta_1,\theta_2)-p_2\Theta(\theta_{i_2}-\theta_2)F(x_{i_2}-x_1,\theta_1,\theta_2)\right] \quad (23a)$$

and

$$W_{21} \equiv \int\int_{S_2} dS_2 2a_1 \int_0^{2\pi} d\theta_1 \left[p_1\Theta(\theta_{e_1}-\theta_1)F(x_2-x_{e_1},\theta_1,\theta_2)-p_1\Theta(\theta_{i_1}-\theta_1)F(x_2-x_{i_1},\theta_1,\theta_2)\right]. \quad (23b)$$

If the integrals were left in this form, it would be necessary to discriminate between the various cases arising out of the possible combinations of positive and negative signs among the four x-values. The formulation of these cases would be tedious and awkward because of their lack of symmetry.

This may be avoided without any loss in generality by transforming all the x-integrations of eq 23 into others in which the x-argument of F has the same algebraic sign throughout the range of integration. To do this, we may write eq 23a in the form

$$W_{12}=2a_1a_2\int_0^{2\pi}d\theta_1\int_0^{2\pi}d\theta_2\left\{p_2\Theta(\theta_{e_2}-\theta_2)\int_{x_{i_1}}^{x_{e_1}}dx_1F(x_{e_2}-x_1,\theta_1,\theta_2)\right.$$

The first x_1 integral is $\qquad\left.-p_2\Theta(\theta_{i_2}-\theta_2)\int_{x_{i_1}}^{x_{e_1}}dx_1F(x_{i_2}-x_1,\theta_1,\theta_2)\right\}$

$$\int_{x_{i_1}}^{x_{e_1}}F(x_{e_1}-x_1)dx_1=\int_0^{x_{e_2i_1}}F(x')dx'-\int_0^{x_{i_2e_1}}F(x')dx'.$$

The second is

$$\int_{x_{i_1}}^{x_{e_1}}F(x_{i_2}-x_1)dx_1=\int_0^{x_{i_2i_1}}F(x')dx'-\int_0^{x_{i_2e_1}}F(x')dx',$$

so that

$$W_{12}=2a_1a_2\int_0^{2\pi}d\theta_1\int_0^{2\pi}d\theta_2\left\{p_2\Theta(\theta_{e_2}-\theta_2)\left[\int_0^{x_{e_2i_1}}F(x',\theta_1,\theta_2)dx'-\int_0^{x_{i_2e_1}}F(x',\theta_1,\theta_2)dx'\right]\right.$$

$$\left.+p_2\Theta(\theta_{i_2}-\theta_2)\left[\int_0^{x_{i_2e_1}}F(x',\theta_1,\theta_2)dx'-\int_0^{x_{i_2i_1}}F(x',\theta_1,\theta_2)dx'\right]\right\}.$$

Similarly,

$$W_{21}=$$

$$2a_1a_2\int_0^{2\pi}d\theta_1\int_0^{2\pi}d\theta_2\Big\{p_1\Theta(\theta_{e_1}-\theta_1)\Big[\int_0^{x_{e_2e_1}}F(x',\theta_1,\theta_2)dx'-\int_0^{x_{i_2e_1}}F(x',\theta_1,\theta_2)dx'\Big]$$
$$+p_1\Theta(\theta_{i_1}-\theta_1)\Big[\int_0^{x_{i_2i_1}}F(x',\theta_1,\theta_2)dx'-\int_0^{x_{e_2i_1}}F(x',\theta_1,\theta_2)dx'\Big].$$

Adding these gives

$$W_{12}+W_{21}=$$
$$=\omega_1(x_{e_2i_1},\theta_{i_1},\theta_{e_2})-\omega_1(x_{e_2e_1},\theta_{e_1},\theta_{e_2})+\omega_1(x_{i_2e_1},\theta_{e_1},\theta_{i_2})-\omega_1(x_{i_2i_1},\theta_{i_1},\theta_{i_2}),\qquad(24)$$

where

$$\omega_1(x_{i_2i_1},\theta_{i_1},\theta_{i_2})\equiv$$
$$2a_1a_2\int_0^{2\pi}d\theta_1\int_0^{2\pi}d\theta_2[p_2\Theta(\theta_{i_2}-\theta_2)-p_1\Theta(\theta_{i_1}-\theta_1)]\int_0^{x_{i_2i_1}}F(x',\theta_1,\theta_2)dx'.\qquad(25)$$

This definition makes ω_1 an odd function of its x argument.

The mutual inductance of the current sheets may be put in a similar form by writing the x_1x_2 integrals of eq 1

$$\int_{x_{i_1}}^{x_{e_1}}dx_1\int_{x_{i_2}}^{x_{e_2}}dx_2F(x_2-x_1)=\int_{x_{i_1}}^{x_{e_1}}dx_1\int_0^{x_{e_2}-x_1}F(x')dx'-\int_{x_{i_1}}^{x_{e_1}}dx_1\int_0^{x_{i_2}-x_1}F(x')d(x').$$

In the first of these double integrals let $x''=x_{e_2}-x_1$, and in the second let $x''=x_{i_2}-x_1$. The first becomes

$$\int_{x_{i_1}}^{x_{e_1}}dx_1\int_0^{x_{e_2}-x_1}F(x')dx'=\int_{x_{e_2}-x_{e_1}}^{x_{e_2}-x_{i_1}}dx''\int_0^{x'}F(x')dx'$$
$$=\int_0^{x_{e_2i_1}}dx''\int_0^{x'}F(x')dx'-\int_0^{x_{e_2e_1}}dx''\int_0^{x'}F(x')\,dx'.$$

The second becomes

$$-\int_{x_{i_1}}^{x_{e_1}}dx_1\int_0^{x_{i_2}-x_1}F(x')dx'=\int_0^{x_{i_2e_1}}dx''\int_0^{x'}F(x')dx'-\int_0^{x_{i_2i_1}}dx''\int_0^{x'}F(x')dx'.$$

Hence eq 1 gives as the mutual inductance, M_0, of the two current sheets

$$M_0=\frac{1}{4\pi^2p_1p_2}\Big\{\omega_0(x_{e_2i_1})-\omega_0(x_{e_2e_1})+\omega_0(x_{i_2e_1})-\omega_0(x_{i_2i_1})\Big\},\qquad(26)$$

where

$$\omega_0(x)\equiv a_1a_2\int_0^{2\pi}d\theta_1\int_0^{2\pi}d\theta_2\int_0^{x}dx''\int_0^{x'}dx'F(x',\theta_1,\theta_2),\qquad(26')$$

which is an even function of x vanishing with x. Its x derivative, $\omega_0'(x)$, is an odd function of x vanishing with it.

An interpretation of the function, $\omega_0(x)$, may be obtained by considering the special case where $x_{t_1}=x_{t_2}$ and $x_{e_1}=x_{e_2}$, which is

$$M=\frac{2\omega_0(x)}{4\pi^2 p_1 p_2}=2n_1n_2\omega_0(x),$$

where

$$x=x_{e_2t_1}=x_{t_2e_1}=l_1=l_2$$

and $n_1=1/2\pi p_1$, $n_2=1/2\pi p_2$=number of turns per unit axial length. This shows that $\omega_0(x)$ is one-half the mutual inductance of the two current sheets, when they have the same end planes, their common length being $|x|$, and when each sheet has one turn per unit axial length (both axial and angular current in the sheets).

Collecting these results, the mutual inductance, M, between the two helices (their Neumann's integral) is

$$M=n_1n_2\{\omega(x_{e_2t_1},\theta_{t_1},\theta_{e_2})-\omega(x_{e_2e_1},\theta_{e_1},\theta_{e_2})+\omega(x_{t_2e_1},\theta_{e_1},\theta_{t_2})$$
$$-\omega(x_{t_2t_1},\theta_{t_1},\theta_{t_2})\}, \qquad (27)$$

where

$$\omega(x_{t_2t_1},\theta_{t_1},\theta_{t_2})=\omega_0(x_{t_2t_1})+\omega_1(x_{t_2t_1},\theta_{t_1},\theta_{t_2})+\omega_2(x_{t_2t_1},\theta_{t_1},\theta_{t_2}), \qquad (28)$$

where ω_0 is given by eq 26[1], ω_1 by eq 25, and ω_2 by eq 21. The x-differences, $x_{t_2t_1}$, between terminal planes of the current sheets and the terminal azimuths, θ_{t_1} and θ_{t_2}, associated with each of these are given in eq 22 and 22[1]. It is now apparent that eq 28 is general, whatever combination of positive and negative signs the four x-differences may have. These signs are automatically taken care of in the definitions, eq 26[1], 25, and 21, of ω_0, ω_1, and ω_2, respectively, which shows that and ω_0 and ω_2 are continuous even functions of x, ω_1 being an odd function of x.

It is evident also from these definitions, that ω_1 and ω_2 (and hence ω) are periodic functions of the terminal azimuths θ_{t_1} and θ_{t_2}, since θ is periodic with period 2π. The period of ω will be seen to be 2π for each angle. Consequently, $\omega(x_{t_1t_2}, \theta_{t_1}, \theta_{t_2})$ is developable in a double Fourier's series of sines and cosines of multiples of these two angles, the development holding for all values of the angles and the coefficients being functions of $x_{t_2t_1}$ (and of r, a_1, a_2)

Since ω_0 is the finite term, both the terms (cos $(\theta_2-\theta_1)$ and p_1p_2/a_1a_2 (constituting the numerator of the expression (eq 2) defining F) must be retained in evaluating ω_0. But since ω_1 is in general an infinitesimal of first order and ω_0 of second order, the term p_1p_2/a_1a_2 is negligible in the definition of F, which is used for evaluating ω_1 and ω_2 (since terms of third order have been neglected).

The system of subscripts in the designation of the three associated variables $(x_{t_1t_1}, \theta_{t_1}, \theta_{t_1})$ has now served its purpose of indicating which pair of terminal azimuths is associated with a given x-difference. From here on in the study of the ω functions we adopt the simpler notation (x, θ_1, θ_2) for these three associated variables and place here for reference, see eq 22 and 22′,

$$\left.\begin{aligned} &x=x_{t_1t_1},\ \theta_1=\theta_{t_1},\theta_2=\theta_{t_1} \\ &\omega(x_1\theta_1,\theta_2)=\omega(x_{t_1t_1},\theta_{t_1},\theta_{t_1}) \end{aligned}\right\}. \qquad (29)$$

This change necessitates a change in the notation of the variables of integration so that eq 26′, 25, and 21 may now be written

$$\omega_0(x)=a_1a_2\int_0^x dx''\int_0^{x''}dx'\int_0^{2\pi}d\theta_1'\int_0^{2\pi}d\theta_2'\frac{[\cos(\theta_1'-\theta_2')+p_1p_2/a_1a_2]}{R_{12}(x',\theta_1',\theta_2')} \tag{30}$$

$$\omega_1(x,\theta_1,\theta_2)=$$

$$2a_1a_2\int_0^x dx'\int_0^{2\pi}d\theta_1'\int_0^{2\pi}d\theta_2'[p_2\Theta(\theta_2-\theta_2')-p_1\Theta(\theta_1-\theta_1')]\frac{\cos\ (\theta_1'-\theta_2')}{R_{12}(x',\theta_1',\theta_2')} \tag{31}$$

$$\omega_2(x,\theta_1,\theta_2)=2a_1a_2\int_0^{2\pi}d\theta_1'\int_0^{2\pi}d\theta_2'\left\{p_1^2\left[\Theta^2(\theta_1-\theta_1')-\frac{\pi^2}{12}\right]\right.$$

$$\left.+p_2^2\left[\Theta^2(\theta_2-\theta_2')-\frac{\pi^2}{12}\right]-2p_1p_2\Theta(\theta_1-\theta_1')\Theta(\theta-\theta_2')\right\}\frac{\cos\ (\theta_1'-\theta_2')}{R_{12}(x,\theta_1',\theta_2')}. \tag{32}$$

Equation 28 becomes

$$\omega(x,\theta_1,\theta_2)=\omega_0(x)+\omega_1(x,\theta_1,\theta_2)+\omega_2(x,\theta_1,\theta_2). \tag{33}$$

In the relatively small terms ω_1 and ω_2, a sufficient approximation to the exact expressions

$$\Theta(\theta)=\sum_{n=1}^{\infty}\frac{\sin\ n\theta}{n}\text{ and }\Theta^2(\theta)-\frac{\pi^2}{12}=\sum_{n=1}^{\infty}\frac{\cos\ n\theta}{n^2} \tag{34}$$

is

$$\Theta(\theta)=\frac{\pi^2}{9}\left(\sin\ \theta+\frac{1}{2}\sin\ 2\theta\right)\text{ and }\Theta^2(\theta)-\frac{\pi^2}{12}=\frac{\pi^2}{9}\left(\cos\ \theta+\frac{\cos\ 2\theta}{4}\right). \tag{35}$$

Using this approximation, eq 31 becomes

$$\omega_1(x,\theta_1,\theta_2)=\frac{2\pi^2}{9}a_1a_2\int_0^x dx'\int_0^{2\pi}d\theta_1'\int_0^{2\pi}d\theta_2'\left\{p_1\left[\sin\ (\theta_1'-\theta_1)+\frac{1}{2}\sin\ 2(\theta_1'-\theta_1)\right]\right.$$

$$\left.-p_2\left[\sin\ (\theta_2'-\theta_2)+\frac{1}{2}\sin\ 2(\theta_2'-\theta_2)\right]\right\}\frac{\cos\ (\theta_1'-\theta_2')}{R_{12}(x',\theta_1',\theta_2'}, \tag{36}$$

and eq 32 becomes

$$\omega_2(x,\theta_1,\theta_2)=\frac{2\pi^2a_1a_2}{9}\int_0^{2\pi}d\theta_1'\int_0^{2\pi}d\theta_2'\left\{p_1^2\left[\cos\ (\theta_1'-\theta_1)+\frac{1}{4}\cos\ 2(\theta_1'-\theta_1)\right]\right.$$

$$\left.+p_2^2\left[\cos\ (\theta_2'-\theta_2)+\frac{1}{4}\cos\ 2(\theta_2'-\theta_2)\right]\right.$$

$$-\frac{2\pi^2p_1p_2}{9}\left[\sin\ (\theta_1'-\theta_1)+\frac{1}{2}\sin\ 2(\theta_1'-\theta_1)\right]$$

$$\left.\left[\sin\ (\theta_2'-\theta_2)+\frac{1}{2}\sin\ 2(\theta_2'-\theta_2\right]\right\}\frac{\cos\ (\theta_1'-\theta_2')}{R_{12}(x,\theta_1',\theta_2')}. \tag{37}$$

For reference is placed here an alternative approximation

$$\left.\begin{aligned}\Theta^2(\theta)&=\frac{\pi^2}{4}\left(1-\sin\frac{\theta}{2}\right),\text{ when }0<\theta<2\pi\\&=\frac{\pi^2}{4}\left(1+\sin\frac{\theta}{2}\right),\text{ when }-2\pi<\theta<0\end{aligned}\right\}, \tag{38}$$

which is seen to be a good approximation, since

$$32/\pi^3 = 1.032$$

and

$$\Theta^2(\theta) = \frac{\pi^2}{4}\left[1 - \frac{32}{\pi^3}\sum_{n=1}^{\infty}\frac{\sin\,(2n-1)\frac{\theta}{2}}{(2n-1)^3}\right], \text{ when } 0<\theta<\pi/2.$$

For the type of expansions required here the three-term approximation for Θ^2 given in eq 35 will be used. It has about the same precision as the two-term approximation, eq 38. The latter is equivalent to one used [3] in considering coaxial helices, as it led to a simple expression for the term corresponding in that case to ω_2, which was in finite terms.

A comparison of the approximate expression adopted for $\Theta(\theta)$ and for $\Theta^2(\theta) - \Pi^2/12$ in (eq 35) with the exact series (eq 34), for these functions shows that we have retained only the first two terms of the series, and have arbitrarily inserted the factor $\pi^2/9$, which is slightly greater than 1, and in fact it is sufficient to replace this by 1 in the second-order terms.

In the following section the ω-functions are expanded in a double Fourier's series in the terminal azimuth angles θ_1 and θ_2.

IV. EXPANSION OF ω IN A DOUBLE FOURIER'S SERIES OF THE AZIMUTHAL ANGLES

In figure 3 is shown the projection of the two parallel cylinders upon the yz plane, and r_{12} is the projection of the distance R_{12} from P_1 to P_2, so that

$$R_{12}^2 = x^2 + r_{12}^2, \text{ where } x = x_2 - x_1. \tag{39}$$

The x axis being taken as the axis of cylindrical coordinates, a_1 and θ_1 are cylindrical coordinates of P_1, but the cylindrical coordinates of P_2 may be taken as r_2 and θ_2', as shown in figure 3. Since r_{12} is one side of the triangle $P_1O_1P_2$, the other two sides, a_1, and r_2, including the angle $\theta_1 - \theta_2'$,

$$r_{12}^2 = a_1^2 - 2a_1r_2\cos\,(\theta_1 - \theta_2') + r_2^2. \tag{40}$$

Since $1/R_{12}$ is an even periodic function of the angle $(\theta_1 - \theta_2')$, its Fourier series may be written

$$\frac{1}{R_{12}} = \frac{2}{\sqrt{a_1r_2}}\sum_{n=0}^{\infty}\epsilon_n\phi_n(x,a_1,r_2)\cos\,n(\theta_1 - \theta_2'), \tag{41}$$

where $\epsilon_0 = \frac{1}{2}$ and $\epsilon_n = 1$, if $n \neq 0$), and where

$$\frac{\phi_n(x,a_1,r_2)}{\sqrt{a_1r_2}} = \frac{1}{2\pi}\int_0^{2\pi}\frac{\cos\,n(\theta_1 - \theta_2')d\theta_1}{R_{12}} \tag{42a}$$

and x, a_1, r_2, θ_2' are held constant in this integration.

[3] Reference 2, p. 259–261.

Another integral representation of this function, which will be derived later and which involves Bessel's function, J_n, is

$$\frac{\phi_n(x,a_1,r_2)}{\sqrt{a_1 r_2}} = \int_0^\infty \overline{e}^{|x|t} J_n(a_1 t) J_n(r_2 t) dt. \tag{42b}$$

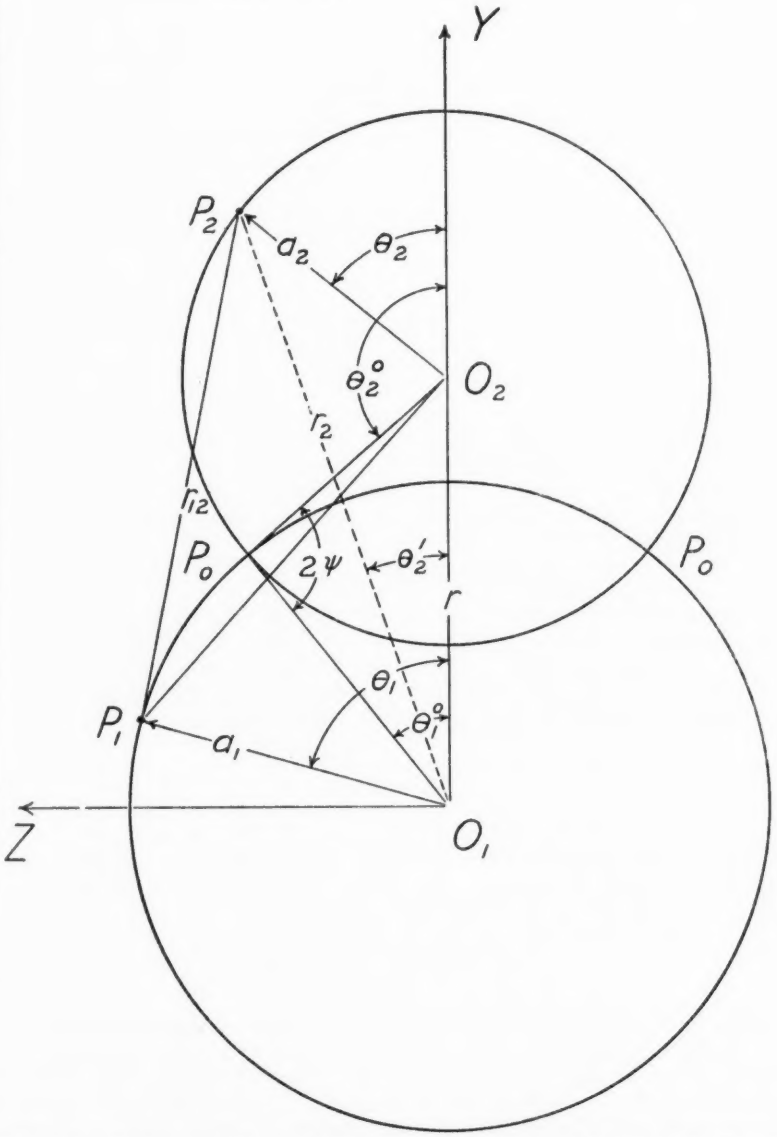

FIGURE 3.—*Projection of the two helices upon a plane perpendicular to their axes.*

This integral may be evaluated, the result being a function of the single dimensionless variable k, so that

$$\frac{\phi_n(x,a_1,r_2)}{\sqrt{a_1 r_2}}=\frac{k^{2n+1}}{2\pi\sqrt{a_1 r_2}}\cdot\frac{\Gamma^2\left(n+\frac{1}{2}\right)}{\Gamma(2n+1)}F\left(n+\frac{1}{2},n+\frac{1}{2},2n+1;k^2\right), \quad (43)$$

where

$$k^2=\frac{4a_1 r_2}{x^2+(a_1+r_2)^2}, \quad (44)$$

and where F is the hypergeometric function. It is evident that the function $\phi_n(x-x_1,r,r_1)/\sqrt{rr_1}$ is a solution of the partial differential equation

$$\left(D_z^2+D_r^2+\frac{1}{r}D_r-\frac{n^2}{r^2}\right)\frac{\phi_n}{\sqrt{rr_1}}=0 \quad (45a)$$

and also of

$$\left(D_{z_1}^2+D_{r_1}^2+\frac{1}{r_1}D_{r_1}-\frac{n^2}{r_1^2}\right)\frac{\phi_n}{\sqrt{rr_1}}=0. \quad (45b)$$

It is further evident that ϕ_n is a symmetrical function of the two sets, x,r, and x_1,r_1, becoming infinite logarithmically when they approach coincidence. It is the Green's function and the nucleus of many integral equations which arise when a solution of eq 45 is required and which have assigned values (or assigned values for its "surface density of charge") on surfaces of revolution about the x-axis. Thus the function

$$V_0(x,r)=\phi_0(x-x_1,r,r_1)/\sqrt{rr_1}$$

is a potential at a point P whose cylindrical coordinates are x and r. It is symmetrical about the x-axis and is due to a unit circular line charge distributed with uniform linear density over the circular arc of radius r_1 in the plane x_1, which is coaxial with the x-axis.

More generally, if n is any integer, the function

$$\frac{\phi_n(x-x_1,r,r_1)}{\sqrt{rr_1}}$$

is the solution of eq 45a at a point x,r, due to a unit circular line "source" at x_1,r_1, in the sense that the solution of eq 45a, whose surface density of source σ is given on any surface of revolution (x_1=function of r_1), is found by integrating

$$\int\frac{\sigma(r_1)\phi_n(x-x_1,r,r_1)}{\sqrt{rr_1}}2\pi r_1 ds_1,$$

where ds_1 is an element of the generating arc of the given surface of revolution, lying in a plane through the x-axis, and the integral is taken between the appropriate limits. If σ is known, this gives the solution, but if the function is assigned, this is an integral equation to determine σ, after which this integral gives the solution. The most appropriate expansions of this nucleus of the integral equations in a given coordinate system are those which are the canonical bilinear expansion of the nucleus in terms of its normal functions for that system.

The role of this function ϕ_n for solutions of eq 45a, having assigned values on surfaces of revolution, is as fundamental as that of $1/R_{p_1p}$ in the general theory of electrostatics, and in fact its expansion in normal functions follows from that of $1/R_{p_1p}$ by eq 42a.

Some coordinates pertinent to the problem of this paper may here be mentioned.

The first is the spherical coordinate system. If the values of a solution U of eq 45a are assigned on the sphere made by revolving the circle $x_1^2+r_1^2=R_1^2$ about the x-axis, and R, ζ, θ are the spherical coordinates of P, while (R_1, ζ_1, θ_1) are those of P_1, where $R=x^2+r^2$, $\zeta=x/R$ and $\tan\theta=y/z$ (where θ is the same as in cylindrical coordinates), then it is known that

$$\frac{1}{R_{P_1P}}=2\sum_{n=0}^{\infty}\epsilon_n\cos n(\theta-\theta_1)\sum_{m=n}^{\infty}\frac{\Gamma(m-n+1)}{\Gamma(m+n+1)}P_m^n(\zeta)R^{-m-1}P_m^n(\zeta_1)R_1^m \qquad (46)$$

when $R>R_1$. (with interchange of R and R_1 for the case $R<R_1$).

The expansion corresponding to eq 41 is

$$\frac{1}{R_{P_1P}}=\frac{2}{\sqrt{r_1r}}\sum_{n=0}^{\infty}\epsilon_n\phi_n(x-x_1,r,r_1)\cos n(\theta-\theta_1), \qquad (47)$$

so that

$$\frac{\phi_n(x-x_1,r,r_1)}{\sqrt{rr_1}}=\sum_{m=n}^{\infty}\frac{\Gamma(m-n+1)}{\Gamma(m+n+1)}P_m^n(\xi)R^{-m-1}P_m^n(\xi_1)R_1^m \qquad (48)$$

when $R>R_1$ (with interchange of R and R_1 when $R<R_1$), where $P_m^n(\xi)$ is the associated Legendre function (Ferrer's). This is the canonical bilinear expansion of the nucleus in terms of normal functions for the spherical surface R_1 by means of which solutions of eq 45a may be found when their values or the values of their source density on the sphere are assigned.

When the solution of eq 45a has assigned values on an oblate spheroid, oblate spheroidal coordinates are used. The bilinear expantion for this nucleus in such coordinates is used in a later section and applied to the limiting case where the spheroid becomes a circular disk.

The expansion in toroidal coordinates is also intimately related to the present problem, the function $\phi_n(k)$ being a toroidal function $\phi_n(k)=\frac{1}{\pi}Q_{n-\frac{1}{2}}\left(\frac{2}{k^2}-1\right)$, where Q_n is Legendre's function of the second kind.

The derivation of eq 42b may be made by use of Heine's integral formula,

$$\frac{1}{R_{12}}=\frac{1}{\sqrt{x^2+r_{12}^2}}=\int e^{-|x|t}J_0(r_{12}t)dt. \qquad (49)$$

Using Neumann's addition formula,

$$J_0(r_{12}t)=\sum_{n_1=-\infty}^{\infty}J_{n_1}(a_1t)J_{n_1}(r_2t)e^{in_1(\theta_1-\theta_2')}$$

$$=2\sum_{n=0}^{\infty}\epsilon_nJ_n(a_1t)J_n(r_2t)\cos n(\theta_1-\theta_2') \qquad (50)$$

gives

$$\frac{1}{R_{12}}=2\sum_{n=0}^{\infty}\epsilon_n \cos n(\theta_1-\theta_2')\int_0^{\infty}e^{-|x|t}.J_n(a_1t)J_n(r_2t)dt, \tag{51}$$

which, by comparison with eq 41, gives eq 42b. In the expansion (eq 41) or its equivalent (eq 51), both r_2 and θ_2' are functions of θ_2. Since r_2 is one side of the triangle, $P_2O_1O_2$ (fig. 3), the other sides, r and a_2, including the angle $(\pi-\theta_2)$,

$$r_2^2=r^2-2ra_2 \cos (\pi-\theta_2)+a_2^2. \tag{52}$$

To obtain the Fourier's cosine series in θ_1 and θ_2 for $1/R_{12}$, the term $J_0(r_{12}t)$ in the integrand of eq 49 must be expressed explicitly in terms of these angles. Hence in the expansion (eq 50), the term $J_{n_1}(r_2t)\ e^{-in_2\theta_2'}$ must be expanded as a Fourier series in θ_2, and for this a more general formula than Neumann's addition formula (eq 50) is required.

Neumann's addition formula is a special case of a more general addition formula derivable from that of Sonin,[4] which, applied to the triangle $P_2O_1O_2$, may be put in the form

$$J_{n_1}(r_2t)e^{-in_1\theta_2'}=\sum_{n_2=-\infty}^{\infty}J_{n_1-n_2}(rt)J_{n_2}(a_2t)e^{-in_2\theta_2}. \tag{53}$$

Using this in eq 50 gives

$$J_0(r_{12}t)=\sum_{n_1=-\infty}^{\infty}\sum_{n_2=-\infty}^{\infty}J_{n_1-n_2}(rt)J_{n_1}(a_1t)J_{n_2}(a_2t).e^{i(n_1\theta_1-n_2\theta_2)}. \tag{54}$$

By use of this expansion in eq 49, the double Fourier's series expansion of the function $1/R_{12}$ defined in eq 3 is found to be

$$\frac{1}{R_{12}(x,\theta_1,\theta_2)}=\frac{1}{\sqrt{a_1a_2}}\sum_{n_1=-\infty}^{\infty}\sum_{n_2=-\infty}^{\infty}\phi_{n_1,n_2}(x,r,a_1,a_2)e^{i(n_1\theta_1-n_2\theta_2)}$$

$$=\frac{1}{\sqrt{a_1a_2}}\sum_{n_1=-\infty}^{\infty}\sum_{n_2=-\infty}^{\infty}\phi_{n_1,n_2}(x,r,a_1,a_2)\cos(n_1\theta_1-n_2\theta_2), \tag{55}$$

which may be written

$$\frac{1}{R_{12}(x,\theta_1,\theta_2)}=\frac{2}{\sqrt{a_1a_2}}\left\{\frac{\phi_{00}}{2}+\sum_{n_1=1}^{\infty}\phi_{n_1,n_1}\cos n_1(\theta_2-\theta_1)\right.$$

$$\left.+\sum_{n=1}^{\infty}\sum_{n_2=-\infty}^{\infty}\phi_{n+n_2,n_2}\cos[(n+n_2)\theta_1-n_2\theta_2]\right\}, \tag{56}$$

or

$$\frac{1}{R_{12}(x,\theta_1,\theta_2)}=$$

$$\frac{2}{\sqrt{a_1a_2}}\sum_{n_1=0}^{\infty}\sum_{n_2=0}^{\infty}\epsilon_{n_1}\epsilon_{n_2}\left\{(\phi_{n_1,n_2}+\phi_{n_1,-n_2})\cos n_1\theta_1\cos n_2\theta_2\right.$$

$$\left.+(\phi_{n_1,n_2}-\phi_{n_1,-n_2})\sin n_1\theta_1\sin n_2\theta_2\right\}. \tag{56'}$$

[4] N. Nielsen, Handbuch der Theorie der Cylinder Funktionen, p. 287, Teubner (1904).

The coefficients $\phi n_1, n_2$ are even functions of x, which are represented by

$$\phi_{n_1,n_2}(x,r,a_1,a_2)=\sqrt{a_1a_2}\int_0^\infty e^{-|x|t}J_{n_1-n_2}(rt)J_{n_1}(a_1t)J_{n_2}(a_2t)dt, \tag{57a}$$

or by Fourier's rule,

$$\phi_{n_1,n_2}(x,r,a_1,a_2)=\frac{\sqrt{a_1a_2}}{4\pi^2}\int_0^{2\pi}d\theta_1\int_0^{2\pi}d\theta_2\,\frac{\cos\,(n_1\theta_1-n_2\theta_2)}{R_{12}(x,\theta_1,\theta_2)}, \tag{57b}$$

which shows that $\phi_{n_1,-n_2}=\phi_{-n_1,n_2}$. On inserting the expansion (eq 56) in the three equations, 30, 31, 32, noting that

$$\int_0^{2\pi}\Theta_1(\theta-\theta_1')\cos n\theta_1'd\theta_1'=\frac{\pi}{n}\sin n\theta_1,\text{ if } n\neq 0,\quad =0\text{ if } n=0$$

$$\int_0^{2\pi}\Theta(\theta_1-\theta_1')\sin n\theta_1'd\theta_1'=-\frac{\pi}{n}\cos n\theta_1\text{ if } n\neq 0,\ =0\text{ if } n=0$$

$$\int_0^{2\pi}\Theta^2(\theta_1-\theta_1')\cos n\theta_1'd\theta_1'=\frac{\pi}{n^2}\cos n\theta_1\text{ if } n\neq 0,\quad =\frac{\pi^3}{6},\text{ if } n=0,$$

the Fourier's series for the function ω is obtained. The term ω_0 corresponding to current sheets may be written

$$\omega_0=\omega_{11}+\frac{p_1p_2}{a_1a_2}\omega_{00}, \tag{58}$$

where the principal part of ω is ω_{11} due to the angular component of current in the sheets. The term

$$\frac{p_1p_2}{a_1a_2}\omega_{00}$$

is due to the axial components of current in the sheets and is an infinitesimal of second order.

The functions ω_{11} and ω_{00} are special cases of the function $\omega_{n_1n_2}$ defined by

$$\omega_{n_1,n_2}(x,r,a_1,a_2)\equiv 4\pi^2\sqrt{a_1a_2}\int_0^x dx''\int_0^{x''}dx'\,\phi_{n_1,n_2}(x',r,a_1,a_2), \tag{59}$$

so that

$$\omega'_{n_1,n_2}(x,r,a_1,a_2)=4\pi^2\sqrt{a_1a_2}\int_0^x dx'\,\phi_{n_1,n_2}(x',r,a_1,a_2). \tag{60}$$

The first-order infinitesimal ω_1 given by eq 31 is found to be

$$\omega_1(x,\theta_1,\theta_2)=-p_1\sum_{n=1}^\infty\frac{\sin\,n\theta_1}{n}[\omega'_{n+1,1}(x,r,a_1,a_2)+\omega'_{n-1,-1}(x,r,a_1,a_2)]$$

$$-p_2\sum_{n=1}^\infty\frac{\sin\,n(\pi-\theta_2)}{n}[\omega'_{n+1,1}(x,r,a_2,a_1)+\omega'_{n-1,-1}(x,r,a_2,a_1)], \tag{61}$$

and the second-order term ω_2, derived from eq 32 becomes

$$\omega_2(x,\theta_1,\theta_2)$$

$$=4\pi^2\sqrt{a_1a_2}\Big\{p_1^2\sum_{n=1}^{\infty}\frac{\cos n\theta_1}{n_2}[\phi_{n+1,1}(x,r,a_1,a_2)+\phi_{n-1,-1}(x,r,a_1,a_2)]$$

$$+p_2^2\sum_{n=1}^{\infty}\frac{\cos n(\pi-\theta_2)}{n^2}[\phi_{n+1,1}(x,r,a_2,a_1)+\phi_{n-1,-1}(x,r,a_2,a_1)]$$

$$+p_1p_2\sum_{n_1=1}^{\infty}\sum_{n_2=1}^{\infty}\frac{1}{n_1n_2}[(\phi_{n_1+1,-n_2+1}+\phi_{n_1-1,-n_2-1})\cos(n_1\theta_1+n_2\theta_2)$$

$$-(\phi_{n_1+1,n_2+1}+\phi_{n_1-1,n_2-1})\cos(n_1\theta_1-n_2\theta_2)]\Big\}, \tag{62}$$

where the arguments of all the ϕ-functions in the double series are (x, r, a_1, a_2), respectively. In deriving these expressions from the expansion (eq 55), we have made use of the fact (shown by eq 57b) that $\phi_{-n_1,-n_2}\equiv\phi_{n_1,n_2}$ and also of the relation (shown by eq 57a that

$$\phi_{n_1,n_2}(x,r,a_1,a_2)=\phi_{n_2,n_1}x,r,a_2,a_1), \tag{63}$$

which obviously hold for the functions $\omega_{n_1n_2}$ and $\omega'_{n_1n_2}$.

The approximate expressions for Θ and Θ^2 given in eq 35 merely indicate that ω_1 is found from eq 61 by retaining only the first two terms of each series and inserting the factor $\pi^2/9$, while the second-order term, ω_2, is sufficiently represented by merely extending the n_1, and n_2 summations each from 1 to 2 in the series given in eq 62.

In the case of coaxial helices ($r=0$), eq 57a, shows that

$$\phi_{n_1n_2}(x,o,a_1,a_2)=\phi_{n_1}(x,a_1,a_2)\delta_{n_1n_2}=\phi_{n_1}(k)\delta_{n_1n_2},$$

where

$$k^2=\frac{4a_1a_2}{x^2+(a_1+a_2)^2}$$

and $\delta_{n_1,n_2}=1$, if $n_1=n_2$,=zero otherwise. Equation 61 shows that $\omega_1=0$, and eq 62 shows that

$$\omega_2\rightarrow-4\pi^2p_1p_2\sqrt{a_1a_2}\sum_{n=1}^{\infty}[\phi_{n-1}(k)+\phi_{n+1}(k)]\frac{\cos n(\theta_1-\theta_2),}{n^2}$$

where $\theta_1-\theta_2$ is the azimuthal difference of the two terminals.

Hence the surviving terms are equivalent to those previously obtained for the coaxial case in eq 49 of the paper quoted (footnote 2). The terms $n_1n_2\omega_{11}(x)$, $n_1n_2\omega_{00}(x)$, $n_1n_2\omega_2(x,\theta_1-\theta_2)$ of this paper correspond to $\omega_0(x)$, $\omega_x(x)$, and $\omega_a(x,\theta_x)(\theta_x=\theta_1-\theta_2)$ of that paper, where $n_1n_2=1/4\pi^2p_1p_2$.

For the coaxial helices in a current balance, the term ω_2 compared with ω_0 was found to be 10 parts in a million.

To derive a formula by which the mutual inductance of the two helices may be computed in the general case, where their axes are merely parallel, it is necessary to obtain expressions by which the functions $\phi_{n_1n_2}$ and their first and second partial integrals with respect to x may be computed. None of the integrals, eq 57a, 57b, 59, and 60, may be integrated in finite terms, so we are driven to expansions

in series. Such expansions in oblate spheroidal harmonics are obtained in the following sections.

By reference to the relation (eq 63) it is evident that ϕ_{n_1,n_2}, where n_1 and n_2 are any integers (positive, negative, or zero), is obtainable (by interchange of the arguments, a_1 and a_2 when necessary) from one of the following three irreducible cases:

Case A; $n_2=n_1\geq 0$
Case B; $0\leq n_2<n_1$
Case C; $n_2<0$ and $n_1>0$

However, this requires that we obtain expansions for $\phi_{n_1n_2}$ in these three cases, without committing ourselves to a restriction that $a_2<a_1$, that is, one that is valid when a_1 and a_2 are interchanged.

V. PARTIAL DIFFERENTIAL EQUATIONS AND BOUNDARY CONDITIONS SATISFIED BY THE FUNCTION ϕ_{n_1,n_2}

From the differential equation satisfied by Bessel's function, combined with the integral representation of ϕ_{n_1,n_2} in (eq 57a), it is found that ϕ_{n_1,n_2} satisfies the two partial differential equations

$$\left\{D_x^2+D_r^2+\frac{1}{r}D_r-\frac{n^2}{r^2}\right\}\frac{\phi_{n_1,n_2}}{\sqrt{a_1a_2}}=0, \text{ where } n=n_1-n_2\geq 0, \tag{64}$$

and

$$\left\{D_x^2+D_{a_1}^2+\frac{1}{a_1}D_{a_1}-\frac{n_1^2}{a_1^2}\right\}\frac{\phi_{n_1,n_2}}{\sqrt{a_1a_2}}=0, \tag{65}$$

and also a similar equation, where a_1 and n_1 are replaced by a_2 and n_2. As to boundary conditions, it is evident that $\dfrac{\phi_{n_1,n_2}}{\sqrt{a_1a_2}}$ vanishes when $\sqrt{x^2+r^2}\to\infty$, or when $\sqrt{x^2+a_1^2}\to\infty$. The function is also regular in the neighborhood of $r=0$ or $(a_1=0)$ and is finite, continuous, and single-valued in general and an even function of x.

The partial derivative with respect to x, ϕ'_{n_1,n_2} is an odd function of x. Defining σ by

$$\sigma\equiv-\frac{\phi'_{n_1,n_2}(+0,r,a_1,a_2)}{2\pi\sqrt{a_1a_2}}=+\frac{\phi'_{n_1,n_2}(-0,r,a_1,a_2)}{2\pi\sqrt{a_1a_2}}$$

$$=\frac{1}{2\pi}\int_0^\infty tJ_{n_1-n_2}(rt)J_{n_1}(a_1t)J_{n_2}(a_2t)dt, \tag{66}$$

it will be seen that σ must be zero when $r<|a_1-a_2|$ and when $r>a_1+a_2$, for the integral representation (eq 57b) exhibits ϕ_{n_1,n_2} as a double line integral around two parallel circles of radii a_1 and a_2, x being the distance between their planes and r the distance between their axes. In the case $n_1=n_2=1$, the function ϕ_{11} multiplied by $4\pi^2\sqrt{a_1a_2}$ is the mutual inductance of the two parallel circles.

Equation 57b may be written

$$4\pi^2\sqrt{a_1a_2}\phi_{n_1,n_2}(x,r)=\int_0^{2\pi}a_2\cos n_2\theta_2 d\theta_2\int_0^{2\pi}\frac{a_1\cos n_1\theta_1 d\theta_1}{R_{12}}$$

$$+\int_0^{2\pi}a_2\sin n_2\theta_2 d\theta_2\int_0^{2\pi}\frac{a_1\sin n_1\theta_1}{R_{12}}d\theta_1. \tag{67}$$

Each of these integrals is a special case of double-line integrals taken around the two circles of type

$$\phi(x)=\int f_2(\theta_2)ds_2\int\frac{f_1(\theta_1)ds_1}{R_{12}}, \tag{68}$$

where

$$ds_1=a_1d\theta_1 \text{ and } ds_2=a_2d\theta_2$$

are elements of arc of the circles, R_{12} being the distance between the two points of integration, P_1 in the first circle and P_2 on the second. The first of radius a_1 may be considered in the plane $x=0$ coaxial with the x-axis, the second parallel to it has its center at a point whose cylindrical coordinates are (x,r,θ). Since $1/R_{12}$ is so fundamental in the theory of electrostatics, and because electrostatic problems are familiar to most of us, some guidance may be obtained by availing ourselves occasionally of an electrostatic interpretation of integrals involving the factor $1/R_{12}$ in the integrand. Thus the first line integral in eq 68, which is

$$V=\int\frac{f_1(\theta_1)ds_1}{R_{12}},$$

is the electrostatic potential at any point P_2 on the second circle when the first circle is a line charge with linear density $f_1(\theta_1)$. Hence, if the second circle is a line charge of linear density $f_2(\theta_2)$, then

$$-\phi'(x)=-D_x\phi=\int_2 f_2(\theta_2)E_xds_2, \text{ where } E_x=-D_xV$$

the x-component of the electric field of the first circle at any point P_2 of the second. Consequently, $-\phi'=F_x=$the x-component of the force which the first circle exerts upon the second. Clearly this vanishes when $x=0$ if the circles do not touch or intersect in this coplanar position, that is,

$$\begin{aligned}\phi'(0)&=0 \text{ if } 0<r<|a_1-a_2|\\&=0 \text{ if } a_1+a_2<r<\infty.\end{aligned} \tag{69}$$

In the remaining case, $|a_1-a_2|<r<a_1+a_2$, the circles intersect if they are brought into the same plane while keeping r constant. This is the case for which figure 3 is drawn, assuming $a_2<a_1$ (but the argument may be made by reference to that figure, keeping in mind the other possibility, $a_1<a_2$). In this case the values of θ_1 and θ_2 corresponding to one point of intersection P_0 are called θ_1^0 and θ_2^0, respec-

tively. The angle 2ψ between the intersecting arcs may be taken as the angle $O_1P_0O_2$, so that

$$\left.\begin{array}{l} 2\psi=\theta_2^0-\theta_1^0, \text{ where } 0\leqq\theta_1^0\leqq\pi \text{ and })\leqq\theta_2^0\leqq\pi, \\ \text{so that } 0\leqq 2\psi\leqq\pi \end{array}\right\}. \tag{70}$$

The coordinates, $\theta_1^0=2\pi-\theta_1^0$ and $\theta'^0_2=2\pi-\theta_2^0$ refer to the other point of intersection P'_0.

When the two circles approach the same plane ($x\to+0$), the infinitesimal arcs in the neighborhood of P_0 (or P'_0) contribute a finite amount to their mutual repulsion F_x in the x-direction, because R_{12} vanishes at P_0 (and P'_0). Arcs at a finite distance from these points contribute a vanishing amount to F_x. The curvature of the intersecting arcs becomes irrelevant, but of course the angle 2ψ at which they intersect is important. The value of the integral may be computed as in the case of two endless straight-line charges approaching intersection, their linear charge densities being variable, but only the values of these densities at P_0 (or P') being effective. If we allow for discontinuities in the functions f_1 (θ_1) and f_2 (θ_2) (as for example in eq 31 and eq 32, in the integrals defining ω_1 and ω_2), we find, when $|a_1-a_2|<r<a_1+a_2$ and ϕ, defined by eq 68, that

$$\begin{aligned} -\phi'(+0)=\frac{2\pi}{\sin 2\psi}\Bigg\{&\left(\frac{f_1(\theta_1^0+0)+f_1(\theta_1^0-0)}{2}\right)\left(\frac{f_2(\theta_2^0+0)+f_2(\theta_2^0-0)}{2}\right) \\ &+\left(\frac{f_1(\theta'^0_1+0)+f_1(\theta'^0_2-0)}{2}\right)\left(\frac{f_2(\theta'^0_2+0)+f_2(\theta'^0_2-0)}{2}\right) \\ +\left(\frac{\pi-4\psi}{\pi}\right)&\Bigg[\left(\frac{f_1(\theta_1^0+0)-f_1(\theta_1^0-0)}{2}\right)\left(\frac{f_2(\theta_3^0+0)-f_2(\theta_2^0-0)}{2}\right) \\ &+\left(\frac{f_1(\theta'^0_1+0)-f_1(\theta'^0_1-0)}{2}\right)\left(\frac{f_2(\theta'^0_2+0)-f_2(\theta'^0_2-0)}{2}\right)\Bigg]\Bigg\}. \end{aligned} \tag{71}$$

For the case where f_1 and f_2 are continuous functions, this becomes

$$-\phi'(+0)=\frac{2\pi}{\sin 2\psi}[f_1(\theta_1^0)f_2(\theta_2^0)+f_1(\theta'^0_2)f_2(\theta'^0_2)]. \tag{71'}$$

Using this in eq 67 leads to the following expression for the σ defined in eq 66:

$$\left.\begin{array}{ll} \sigma=0 & \text{if } 0\leqq r<A_2 \\ =\dfrac{2}{n^2(A_1^2-A_2^2)}\dfrac{\cos(n_1\theta_1^0-n_2\theta_2^0)}{\sin 2\psi} & \text{if } A_2<r<A_1 \\ =0 & \text{if } A_1<r\leqq\infty \end{array}\right\}, \tag{72}$$

where

$$\left.\begin{array}{l} A_1\equiv a_1+a_2 \\ A_2\equiv|a_1-a_2| \end{array}\right\}, \text{ so that } 0<A_2<A_1. \tag{73}$$

The absolute value $|a_1-a_2|$ is used for A_2, so that we need not commit ourselves on the question as to which of the two circular radii, a_1 or a_2, is the larger.

The second member of eq 72 is a function of r, since θ_1^0 and θ_2^0 and $2\psi=\theta_2^0-\theta_1^0$ are functions of r. However, it is more convenient to reverse this and to express σ and r as functions of ψ, which may be done by expressing θ_1^0 as functions of ψ.

To do this we define ξ_0' by

$$\left.\begin{aligned}\xi_0'&=\frac{a_1-a_2}{a_1+a_2}\\ \xi_0&=\sqrt{1-\xi_0'^2}=\frac{2\sqrt{a_1a_2}}{a_1+a_2}=\sqrt{1-\left(\frac{A_2}{A_1}\right)^2}\end{aligned}\right|\begin{matrix}-1<\xi_0'<1\\ 0<\xi_0<1\end{matrix}. \tag{74}$$

Considering the triangle $O_1P_0O_2$ of figure 3, it is evident that

$$\begin{aligned}r&=(a_1^2-2a_1a_2\cos 2\psi+a_2^2)^{\frac{1}{2}}=A_1(1-\xi_0^2\cos^2\psi)^{\frac{1}{2}}\\ &=a_1\left(1-\frac{a_2}{a_1}e^{2i\psi}\right)^{\frac{1}{2}}\left(1-\frac{a_2}{a_1}e^{-2i\psi}\right)^{\frac{1}{2}}\end{aligned} \tag{75}$$

$$\sin 2\psi=\frac{2}{A_1^2-A_2^2}\sqrt{(A_1^2-r^2)(r^2-A_2^2)} \tag{75'}$$

$$\left.\begin{aligned}\cos\theta_1^0&=\frac{a_1-a_2\cos 2\psi}{r}\\ \sin\theta_1^0&=\frac{a_2\sin 2\psi}{r}\end{aligned}\right\}\text{ and }\left\{\begin{aligned}\cos\theta_2^0&=\frac{a_1\cos 2\psi-a_2}{r}\\ \sin\theta_2^0&=\frac{a_1\sin 2\psi}{r}\end{aligned}\right\}. \tag{76}$$

From these relations it follows that

$$e^{i\theta_1^0}=\frac{a_1-a_2e^{-2i\psi}}{r}=\left(\frac{a_1-a_2e^{-2i\psi}}{a_1-a_2e^{2i\psi}}\right)^{\frac{1}{2}}=\frac{1+\xi_0}{2}\frac{1-\dfrac{1-\xi_0'}{1+\xi_0}e^{-2i\psi}}{(1-\xi_0^2\cos^2\psi)^{\frac{1}{2}}} \tag{77a}$$

$$e^{i\theta_2^0}=\frac{a_1e^{2i\psi}-a_2}{r}=e^{i(\theta_1^0+2\psi)}. \tag{77b}$$

When considering θ_1^0 and θ_2^0 as functions of r, a_1, and a_2, this may be indicated by writing $\theta_1^0=\theta_1^0(r,a_1,a_2)$ and $\theta_2^0=\theta_2^0(r,a_1,a_2)$. It is evident from these definitions that when we interchange the arguments a_1 and a_2, θ_1^0 goes into $\pi-\theta_2^0$ and θ_2^0 goes into $\pi-\theta_1^0$, that is,

$$\theta_1^0(r,a_2,a_1)=\pi-\theta_2^0(r,a_1,a_2) \tag{78a}$$

and

$$\theta_2^0(r,a_2,a_1)=\pi-\theta_1^0(r,a_1,a_2). \tag{78b}$$

On the other hand, $2\psi(=\theta_2^0-\theta_1^0)$ is unaltered by interchange of arguments a_1 and a_2.

By eq 77 we may write (if $\mathscr{R}$ ( ) denotes the real part)

$$\cos(n_1\theta_1^0 - n_2\theta_2^0) = \mathscr{R}\left(\frac{1+\xi_0'}{2}\right)^{n_1-n_2} \frac{e^{-2in_2\psi}\left[1-\frac{1-\xi_0'}{1+\xi_0'}e^{-2i\psi}\right]^{n_1-n_2}}{[1-\xi_0^2\cos^2\psi]^{\frac{n_1-n_2}{2}}}$$

$$= \frac{\left(\frac{1+\xi_0'}{2}\right)^{n_1-n_2}}{(1-\xi_0^2\cos^2\psi)^{\frac{n_1-n_2}{2}}}\Gamma(n_1-n_2+1)\cdot$$

$$\cdot\sum_{k=0}^{n_1-n_2}(-1)^k\left(\frac{1-\xi_0'}{1+\xi_0'}\right)^k \frac{\cos 2(k+n_2)\psi}{\Gamma(k+1)\Gamma(1+n_1-n_2-k)}$$

$$= \frac{(-1)^{n_2}\left(\frac{a_1}{A_1}\right)^{n_1}\left(\frac{a_2}{A_1}\right)^{-n_2}\Gamma(n_1-n_2+1)}{(1-\xi_0^2\cos^2\psi)^{\frac{n_1-n_2}{2}}}\cdot$$

$$\cdot\sum_{k=n_2}^{n_1}\frac{(-1)^k\left(\frac{a_2}{a_1}\right)^k\cos 2k\psi}{\Gamma(1+n_1-k)\Gamma(1-n_2+k)}.$$

Hence, if we define the integer n by

$$n = n_1 - n_2, \text{ so that } n \geqq 0 \text{ in all cases, } A, B, \text{ and } C, \tag{79}$$

while n_2 may be positive or negative, then

$$\left.\begin{aligned}
\sigma &= 0 \quad \text{— — — — — — — — — — — —} \quad \text{when } 0 \overline{\geqq} r < A_2 \\
&= \frac{2}{\xi_2^2\pi^2A^2\sin 2\psi}\left(\frac{1+\xi_0'}{2}\right)^n \frac{\Gamma(n+1)}{(1-\xi_0'^2\cos^2\psi)^{\frac{n}{2}}}\cdot \\
&\qquad \cdot\sum^{n}(-1)^k\left(\frac{1-\xi_0'}{1+\xi_0'}\right)^k \frac{\cos 2(k+n_2)\psi}{\Gamma(k+1)\Gamma(1+n-k)} \\
&\qquad \text{when } A_2 < r < A_1 \\
&= 0 \quad \text{— — — — — — — — — — — —} \quad \text{when } A_1 < r \overline{\leqq} \infty
\end{aligned}\right\} \tag{80}$$

In case $n=0$, this series reduces to the simple term $\cos 2n_2\psi$, so tha

$$\sigma_{m,m} = \frac{2\cos 2m\psi}{\pi^2(A_1^2-A_2^2)\sin 2\psi}.$$

Quite a different electrostatic interpretation of $\phi_{n_1n_2}$ will now be useful. If x, r, and θ are considered as the cylindrical coordinates of a point P in space, the function $V(x,r,\theta) = (a_1a_2)^{-\frac{1}{2}}\phi_{n1,n2}(x,r,a_1,a_2)\cos(n_1-n_2)\theta$ is the Newtonian potential at any point P due to a simple distribution of charge upon the annular surface $(A_2<r<A_1, x=0)$, whose surface density is $\sigma\cos(n_1-n_2)\theta$, so that the σ defined by eq 66 or 80 plays the same part for solutions of eq 64 that surface density on the annulus plays for solutions of Laplace's equation.

In the following section an expansion for ϕ_{n_1,n_2} is obtained in terms of the normal functions of oblate spheroidal coordinates, these being

used because in terms of them ϕ_{n_1,n_2} admits of a single expansion valid for all real values of x and for all positive or zero values of r, a_1, and a_2, whereas ordinary spherical coordinates require three different expansions according as $0 \leqq r \leqq A_2$, $A_2 \leqq r \leqq A_1$, or $A_1 \leqq r \leqq \infty$, and the expansion in the second of these cases is somewhat complicated. In this respect, toroidal coordinates are superior to spherical but inferior to spheroidal, as the expansions require only two cases.

VI. EXPANSION OF $\phi_{n_1 n_2}$ IN OBLATE SPHEROIDAL COORDINATES

Instead of the cylindrical coordinates (x, r, θ) the (oblate) spheroidal coordinates, ξ, η, θ (the same θ), may be used to designate a point in space, where

$$\left.\begin{aligned} x &= A_1 \xi \eta \\ r &= A_1 \sqrt{(1-\xi^2)(1+\eta^2)} \end{aligned}\right\}, \text{ where } \left\{\begin{matrix} -1 \leqq \xi \leqq 1 \\ 0 \leqq \eta \leqq \infty \end{matrix}\right\}. \tag{81}$$

Solving for ξ ad η gives

$$\left.\begin{aligned} \xi^2 &= \frac{1}{2A_1^2}\left\{A_2^1 - x^2 - r^2 + \sqrt{[x^2+(r+A_1)^2][x^2+(r-A_1)^2]}\right\} \\ \eta^2 &= \frac{1}{2A_1^2}\left\{x^2 + r^2 - A_1^2 + \sqrt{[x^2+(r+A_1)^2][x^2+(r-A_1)^2]}\right\} \end{aligned}\right\}. \tag{82}$$

Also from eq 81, we find

$$dx^2 + dr^2 = A_1^2(\xi^2+\eta^2)\left[\frac{d\xi^2}{1-\xi^2} + \frac{d\eta^2}{1+\eta^2}\right]. \tag{83}$$

The locus of the equation, η=constant, is the entire surface of the oblate spheroid, whose equation is

$$x^2/A_1^2\eta^2 + r^2/A_1^2(1+\eta^2) = 1,$$

whose foci are at $(x=0,\ r=\pm A_1)$. In particular, the locus of $\eta=0$ is both sides of the circular disk $(x=0,\ 0 \leqq r,\ \leqq A_1)$, at the edge of which $\xi=0$, and ξ increases from zero to 1 on the side $x=+0$ as the point passes from the edge to the origin, or x-axis, while ξ decreases from 0 to -1 on the side $x=-0$ as the point moves down to the axis. The locus $\xi=+1$ is the positive x-axis, and $\xi=-1$ is the negative x-axis.

The hyperboloid which is confocal with every such spheroid whose equation is

$$-x^2/A_1^2\xi^2 + r^2/A_1^2(1-\xi^2) = 1$$

must be considered as the two loci, that half for which $x>0$ being the locus $\xi=\xi_1>0$, and that for which $x<0$ being the locus $\xi=-\xi_1<0$. Large values of η correspond to points far away from the origin, since $1+\eta^2=(x^2+r^2)/A_1^2+\xi^2$. The differential equation (64) becomes

$$\left\{D_\xi[(1-\xi^2)D_\xi] - \frac{n^2}{1-\xi^2}\right\}\frac{\phi_{n_1,n_2}}{\sqrt{a_1 a_2}} = -\left\{D_\eta[(1+\eta^2)D_\eta] + \frac{n^2}{1+\eta^2}\right\}\frac{\phi_{n_1,n_2}}{\sqrt{a_1 a_2}}, \tag{84}$$

which has solutions of the form

$$\frac{\phi_{n_1 n_2}}{\sqrt{a_1 a_2}} = P(\xi)R(\eta), \tag{85}$$

where $P(\xi)$ is a solution of

$$D_\xi[(1-\xi^2)P'] + \left[\mu(\mu+1) - \frac{n^2}{1-\xi^2}\right]P = 0, \text{ where } P' = D_\xi P \tag{86}$$

and $R(\eta)$ is a solution of

$$D_\eta[(1+\eta^2)R'] - \left[\mu(\mu+1) - \frac{\eta^2}{1+\eta^2}\right]R = 0 \tag{87}$$

$$n \equiv n_1 - n_2. \tag{88}$$

As shown in the preceding section, it is sufficient to consider $n = n_1 - n_2$, where n is a positive integer, or zero, while n_2 is either positive, negative, or zero, and $n_1 \geq 0$. Equation 87 goes into the same type as eq 86 in the independent variable z, where $\eta = iz$.

One solution of eq 86 for the case where $-1 < \xi < 1$ may be taken as $P = P_\mu^n(\xi)$, which is (Ferrer's) associated Legendre function. This reduces to the accepted value when $\nu =$ an integer, if we define it, for general values of μ, ν when $|1-\xi| < 2$ by

$$P_\mu^\nu(\xi) = \frac{(1-\xi^2)^{\frac{\nu}{2}}\Gamma(\mu+\nu+1)}{2^\nu \Gamma(\mu-\nu+1)\Gamma(\nu+1)} F\left(\nu-\mu, \nu+\mu+1, \nu+1; \frac{1-\xi}{2}\right). \tag{89}$$

We make use of the two recurrence relations

$$(2\mu+1)\xi P_\mu^\nu(\zeta) = (\mu-\nu+1)P_{\mu+1}^\nu(\zeta) + (\mu+\nu)P_{\mu-1}^\nu(\zeta) \tag{90}$$

$$(2\mu+1)(1-\zeta^2)P_\mu'^\nu(\xi) = -(\mu-\nu+1)\mu P_{\mu+1}^\nu(\xi) + (\mu+\nu)(\mu+1)P_{\mu-1}^\nu(\xi). \tag{91}$$

Also when n is a positive integer

$$P_\mu^n(\xi) = (1-\xi^2)^{\frac{n}{2}} D_\xi^n P_\mu(\xi). \tag{92}$$

We require also the following expressions when $\mu = \nu + s$, where s is a positive integer or zero.

$$P_{\nu+s}^\nu(\xi) = \frac{(1-\xi^2)^{\frac{\nu}{2}}}{2^\nu} \frac{\Gamma(s+2\nu+1)}{\Gamma(s+1)\Gamma(\nu+1)}$$

$$F\left(-s, s+2\nu+1, \nu+1; \frac{1-\xi}{2}\right), \text{ if } |1-\xi| < 2 \tag{93}$$

$$P_{\nu+2s}^\nu(\xi) = \frac{(-1)^s 2^\nu (1-\xi^2)^{\frac{\nu}{2}}}{\sqrt{\pi}} \frac{\Gamma(s+\nu+\frac{1}{2})}{\Gamma(s+1)} F\left(-s, s+\nu+\tfrac{1}{2}, \tfrac{1}{2}; \xi^2\right) \tag{94a}$$

$$P_{\nu+2s+1}^\nu(\xi) = \frac{(-1)^s 2^{\nu+1} (1-\xi^2)^{\frac{\nu}{2}}}{\sqrt{\pi}} \frac{\Gamma(s+\nu+\frac{3}{2})}{\Gamma(s+1)} \xi F\left(-s, s+\nu+\tfrac{3}{2}, \tfrac{3}{2}; \xi^2\right) \tag{94b}$$

if $|\xi| < |$.

Also when $|1-\xi^2|<1$, there are the two relations:

$$P^{\nu}_{\nu+2s}(\xi)=\frac{2^{\nu}(1-\xi^2)^{\frac{\nu}{2}}\,\Gamma(s+\nu+1)\Gamma(s+\nu+\frac{1}{2})}{\Gamma(\nu+1)\;\Gamma(s+1)\;\Gamma(s+\frac{1}{2})}\cdot$$

$$F(-s,s+\nu+\tfrac{1}{2},\nu+1;1-\xi^2) \quad (95a)$$

$$P^{\nu}_{\nu+2s+1}(\xi)=\frac{2^{\nu}(1-\xi^2)^{\frac{\nu}{2}}\;\Gamma(s+\nu+1)\;\Gamma(s+\nu+\frac{3}{2})}{\Gamma(\nu+1)\;\Gamma(s+1)\;\Gamma(s+\frac{3}{2})}\cdot$$

$$\xi\,F\,(-s,s+\nu+\tfrac{3}{2},\nu+1;1-\xi^2). \quad (95b)$$

The hypergeometric functions in the last five expressions are polynomials, if s is a positive integer or zero, but eq 93, 95a, and 95b are valid if ν and s are unrestricted.

The importance of the case $\mu=\nu+s$ lies in the fact that if ν is any given constant greater than -1, the infinite set of functions $P^{\nu}_{\nu+s}$ constitute a complete set of orthogonal functions for the range $-1<\xi<1$, for

$$\int_{-1}^{1}P^{\nu}_{\nu+s_1}(\xi)P^{\nu}_{\nu+s_2}(\xi)d\xi=0 \text{ if } s_1\neq s_2 \quad (96)$$

and

$$\int_{-1}^{1}[P^{\nu}_{\nu+s}(\xi)]^2d\xi=\frac{2\Gamma(s+2\nu+1)}{(2s+2\nu+1)\Gamma(s+1)}\cdot \quad (97)$$

For the range $0<\xi<1$ the set of even functions of ξ, $P^{\nu}_{\nu+2s}\xi$, are a closed set of orthogonal functions, as also are the odd functions.

If a function is developable in terms of these normal functions, its development is

$$f(\xi)=\sum_{s=0}^{\infty}(s+\nu+\tfrac{1}{2})\frac{\Gamma(s+1)}{\Gamma(s+2\nu+1)}P^{\nu}_{\nu+s}(\xi)\int_{-1}^{1}f(\xi_1)P^{\nu}_{\nu+s}\,\xi_1)d\xi_1 \text{ for} -1<\xi<1. \quad (98)$$

A special case is

$$f(\xi)=2\sum_{s=0}^{\infty}(2s+\nu+\tfrac{1}{2})\frac{\Gamma(2s+1)}{\Gamma(2s+2\nu+1)}P^{\nu}_{\nu+2s}(\xi)$$

$$\int_{0}^{1}f(\xi_1)P^{\nu}_{\nu+2s}(\xi)d\xi_1 \text{ for } 0<\xi<1. \quad (98^1)$$

For the range here needed, $0\leqq\eta\leqq\infty$, it is convenient to take the general solution of eq 87 in the form

$$R(\eta)=C_1R^{n}_{\mu}(\eta)+C_2S^{n}_{\mu}(\eta),$$

where

$$R^{\nu}_{\mu}(\eta)\equiv\frac{(1+\eta^2)^{-\left(\frac{\mu+1}{2}\right)}}{2^{\mu}}\cdot\frac{\Gamma(\mu-\nu+1)}{\Gamma\left(\mu+\frac{3}{2}\right)}\cdot F\left(\frac{\mu+\nu+1}{2},\frac{\mu-\nu+1}{2},\mu+\frac{3}{2};\frac{1}{1+\eta^2}\right)$$

$$=\frac{2\Gamma(\mu-\nu+1)i^{\mu+1}}{\sqrt{\pi}\cos\nu\pi\Gamma(\mu+\nu+1)}Q^{\nu}_{\mu}(i\eta) \tag{99a}$$

$$S^{\nu}_{\mu}(\eta)=\frac{(1+\eta^2)^{\frac{\mu}{2}}2^{\mu}\pi}{\Gamma(\mu-\nu+1)\Gamma\left(\frac{1}{2}-\mu\right)}F\left(-\frac{\mu}{2}+\frac{\nu}{2},-\frac{\mu}{2}-\frac{\nu}{2},\frac{1}{2}-\mu;\frac{1}{1+\eta^2}\right)$$

$$=-\frac{\sin(\mu+\nu)\pi}{2}R^{\nu}_{-\mu-1}(\eta). \tag{99b}$$

The relation

$$(1+\eta^2)[R^{\nu}_{\mu}S'^{\nu}_{\mu}-R'^{\nu}_{\mu}S^{\nu}_{\mu}]=2\cos\mu\pi\frac{\Gamma(\mu-\nu+1)}{\Gamma(\mu+\nu+1)} \tag{100}$$

shows that these two functions are linearly independent when $\nu=n$ and $\mu=m\geq n$. The two recurrence relations

$$(2\mu+1)\eta R^{\nu}_{\mu}=(\mu-\nu)R^{\nu}_{\mu-1}-(\mu+\nu+1)R^{\nu}_{\mu+1} \tag{101a}$$

$$(2\mu+1)(1+\eta^2)R'^{\nu}_{\mu}=-(\mu-\nu)(\mu+1)R^{\nu}_{\mu-1}-(\mu+\nu+1)\mu R^{\nu}_{\mu+1} \tag{101b}$$

are also satisfied by the functions S^{ν}_{μ}.

Since $Q^{n}_{\mu}(z)=(z^2-1)^{\frac{n}{2}}D^{n}_{z}Q_{\mu}(z)$, the analogs of eq 92 are

$$R^{n}_{\mu}(\eta)=\frac{(-1)^n\Gamma(\mu-n+1)}{\Gamma(\mu+n+1)}(1+\eta^2)^{\frac{n}{2}}D^{n}_{\eta}R_{\mu}(\eta) \tag{102a}$$

$$S^{n}_{\mu}(\eta)=\frac{\Gamma(\mu-n+1)}{\Gamma(\mu+n+1)}(1+\eta^2)^{\frac{n}{2}}D^{n}_{\eta}S_{\mu}(\eta). \tag{102b}$$

By use of the recurrence relations, eq 90, 91, 101a, and 101b, we obtain equations of the form

$$(2\mu+1)P^{\nu}_{\mu}(\xi)R^{\nu}_{\mu}(\eta)=-A_1D_x[P^{\nu}_{\mu-1}(\xi)R^{\nu}_{\mu-1}(\eta)+P^{\nu}_{\mu+1}(\xi)R^{\nu}_{\mu+1}(\eta)] \tag{103}$$

and three others obtained by replacing $R^{\nu}_{\mu}(\eta)$ by $S^{\nu}_{\mu}(\eta)$ and then $P^{\nu}_{\mu}(\xi)$ by $Q^{\nu}_{\mu}(\xi)$ in each of the two relations. It is evident from eq 99

that $R_\mu^\nu \to 0$ when $\eta \to \infty$ if $\mu > -1$, while $S_\mu^\nu \to \infty$ if $\mu > 0$. We also place here for reference

$$\left.\begin{aligned} R_\mu^\nu(0) &= \frac{\Gamma\left(\frac{\mu-\nu+1}{2}\right)}{2^\nu \Gamma\left(\frac{\mu+\nu}{2}+1\right)} \quad \text{and} \quad R'^\nu_\mu(0) = -\frac{\Gamma\left(\frac{\mu-\nu}{2}+1\right)}{2^{\nu-1}\Gamma\left(\frac{\mu+\nu+1}{2}\right)} \\ S_\mu^\nu(0) &= \frac{(\cos \mu\pi + \cos \nu\pi)}{2^{\nu+1}} \frac{\Gamma\left(\frac{\mu-\nu+1}{2}\right)}{\Gamma\left(\frac{\mu+\nu}{2}+1\right)} \text{ and } S'^\nu_\mu(0) \\ &= \frac{(\cos \mu\pi - \cos \nu\pi)}{2^\nu} \frac{\Gamma\left(\frac{\mu-\nu}{2}+1\right)}{\Gamma\left(\frac{\mu+\nu+1}{2}\right)} \end{aligned}\right\} \quad (104)$$

The reciprocal distance from $P_1(\xi_1,\eta_1,\theta_1)$ to $P(\xi,\eta,\theta)$ has the known expansion

$$\frac{1}{R_{P_1P}} = \frac{2}{A_1} \sum_{n=0}^{\infty} \epsilon_n \cos n(\theta-\theta_1) \sum_{m=n}^{\infty} (-1)^m (m+\tfrac{1}{2})\, P_m^n(\xi) R_m^n(\eta) P_m^n(\xi_1) S_m^n(\eta_1), \quad (105)$$

provided that $\eta > \eta_1$, that is, the point P lies outside the ellipsoid, η_1, passing through P_1. When it is inside, $\eta < \eta_1$ and the above expansion is merely modified by interchanging the arguments η and η_1. This expansion is very similar in form to that of spherical coordinates given in eq 46. A comparison of eq 105 with eq 47 gives the expansion in spheroidal coordinates when $\eta > \eta_1$

$$\frac{\phi_n(x-x_1,r,r_1)}{\sqrt{rr_1}} = \frac{1}{A_1} \sum_{m=n}^{\infty} (-1)^m (m+\tfrac{1}{2})\, P_m^n(\xi) R_m^n(\eta) P_m^n(\xi_1) S_m^n(\eta_1) \quad (106)$$

with interchange of η and η_1 in case $\eta < \eta^1$. This is similar to the expansion of the same function in spherical coordinates given in eq 48.

Passing now to the case $\eta = 0$, which corresponds to $x_1 = 0$ and $0 \leq r_1 = A_1(1-\xi^2)^{\frac{1}{2}} < A_1$ so that the ellipsoid, η_1, shrinks into the circular disc, we find from eq 104 that

$$S_{n+2s+1}^n(0) = 0 \text{ and } S_{n+2s}^n(0) = \frac{(-1)^n}{2^n} \frac{\Gamma(s+\frac{1}{2})}{\Gamma(s+n+1)}.$$

Hence if

$$k^2 = \frac{4rr_1}{x^2+(r+r_1)^2} \quad (107)$$

then

$$\frac{\phi_n(x,r,r_1)}{\sqrt{rr_1}} = \frac{\phi_n(k)}{\sqrt{rr_1}}$$

$$= \frac{1}{A_1 2^n} \sum_{s=0}^{\infty} (2s+n+\tfrac{1}{2}) \frac{\Gamma(s+\frac{1}{2})}{\Gamma(s+n+1)} P_{n+2s}^n(\xi)\, R_{n+2s}^n(\eta)\, P_{n+2s}^n(\xi_1), \quad (108)$$

which is valid for all values of η, as is also the integral representation

$$\frac{\phi_n(k)}{\sqrt{rr_1}} = \int_0^\infty e^{-|x|t} J_n(rt) J_n(r_1 t) dt. \tag{109}$$

If U is a solution of eq 64, which vanishes when $x^2+r^2 \to \infty$ and such that

$$\sigma \equiv -\frac{1}{2\pi}[D_x U]_{x=+0} = +\frac{1}{2\pi}[D_x U]_{x=-0}$$

is a given function of $r_1 (= A_1(1-\xi_1^2)^{\frac{1}{2}})$

on the circular annulus $x=0 A_2 < r_1 < A_1$, and $\sigma = 0$ when $0 \leq r_1 < A_2$, and when $r > A_1$, then ξ_0 being defined as in eq 74

$$U = 2\pi \int_{A_2}^{A_1} \frac{r_1 \sigma(r_1) \phi_n(k) dr_1}{\sqrt{rr_1}} = 2\pi A_1^2 \int_0^{\xi_0} \frac{\xi_1 \sigma(\xi_1) \phi_n(k)}{\sqrt{rr_1}} d\xi_1. \tag{110}$$

Using eq 108 in this gives

$$U = \frac{2\pi A_1}{2^n} \sum_{s=0}^{\infty} (2s+n+\tfrac{1}{2}) \frac{\Gamma(s+\frac{1}{2})}{\Gamma(s+n+1)}$$

$$P_{n+2s}^n(\xi) . R_{n+2s}^n(\eta) . \int_0^{\xi_0} \xi_1 \sigma(\xi_1) P_{n+2s}^n(\xi_1) d\xi_1. \tag{111}$$

To confirm this result we note that the function U given by eq 111 is a solution of eq 64, which vanishes when $x^2+r^2 \longrightarrow \infty$.

Also $D_x U_{x=\pm 0} = 0$ when $r > A_1$, since $(D_x U_{x=0}) = \left(\frac{1}{A_1 \eta} D_\xi U\right)_{\xi=0}$ and $P'^n_{n+2s}(0) = 0$.

When $r < A_1$, $2\pi\sigma = -(D_x U)_{x=+0} = -\frac{1}{A_1 \xi}(D_\eta U)_{\eta=0}$ and eq 111 gives, by use of eq 104,

$$\xi\sigma(\xi) = 2 \sum_{s=0}^{\infty} (2\xi+n+\tfrac{1}{2}) \frac{\Gamma(2s+1)}{\Gamma(2s+2n+1)} P_{n+2s}^n(\xi) . \int_0^{\xi_0} \xi_1 \sigma(\xi_1) P_{n+2s}^n(\xi_1) d\xi_1 \tag{112}$$

for $0 < \xi < 1$.

Reference to eq 98′ for the case $\nu = n$ shows that the second member of eq 112 is the development in normal functions of the function $\xi\sigma(\xi)$, which is zero when $\xi_0 < \xi < 1$, that is, when $0 \leq r < A_2$, which shows that eq 111 is the required solution.

The same confirmation results by using eq 109 in eq 110, which give

$$U = 2\pi \int_0^\infty e^{-|x|t} J_n(rt) dt \int_{A_2}^{A_1} r_1 \sigma(r_1) J_n(r_1 t) dr_1, \tag{113}$$

which gives

$$\sigma \equiv -\frac{1}{2\pi}(D_x U)_{x=+0} = \int_0^\infty t J_n(rt) dt \int_{A_2}^{A_1} r_1 \sigma(r_1) J_n(r_1 t) dr_1, \tag{114}$$

which is Hankel's integral representation of a function of r, which is equal to σ when $A_2 < r < A_1$ and is zero when $0 \leq r < A_2$ and when $r > A_1$.

The function

$$\frac{\phi_{n_1 n_2}}{\sqrt{a_1 a_2}}$$

is equal to U if the density (eq 80) is used. It is then necessary to evaluate the integral

$$C_s^{n_1,n_2} \equiv \int_0^{\xi_0} \xi_1 \sigma(\xi_1) P_{n+2s}^n(\xi_1) d\xi_1 = \frac{1}{\pi^2 A_1^2}\left(\frac{1+\xi_0'}{2}\right)^n \cdot \frac{2\Gamma(n+1)}{{\xi_0}^2} \cdot$$

$$\cdot \sum_{k=0}^{n} \frac{(-1)^k \left(\frac{1-\xi_0'}{1+\xi_0'}\right)^k}{\Gamma(k+1)\Gamma(1+n-k)} \int_0^{\xi_0} \frac{\xi_1 \cos 2(k+n_2)\psi P_{n+2s}^n(\xi_1) d\xi_1}{(1-{\xi_0}^2 \cos^2\psi)_2^n \cdot \sin 2\psi}. \quad (115)$$

Now by eq 75 and eq 81, when $\eta=0$

$$\frac{r_1}{A_1} = (1-\xi_1^2)^{\frac{1}{2}} = (1-{\xi_0}^2\cos^2\psi)^{\frac{1}{2}}, \text{ so that } \xi_1 = \xi_0 \cos\psi$$

and

$$\xi_1 d\xi_1 = -\frac{{\xi_0}^2}{2} \sin 2\psi d\psi = -\frac{r_1 dr_1}{{A_1}^2},$$

so this becomes

$$C_s^{n_1,n_2} = \frac{\Gamma(n+1)}{\pi^2 A_1^2}\left(\frac{1+\xi_0'}{2}\right)^n \sum_{k=0}^{n} \frac{(-1)^k \left(\frac{1-\xi_0'}{1+\xi_0'}\right)^k}{\Gamma(k+1)\Gamma(1+n-k)} \cdot$$

$$\cdot \int_0^{\pi/2} \frac{\cos 2(k+n_2)\psi \; P_{n+2s}^n(\xi_0\cos\psi)}{(1-{\xi_0}^2\cos^2\psi)_2^n} d\psi. \quad (116)$$

Referring to the eq 94a, we find that

$$\frac{P_{n+2s}^n(\xi_0\cos\psi)}{(1-\xi_0^2\cos^2\psi)_2^n} = \frac{(-1)^s 2^n \Gamma(s+n+\frac{1}{2})}{\sqrt{\pi}\Gamma(s+1)} F(-s,\, s+n+\tfrac{1}{2},\, \tfrac{1}{2};\, \xi_0^2\cos^2\psi)$$

$$= (-1)^s 2^n \sum_{t=0}^{s} (-1)^t \xi_0^{2t} \frac{\Gamma(t+s+n+\frac{1}{2})\cos^{2t}\psi}{\Gamma(1+s-t)\Gamma(t+1(\Gamma t t\tfrac{1}{2})}. \quad (117)$$

Now

$$\int_0^{\pi/2} \frac{\cos 2(k+n_2)\psi \cos^{2t}\psi}{\Gamma(t+1)\Gamma(t+\frac{1}{2})} d\psi = \frac{\sqrt{\pi}}{2\Gamma(t+k+n_2+1)\Gamma(t-k-n_2+1)}. \quad (118)$$

Hence

$$\int_0^{\pi/2} \frac{\cos 2(k+n_2)\psi P_{n+2s}^n(\xi_0\cos\psi)}{(1-\xi_0^2\cos^2\psi)^{\frac{n}{2}}} d\psi$$

$$= (-1)^s 2^{n-1}\sqrt{\pi} \sum_{t=0}^{s} (-1)^t \xi_0^{2t} \frac{\Gamma(t+s+n_2+\frac{1}{2})}{\Gamma(1+s-t)\Gamma(t+k+n_2+1)\Gamma(t-k-n_2+1)}. \quad (119)$$

Using this in eq 116 gives

$$C_s^{n_1,n_2}=\frac{(-1)^s(1+\xi_0')^n}{2\pi^{3/2}A_1^2}\sum_{t=0}^{s}(-1)^t\xi_0^{2t}\frac{\Gamma(t+s+n+\frac{1}{2})}{\Gamma(1+s-t)}S_t, \qquad (120)$$

where

$$S_t\equiv\Gamma(n+1)\sum_{k=0}^{n}\frac{(-1)^k\left(\frac{1-\xi_0'}{1+\xi_0'}\right)^k}{\Gamma(k+1)\Gamma(k+t+n_2+1)\Gamma(1+t-n_2-k)\Gamma(1+n-k)}. \qquad (121)$$

In case $t\geqq-n_2$, that is, $t+n_2\geqq0$,

$$S_t=\frac{F\left(-n,n_2-t,t+n_2+1;-\left(\frac{1-\xi_0'}{1+\xi_0'}\right)\right)}{\Gamma(t-n_2+1)\Gamma(t+n_2+1)}$$

$$=\left(\frac{1+\xi_0'}{2}\right)^{n_2-t}\frac{F\left(n_2-t,t+n_2+n+1,t+n_2+1;\frac{1-\xi_0'}{2}\right)}{\Gamma(t-n_2+1)\Gamma(t+n_2+1)} \qquad (122a)$$

the last form being obtained by Euler's transformation of the first hypergeometric function. Since t is never negative in eq 120, it is evident that eq 122a is applicable whenever $n_2\geqq0$, and also for negative values of n_2 when the unequality $t>-n_2$ holds. In the remaining case, where $0\leqq t<-n_2$, we may write $n_2=-m$, where m is a positive integer, so that, $0\leqq t\leqq m$.
In this case

$$S_t=\Gamma(n+1)(-1)^{m-t}\left(\frac{1-\xi_0'}{1+\xi_0'}\right)^{m-t}\frac{F\left(-2t,m-t-n,m-t+1;-\left(\frac{1-\xi_0'}{1+\xi_0'}\right)\right)}{\Gamma(2t+1)\Gamma(1+n-m+t)\Gamma(m-t+1)}$$

$$=\Gamma(n+1)(-1)^m\left(\frac{1-\xi_0'}{1+\xi_0'}\right)^m\frac{(-1)^t\xi_0^{-2t}2^{2t}F\left(-2t,n+1,m-t+1;\frac{1-\xi_0'}{2}\right)}{\Gamma(2t+1)\Gamma(t+n-m+1)\Gamma(m-t+1)}. \qquad (122b)$$

This expression however is that which eq122a becomes when $t+n_2<0$, so that either eq 122a or 122b may be used, as they are both valid for positive and negative values of n_2. Using the latter, where m is replaced by $-n_2$ gives

$$(-1)^t\xi_0^{2t}S_t=$$

$$(-1)^{n_2}\left(\frac{1+\xi_0'}{1-\xi_0'}\right)^{n_2}\Gamma(n+1)\frac{2^{2t}F\left(-2t,n+1,1-n_2-t;\frac{1-\xi_0'}{2}\right)}{\Gamma(t+n+n_2+1)\Gamma(2t+1)\Gamma(1-n_2-t)}. \qquad (123)$$

Using this, eq 120 becomes

$$C_s^{n_1,n_2}=\frac{(-1)^{s+n_2}(1+\xi_0')^{n+n_2}\cdot(1-\xi_0')^{-n_2}}{2\pi^{3/2}A_1^2}\Gamma(n+1)$$
$$\sum_{t=0}^{s}\frac{2^{2t}\Gamma(t+s+n+\frac{1}{2})\,F\left(-2t,n+1,1-n_2-t;\ \frac{1-\xi_0'}{2}\right)}{\Gamma(1+s-t)\Gamma(t+n+n_2+1)\Gamma(2t+1)\Gamma(1-n_2-t)}$$
$$=\frac{(-1)^{s+n_2}(1+\xi_0')^{n+n_2}(1-\xi_0')^{-n_2}}{2\pi^{3/2}A_1^2}\sum_{t=0}^{s}\frac{2^{2t}\Gamma(t+s+n+\frac{1}{2})}{\Gamma(1+s-t)\Gamma(t+n+n_2+1)}$$
$$\sum_{k=0}^{2t}\frac{(-1)^k\left(\frac{1-\xi_0'}{2}\right)^k\Gamma(k+n+1)}{\Gamma(k+1)\Gamma(k-t-n_2+1)\Gamma(1+2t-k)}.$$

Interchanging the order of summation gives

$$C_s^{n_1,n_2}=\frac{(-1)^{s+n_2}(1+\xi_0')^{n+n_2}(1-\xi_0')^{-n_2}}{2\pi^{3/2}A^2{}_1}\sum_{k=0}^{2s}(-1)^k\left(\frac{1-\xi_0'}{2}\right)^k\frac{\Gamma(k+n+1)}{\Gamma(k+1)}G_k, \tag{124}$$

where

$$G_k\equiv\sum_{t=0}^{s}\frac{2^{2t}\Gamma(t+s+n+\frac{1}{2})}{\Gamma(2t+1-k)\Gamma(t+n+n_2+1)\Gamma(1+s-t)\Gamma(1+k-n_2-t)}. \tag{125}$$

In order to evaluate G_k (eq 125) as a single term, we define the function G (z) as follows:

$$\mathcal{G}(z)\equiv\sum_{k=-\infty}^{\infty}(-z)^kG_k$$
$$\equiv\sum_{k=-\infty}^{\infty}\sum_{t=0}^{s}\frac{(-z)^k2^{2t}\Gamma(t+s+n+\frac{1}{2})}{\Gamma(2t+1-k)\Gamma(t+n+n_2+1)\Gamma(1+s-t)\Gamma(1+k-n_2-t)}. \tag{126}$$

Since n and n_2 are integers, this function is a polynomial in positive and negative powers of z. It is therefore analytic at every finite point in the z-plane except at $z=0$. After inverting the order of summation, we may substitute $k=\mu+n_2+t$ and sum first over μ

$$\mathcal{G}(z)=\sum_{t=0}^{s}\frac{(-z)^{n_2+t}2^{2t}\Gamma(t+s+n+\frac{1}{2})}{\Gamma(t+n+n_2+1)\Gamma(1+s-t)\Gamma(t-n_2+1)}\cdot$$
$$\cdot\sum_{\mu=-\infty}^{\infty}\frac{(-z)^\mu\Gamma(t-n_2+1)}{\Gamma(t-n_2+1-\mu)\Gamma(\mu+1)} \tag{127}$$

or

$$\mathcal{G}(z)=\sum_{t=0}^{s}\frac{2^{2t}\Gamma(t+s+n+\frac{1}{2})(-z)^{n_2+t}(1-z)^{t-n_2}}{\Gamma(t+n+n_2+1)\Gamma(1+s-t)\Gamma(t-n_2+1)} \tag{128}$$

This series starts not below $t=n_2$. Let $\lambda=t-n_2$, then

$$\mathcal{G}(z)=(-2z)^{2n_2}\sum_{\lambda=0}^{\infty}\frac{[-4z(1-z)]^\lambda\Gamma(\lambda+s+n+n_2+\frac{1}{2})}{\Gamma(\lambda+1)\Gamma(\lambda+n+2n_2+1)\Gamma(1+s-n_2-\lambda)}. \tag{129}$$

The sum is of the form

$$\sum_{\lambda=0}^{\infty}\frac{[-4z(1-z)]^{\lambda}\Gamma(\lambda+\alpha)}{\Gamma(\lambda+1)\Gamma(\lambda+\alpha+\beta+\frac{1}{2}\Gamma(1-\beta-\lambda)}=\frac{\Gamma(\alpha)F(\alpha,\beta,\alpha+\beta+\frac{1}{2};4z(1-z))}{\Gamma(1-\beta)\Gamma\alpha+\beta+\frac{1}{2}}$$

with $\alpha=s+n+n_2+\frac{1}{2}$ and $\beta=n_2-s$.

By a special transformation due to Gauss

$$F(\alpha,\beta,\alpha+\beta+\tfrac{1}{2};4z(1-z))=F(2\alpha,2\beta,\alpha+\beta+\tfrac{1}{2};z)$$

and by use of the equation

$$\frac{\Gamma(\alpha)}{\Gamma(1-\beta)\Gamma(\alpha+\beta+\frac{1}{2})}F(2\alpha,2\beta,\alpha+\beta+\tfrac{1}{2};z)$$

$$=\frac{2\Gamma(\frac{1}{2}-\beta)}{2^{2\alpha+2\beta}\Gamma(\alpha+\frac{1}{2})}\sum_{\lambda=0}^{\infty}\frac{(-z)^{\lambda}\Gamma(\lambda+2\alpha)}{\Gamma(\lambda+1)\Gamma(\lambda+\alpha+\beta+\frac{1}{2})\Gamma(1-2\beta-\lambda)}. \quad (130)$$

We get

$$\mathcal{G}(z)=\sum_{k=-\infty}^{\infty}(-z)^kG_k$$

$$=\frac{(-z)^{2n_2}\Gamma(s-n_2+\frac{1}{2})}{2^{2s+2n_2}\Gamma(s+n+n_2+1)}\sum_{\lambda=0}^{\infty}\frac{(-z)^{\lambda}\Gamma(\lambda+2s+2n+2n_2+1)}{\Gamma(\lambda+1)\Gamma(\lambda+n+2n_2+1)\Gamma(1+2s-2n_2-\lambda)} \quad (131)$$

from which, by equating equal powers of (z), we get for G_k with $k=\lambda+2n_2$ the expression (eq 132) below. This brief method of deriving eq 132 from eq 125 was suggested to me by C. L. Critchfield, whose helpful criticism in other respects may be acknowledged here.

$$\Gamma(k+n+1)G_k=\frac{\Gamma(s-n_2+\frac{1}{2})\Gamma(k+2s+2n+1)}{2^{2s+2n_2}\Gamma(s+n+n_2+1)\Gamma(1+2s-k)\Gamma(k+1-2n_2)}. \quad (132)$$

Using this in eq 124 gives

$$C_s^{n_1,n_2}=\frac{(-1)^{s+n_2}\Gamma(s-n_2+\frac{1}{2})}{A_1^2\pi^{\frac{1}{2}}2^{n+2n_2+1}\Gamma(s+n+n_2+1)}\left(\frac{1+\xi_0'}{2}\right)^n\left(\frac{1-\xi_0'}{1+\xi_0'}\right)^{-n_2}\cdot$$

$$\cdot\sum_{k=0}^{2s}(-1)^k\left(\frac{1-\xi_0'}{2}\right)^k\frac{\Gamma(k+2s+2n+1)}{\Gamma(k+1)\Gamma(k+1-2n_2)\Gamma(1+2s+k)}.$$

Now

$$\sum_{k=0}^{2s}(-1)^k\left(\frac{1-\xi_0'}{2}\right)^k\frac{\Gamma(k+2s+2n+1)}{\Gamma(k+1)\Gamma(k+1-2n_2)\Gamma(1+2s-k)}=$$

$$=\frac{\Gamma(2s+2n+1)}{\Gamma(2s+1)\Gamma(1-2n_2)}F\left(-2s,2s+2n+1,1-2n_2;\frac{1-\xi_0'}{2}\right)$$

$$=\left(\frac{a_1}{A_1}\right)^{2s}\frac{\Gamma(2s+2n+1)}{\Gamma(2s+1)\Gamma(1-2n_2)}F\left(-2s,-2s-2n-2n_2,1-2n_2;-\frac{a_2}{a_1}\right) \quad (133)$$

by Euler's transformation, remembering that $1-\xi_0'=2a_2/A_1$ and $1+\xi_0'=2a_1/A_1$.

We thus obtain the following

$$\frac{2\pi A_1\Gamma(s+\frac{1}{2})}{2^n\Gamma(s+n+1)}\cdot C_s^{n_1,n_2}=\frac{(-1)^{n_2+s}}{A_1\pi^{3/2}}\cdot A_{2s}^{2n+2n_2,-2n_2}(a_1,a_2), \tag{134}$$

where the A-function is defined by

$$A_{2s}^{2n_1,2n_2}(a_1,a_2)\equiv$$

$$\equiv\frac{\Gamma(s+n_1+\frac{1}{2})\Gamma(s+n_2+\frac{1}{2})\Gamma(s+n_1+n_2+\frac{1}{2})\Gamma(s+\frac{1}{2})}{\Gamma(2s+1)\Gamma(2s+2n_1+1)\Gamma(2n_2+1)}$$

$$\cdot\left(\frac{a_1}{a_1+a_2}\right)^{n_1+2s}\cdot\left(\frac{a_2}{a_1+a_2}\right)^{n_2}\cdot F\left(-2s,-2s-2n_1,2n_2+1;-\frac{a_2}{a_1}\right) \tag{135}$$

On expressing this as a polynomial and summing it in the reverse order, we find, since s is an integer,

$$\mathrm{A}_{2s}^{2n_1,2n_2}(a_1,a_2)=\mathrm{A}_{2s}^{2n_2,2n_1}(a_2,a_1). \tag{136}$$

Also since n_2 is an integer, it is found that

$$\mathrm{A}_{2s}^{2n_1,-2n_2}(a_1,a_2)=\mathrm{A}_{2(s-n_1)}^{2n_1,2n_2}(a_1,a_2), \tag{137}$$

which vanishes if $s-n_2<0$.

If $n_2=n_1$ in this, it is found that

$$\mathrm{A}_{2s}^{2n_1,-2n_1}(a_1,a_2)=\mathrm{A}_{2s}^{-2n_1,2n_1}(a_1,a_2)=\frac{\pi\Gamma(s+\frac{1}{2})\Gamma(s-n_1+\frac{1}{2})}{2^{2n_1}\Gamma(s+1)\Gamma(s+n_1+1)}\cdot\mathrm{P}_{2s}^{2n_1}(\xi_0'), \tag{138}$$

which vanishes when $s<n_1$.

Recalling that $n=n_1-n_2\geq 0$ and $n_1\geq 0$, it is evident that eq 134 may be written

$$\frac{2\pi A_1\Gamma(s+\frac{1}{2})}{2^n\Gamma(s+n+1)}\mathrm{C}_s^{n_1,n_2}=\frac{(-1)^{n_2+s}}{A_1\pi^{\frac{1}{2}}}\mathrm{A}_{2s}^{2n_1,-2n_2}(a_1a_2). \tag{139}$$

In this equation $C_s^{n_1,n_2}$ is the value of $\int_0^{\xi_0}\xi_1 P_{n+2s}^n(\xi_1)\sigma(\xi_1)d\xi_1$, where the expression (eq 80) has been used for the density σ, so that with this value of the integral the formula (111) is the expansion of the function $U=\phi_{n_1,n_2}(x,r,a_1,a_2)/\sqrt{a_1a_2}$.

We have, therefore, obtained the following development when $n=n_1-n_2\geq 0$, which is valid for all positions of the two parallel circles, which converges to a finite value except in the case where the circles are equal in radii, and approach coincidence (in which case it becomes logarithmically infinite).

$$\frac{\phi_{n_1,n_2}(x,r,a_1,a_2)}{\sqrt{a_1,a_2}}$$

$$=\frac{(-1)^{n_2}}{\pi^{\frac{1}{2}}A_1}\sum_{s=0}^{\infty}(-1)^s(2s+n+\tfrac{1}{2})A_{2s}^{2n_1,-2n_2}(a_1,a_2)P_{n+2s}^n(\xi)R_{n+2s}^n(\eta). \tag{140}$$

When $n_2=n_1\geq 0$, this becomes by use of eq 138

$$\frac{\phi_{n_1,n_1}(x,r,a_1,a_2)}{\sqrt{a_1a_2}}=$$

$$\frac{(-1)^{n_1}}{2^{2n_1}\sqrt{\pi}A_1}\sum_{s=n_1}^{\infty}(-1^s)(2s+\tfrac{1}{2})\frac{\Gamma(s+\frac{1}{2})\Gamma(s-n_1+\frac{1}{2})}{\Gamma(s+1)\Gamma(s+n_1+1)}P_{2s}^{2n_1}(\xi_0^1)P_{2s}(\xi)R_{2s}(\eta). \quad (141)$$

From eq 137 it is seen that the expansion (eq≤140) begins with the term $s=n_2$ when $0\leq n_2\leq n_1$, but with $s=0$ when $n_1\geq 0$ and $n_2<0$.

It may be noted that if $n\equiv|n_1-n_2|$ and if we write $A_{2s}^{\pm 2n_1,\mp 2n_2}(a_1,a_2)$ in eq 140, the expansion is valid for all integral values of n_1 and n_2, with the understanding that the upper of the double signs is to be taken when $n_1-n_2>0$, the lower when $n_1-n_2<0$. The ambiguity disappears when $n_1-n_2=0$.

From the integral representation (eq 57a) of $\frac{\phi n_1 n_2}{\sqrt{a_1a_2}}$ it is evident that this function is unaltered if we interchange the arguments a_1 and a_2 and corresponding parameters n_1 and n_2 and multiply by $(-1)^{n_1-n_2}$. This fact is derivable from eq 140 by use of the relation eq 136, noting that A_1, A_2, ξ, and η are all unaffected by interchange of a_1 and a_2.

The integral representation shows also that

$$\frac{\phi_{n_1,n_2}(x,r,a_1,a_2)}{\sqrt{a_1a_2}}=\frac{(-1)^{n_2}\phi_{\bar{n}_1,\bar{n}_2}(x,a_1,r,a_2)}{\sqrt{ra_2}},$$

Where

$$\left.\begin{aligned}\bar{n}_1&=n_1-n_2\\ \bar{n}_2&=-n_2\\ \bar{n}&=|\bar{n}_1-\bar{n}_2|=|n_1|\end{aligned}\right\}. \quad (142)$$

This interchange of arguments r and a_1 in the light of eq 65 amounts to viewing x and a_1 as the cylindrical coordinates of a point, while r and a_2 are constants playing the part which a_1 and a_2 held in the preceding formulas.

Hence, as in eq 173, we let

$$\bar{A}_1=r+a_2,\ x=\bar{A}_1\bar{\xi}\bar{\eta},\ a_1=\bar{A}_1\sqrt{(1-\bar{\xi}^2)(1+\bar{\eta}^2)}, \quad (143)$$

so that $\bar{\xi}$ and $\bar{\eta}$ are computed from the second members of eq 82, after replacing A_1 by $r+a_2$ and r by a_1.

The function on the right of eq 142 is then given by a development obtainable from eq 140 by replacing A_1, a_1, ξ, η, n_1, n_2, and n by $\bar{A}_1$, r, $\bar{\xi}$, $\bar{\eta}$, n_1-n_2, $-n_2$, and $|n_1|$, respectively. This gives

$$\frac{\phi_{n_1,n_2}(x,r,a_1,a_2)}{\sqrt{a_1a_2}}=\frac{1}{\pi^{3/2}(r+a_2)}$$

$$\sum_{s=0}^{\infty}(-1)^s)2s+|n_1|+\tfrac{1}{2})A_{2s}^{\pm 2(n_1-n_2),\pm 2n_2}(r,a_2)P\cdot_{|n_1|+2s}^{|n_1|}(\bar{\xi})R_{|n_1|+2s}^{|n_1|}(\bar{\eta}), \quad (144)$$

the upper or lower sign being taken according as n_1 is positive or negative. Similarly, from interchange of r and a_2,

$$\frac{\phi_{n_1,n_2}(x,r,a_1,a_2)}{\sqrt{a_1a_2}}=\frac{\phi_{\bar{n}_1\bar{n}_2}(x,a_2,a_1,r)}{\sqrt{a_1r}},$$

where

$$\left.\begin{aligned}\bar{n}_1&=n_1\\ \bar{n}_2&=n_1-n_2\\ \bar{n}&=|\bar{n}_1-\bar{n}_2|=|n_2|\end{aligned}\right\}. \tag{145}$$

This gives a third expansion

$$\frac{\phi_{n_1,n_2}(x,r,a_1,a_2)}{\sqrt{a_1a_2}}=\frac{(-1)^{n_1-n_2}}{\pi^{3/2}(r+a_1)}$$

$$\sum_{s=0}^{\infty}-1^s\left(2s+|n_2|+\frac{1}{2}\right)A_{2s}(r,a_1)^{\pm 2(n_2-n_1),\pm 2n_1}\cdot P_{|n_2|+2s}^{|n_2|}(\bar{\bar{\xi}})\cdot R_{|n_2|+2s}^{|n_2|}(\bar{\bar{\eta}}), \tag{146}$$

where the upper or lower sign is taken according as n_2 is positive or negative

$$x=(r+a_1)\bar{\bar{\xi}}\bar{\bar{\eta}} \text{ and } a_2=(r+a_1)\cdot\sqrt{(1-\bar{\bar{\xi}}^2)(1+\bar{\bar{\eta}}^2)}, \tag{147}$$

so that $\bar{\bar{\xi}}$ and $\bar{\bar{\eta}}$ are computed from the second members of eq 82 after replacing A_1 by $r+a_1$ and r by a_2.

The following section is concerned with the partial integrals with respect to x derivable from the expansion (eq 140).

VII. EXPANSION OF ω_{n_1,n_2} IN SPHEROIDAL COORDINATES

The function $\omega_{n_1,n_2}(x,r,a_1,a_2)$, or more briefly, $\omega_{n_1,n_2}(xr)$ is represented in eq 59 by the integral

$$\omega_{n_1,n_2}(x,r)\equiv 4\pi^2\sqrt{a_1a_2}\int_0^x dx''\int_0^{x'}\phi_{n_1,n_2}(x',r)dx'. \tag{148}$$

We exclude for the present the exceptional case where n_1 and n_2 are both zero. In all other cases we may write

$$\omega_{n_1,n_2}(x,r)=V_{n_1,n_2}(x,r)-V_{n_1,n_2}(0,r)+2\pi|x|S_{n_1,n_2}(r) \tag{149}$$

$$\omega'_{n_1,n_2}(x,r)=V'_{n_1,n_2}(x,r)\pm 2\pi S_{n_1,n_2}(r), \tag{150}$$

the upper or lower sign being taken according as x is positive or negative. The function $V_{n_1,n_2}(x,r)$ is an even function of x defined by

$$V_{n_1,n_2}(x,r)\equiv 4\pi^2a_1a_2\int_0^{\infty}e^{-|x|t}J_{n_1-n_2}(rt)J_{n_1}(a_1t)J_{n_2}(a_2t)\frac{dt}{t^2}. \tag{151}$$

The function $V'_{n_1,n_2}(x_1r)$ is an odd function of x defined by

$$V'_{n_1,n_2}(x,r)\equiv\mp 4\pi^2a_1a_2\int_0^{\infty}e^{-|x|t}J_{n_1-n_2}(rt)J_{n_1}(a_1t)J_{n_2}(a_2t)\frac{dt}{t}, \tag{152}$$

the upper or lower sign being taken according as x is positive or negative. Also

$$2\pi S_{n_1,n_2}(r) = -V'_{n_1,n_2}(+0,r) = +V'_{n_1,n_2}(-0,r)$$
$$= 4\pi^2 a_1 a_2 \int_0^\infty J_{n_1-n_2}(rt) J_{n_1}(a_1 t) J_{n_2}(a_2 t) \frac{dt}{t}. \quad (153)$$

These relations are all obtained by introducing into eq 148 the integral representation (eq 57a) for $\phi_{n_1 n_2}$, which gives

$$\omega_{n_1,n_2}(x,r) = 4\pi^2 a_1 a_2 \int_0^\infty \left[\frac{e^{-|x|t} - 1 + |x|t}{t^2}\right] J_{n_1-n_2}(rt) J_{n_1}(a_1 t) J_{n_2}(a_2 t) dt. \quad (154)$$

If the exceptional case $n_1 = n_2 = 0$ be excluded, this may be separated into three integrals, each of which converges, thus giving the eq 149 to 153.

From 152 and 57a it is evident that

$$V'_{n_1,n_2}(x,r) = -4\pi^2 \sqrt{a_1 a_2} \int_x^\infty \phi_{n_1,n_2}(x',r) dx' \quad (155)$$

if $x > 0$,

and

$$V_{n_1,n_2}(x,r) = -\int_x^\infty V'_{n_1,n_2}(x^1,r) dx' \quad (156)$$

if $x > 0$. In both of these integrals, the integration must be performed, while r is held constant.

The functions V_{n_1,n_2} and V'_{n_1,n_2} each satisfy the partial differential eq 64. The function V'_{n_1,n_2} vanishes when the point $P(x,r)$ goes to infinity in any direction in the (x,r) plane, while V_{n_1,n_2} vanishes in general if $x \to \pm\infty$, while r has any fixed finite value.

To perform the integrations in eq 155 we write eq 103 in the two forms:

$$(2s+n+\tfrac{1}{2}) P^n_{n+2s}(\xi) R^n_{n+2s}(\eta) =$$
$$-\frac{A_1}{2} D_x [P^n_{n+2s-1}(\xi) \cdot R^n_{n+2s-1}(\eta) + P^n_{n+2s+1}(\xi) \cdot R^n_{n+2s+1}(\eta)] \quad (157)$$

$$(2s+n+\tfrac{3}{2}) P^n_{n+2s+1}(\xi) R^n_{n+2s+1}(\eta) =$$
$$-\frac{A_1}{2} D_x [P^n_{n+2s}(\xi) \cdot R^n_{n+2s}(\eta) + P^n_{n+2s+2}(\xi) \cdot R^n_{n+2s+2}(\eta)]. \quad (158)$$

The expansion for V'_{n_1,n_2} is obtained by using the expansion (eq 140) for ϕ_{n_1,n_2} in eq 155 and then performing the integration with respect to x by use of eq 157. Since r is held at a finite constant value in this integration, the value of the integrated terms at $x = \infty$ (r finite) are found by letting $\eta \to \infty$, while at the same time $\xi^2 \to 1$, the two

variables being connected, as shown in eq 81, in such a manner that limit

$$\begin{matrix}\eta\to\infty\\ \xi^2\to 1\end{matrix}\left[\eta(1-\xi^2)^{\frac{1}{2}}\right]=\frac{r}{A_1}.$$

It is thus found that for the case $n\equiv n_1-n_2>0$

$$V'_{n_1,n_2}(x,r,a_1,a_2)=$$

$$=(-1)^{n_2+1}2a_1a_2\sqrt{\pi}\left\{\frac{A_0^{2n_1,-2n_2}(a_1,a_2)}{n\sqrt{\pi}}\left(\frac{1-\xi^2}{1+\eta^2}\right)^{\frac{n}{2}}\xi F(1,n+\tfrac{1}{2},n+1;1-\xi^2)\right.$$

$$\left.+\sum_{s=0}^{\infty}(-1)^s[A_{2s}^{2n_1,-2n_2}(a_1,a_2)-A_{2s+2}^{2n_1,-2n_2}(a_1,a_2)]P^n_{n+2s+1}(\xi)R^n_{n+2s+1}(\eta)\right\} \quad (159)$$

and for the case $n_2=n_1>0 (n=0)$

$$V'_{n_1,n_1}(x,r,a_1,a_2)=(-1)^{n_2+1}2a_1a_2\sqrt{\pi}\sum_{s=n_1-1}^{\infty}(-1)^s[A_{2s}{}^{2n_1,-2n_1}(a_1,a_2)$$

$$-A_{2s+2}{}^{2n_1,-2n_1}(a_1,a_2)]P_{2s+1}(\xi)R_{2s+1}(\eta). \quad (160)$$

The first term inside the brace of eq 159 is

$$A_0{}^{2n_1,-2n_2}(a_1,a_2)[P^n_{n+2s-1}(\xi)R^n_{n+2s-1}(\eta)]_{s=0}$$

$$=\frac{A_0{}^{2n_1,-2n_2}(a_1,a_2)}{n\sqrt{\pi}}\left(\frac{1-\xi^2}{1+\eta^2}\right)^{\frac{n}{2}}\xi F(1,n+\tfrac{1}{2},n+1;1-\xi^2), \quad (161)$$

for from eq 95b we find

$$\left[\frac{P^n_{n+2s-1}(\xi)}{s}\right]_{s=0}=\frac{2^n}{n\sqrt{\pi}}\Gamma(n+\tfrac{1}{2})(1-\xi^2)^{\frac{n}{2}}\cdot\xi F(1,n+\tfrac{1}{2},n+1;1-\xi^2), \quad (162a)$$

and from the eq 99a we find

$$[sR^n_{n+2s-1}(\eta)]_{s=0}=\frac{(1+\eta^2)^{-\frac{n}{2}}}{2^n\Gamma(n+\frac{1}{2})}. \quad (162b)$$

Also from eq 95a we find

$$\left[\frac{1}{s}P^n_{n+2s-2}(\xi)\right]_{s=0}=-\frac{2^{n-1}\Gamma(n-\frac{1}{2})(1-\xi^2)^{\frac{n}{2}}}{n\sqrt{\pi}}\cdot F(1,n-\tfrac{1}{2},n+1;1-\xi^2),$$

and from eq 99a

$$[sR^n_{n+2s-2}(\eta)]_{s=0}=-\frac{\eta}{2^{n-1}\Gamma(n-\frac{1}{2})(1+\eta^2)^{\frac{n}{2}}}$$

Hence

$$[P^n_{n+2s-2}(\xi).R^n_{n+2s-2}(\eta)]_{s=0}=\frac{\eta}{n\sqrt{\pi}}\left(\frac{1-\xi^2}{1+\eta^2}\right)^{\frac{n}{2}}F(1,n-\tfrac{1}{2},n+1;1-\xi^2).$$

Inserting the expansion (eq 159) in (eq 156) and integrating by use of (eq 158) gives for the case $n>0$.

$$V_{n_1,n_2}(x,r,a_1,a_2)=$$

$$=(-1)^{n_2}a_1a_2A_1\sqrt{\pi}\left\{\frac{A_0^{2n_1,-2n_2}(a_1,a_2)}{n(n-\frac{1}{2})\sqrt{\pi}}\left(\frac{1-\xi^2}{1+\eta^2}\right)\eta F(1,n-\tfrac{1}{2},n+1;1-\xi^2)\right.$$

$$+\sum_{s=0}^{\infty}(-1)^s\left[\frac{A_{2s}^{2n_1,-2n_2}(a_1,a_2)-A_{2s+2}^{2n_1,-2n_2}(a_1,a_2)}{2s+n+\frac{3}{2}}-\right.$$

$$\left.\left.\frac{A_{2s-2}^{2n_1,-2n_2}(a_1a_2)-A_{2s}^{2n_1,-2n_2}(a_1a_2)}{2s+n-\frac{1}{2}}\right]P_{n+2s}^{n}(\xi)R_{n+2s}^{n}(\eta)\right\} \quad (163)$$

and for the case $n=0$, $n_2=n_1>0$

$$V_{n_1,n_1}(x,r,a_1,a_2)=$$

$$=(-1)^{n1}a_1a_2A_1\sqrt{\pi}\sum_{s=n_1-1}^{\infty}(-1)^s\left[\frac{A_{2s}^{2n_1,-2n_1}(a_1,a_2)-A_{2s+2}^{2n_1,-2n_2}(a_1,a_2)}{2s+\frac{3}{2}}-\right.$$

$$\left.\frac{A_{2s-2}^{2n_1,-2n_1}(a_1,a_2)-A_{2s}^{2n_1,-2n_1}(a_1,a_2)}{2s-\frac{1}{2}}\right]P_{2s}(\xi)R_{2s}(\eta). \quad (164)$$

The value of $V_{n_1,n_2}(0,r,a_1,a_2)$ for the range $0\leqq r\leqq A_1$ is found by placing $\eta=0$ and $\xi=\sqrt{1-\frac{r^2}{A_1^2}}$ in eq 163. For the range $r>A_1$ we place $\xi=0$ and $\eta=\sqrt{\frac{r_1^2}{A_1^2}-1}$. Similarly, from eq 159 the value of $2\pi S_{n_1n_2}(r)=-V'_{n_1n_2}(+0,r,a_1a_2)$ could be found, but such expansions are unnecessary, for we now find that $S_{n_1n_2}(r)$ may be obtained in finite form.

It should be noticed that the term $\xi F(1,n+1/2,n+1;1-\xi^2)$ in eq 159 is an odd function of ξ (and therefore of x), as are all the terms in $P_{n+2s+1}^{n}(\xi)$ in the series. The latter all vanish with ξ, but the former does not, as may be seen by the transformation

$$\xi F(1,n+\tfrac{1}{2},n+1;1-\xi^2)=\pm F(\tfrac{1}{2},n,n+1;\ 1-\xi^2)=\frac{\pm\sqrt{\pi}\Gamma(n+1)}{\Gamma(n+\frac{1}{2})}, \quad (165)$$

when $\xi\to\pm 0$.

Hence when $x\to+0$ and $r>A_1$, i. e., $\xi\to+0$ and $\sqrt{\frac{1}{1+\eta^2}}=\frac{A_1}{r}$, eq 159 gives for $r>A_1$

$$S_{n_1,n_2}(r)=-\frac{V'_{n_1n_2}(+0,r,a_1a_2)}{2\pi}=\frac{a_1a_2(-1)^{n_2}\Gamma(n)}{\sqrt{\pi}\Gamma(n+\frac{1}{2})}A_0^{2n_1,-2n_2}(a_1,a_2)\left(\frac{A_1}{r}\right)^n \quad (166)$$

if $n\neq 0$. Referring to eq 135, we find

$$\frac{A_0^{2n_1,-2n_2}(a_1,a_2)}{\sqrt{\pi}\Gamma(n+\frac{1}{2})}=\frac{\pi}{A_1^n}\left(\frac{a_1^{n_1}}{\Gamma(1+n_1)}\right)\left(\frac{a_2^{-n_2}}{\Gamma(1-n_2)}\right), \quad (167)$$

when $n_1>0$ and $n_2<n_1$.

Hence eq 166 becomes

$$S_{n_1,n_2}(r)=\pi a_1 a_2(-1)^{n_2}\frac{\Gamma(n)}{r^n}\left(\frac{a_1^{n_1}}{\Gamma(n_1+1)}\right)\left(\frac{a_2^{-n_2}}{\Gamma(1-n_2)}\right) \tag{168}$$

when $r\geq A_1=a_1+a_2$ and $n_1>0$, $n_2<n_1$. This vanishes if n_2 is a positive integer less than n_1.

This relation may be used to obtain the value of $S_{n_1n_2}(r)$ for the range $0\leq r<A_2$ by considering the effect of interchanging r with a_1 or a_2, which is determined by the integral definition (eq 153 of $S_{n_1n_2}(r)$, which is an abbreviation for $S_{n_1n_2}(r,a_1,a_2)$. It is thus found for the case $n_1>0$ and $n_2<n_1$ that when $0\leq r\leq A_2=|a_1-a_2|$

$$\left.\begin{aligned} S^{n_1,n_2}(r)&=\pi a_1 a_2\frac{r^n\Gamma(n_1)a_2^{n_2}}{\Gamma(n+1)a_1^{n_1}\Gamma(n_2+1)}, \text{ when } a_2<a_1\\ &=0 \qquad\qquad\qquad\qquad\qquad\quad \text{when } a_2>a_1\end{aligned}\right\} \tag{169}$$

Similarly, for the case $n_2=n_1>0$ it is found that

$$\left.\begin{aligned} S_{n_1,n_1}(r)&=0 \text{ when } A_1\leq r\leq\infty\\ &=\frac{\pi a_1 a_2}{n_1}\left(\frac{a_2}{a_1}\right)^{|n_1|} \text{ if } a_2<a_1\\ &=\frac{\pi a_1 a_2}{n_1}\left(\frac{a_1}{a_2}\right)^{|n_1|} \text{ if } a_2>a_1\end{aligned}\right\} \text{when } 0\leq r<A_2. \tag{170}$$

In all these statements the case $n_1=n_2=0$ is excluded. It is evident therefore that $S_{n_1,n_2}(r)$ vanishes when $r=\infty$ and also if $n_1\neq n_2$ when $r=0$. It may be shown from its definition (eq 153) that $S_{n_1,n_2}(r)$ is a continuous function of r, in particular at $r=A_1$ and $r=A_2$. To find its value for the range $A_2<r<A_1$, we find from eq 152 that when $x>0$

$$\left[\frac{1}{r}D_r(rD_r)-\frac{n^2}{r^2}\right]\frac{V'_{n_1,n_2}(x_1r)}{2\pi}=-D_x^2\frac{V'_{n_1,n_2}(x,r)}{2\pi}$$

$$=2\pi a_1 a_2\int_0^\infty te^{-xt}J_{n_1-n_2}(rt)J_{n_1}(a_1t)J_{n_2}(a_2t)dt.$$

Letting x approach zero in this, and noting that by eq 153 $V'_{n_1,n_2}(+0,r)=-2\pi S_{n_1,n_2}(r)$, and that the integral on the right approaches that which defines $2\pi\sigma(r)$ in eq 66, we find that $S_{n_1,n_2}(r)$ satisfies the ordinary nonhomogeneous differential equation

$$\frac{1}{r}D_r(rD_rS_{n_1,n_2})-\frac{n^2S_{n_1,n_2}}{r^2}=-4\pi^2a_1a_2\sigma(r)$$

$$=-2\frac{\cos\ (n_1\theta_1^0-n_2\theta_2^0)}{\sin\ (\theta_2^0-\theta_1^0)} \tag{171}$$

for the range $A_2<r<A_1$, this value of σ being taken from eq 72. If r lies outside this range $\sigma_{n_1n_2}=0$, the homogeneous equation having solution $C_1r^n+C_2r^{-n}$ if $n\pm0$ and $C_1+C_2\log r$ if $n=0$. The values just found are of this form. Hence if any particular integral of eq 171 is found for the range $A_2<r<A_1$, this increased by $C_1r^n+C_2r^{-n}$ is the

general solution for that range, and the values of the two constants of integration, C_1 and C_2, are then determined by the fact that this solution must be continuous at $r=A_2$ and at $r=A_1$ with the solutions previously found and given by eq 168 and 169. Similarly, in the case $n=0$.

To derive a particular integral of eq 171 in finite form for the case $n_1>0$ and $n_2<n_1$, so that $n=n_1-n_2>0$, we begin with the elementary integral form of the solution

$$S(r)=\frac{a_1a_2}{n}[r^{-n}I_1-r^nI_2], \tag{172}$$

where

$$I_1=\int r^n\cos\,(n_1\theta_1^0-n_2\theta_2^0)d2\psi$$

$$I_2=\int r^{-n}\cos\,(n_1\theta_1^0-n_2\theta_2^0)d2\psi.$$

Now by eq 77

$$r^n\cos\,(n_1\theta_1^0-n_2\theta_2^0)=\mathscr{R}\,a_1^ne^{-2in_2\psi}\left(1-\frac{a_2e^{-2i\psi}}{a_1}\right)^n$$

$$=a_1^n\Gamma(n+1)\sum_{k=0}^{n}\frac{(-1)^k\left(\frac{a_2}{a_1}\right)^k\cos\,2(k+n_2)\psi}{\Gamma(k+1)\,\Gamma(1+n-k)}$$

$$=(-1)^{n_2}\frac{a_1^{n_1}}{a_2^{n_2}}\Gamma(n+1)\sum_{k=n_1}^{n_1}\frac{(-1)^k\left(\frac{a_2}{a_1}\right)^k\cos\,2k\psi}{\Gamma(k-n_2+1)\Gamma(1+n_1-k)},$$

so that

$$r^{-n}I_1=(-1)^{n_2}\frac{\Gamma(n+1)}{r^n}a_1{}^{n_1}a_2{}^{-n_2}\left\{\frac{2\psi}{\Gamma(n_1+1)\Gamma(1-n_2)}+\right.$$

$$\left.\sum_{k=n_1}^{n_1}{}'\frac{(-1)^k\left(\frac{a_2}{a_1}\right)^k}{\Gamma(k-n_2+1)\Gamma(1+n_1-k)}\frac{\sin\,2k\psi}{k}\right\}, \tag{173}$$

where Σ' indicates that the term $k=0$ is omitted. To evaluate I_2 we derive from eq 77

$$r^{-n}\cos\,(n_1\theta_1^0-n_2\theta_2^0)=\mathscr{R}\frac{a_2{}^{n_2}}{a_1{}^{n_1}}\left(\frac{re^{i\theta_1^0}}{a_2}\right)^{-n}\cdot\left(1+\frac{re^{i\theta_2^0}}{a_2}\right)^{n1}$$

and

$$d2\psi=-i\left(1+\frac{re^{i\theta_2^0}}{a_2}\right)^{-1}d\left(\frac{re^{i\theta_2^0}}{a_2}\right),$$

so that

$$I_2=-\frac{ia_2{}^{n_2}}{a_1{}^{n_1}}\int\left(\frac{re^{i\theta_2^0}}{a_2}\right)\left[1+\frac{re^{i\theta_2^0}}{a_2}\right]^{n_1-1}d\left(\frac{re^{i\theta_2^0}}{a_2}\right),$$

where the real part is to be taken.

Since $n_1>0$, the expansion of the binomial $\left[1+\frac{re^{i\theta_2^0}}{a_2}\right]^{n_1-1}$ is a finite

polynomial in $re^{i\theta_2^0}a_2$. This gives

$$r^n I_2 = \frac{r^n \Gamma(n_1) a_2^{n_2}}{a_1^{n_1}} \left\{ \frac{\theta_2^0}{\Gamma(n)\Gamma(n_2+1)} + \sum_{k=-n_1}^{n-1} \frac{\left(\frac{a_2}{r}\right)^k}{\Gamma(k+n_2+1)\Gamma(n-k)} \frac{\sin k\theta_2^0}{k} \right\}, \quad (174)$$

Using eq 173 and 174 in eq 172 gives a particular integral $S(r)$ of eq 171 for the range $A_2<r<A_1$, when $n_1>0$ and $n_2<n_1$. Hence if $A_2 \leqq r<A_1$, $n_1>0$ and $n_2<n_1$, we find

$$S_{n_1 n_2}(r) = \\ = a_1 a_2 \left\{ \frac{(-1)^{n_2}\Gamma(n) a_1^{n_1} a_2^{-n_2}}{\Gamma^n} \left[\frac{2\psi}{\Gamma(n_1+1)\Gamma(1-n_2)} + \sum_{k=n_2}^{n_1} \frac{(-1)^k \left(\frac{a_2}{a_1}\right)^k}{\Gamma(k-n_2+1)\Gamma(1+n_1-k)} \frac{\sin 2k\psi}{k} \right] \right. \\ \left. + \frac{r^n \Gamma(n_1) a_2^{n_2}}{a_1^{n_1}} \left[\frac{\pi-\Theta_2^0}{\Gamma(n+1)\Gamma(n_2+1)} - \frac{1}{n} \sum_{k=-n_2}^{n-1} \frac{\left(\frac{a_2}{r}\right)^k}{\Gamma(k+n_2+1)\Gamma(n-k)} \frac{\sin k\theta_2^0}{k} \right] \right\}, \quad (175)$$

where the constants C_1 and C_2 have been so chosen as to make $S_{n_1 n_2}(r)$ continuous at $r=A_1$ and at $r=A_2$, its values at these points being given by eq 168 and 169 when $r=A_1$ or A_2, respectively.

The terms in the summation vanish at each of these values of r, for, when $r=A_1$, $\theta_1^0=0$, $\theta_2^0=\pi$, and $2\psi=\theta_2^0-\theta_1^0=\pi$, and when $r=A_2$, $2\psi=0$, and $\begin{cases} \theta_1^0=\theta_2^0=0 \text{ if } a_2<a_1 \\ \theta_1^0=\theta_2^0=\pi \text{ if } a_2>a_1 \end{cases}$.

This shows that the second member of eq 175 reduces to eq 168 when $r=A_1$ and to eq 169 when $r=A_2$. Therefore, eq 168, 169, and 175 give Sr_{n1n2} in finite terms for all values of r when $n_1>0$ and $n_2<n_1$.

In eq 175 $S_{n_1 n_2}(r)$ is $S_{n_1 n_2}(r, a_1 a_2)$. In order to find $S_{n_1 n_2}(r, a_2, a_1)$, we must not only interchange a_1 and a_2 where they occur explicitly in the second member of eq 172 but must also replace θ_2 by $\pi-\theta_1$, as shown by eq 78b.

The remaining irreducible cases are for $n_2=n_1>0$ and $n_2=n_1=0$. In the case $n_2=n_1>0(n=0)$, we start with the particular integral of eq 171

$$S(r)=4n^2a_1a_2\int r_1\sigma(r_1)\log\frac{r_1}{r}dr_1=2a_1a_2\int\cos 2n_1\psi'\log\frac{r_1}{r}d2\psi'$$

$$=a_1a_2\left\{\frac{2\sin 2n_1\psi}{n_1}\log\frac{1}{r}+2\int\cos 2n_1\psi'\log r_1 d2\psi'\right\}$$

$$=a_1a_2\left\{\frac{2\sin 2n_1\psi}{n_1}\log\frac{a_1}{r}-2\sum_{k=1}^{\infty}\frac{1}{k}\left(\frac{a_2}{a_1}\right)^k\int\cos\ 2n_1\psi'\ \cos\ 2k\psi' d2\psi'\right\}$$

$$=a_1a_2\left\{\frac{2\sin 2n_1\psi}{n_1}\log\frac{a_1}{r}\right.$$

$$\left.-\sum_{k=1}^{\infty}\frac{1}{k}\left(\frac{a_2}{a_1}\right)^k\left[\frac{\sin 2(k+n_1)\psi}{k+n_1}+\frac{\sin 2(k-n_1)\psi}{k-n_1}\right]\right\}.$$

This may be reduced to finite terms by use of the expansion

$$\frac{2\sin 2n_1\psi}{n_1}\log\frac{a_1}{r}=\sum_{k=1}^{\infty}\frac{1}{k}\left(\frac{a_2}{a_1}\right)^k\frac{2\sin 2n_1\psi\cos 2k\psi}{n_1}$$

$$=\sum_{k=1}^{\infty}\frac{1}{k}\left(\frac{a_2}{a_1}\right)^k\left[\frac{\sin 2(k+n_1)\psi}{n_1}-\frac{\sin 2(k-n_1)\psi}{n_1}\right],\quad(176)$$

so that

$$S(r)=\frac{a_1a_2}{n_1}\sum_{k=1}^{\infty}\left(\frac{a_2}{a_1}\right)^k\left[\frac{\sin 2(k+n_1)\psi}{k+n_1}-\frac{\sin 2(k-n_1)\psi}{k-n_1}\right]$$

$$=\frac{a_1a_2}{n_1}\left\{-2\psi\left(\frac{a_2}{a_1}\right)^{n_1}-\left[\left(\frac{a_2}{a_1}\right)^{n_1}-\left(\frac{a_1}{a_2}\right)^{n_1}\right]\sum_{k=1}^{\infty}\left(\frac{a_2}{a_1}\right)^k\frac{\sin 2k\psi}{k}\right.$$

$$\left.-\sum_{k=1}^{n_1}\left[\left(\frac{a_2}{a_1}\right)^{k-n_1}+\left(\frac{a_1}{a_2}\right)^{k-n_1}\right]\frac{\sin 2k\psi}{k}+\frac{\sin 2n_1\psi}{n_1}\right\}.$$

Now

$$e^{i\theta_1^0}=\left(\frac{1-\frac{a_2}{a_1}e^{-2i\psi}}{1-\frac{a_2}{a_1}e^{2i\psi}}\right)^{\frac{1}{2}},$$

so that taking the logarithm of both sides we obtain

$$\theta_1^0=\sum_{k=1}^{\infty}\left(\frac{a_2}{a_1}\right)^k\frac{\sin 2k\psi}{k}.\quad(177)$$

The particular integral then becomes for the case $n_2=n_1>0$.

$$S(r)=\frac{a_1a_2}{n_1}$$

$$\left\{\left(\frac{a_1}{a_2}\right)^{n_1}\theta_1^0-\left(\frac{a_2}{a_1}\right)^{n_1}\theta_2^0+\frac{\sin 2n_1\psi}{n_1}-\sum_{k=1}^{n_1}\left[\left(\frac{a_2}{a_1}\right)^{k-n_1}+\left(\frac{a_1}{a_2}\right)^{k-n_1}\right]\frac{\sin 2k\psi}{k}\right\},$$

which contains only a finite number of terms and is valid whichever of the two circles is the larger.

With this particular integral we find, after determining the two constants of integration by making $S_{n_1 n_2}(r)$ continuous at $r=A_2$ and at $r=A_1$ with the values given in eq 170,

$$\left.\begin{aligned} S_{n_1 n_2}(r) &= \frac{\pi a_1 a_2}{n_1}\left(\frac{a_2}{a_1}\right)^{n_1} \text{ if } a_2<a_1 \\ &= \frac{\pi a_1 a_2}{n_1}\left(\frac{a_1}{a_2}\right)^{n_1} \text{ if } a_1<a_2 \end{aligned}\right\} \text{when } 0\leqq r\leqq A_2,$$

$$= \frac{a_1 a_2}{n_1}\left\{\left(\frac{a_1}{a_2}\right)^{n_1}\theta_1^0 + \left(\frac{a_2}{a_1}\right)^{n_1}(\pi-\theta_2^0) + \frac{\sin 2n_1\psi}{n_1} - \sum_{k=1}^{n_1}\left[\left(\frac{a_2}{a_1}\right)^{k-n_1}+\left(\frac{a_1}{a_2}\right)^{k-n_1}\right]\frac{\sin 2k\psi}{k}\right\}$$

$$\text{when } A_2\leqq r\leqq A_1$$

$$=0 \qquad \text{when } A_1\leqq r\leqq\infty, \tag{178}$$

provided that $n_1>0$.

In the particular case of greatest importance, $n_1=1$,

$$S_{11}(r)=\left\{\begin{matrix}\pi a_2^2 \text{ if } a_2<a_1 \\ \pi a_1^2 \text{ if } a_1<a_2\end{matrix}\right\} \qquad \text{when } 0\leqq r\leqq A_2$$

$$= a_1^2\theta_1^0 + a_2^2(\pi-\theta_2^0) - a_1 a_2 \sin 2\psi \quad \text{when } A_2\leqq r\leqq A_1$$

$$=0 \qquad \text{when } A_1\leqq r\leqq\infty. \tag{179}$$

This shows that $S_{11}(r)$ is the area common to the two coplanar circles of radii a_1 and a_2, when r is the distance between their axes.

By the preceding formulas every $\omega_{n_1 n_2}$ is evaluated with the exception of the case $n_1=n_2=0$. Before considering it, attention may be called to the interesting fact that although every V_{n_1,n_2} vanishes when $x\to\pm\infty$ holding r finite, there are two cases of eq 163 namely, $V_{1,0}(x,r,a_1,a_2)$ and $V_{0,-1}(x,r,a_1,a_2)$ which do not vanish when the point $P(x,r)$ goes to infinity in directions other than the x-direction.

By use of eq 163 and 167 it is found that when $x^2+r^2\to\infty$ in the direction ϕ defined by $\cos\phi=\dfrac{x}{\sqrt{x^2+r^2}}$ then

$$\left.\begin{aligned} V_{1,0}(x,r,a_1,a_2) &\to 2\pi^2 a_1^2 a_2\left|\tan\frac{\phi}{2}\right| \\ V_{0,-1}(x,r,a_1,a_2) &\to -2\pi^2 a_1 a_2^2\left|\tan\frac{\phi}{2}\right| \end{aligned}\right\}. \tag{180}$$

In the exceptional case where $n_2=n_1=0$, the integrals involving Bessel's functions, which served to define the functions V_{n_1,n_2} and V'_{n_1,n_2} in eq 151 and 152, are not convergent. Neither are the definitions of these functions by the integrals, eq 155 and 156. Nevertheless, functions

$$V_{00}(x,r),\ V'_{00}(x,r)\equiv D_x V_{00}(x,r), \text{ and } S_{00}(r)$$

may be defined in this case, so that eq 149 and 150 are applicable. To find these functions we begin with

$$\omega_{00}(x,r)=\int_0^x \omega'_{00}(x',r)dx'=4\pi^2 a_1 a_2\int_0^x dx''\int_0^{x''}\frac{\phi_{00}(x',r)}{\sqrt{a_1a_2}}\,dx' \tag{181}$$

$$\omega'_{00}(x,r)=D_x\omega_{00}(x,r)=4\pi^2 a_1 a_2\int_0^x\frac{\phi_{00}(x',r)}{\sqrt{a_1a_2}}\,dx'. \tag{182}$$

Applying the operator $r^{-1}D_r(rD_r)$ to the latter gives

$$\begin{aligned}\frac{1}{r}D_r(rD_r\omega'_{00})&=4\pi^2a_1a_2\int_0^x\frac{1}{r}D_r\left(\frac{rD_r\phi_{00}(x',r)}{\sqrt{a_1a_2}}\right)dx'\\&=-4\pi^2a_1a_2\int_0^x D_{x'}^2\left(\frac{\phi_{00}(x',r)}{\sqrt{a_1a_2}}\right)dx'\\&=-4\pi^2a_1a_2D_x\left(\frac{\phi_{00}(x,r)}{\sqrt{a_1a_2}}\right)+4\pi^2a_1a_2\left[D_x\left(\frac{\phi_{00}(x,r)}{\sqrt{a_1a_2}}\right)\right]_{x\to0}.\end{aligned}$$

Also applying the operator D_x^2 to eq 182 gives

$$D_x^2\omega'_{00}=4\pi^2a_1a_2D_x\frac{\phi_{00}(x,r)}{\sqrt{a_1a_2}},$$

so that

$$\nabla^2\omega'_{00}(x,r)=\left[D_x^2+\frac{1}{r}D_r(rD_r)\right]\omega'_{00}(x,r)=4\pi^2a_1a_2\left[D_x\frac{\phi_{00}(x,r)}{\sqrt{a_1a_2}}\right]_{x\to0}.$$

That is, by eq 66

$$\nabla^2\omega'_{00}(x,r)=\mp4\pi^2a_1a_2.2\pi\sigma_{00}(r) \tag{183}$$

the upper sign if $x>0$ the lower if $x<0$. This shows that $\omega'_{00}(x,r)$ is of the form as in eq 150

$$\omega'_{00}(x,r)=V'_{00}(x,r)\pm2\pi S_{00}(r), \tag{184}$$

where $V'_{00}(x,r)$ is an odd function of x satisfying

$$\nabla^2V'_{00}(x,r)=0, \tag{185}$$

and $S_{00}(r)$ is a solution of

$$\nabla^2S_{00}(r)=\frac{1}{r}D_r(rD_rS_{00}(r))=-4\pi^2{}_{a1}a_2\sigma_{00}(r)=\frac{-2}{\sin 2\psi}, \tag{186}$$

as in eq 171.

Since ω'_{00} and ω_{00} both vanish with x,

$$S_{00}(r)=-\frac{V'_{00}(+0,r)}{2\pi}=+\frac{V'_{00}(-0,r)}{2\pi}, \tag{187}$$

as in eq 153.
Also by eq 184

$$\omega_{00}(x,r)=\int_0^x\omega'_{00}(x',r)dx'=V_{00}(x,r)-V_{00}(0,r)+2\pi|x|S_{00}(r), \tag{188}$$

as in eq 149.

If in the integral (eq 182) we introduce for $\phi_{00}(x',r)/\sqrt{a_1a_2}$ its expansion (eq 140), where $A^{0,0}_{2s}=\frac{\pi\Gamma^2(s+\frac{1}{2})}{\Gamma^2(s+1)}P_{2s}(\xi_0')$ by eq 138, this gives

$$\omega'_{00}(x,r)=\frac{4a_1a_2\sqrt{\pi}}{A_1}$$
$$\left\{\frac{\pi^2}{2}\int_0^x P_0(\xi)R_0(\eta)dx+\sum_{s=1}^{\infty}(-1)^s(2s+\tfrac{1}{2})A^{0,0}_{2s}(a_1,a_2)\int_0^x P_{2s}(\xi)R_{2s}(\eta)dx\right\} \quad (189)$$

where

$$P_0(\xi)R_0(\eta)=R_0(\eta)=\frac{2}{\sqrt{\pi}}\cot^{-1}\eta. \quad (190)$$

The terms in the series of eq 189, for which $s>0$, may be integrated by the use of formula 157, but the present case is again exceptional for eq 157 now fails entirely, for the term $s=0$ becomes infinite instead of merely becoming indeterminate of the form 0/0, as in the case of P^n_s where $n=0$.

This breakdown of the formula may be repaired by writing

$$P_0(\xi)R_0(\eta)=\frac{1}{2\pi i}\int_{\mu=0}P_\mu(\xi)R_\mu(\eta)\frac{d\mu}{\mu}, \quad (191)$$

where the integral is a contour integral taken around a small closed curve in the complex μ-plane, encircling the point $\mu=0$. Since μ does not vanish at any point on this curve, the integrand may be written by eq 103

$$P_\mu(\xi)R_\mu(\eta)=-\frac{A_1}{2\mu+1}D_x[P_{\mu-1}(\xi)R_{\mu-1}(\eta)+P_{\mu+1}(\xi)R_{\mu+1}(\eta)],$$

which gives by Cauchy's theorem

$$P_0(\xi)R_0(\eta)=\frac{2}{\sqrt{\pi}}\cot^{-1}\eta=-A_1D_x\left\{D_\mu\left[\frac{\mu P_{\mu-1}(\xi)R_{\mu-1}(\eta)}{2\mu+1}\right]_{\mu=0}+P_1(\xi)R_1(\eta)\right\}. \quad (192)$$

It is found that

$$\frac{\sqrt{\pi}}{2}D_\mu\left[\frac{\mu P_{\mu-1}(\xi)R_{\mu-1}(\eta)}{2\mu+1}\right]=-\log\frac{(1+\xi)\sqrt{1+\eta^2}}{2}. \quad (193)$$

If we define the function $v(x,r)$ by

$$\left.\begin{aligned}v(x,r)&\equiv-\frac{2}{\sqrt{\pi}}\log\left[(1+\xi)\cdot\sqrt{1+\eta^2}\right]\text{ when }x>0\\&\equiv+\frac{2}{\sqrt{\pi}}\log\left[(1-\xi)\sqrt{1+\eta^2}\right]\text{ when }x<0\end{aligned}\right\}, \quad (194)$$

then $v(x,r)$ is an odd function of x, which is an axially symmetrical solution of Laplace's equation, and eq 192 becomes

$$P_0(\xi)R_0(\eta)=\frac{2}{\sqrt{\pi}}\cot^1\eta=-A_1D_x\{v(x,r)+P_1(\xi)R_1(\eta)\}. \quad (195)$$

A further integration may be made by the same method. This gives

$$v(x,r)=D_x\left\{xv(x,r)+\frac{2A_1}{\sqrt{\pi}}(\eta+\cot^{-1}\eta)\right\}. \quad (196)$$

The function within the parentheses of eq 196 is an even function of x, satisfying Laplace's equation. Integrating eq 189 by use of eq 157 and 195 leads to the following definition of V'_{00}

$$V'_{00}(x,r) = -2a_1a_2\sqrt{\pi} \left\{\pi^2 v(x,r) + \sum_{s=0}^{\infty}(-1)^s[A^{00}_{2s}(a_1a_2) - A^{00}_{2s+2}(a_1a_2)]P_{2s+1}(\xi)R_{2s+1}(\eta)\right\}. \quad (197)$$

Integrating this from $x=0$ to $x=x$ by eq 158 and 196 leads to

$$V_{00}(x,r) = -a_1a_2\sqrt{\pi}\left\{2\pi^2\left[xv(x,r) + \frac{2A_1}{\sqrt{\pi}}\eta\right] + A_1\sum_{s=0}^{\infty}(-1)^s \left[\frac{A^{00}_{2s-2}(a_1,a_2) - A^{00}_{2s}(a_1,a_2)}{2s-\frac{1}{2}} - \frac{A^{00}_{2s}(a_1,a_2) - A^{00}_{2s+2}(a_1,a_2)}{2s+\frac{3}{2}}\right]P_{2s}(\xi)R_{2s}(\eta)\right\}. \quad (198)$$

From eq 197, 194, and 187 we find

$$S_{00}(r) = -2\pi a_1a_2 \log\left(\frac{r}{A_1}\right) \text{when } r > A_1. \quad (199)$$

When $0<r<A_1$, $S_{00}(r)$ is found from eq 187 and 197 by placing $\eta=0$ and $\xi=\xi_r=\sqrt{1-\frac{r^2}{A_1^2}}$

$$S_{00}(r) = -\frac{a_1a_2}{2}\left\{4\pi \log(1+\xi_r) + \frac{2}{\sqrt{\pi}}\sum_{s=0}^{\infty}(-1)^s\frac{\Gamma(s+1)}{\Gamma(s+\frac{3}{2})}[A^{00}_{2s+2}(a_1,a_2) - A^{00}_{2s}(a_1,a_2)]P_{2s+1}(\xi_r)\right\} \quad (200)$$

for the range $0<r<A_1$. In the part of this range $0<r<A_2$ where $\sigma_{00}=0$, this development must represent

$$S_{00}(r) = C_0 + C_1 \log r, \quad (201)$$

as shown by eq 186.

If the development eq 200 converges when $r=0(\xi_r=1)$, the constant C_1 must be zero.

Now by eq 200, when $r=0$, $\xi_r=1$ and $P_{2s+1}(1)=1$. Also reference to eq 138 shows that

$$A^{00}_{2s} = \frac{\pi\Gamma^2(s+\frac{1}{2})}{\Gamma^2(s+1)}P_{2s}(\xi'_0).$$

Hence from eq 200 we find

$$S_{00}(0) = -2\pi a_1a_2\{\log 2 - F(\xi'_0)\},$$

where

$$F(\xi'_0) \equiv 1 + \frac{1}{\sqrt{\pi}}\sum_{s=1}^{\infty}(-1)^s\frac{\Gamma(s+\frac{1}{2})}{\Gamma(s+1)}\left[\frac{1}{2s} + \frac{1}{2s+1}\right]P_{2s}(\xi'_0).$$

Since this series converges, the constant C_1 in eq 201 is zero. It is readily found that $F(\xi'_0)$ is the development

$$F(\xi'_0) = -\log\left[\frac{1+|\xi'_0|}{4}\right] = -\log\frac{A_1+A_2}{4A_1},$$

so that

$$S_{00}(0)=-2\pi a_1 a_2 \log \frac{A_1+A_2}{2A_1}, \text{ where } \frac{A_1+A_2}{2}=a_1 \text{ if } a_2<a_1$$
$$=a_2 \text{ if } a_2>a_1.$$

Hence eq 201 becomes

$$\left.\begin{aligned} S_{00}(r)&=-2\pi a_1 a_2 \log\left(\frac{a_1}{a_1+a_2}\right) \text{ if } a_2<a_1 \\ &=-2\pi a_1 a_2 \log\left(\frac{a_2}{a_1+a_2}\right) \text{ if } a_2>a_1 \end{aligned}\right\} \text{when } 0\leq r\leq A_2. \quad (202a)$$

Also for the range $A_2<r<A_1$, we have

$$\left.\begin{aligned} S_{00}(r)&=2a_1a_2\left\{2\psi \log\frac{a_1}{r}+\pi \log\left(\frac{a_1+a_2}{a_1}\right)-\sum_{k=1}^{\infty}\left(\frac{a_2}{a_1}\right)^k \frac{\sin 2k\psi}{k^2}\right\} \text{ if } a_2<a_1 \\ &=2a_1a_2\left\{2\psi \log\frac{a_2}{r}+\pi \log\left(\frac{a_1+a_2}{a_2}\right)-\sum_{k=1}^{\infty}\left(\frac{a_1}{a_2}\right)^k \frac{\sin 2k\psi}{k^2}\right\} \text{ if } a_2>a_1 \end{aligned}\right. \quad (202b)$$

Finally, for the remaining range of r,

$$S_{00}(r)=-2\pi a_1 a_2 \log\left(\frac{r}{a_1+a_2}\right) \text{ when } A_1<r<\infty. \quad (202c)$$

This completes the expansions required. Before summarizing the results, we should consider a small correction which takes account of the diameter of the wires.

VIII. CORRECTIONS FOR THE DIAMETER OF THE WIRES

If a helix is made with ordinary wire, a plane section of the wire by a plane through the x-axis may be considered circular. Let ρ_1 and ρ_2 be the wire radii, and let a_1 and a_2 represent the cylindrical radii of the central helical filament of the actual helices. Since ρ_1 and ρ_2 cannot be larger than πp_1 or πp_2 the correction terms for finite thickness of the wire will be second-order infinitesimals.

Assume that the current density at any point in the wire is in the direction of the generating helical filament passing through that point, its magnitude being a function of the distance r, of the point from the axis of the cylinder on which the wire is wound. Let γ_1 (or γ_2) be the value, at the central filament, of the r-derivative of the current density.

It may then be shown that the correction for the thickness of the wires may be made by using for the cylindrical radii a_1, a_2 in the principal term not a_1, a_2 of the central filaments of the wires, but $\bar{a}_1$, $\bar{a}_2$ of their equivalent helices, where

$$\bar{a}_1=a_1+\frac{\rho_1^2}{8}\left(\frac{1}{a_1}+2\gamma_1\right) \text{ and } \bar{a}_2=a_2+\frac{\rho_2^2}{8}\left(\frac{1}{a_2}+2\gamma_2\right). \quad (203)$$

If the current is uniform, $\gamma_1=\gamma_2=0$. If it is the "natural" distribution in both wires (inversely proportional to r) then $\gamma_1=-1/a_1$ and

$\gamma_2 = -1/a_2$, so that the correction is equal in magnitude but opposite in sign to that of the uniform distribution.

The derivation of eq 203 is almost verbatim, the same as that given in the paper on coaxial helices (footnote 2). It depends essentially on the fact that ϕ_{11} satisfies the partial differential equation 65.

IX. SUMMARY

The mutual inductance, M, between two parallel helices is expressed in eq 27 in terms of a function $\omega\ (x,\theta_1,\theta_2)$ involving four sets of terminal x-differences defined in eq 22 and 22′, where θ_1 and θ_2 are the associated terminal azimuths, as given in eq 29. In eq 33 and 58 ω is resolved into four others, $\omega_{11}+p_1p_2\omega_{00}/a_1a_2+\omega_1+\omega_2$, the first two, $\omega_{11}+p_1p_2\omega_{00}/a_1a_2$, corresponding to the mutual inductance of the two associated current sheets, the principal term ω_{11} representing the effect of angular components of current, the relatively small term, $p_1p_2\omega_{00}/a_1a_2$, of second order representing their axial currents. The terms ω_1 and ω_2 depend upon x and the terminal azimuths. These are expanded, eq 61 and 62, in Fourier's series of the terminal azimuths, the coefficients involving functions ω'_{n_1,n_2} and $\phi_{n_1n_2}$. It is shown that two terms of the series for the first-order quantity ω_1 are sufficient in general, the second-order term ω_2 being given by retaining terms in the single and double series corresponding to $n_1=1$, 2 and $n_2=1$, 2.

In eq 140, 144, and 146 three different types of expansions for any function $\phi_{n_1n_2}$ in oblate spheroidal harmonics are given. In section VII the first and second partial integrals of these expansions are evaluated, giving the functions $\omega'_{n_1n_2}$ and ω_{n_1,n_2} in spheroidal harmonics. The results are found in eq 149 to 202. Finally, in eq 203, is given the effect of diameter of the wires.

WASHINGTON, August 8, 1940.

U. S. DEPARTMENT OF COMMERCE NATIONAL BUREAU OF STANDARDS

RESEARCH PAPER RP1347

Part of Journal of Research of the National Bureau of Standards, Volume 25, December 1940

EFFECT OF LOW TEMPERATURES ON THE PROPERTIES OF AIRCRAFT METALS

By Samuel J. Rosenberg

ABSTRACT

The effect of subzero temperatures down to −78° C was determined upon the tensile properties, hardness, and impact resistance of metals commonly used in aircraft construction. The materials were divided into three general groups: (1) Ferritic steels, (2) austenitic stainless steels and nickel alloys, and (3) light metal alloys (Al- and Mg-base).

None of these properties of any of the materials tested was adversely affected by low temperatures with the exception of the impact resistance of the ferritic steels. A decrease in impact resistance as the test temperature was lowered was characteristic of these steels.

CONTENTS

	Page
I. Introduction	673
II. Previous investigations	674
III. Apparatus and methods of test	675
1. Methods of securing test temperatures	675
2. Tensile tests	675
3. Hardness tests	678
4. Impact tests	679
IV. Materials tested	680
1. Ferritic steels	680
2. Austenitic stainless steels and nickel alloys	680
3. Light metal alloys	681
V. Results of tests	682
1. Ferritic steels	682
(a) Tensile tests	682
(b) Hardness tests	682
(c) Impact tests	682
2. Austenitic stainless steels and nickel alloys	689
(a) Tensile tests	689
(b) Hardness tests	690
(c) Impact tests	690
3. Light metal alloys	691
(a) Tensile tests	691
(b) Hardness tests	696
(c) Impact tests	696
VI. Summary and conclusions	698
VII. References	701

I. INTRODUCTION

The temperature of the atmosphere in which aircraft operate frequently is considerably lower than the temperatures on the earth's surface and may reach a minimum of −60° C at high altitudes. It is known that such subzero temperatures may have marked effects upon certain mechanical properties of metals. Although the general relationship of mechanical properties and low temperatures is familiar

to many metallurgists and engineers, test data on specific commercial materials are usually a welcome addition to technical literature.

This paper contains the results of tests to determine the effect of low temperatures upon specific alloys used or considered for use in aircraft. The tests were made at the National Bureau of Standards, under the sponsorship and direction of the Bureau of Aeronautics, U. S. Navy Department.

II. PREVIOUS INVESTIGATIONS

Various investigators are in agreement that yield and tensile strengths, endurance limit, and hardness of metals increase as the temperature of test decreases. Ductility, as evidenced by elongation and reduction of area, usually varies but slightly down to about −80° C. At extremely low temperatures, however (liquid air or liquid hydrogen), elongation and reduction of area are markedly decreased.

The property most deleteriously affected by low temperatures is impact resistance. In most nonaustenitic steels the resistance to impact decreases more or less rapidly as the temperature drops from about +20° to −80° C (with the ordinary type of impact test specimen and velocity of blow). The major decrease, from maximum to minimum values, frequently occurs within narrow temperature limits termed the "transition range" to cold brittleness. Below −80° C the impact values decline at a much slower rate.

The deleterious effect of notches becomes considerably more pronounced at low temperatures. The impact resistance of notched bars drops with decreasing test temperatures. Decreased sharpness of notch causes the transition range to appear at lower temperatures and in unnotched bars the impact resistance may not be materially affected until considerably lower temperatures are reached.

So many factors influence the impact resistance of metals that, in order to secure some idea of the relative value and proper interpretation of impact test data, it is practically imperative that an understanding of the general theoretical facts underlying impact testing be had. McAdam and Clyne [1] [1] review the theory of impact testing and explain the influence of velocity of blow, form, and size of specimen, size of notch, and other variables on cold brittleness. According to these authors, test factors contributing to an increased tendency to cold brittleness are increased velocity of deformation, increased size of specimen, and increased depth and sharpness of notch.

Russell [2], in a paper summarizing the literature, gave a list of the changes in properties caused by low temperatures as follows:

Yield point	Increase.
Tensile strength	Do.
Elongation	Probably small decrease.
Reduction of area	Decrease.
Impact resistance	Do.
Hardness	Increase.
Endurance limit	Do.
Modulus of elasticity	Do.
Compressibility	Decrease.
Thermal expansion	Do.
Specific heat	Do.
Thermal conductivity	Increase.
Electrical conductivity	Do.

[1] Figures in brackets refer to the literature references at the end of this paper.

In discussion of Russell's paper, Strauss maintained that not all of these generalizations were warranted.

The selected references at the end of this paper contain material which is either of general interest to the subject of impact testing at low temperatures or else gives data on the low-temperature properties of metals similar to some included in the present work.

III. APPARATUS AND METHODS OF TEST

Since the minimum temperature to which aircraft may be subjected in service is approximately −60° C (−76° F), the sublimation point of carbon dioxide (−78.5° C) (−109° F) was chosen as the lowest temperature of test. Tensile, hardness, and impact tests were made at the following temperatures:

Tensile tests—room temperature and −78° C
Hardness tests—room temperature, 0°, −40°, and −78° C
Impact tests—+100° C (certain steels only), room temperature, 0°, −20°, −40°, and −78° C.

Tests were also made at room temperature after previous exposure of specimens at −78° C to determine whether any change in mechanical properties occurred after temporary exposure to this temperature. It may be noted here that testing at room temperature after prolonged exposure at −78° C had no effect upon the tensile, hardness, or impact properties of any of the metals tested, with but one or two exceptions, which will be noted in the proper place.

1. METHODS OF SECURING TEST TEMPERATURES

The temperature of +100° C was obtained by the use of boiling water. The temperature of 0° C was readily obtained by the use of melting crushed ice. An excess of solid carbon dioxide in a mixture of equal parts of carbon tetrachloride and chloroform was used for temperature maintenance at −78° C. Since carbon dioxide passes directly to a gas from the solid state, no dilution or other change occurred in the liquid bath and carbon dioxide could be added as needed. Temperatures between 0° and −78° C were easily maintained by regulated additions of carbon dioxide. The mixture utilized for the bath had the added advantage of being nonflammable.

The temperature of the cooling bath at −20° and −40° C was measured with a copper-constantan thermocouple. No measurements, except during calibration, were made at the other temperatures.

2. TENSILE TESTS

In view of the fact that a study of the literature revealed that the tensile properties of metallic materials are not adversely affected at temperatures down to −80° C, and since these tests are very time-consuming, it was decided to make tensile tests at room temperature and −78° C only. The only adverse effect of low temperature on tensile properties which might be expected would be exhibited in the ductility and it was felt that this property could be better evaluated by means of the impact tests.

All tensile tests were made in duplicate in an Amsler hydraulic testing machine of 50,000-lb capacity. The type of specimen used for the tensile tests of all materials except the wrought aluminum

alloys is shown in figure 1. Because of the deleterious effect of notches the diameter of the tensile specimen at the gage marks was made appreciably greater than the diameter of the gage length itself. This design was effective in preventing breaks through the gage marks. Strain readings taken on such a specimen, however, were slightly lower than the true strain readings over the full gage length

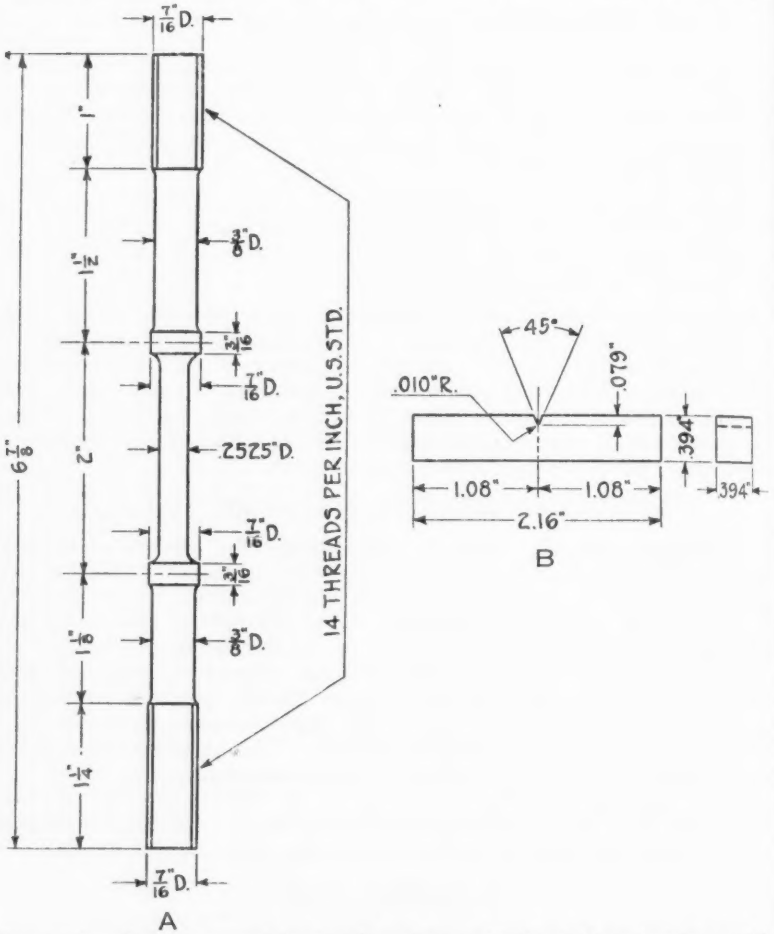

FIGURE 1.—*Specimens used for tensile and impact tests of all materials except the wrought aluminum alloys.*

A, tensile specimen; *B*, impact specimen.

of uniform diameter and the resultant stress-strain curve gave a modulus of elasticity which was higher than the actual value. A correction (−6.5 percent) calculated from the shape of the specimen, was applied to all determinations of modulus of elasticity.

Since the wrought aluminum alloys were supplied in plates ½ in. thick, it was necessary to use a different type of tensile specimen (fig. 2) for these alloys. As before, the cross-sectional area at the gage marks was somewhat greater than the area of the reduced sec-

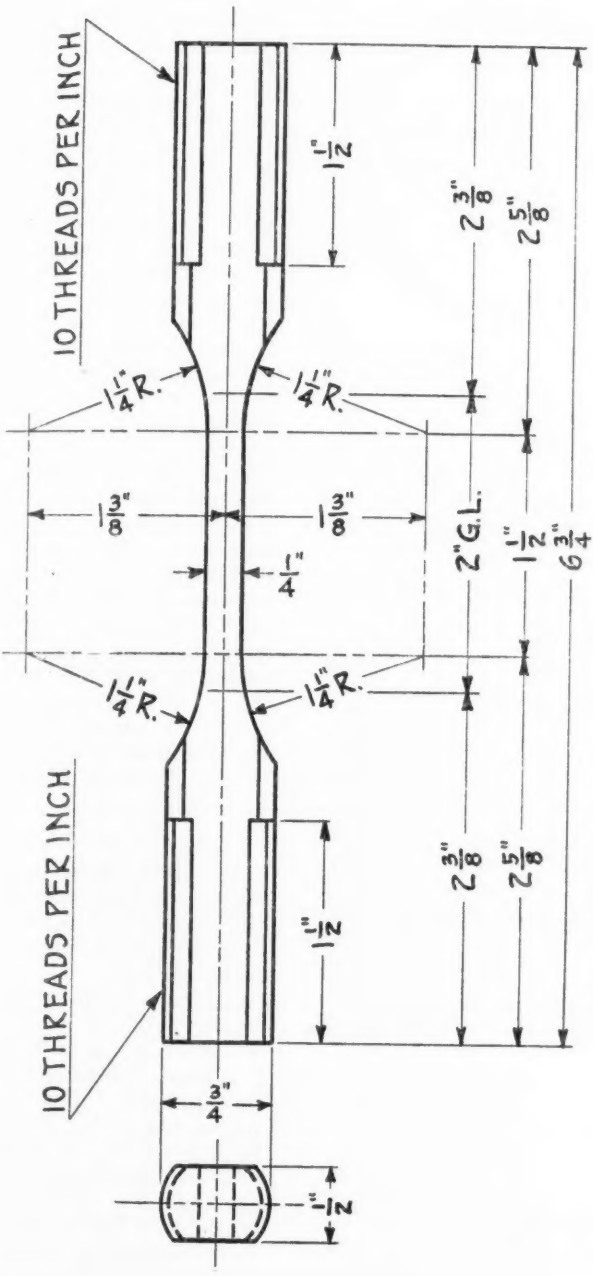

FIGURE 2.—*Specimen used for tensile tests of the wrought aluminum alloys.*

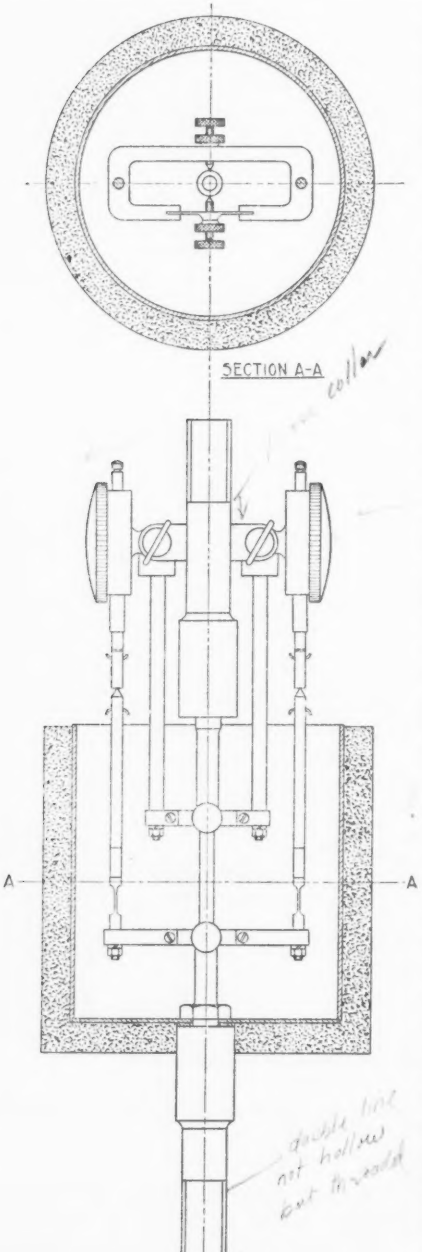

FIGURE 3.—*Extensometer and cooling-bath assembly used in the tensile tests.*

tion and a correction (−2.4 percent) was applied to all calculations of modulus of elasticity. Tensile tests of all wrought aluminum alloys were made on specimens taken both longitudinally and transversely to the direction of rolling.

It was necessary to design and construct a special extensometer (fig. 3) to obtain strain measurements at the low temperature. The strain gages were Ames dials reading directly to 0.001 in. and strain measurements were estimated to the nearest 0.0001 in. In making tensile tests at −78° C an insulated container (fig. 3) was screwed on the bottom of the specimen directly above the lower adapter. This container was then filled with cracked carbon dioxide and the 50–50 mixture of carbon tetrachloride and chloroform. Specimens were held at temperature for about 20 or 30 min before testing. Preliminary surveys of this set-up showed a temperature variation in the gage length of the specimen of about ±1° at −78°C.

3. HARDNESS TESTS

Hardness tests were made with a Rockwell machine, using the appropriate scale, and five determinations were made on each specimen. An insulated container, made integral with an anvil which fitted into the elevating screw of the machine, was used to hold the refrigerating mixture. The anvil projected about 1½ in. above the bottom of the container. An adapter, fitted into the head of the machine, carried the penetrator well below the surface of the refrigerating mixture. Thus the test specimen, anvil, and penetrator were all immersed

in the cooling bath during the test. Specimens were held at temperature for about 20 or 30 min before testing.

4. IMPACT TESTS

The type of test specimen used for impact tests of all materials except the wrought aluminum alloys is shown in figure 1. A modified specimen (fig. 4) was used for the latter in order to get some measure of the differences in impact resistance caused by the cold-worked skin. With the wrought aluminum alloys, impact tests were made on specimens taken both longitudinally and transversely with respect to the direction of rolling. Impact tests on the SAE steels were made

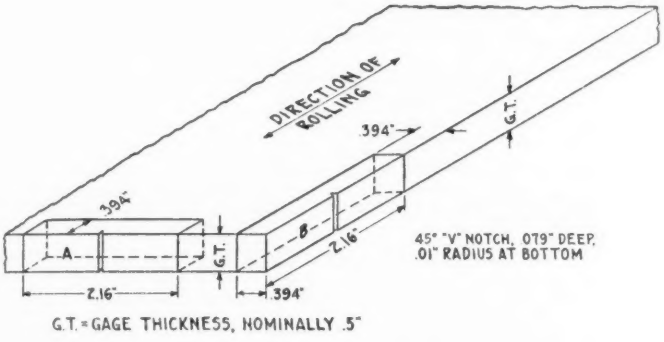

FIGURE 4.—*Location of Charpy impact specimens in wrought aluminum alloy plate. A*, transverse specimen; *B*, longitudinal specimen.

in duplicate at all temperatures except +100° C, at which temperature four specimens were tested; impact tests on all other materials were made in quadruplicate. The light metal alloys, with the exception of alloys 3S and 52S, were tested in a Charpy machine of 30 ft-lb capacity; all other materials were tested in a machine of 224 ft-lb capacity. The constants of these two Charpy machines were as follows:

Capacity	224.1 ft-lb	30 ft-lb.
Weight of hammer	50. 8 lb	8.436 lb.
Height of drop of hammer	4.411 ft	3.556 ft.
Distance from center of axis of rotation to center of gravity of striking mass	2.277 ft	1.583 ft.
Distance from center of axis of rotation to center of percussion	2.478 ft	1.833 ft.
Velocity of hammer at time of impact	16.85 ft/sec	15.14 ft/sec.
Distance between supports	1.6 in	1.6 in.

The specimens were placed in an insulated container holding the cooling bath, held at temperature for at least 30 min., and then quickly transferred to the impact machine and broken. The average time required to transfer the specimens from the cooling bath to the machine and then to trip the hammer was about 2 sec. Calibration of dummy specimens showed no appreciable changes in temperature during this interval.

IV. MATERIALS TESTED

The materials tested may be divided into three general groups, as follows: (1) Ferritic steels; (2) austenitic stainless steels and nickel alloys; and (3) light metal alloys (Al- and Mg-base).

1. FERRITIC STEELS

The term "ferritic steels" is used in this report to designate all steels which contain alpha iron at room temperature, regardless of the method of cooling. The steels used in this study which fall into this classification are various SAE steels, a Cr-Ni-Mo steel and a hardenable stainless steel of the 16-Cr–2-Ni type.

TABLE 1.—*Chemical compositions and heat treatments of the ferritic steels*

[Analyses of the SAE steels were made at the National Bureau of Standards. Compositions of the Cr-Ni-Mo and the high-Cr–low-Ni steels are mill analyses. The high-Cr–low-Ni steel was furnished by the Rustless Iron and Steel Corporation. All other steels were furnished by the Bethlehem Steel Corporation, through the courtesy of P. E. McKinney.]

SAE Number	Composition									Heat treatment
	C	Mn	P	S	Si	Ni	Cr	Mo	V	
	%	%	%	%	%	%	%	%	%	
1045	0.45	0.77	0.013	0.022	0.21					Normalized—1 hr at 1,600° F, air-cooled. Heat treated—¾ hr at 1,475° F, water quenched; 1 hr at 1,000° F, air-cooled. Cold drawn.
1095	.93	.27	.014	.023	.15					Normalized—1 hr at 1,475 °F, air-cooled. Heat treated (low draw)—½ hr at 1,425° F, oil quenched; 1 hr at 600° F, air-cooled. Heat treated (high draw)[1]—1 hr at 1,425° F, oil quenched; 1 hr at 1,075° F, air-cooled.
2330	.34	.72	.018	.017	.26	3.30				Normalized—1 hr at 1,700° F, air-cooled. Heat treated—½ hr at 1,475 °F, oil quenched; 1 hr at 1,000 °F, air-cooled.
X4130	.29	.50	.015	.013	.16		0.98	0.21		Normalized—1 hr at 1,600 °F, air-cooled. Heat treated (low draw)—¾ hr at 1,575 °F, oil quenched; 1 hr at 600° F, air-cooled. Heat treated (high draw)[1]—½ hr at 1,575° F, oil quenched; 1 hr at 1,075° F, air-cooled.
6130	.29	.69	.017	.022	.01		.96		0.17	Normalized—1 hr at 1,700° F, air-cooled. Heat treated—½ hr at 1,625° F, oil quenched; 1 hr at 1,175° F, air-cooled.
Cr-Ni-Mo	.47	.80	.014	.025	.29	1.80	1.04	.22		Annealed—4 hr at 1,450° F, furnace cooled 1 hr, then cooled to 1,100° F at the rate of approximately 150° F per hr and then cooled to 850° F at the rate of approximately 250° F per hr. Heat treated—annealing treatment as above, then ¾ hr at 1,520° F, oil quenched; 1 hr at 1,100° F, air-cooled.
High-Cr–low-Ni	.11	.44	.014	.024	.26	1.72	16.27			Heat treated—1,800° F, oil quenched; 850° F, air-cooled.

[1] Impact tests only were made on these materials.

All steels were received in the form of ⅝-in. diameter rods. Heat treatments were carried out on the ⅝-in. rods, the test specimens being subsequently machined therefrom. The SAE steels, with the single exception of one cold-drawn steel, were received in the hot-rolled condition. The Cr-Ni-Mo steel and the high-Cr–low-Ni steel were received as heat treated. Details of composition and heat treatment are given in table 1.

2. AUSTENITIC STAINLESS STEELS AND NICKEL ALLOYS

All these materials were received in the form of ⅝-in. diameter rods. Details of compositions and heat treatments are given in table 2.

TABLE 2.—*Chemical compositions and treatments of the austenitic stainless steels and nickel alloys*

Material	Composition													Treatment
	C	Mn	P	S	Si	Ni	Cr	Ti	Cb	Mo	Al	Fe	Cu	
	%	%	%	%	%	%	%	%	%	%	%	%	%	
18-8	0.07	0.44	0.012	0.018	0.50	8.63	18.22							Annealed—1 hr at 1,900° F, water quenched. Hot-rolled. Cold drawn.
18-8, stabilized with Ti.	.05	.39	.010	.015	.62	9.15	19.04	0.29						Annealed—1 hr. at 1,900° F, water quenched. Hot-rolled. Cold drawn.
18-8, stabilized with Cb.	.07	.42	.027	.028	.32	10.29	18.97		0.95					Annealed—1 hr. at 1,900° F, water quenched. Hot-rolled. Cold drawn.
18-8, stabilized with Mo.	.07	.93	.026	.012	.42	8.93	18.58			3.36				Annealed (exact treatment unknown).
	.07	.73	.017	.019	.48	7.88	18.41			2.80				Cold drawn.
K Monel	.23	.25			.27	diff.					3.1	1.7	29.9	Cold drawn and then tempered to grade C (300 BHN).
Monel metal	.18	1.0			.06	diff.					0.10	1.7	29.2	Cold drawn.
Nickel	.14	0.24			.03	diff.					nd [1]	0.10	0.03	Do.
Inconel	.06	.53				diff.	13.4					7.4		Hot-rolled, then annealed 2 hr at 1,750° F and quenched in alcohol. Cold drawn, then normalized at 525° F and air-cooled.

[1] nd = not detected.

3. LIGHT METAL ALLOYS

The light metal alloys were furnished in the following forms: (1) Cast aluminum alloys, bars 12 in. long, ¾ in. diameter; (2) cast magnesium alloys, bars 8 in. long, ⅝ in. diameter; (3) wrought aluminum alloys, plates 30 in. (in the direction of rolling), 12 in. wide, ½ in. thick; and (4) extruded magnesium alloys, bars about 15 ft long, ½ in. square. Details of composition and treatments are given in table 3.

TABLE 3.—*Chemical compositions and treatments of the light metal alloys*

[All analyses were made at the National Bureau of Standards except those of alloys 195–T4, 220–T4, 355–T4, 356–T4, which were furnished by the Aluminum Company of America. Referring to the wrought aluminum alloys, items finishing in the as-rolled or heat-treated condition were hotrolled directly to the finished gage. Items finishing in the RT temper were hot rolled to 5½ percent above the finished thickness, heat treated, and cold rolled to the final gage. All treatments applied to both the aluminum- and magnesium-base alloys were performed by the manufacturer]

Material	Composition									Treatment
	Si	Fe	Cu	Mn	Zn	Mg	Al	Sn	Cr	
	%	%	%	%	%	%	%	%	%	
3S	0.14	0.45	0.12	1.04			diff.			As rolled.
17ST	.46	.43	3.72	0.59		0.62	diff.			1 hr at 935° to 945° F, water quenched.
17SRT	.46	.29	3.90	.63		.63	diff.			
24ST	.14	.16	4.32	.48		1.44	diff.			1 hr at 916° to 924° F, water quenched.
24SRT										
25ST	.70	.50	4.26	.82		0.03	diff.			2 hr at 960° to 970° F, water quenched; aged 18 hr at 290° F.
25SRT	.73	.48	4.41	.80		.02	diff.			
27ST	.81	.36	3.99	.79		.01	diff.	0.04		1½ hr at 960° to 970° F, water quenched; aged 18 hr at 320° F.
52S	.12	.14	0.05			2.35	diff.		0.27	As rolled.
195–T4	.84	.53	4.35				diff.			As cast, 16 hr at 960° F, quenched in water at 200° to 212° F.
220–T4	.07	.13	0.03			10.49	diff.			As cast, 16 hr at 810° F, quenched in oil at 250° F.
355–T4	4.76	.26	1.25			0.49	diff.			As cast, 16 hr at 980° F, quenched in water at 200° to 212° F.

TABLE 3.—*Chemical compositions and treatments of the light metal alloys*—Con.

Material	Composition									Treatment
	Si	Fe	Cu	Mn	Zn	Mg	Al	Sn	Cr	
	%	%	%	%	%	%	%	%	%	
356-T4	6.71	.26	0.08	....	....	.25	diff.	....	....	As cast, 16 hr at 1,000° F, quenched in water at 200° to 212° F.
Dowmetal M	....	.01	....	1.6	[1]nd	diff.	0.02	....	....	16 hr at 750° F, followed at once, without quenching, by extrusion at 750° F and then air-cooled.
Dowmetal J	....	.06	....	0.22	1.0	diff.	5.8	....	....	Do.
Experimental Dowmetal.	....	.01	....	1.5	4.0	diff.	0.02	....	....	16 hr at 700° F, followed at once, without quenching, by extrusion at 750° F and then air-cooled.
Dowmetal G	....	.02	....	0.24	[1]nd	diff.	10.5	....	....	As sand cast. As sand cast, then 16 hr at 770° F and air-cooled. As sand cast, then 16 hr at 770° F, air-cooled, and aged 16 hr at 350° F.
Dowmetal H	....	.02	....	.28	2.7	diff.	6.3	....	....	As sand cast. As sand cast, then 4 hr at 630° F plus 16 hr at 720° F and air-cooled. As sand cast, then 4 hr at 630° F plus 16 hr at 715° F, quenched in hot water, and aged 16 hr at 350° F.

[1] nd=not detected.

Since the cold work given to heat-treated aluminum alloys is essentially a skin effect, it would not be expected that material ½-in. thick would be representative of fully worked aluminum alloys. It was felt, however, that the trend in mechanical properties caused by cold working would be indicated by the tests.

V. RESULTS OF TESTS

1. FERRITIC STEELS

(a) TENSILE TESTS

The tensile tests (figs. 5 and 6) on the ferritic steels showed the following changes in properties at −78° C as compared to room temperature: (1) The tensile strengths increased between 10,000 and 20,000 lb/in.^{2}; (2) the yield strengths increased between 7,000 and 22,000 lb/in.^{2}, with the greater increases occurring in the heat-treated steels; (3) the modulus of elasticity was unaffected, except for the normalized SAE 2330 steel, where loss resulted; and (4) the elongation values usually exhibited a slight increase, while reductions of area were sometimes lower, thus indicating no significant changes in ductility. The modulus of elasticity of the normalized SAE 2330 steel was also decreased at room temperature after previous exposure at −78° C. With this one exception, the results of these tests indicated quite definitely that the temperature of −78° C had no deleterious effect upon the tensile properties of any of the ferritic steels studied.

(b) HARDNESS TESTS

As a general rule, the hardness of the ferritic steels tended to increase slightly as the test temperature decreased to −78° C (fig. 7).

(c) IMPACT TESTS

The results of the impact tests on the ferritic steels are given in figure 8. An examination of this figure reveals that all steels which had an appreciable resistance to impact at room temperature lost a great portion of this impact resistance at −78° C.

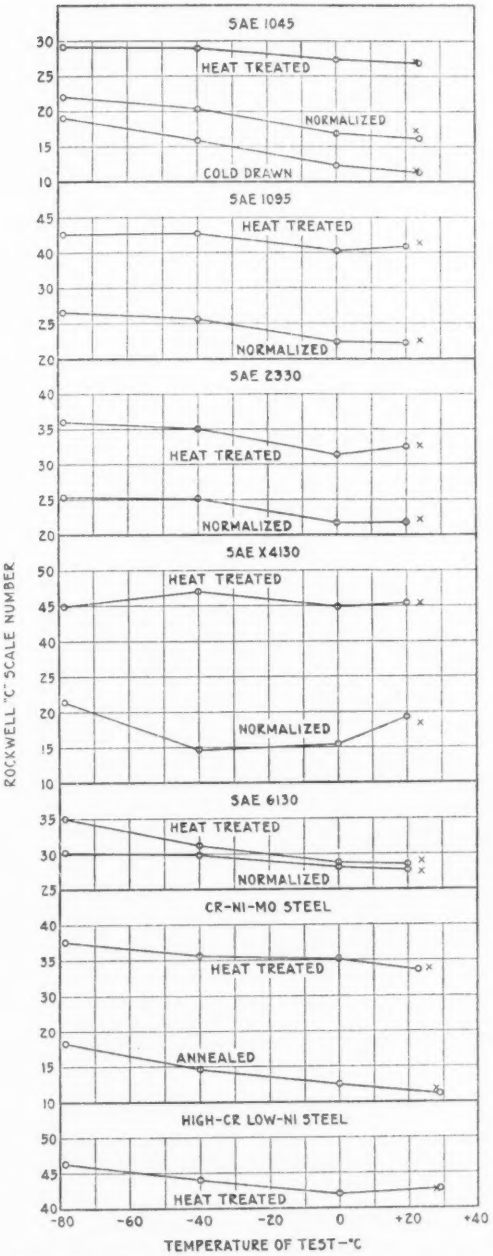

FIGURE 5.—*Effect of test temperature upon the yield strength, ultimate tensile strength, and modulus of elasticity of the ferritic steels.*

Decreasing temperatures had but little effect upon the impact resistance of the steels which were relatively brittle at room temperature. At +100° C, however, the impact resistance of some of these steels was considerably increased. These steels, then, are those which undergo the transition from tough to brittle material at some tem-

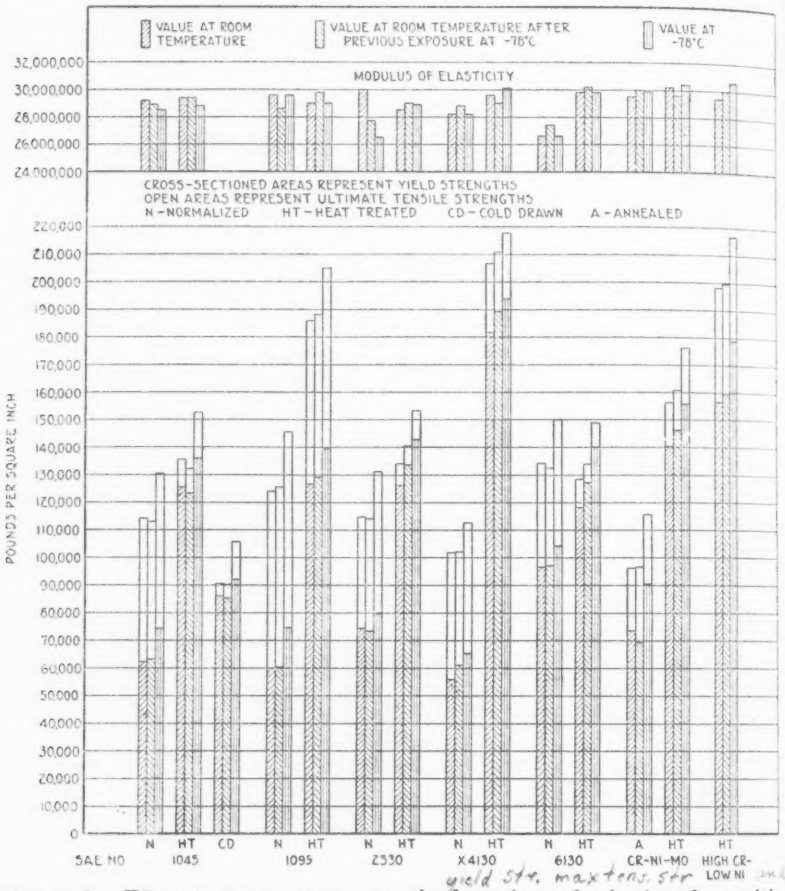

FIGURE 6.—*Effect of test temperature upon the ~~elongation and reduction of area~~ yield str. max tens. str and of the ferritic steels.*

perature above room temperature and are, therefore, most unsuited for use at low temperature. The steels in which the transition range occurred above room temperature under the test conditions described in this report are as follows:

SAE 1045 as cold drawn and as normalized.
SAE 1095 as normalized and as heat treated (both high and low draw).
SAE 2330 as normalized.
SAE X4130 as normalized and as heat treated (low draw).
SAE 6130 as normalized.
High-Cr-low-Ni steel as heat treated.

Decreasing temperatures had a marked deleterious effect, however, upon those steels which had a relatively high resistance to impact at room temperature. It is worthy of note that at +100° C the impact resistance of these steels was no better than at room temperature; in fact in the case of the heat-treated SAE 6130 steel it was decidedly less. In these steels the temperature at which considerable resistance to impact is developed is room temperature or even lower; the transition range is thus moved to lower temperatures and therefore these

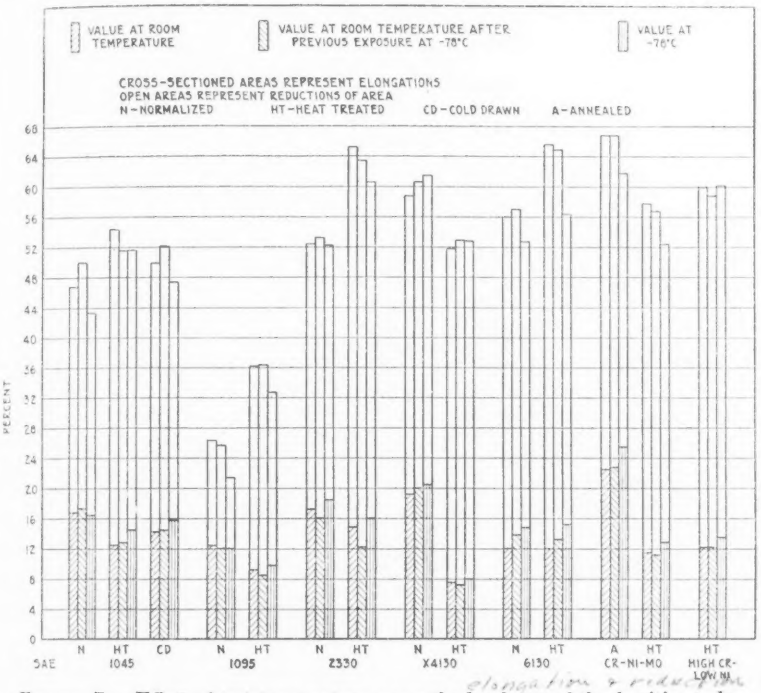

FIGURE 7.—*Effect of test temperature upon the hardness of the ferritic steels.*

The points indicated by the symbol "X" represent specimens which had been cooled to and held at −78° C for several hours prior to testing at room temperature.

steels are more suitable for use at sub-zero temperatures. These steels were as follows:

SAE 1045 as heat treated.
SAE 2330 as heat treated.
SAE X4130 as heat treated (high draw).
SAE 6130 as heat treated.
Cr-Ni-Mo steel as annealed and as heat treated.

It may be noted that the normalized SAE steels tested did not have a very great measure of resistance to impact at room temperature and even less at −78°C. When they were properly heat treated, however, the impact resistance was considerably improved. It is well known that maximum impact resistance is developed in steels which have been completely sorbitized. The effect of a high and low tempering treatment upon the impact resistance may be observed in the case of

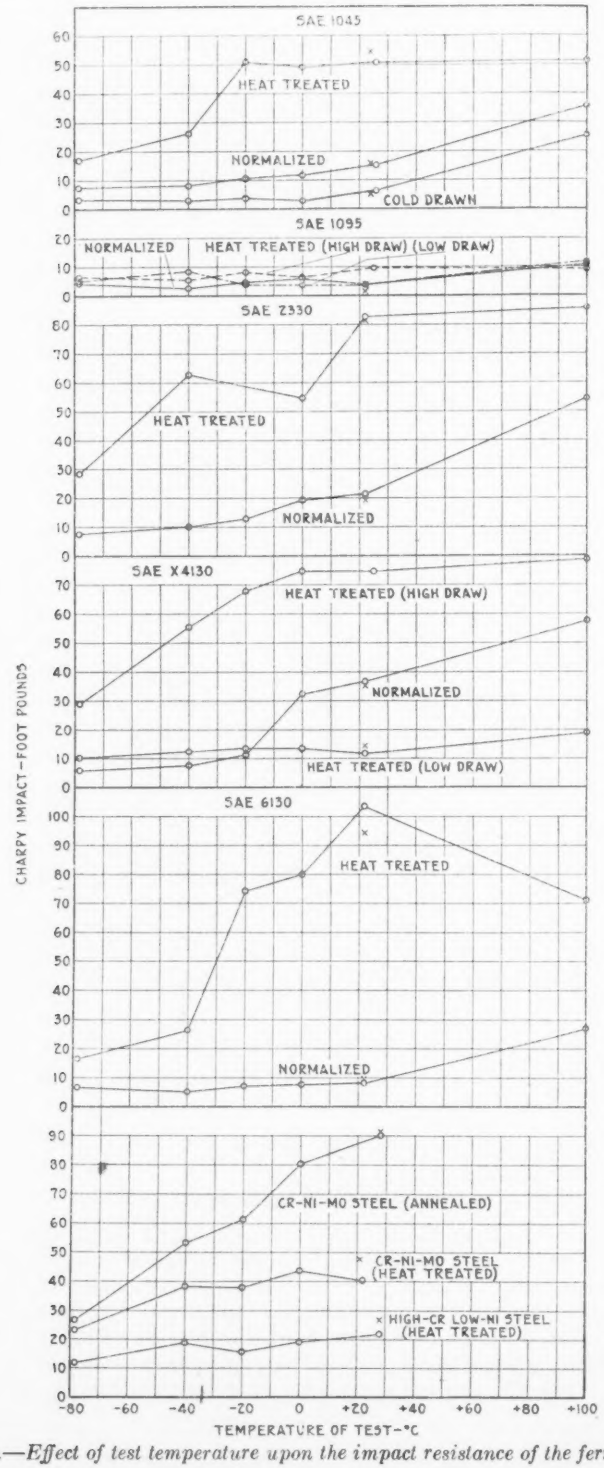

FIGURE 8.—*Effect of test temperature upon the impact resistance of the ferritic steels.*

The points indicated by the symbol "X" represent specimens which had been cooled to and held at −78° C for several hours prior to testing at room temperature.

the SAE X4130 steel. When tempered at 600° F subsequent to hardening this steel had an impact resistance of only 12 ft-lb at room temperature and 10 ft-lb at −78°C. When tempered at 1,075° F, however, the values were 75 and 29 ft-lb, respectively. The effect of this higher tempering treatment was to move the transition range in this steel from above +100° C to below −40° C. The SAE 1095 steel was normally coarse-grained and brittle and tempering at 1,075° F failed to cause any significant improvement in impact resistance as compared with the steel tempered at 600° F.

The test data showed that the 16-Cr–2-Ni steel did not have very good impact resistance when tempered at 850° F. Some data, not yet available for publication, indicated that high impact resistance in this steel may be obtained with lower tempering temperatures. This is an extremely unusual trend and a detailed study of this particular type of steel is in progress.

It is incorrect to assume that a steel having the highest resistance to impact at room temperature would always maintain this superi-

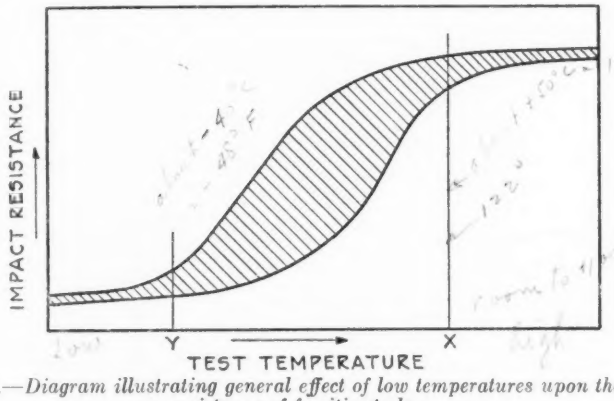

FIGURE 9.—*Diagram illustrating general effect of low temperatures upon the impact resistance of ferritic steels.*

ority at −78° C. For instance, at room temperature the heat-treated SAE X4130 steel (high draw) had an impact value of 75 ft-lb as compared with 104 ft-lb for the heat-treated SAE 6130 steel; but at −78° C this order was reversed, the values being, respectively, 29 and 17 ft-lb (fig. 8). Also, SAE 1045 as heat treated had only about one-half the impact resistance of SAE 6130, at room temperature but both steels had the same values at −40° and at −78° C.

The rate at which the impact resistance drops with decreasing temperature is also important, being rapid in some steels and gradual in others. As a general rule, the steels showing a gradual drop in impact resistance with decreasing temperature should be more suitable for sub-zero service than those showing a more abrupt drop.

The general effect of low temperatures upon the impact resistance of ferritic steels is diagrammatically illustrated in figure 9. The shaded area represents the scatter of energy absorbed. In the transition range, in which the impact resistance decreases more or less rapidly, there frequently occurs a marked scattering of test values. The results of tests at temperatures above "X" and below "Y" are usually in fair agreement.

An examination of the fractured surfaces of impact test specimens reveals a certain correlation between their appearances and the shape of the impact-temperature curve. At temperatures above "X" the fractures have a dull, fibrous appearance; there is a considerable amount of deformation and they are typical of what are usually referred to as tough fractures. Below temperature "Y" the fractures have a bright, crystalline appearance; there is very little deformation and they are typical of what are usually referred to as brittle fractures. Between these two temperatures (the transition range), fractures having a partly tough and partly brittle appearance are not uncommon.

This is exemplified in figure 10 which shows duplicate impact specimens from a steel tested at room temperature (SAE X4130 as normalized). Sample *A* broke with almost an entirely brittle fracture. A small part of the fracture, representing the area occupied by a slight cup and cone at the sides and a small area at the bottom, had the characteristics of the tough type. About 85 percent of the area covered by the fracture was of the brittle type and about 15 percent of the tough type, and the impact value absorbed in breaking was 19 ft-lb. In check specimen *B*, a thin layer of fibrous appearance existed immediately below the notch. The cup and cone was deeper and there was a considerable amount of deformation at the bottom, while in sample *A* there was none. About 60 percent of the area was of the tough type and about 40 percent was of the brittle type, and the energy absorbed in breaking was 54 ft-lb. The same phenomenon was also observed at 0° C.

At −20° C and below, only the brittle type of fracture was observed and the impact resistance was relatively low. At +100° C only the tough type of fracture was observed and the impact resistance was high. It is probable that, had tests been made at some temperature between room temperature and +100° C, good check results would have been obtained. It is apparent, then, that in this particular steel and under the test conditions described, the transition range exists between about −20° C and some temperature between room temperature and +100° C. As a matter of safety, only the lower impact values obtained in the transition range should be used in evaluating the impact resistance of all steels.

The appearances of the fractures are good indices of whether or not the materials are cold brittle at the temperature of testing. This is illustrated in figure 11, which shows the impact fractures of SAE 1045 steel as normalized, as heat treated, and as cold drawn. Both the normalized and cold-drawn steels exhibited brittle fractures at room and lower temperatures; reference to figure 8 corroborates the fact that the transition range of the steel thus treated exists above room temperature. At +100° C the normalized steel exhibited a fracture which was almost entirely of the tough type (fig. 12). The heat-treated steel, however, exhibited a fibrous fracture at test temperatures down to −20° C, while evidence of a brittle fracture was first found at −40° C. The impact-temperature curve (fig. 8) locates the transition range of the heat-treated steel below −20° C.

The fact that temperature is only one of the variables which affect the brittleness of materials should be emphasized. Other important variables are shape and size of specimen and the velocity of deformation. In the impact tests described in this report all these variables

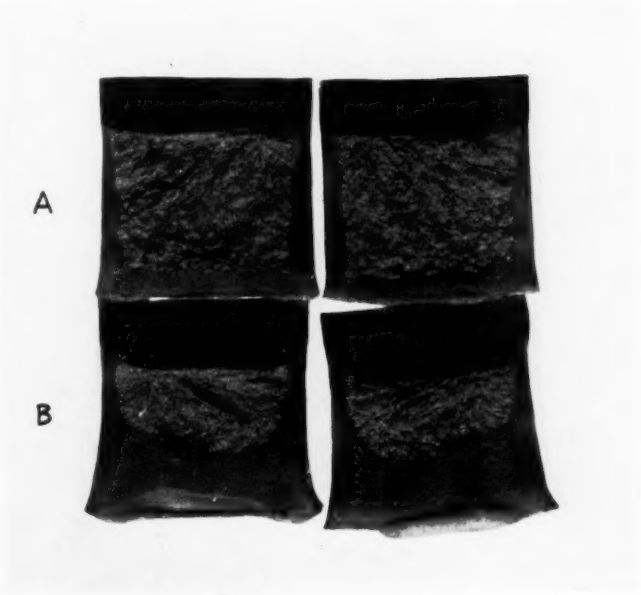

FIGURE 10.—*Appearance of the impact fracture of normalized SAE X4130 steel broken at room temperature.* ×3.

A, Brittle fracture, 19 foot-pounds.
B, Tough fracture, 54 foot-pounds.

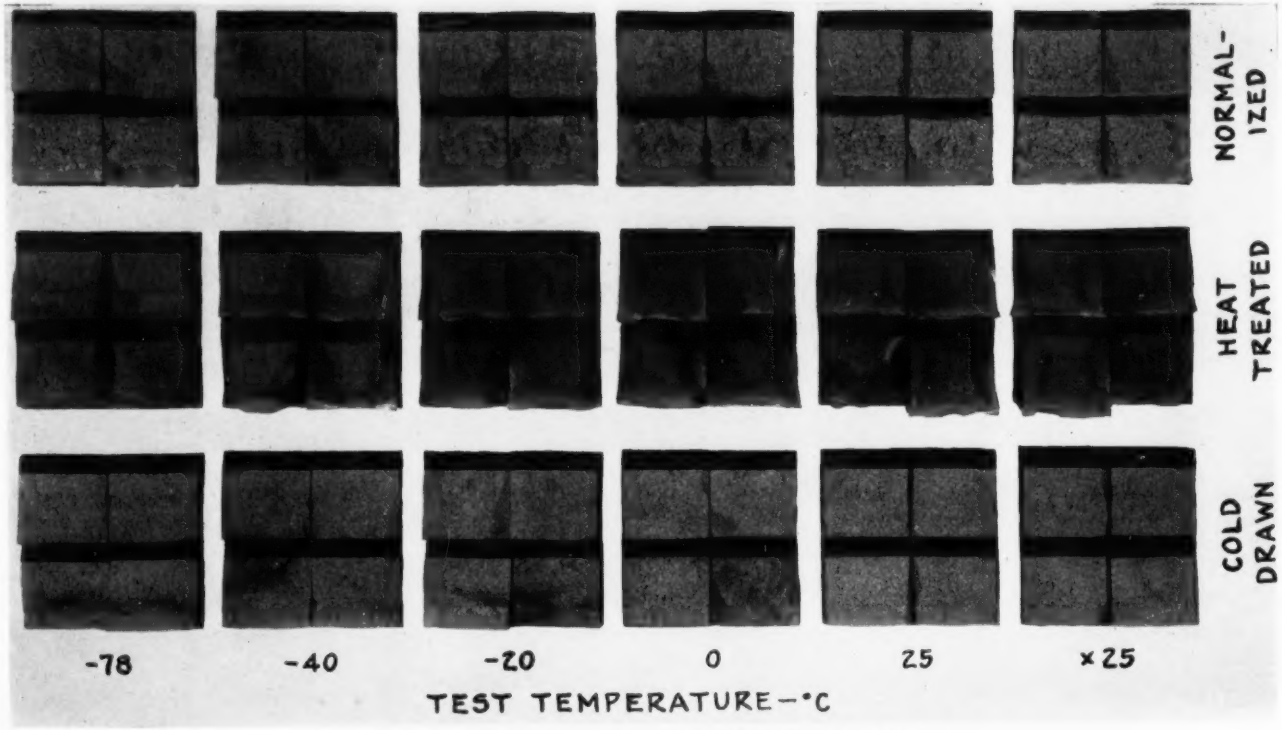

FIGURE 11.—*Impact fractures of SAE 1045 steel.* ×1.

Symbol "X" at the test temperature of 25° C indicates that these specimens had been cooled to and held at −78° C prior to breaking at room temperature.

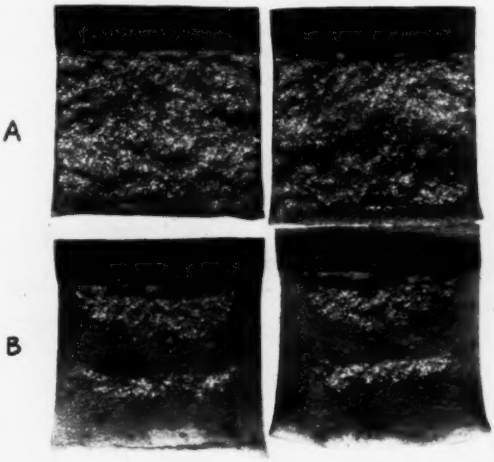

FIGURE 12.—*Appearance of the impact fracture of normalized SAE 1045 steel.* × 3.

A, Broken at room temperature, 15 foot-pounds.
B, Broken at +100° C, 35 foot-pounds.

except temperature, were arbitrarily fixed and the data thus secured gave information about the relative value of these steels at low temperatures. If any one of the other variables had been changed,

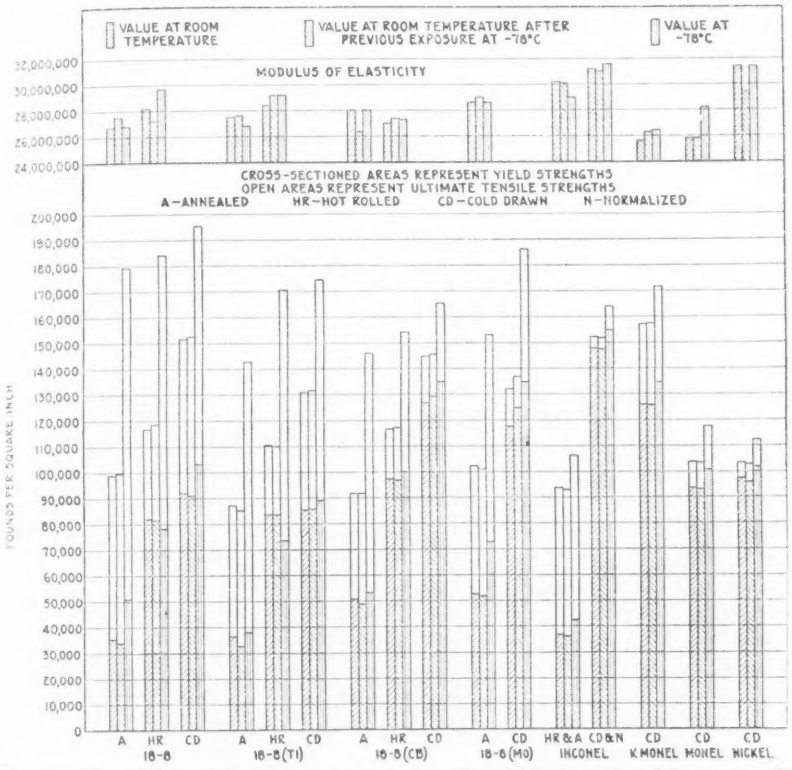

FIGURE 13.—*Effect of test temperature upon the yield strength, ultimate tensile strength, and modulus of elasticity of the austenitic stainless steels and the nickel alloys.*

the temperatures at which cold brittleness appeared might have been different.

2. AUSTENITIC STAINLESS STEELS AND NICKEL ALLOYS

(a) TENSILE TESTS

The tensile tests (fig. 13 and 14) on the austenitic stainless steels and nickel alloys showed the following changes in properties at −78° C as compared with room temperature:

Stainless Steels.—(1) The tensile strengths increased between 20,000 and 80,000 lb/in^2; (2) the yield strengths generally increased between 3,000 and 20,000 lb/in^2, although in some cases there was no change or even a small decrease; (3) the modulus of elasticity was unaffected; and (4) the ductility showed no significant changes, although the elongation values usually exhibited a slight increase, while reductions of area were usually lower.

Nickel Alloys.—(1) The tensile strengths increased between 8,000 and 15,000 lb/in^2; (2) the yield strengths increased approximately 5,000 lb/in^2; (3) the modulus of elasticity varied somewhat but the changes were not significant; and (4) the ductility showed no significant changes, although the values for elongation increased slightly.

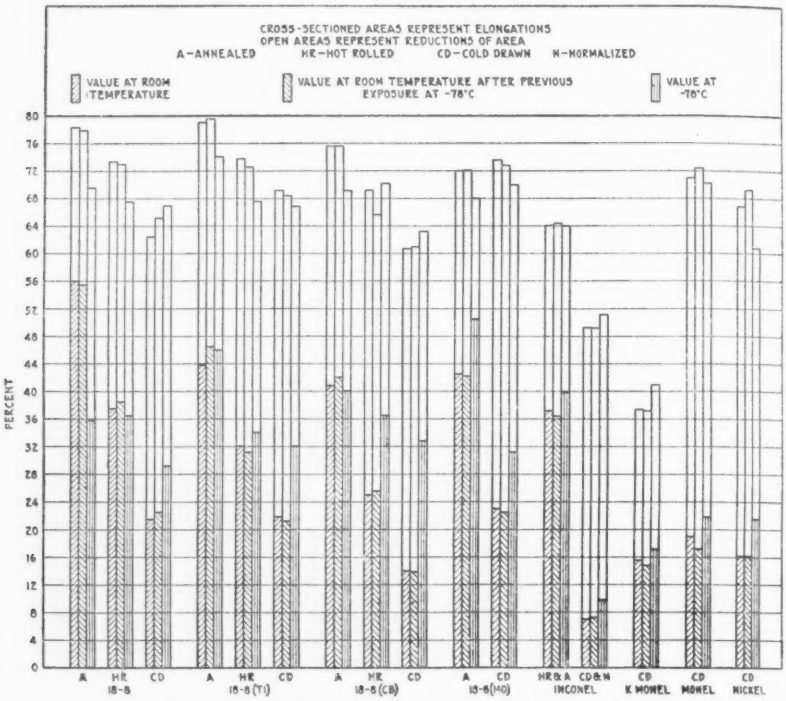

FIGURE 14.—*Effect of test temperature upon the elongation and reduction of area of the austenitic stainless steels and the nickel alloys.*

(b) HARDNESS TESTS

The hardness of these materials, in general, tended to increase slightly as the test temperature decreased (fig. 15).

(c) IMPACT TESTS

The results of the impact tests on the austenitic stainless steels and the nickel alloys are given in figure 16. Neither the nickel alloys nor the austenitic stainless steels were much affected at the lower temperatures.

In view of the remarkable toughness of these materials at room temperature and the negligible effect of temperatures as low as −78° C upon this property, it was apparent that these materials are well-suited for low temperature service. Under the test conditions used, this class of materials exhibited no evidence of cold brittleness down to temperatures as low as −78° C.

3. LIGHT METAL ALLOYS

(a) TENSILE TESTS

The results of the tensile tests on the aluminum-base alloys are summarized in figures 17 and 18. The tensile and yield strengths of these materials were but very slightly increased, while the elongation and reduction of area showed no consistent change at −78° C. The results justified the conclusion that there was no significant change in

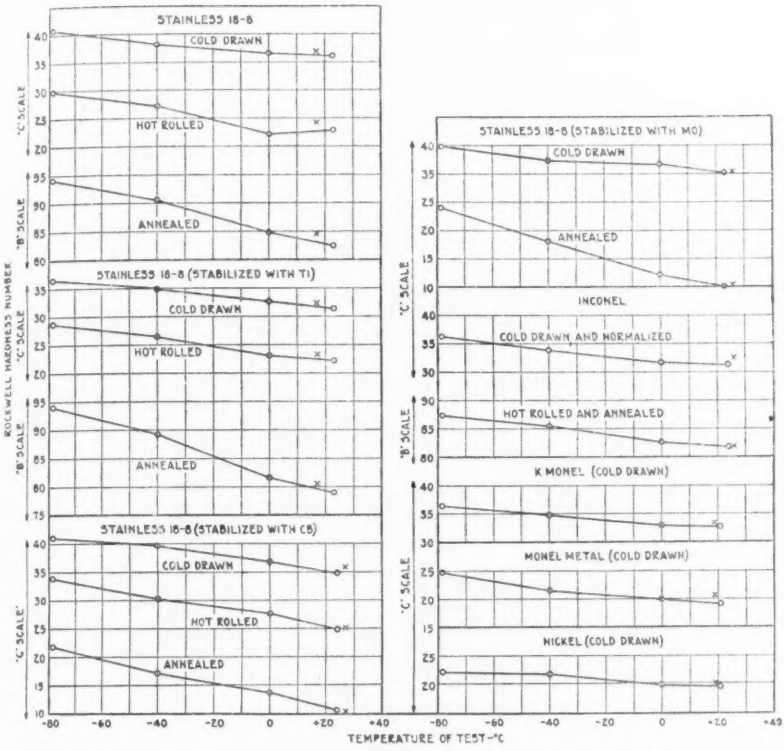

FIGURE 15.—*Effect of test temperature upon the hardness of the austenitic stainless steels and the nickel alloys.*

The points indicated by the symbol "X" represent specimens which had been cooled to and held at −78° C for several hours prior to testing at room temperature.

these properties at the low temperature. The modulus of elasticity tended to increase somewhat at −78° C.

Although not a full measure of the benefits derived from cold working subsequent to heat treatment, the data (figs. 17 and 18) show conclusively the trend in tensile properties caused by cold work. The tensile properties of specimens taken transversely to the direction of rolling were generally somewhat inferior to those of specimens taken longitudinally with the direction of rolling.

The results of the tensile tests on the magnesium-base alloys are summarized in figures 19 and 20. The yield strengths of all these alloys were higher at −78° C than at room temperature. The tensile

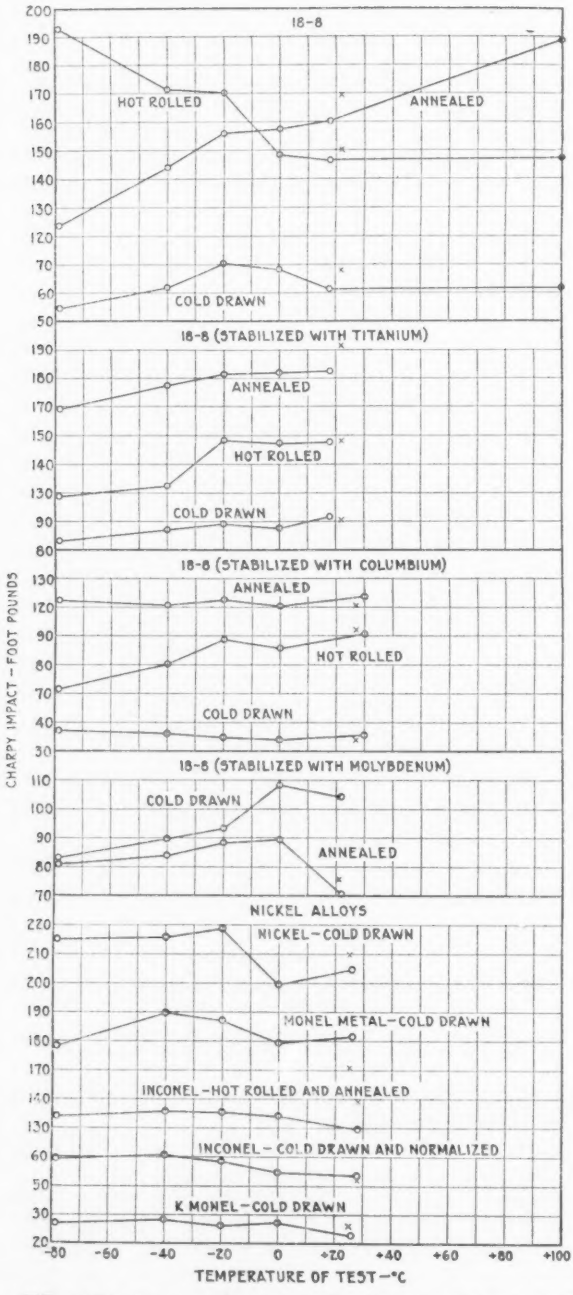

FIGURE 16.—*Effect of test temperature upon the impact resistance of the austenitic stainless steels and the nickel alloys*

The points indicated by the symbol "X" represent specimens which had been cooled to and held at −78° C for several hours prior to testing at room temperature.

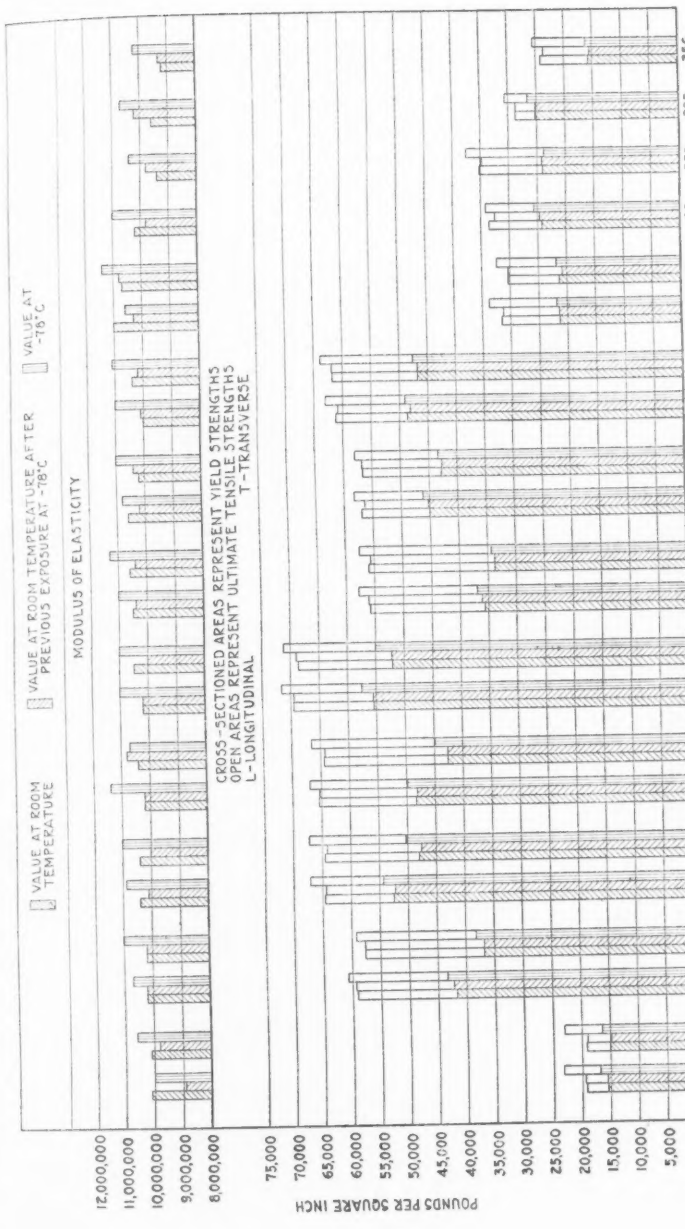

FIGURE **17.**—*Effect of test temperature upon the yield strength, ultimate tensile strength, and modulus of elasticity of the aluminum alloys.*

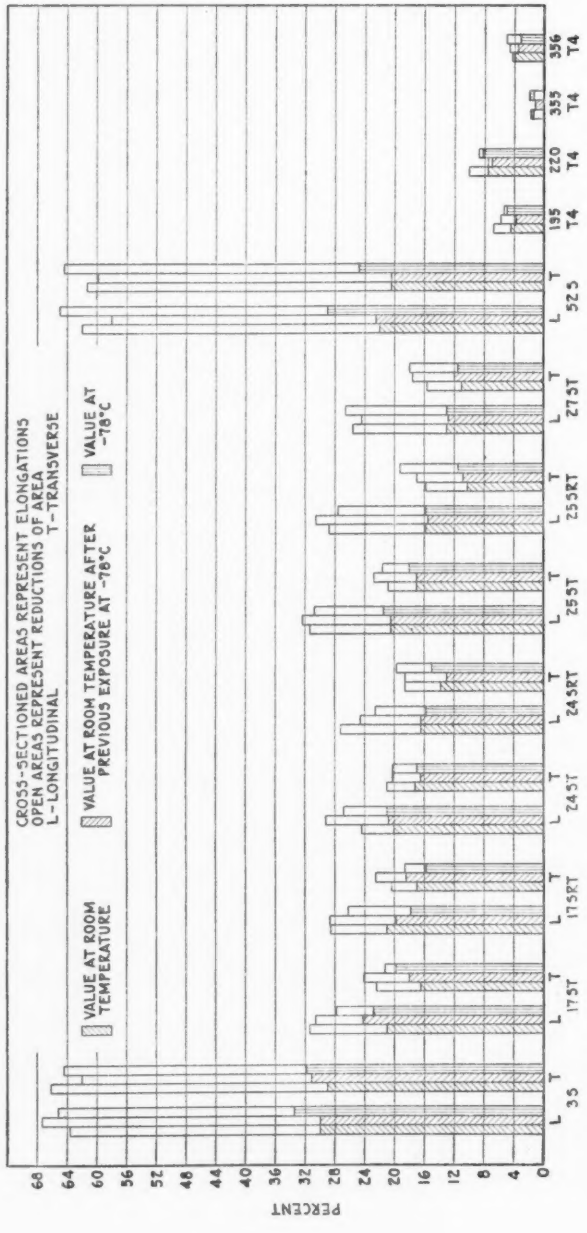

FIGURE 18.—*Effect of test temperature upon the elongation and reduction of area of the aluminum alloys.*

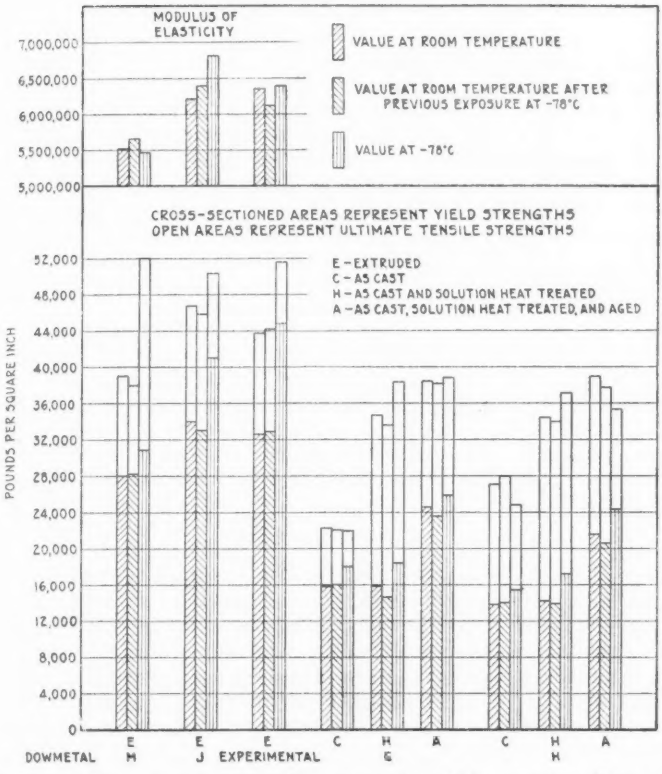

FIGURE 19.—*Effect of test temperature upon the yield strength, ultimate tensile strength, and modulus of elasticity of the magnesium alloys.*

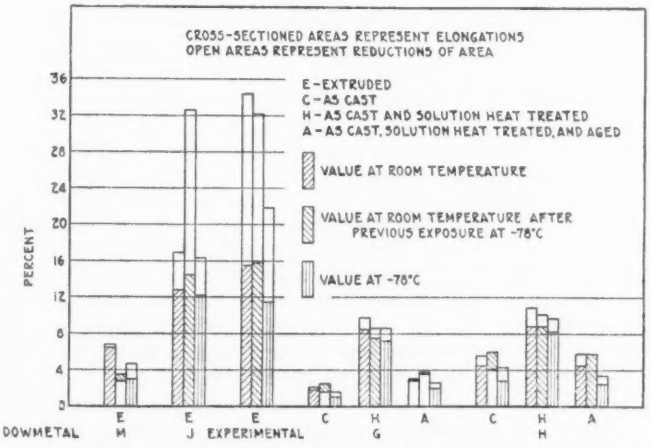

FIGURE 20.—*Effect of test temperature upon the elongation and reduction of area of the magnesium alloys.*

strengths of the extruded Dowmetals were also higher at the low temperature but the effect of low temperature on the cast Dowmetals was rather irregular. Elongation and reduction of area were generally slightly decreased at −78° C. Measurements of the modulus of elasticity could be made only on the extruded Dowmetal, because of the type of specimen used. In the case of Dowmetal M and the experimental Dowmetal, no change in the modulus was observed at −78° C, but a definite increase occurred in Dowmetal J. Prolonged exposure at −78° C prior to testing at room temperature generally caused no significant change in any of the tensile properties, with but one exception—the reduction of area of Dowmetal J was markedly increased after this treatment.

(b) HARDNESS TESTS

The results of the hardness tests on the aluminum- and magnesium-base alloys are summarized in figures 21 and 22, respectively. All of the materials increased in hardness as the test temperature decreased. Prolonged exposure at −78° C prior to testing at room temperature had no significant effect upon the hardness of any of these alloys except in the case of the cast Dowmetals, in which this treatment seemed to cause a slight increase.

(c) IMPACT TESTS

The results of the impact tests on the wrought aluminum alloys are summarized in figure 23. The general effect of decreasing test temperatures was either to increase slightly or else not to affect the resistance to impact of these materials. In some cases in which there was an apparent decrease in the impact resistance at certain temperatures, the resistance at −78° C was still not inferior to the impact resistance at room temperature. The relatively low ratio of cold-worked area to the total cross section of the alloys finished in the RT temper was sufficient to cause some decrease in the impact resistance; low temperatures, however, were not injurious to this property. The impact resistance of specimens taken transversely to the direction of rolling was definitely inferior to that of specimens taken longitudinally with the direction of rolling. Since the impact tests on these alloys were secured on the type of specimen shown in figure 4, these values, except to indicate the trend of the effect of temperature, cannot be compared numerically with values of the impact resistance of the cast aluminum alloys nor of the Dowmetals.

The effect of temperature upon the impact resistance of the cast aluminum alloys is summarized in figure 24. Although the resistance to impact of these cast alloys was generally quite low, temperatures down to −78° C had no adverse effect except on alloy 220–T4.

The results of the impact tests upon the Dowmetals are summarized in figure 25. The impact resistance of the cast Dowmetals G and H was quite low in all three conditions tested and was unaffected by temperatures down to −78° C. Of the extruded magnesium alloys, Dowmetal M showed no greater impact resistance at room temperature than did some of the cast magnesium alloys, but Dowmetal J and the experimental Dowmetal showed a definite improvement in this property. However, the impact resistance of all three of these alloys decreased steadily as the test temperature decreased.

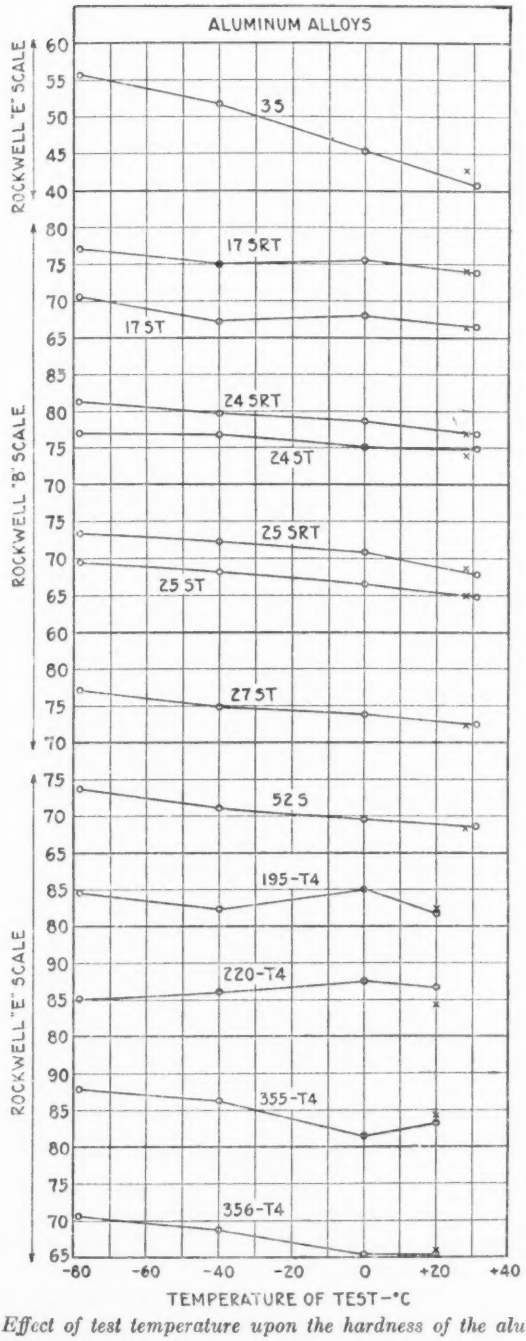

FIGURE 21.—*Effect of test temperature upon the hardness of the aluminum alloys.*

The points indicated by the symbol "X" represent specimens which had been cooled to and held at −78° C for several hours prior to testing at room temperature.

269047—41——6

VI. SUMMARY AND CONCLUSIONS

The effect of sub-zero temperatures down to −78° C was determined upon the tensile, hardness, and impact properties of metals commonly used in aircraft construction. These materials were

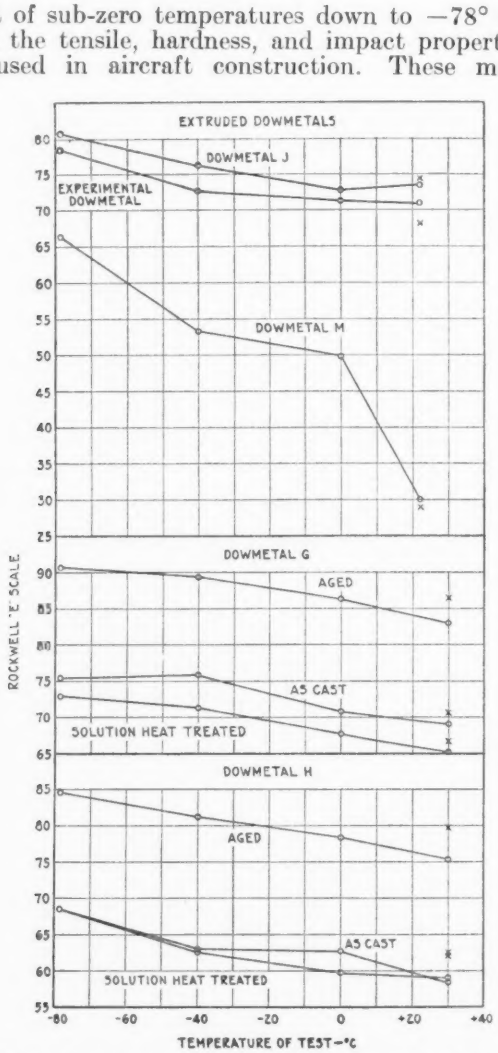

FIGURE 22.—*Effect of test temperature upon the hardness of the magnesium alloys.*
The points indicated by the symbol "X" represent specimens which had been cooled to and held at −78° C for several hours prior to testing at room temperature.

divided into three general groups: (1) Ferritic steels, (2) austenitic stainless steels and nickel alloys, and (3) light-metal alloys.

The tensile properties and the hardness of all materials were generally improved at low temperatures. The resistance to impact of the ferritic steels decreased generally as the test temperature was lowered, the rate and nature of the decrease being dependent upon the type of steel and its treatment. The impact resistance of the austenitic stainless steels and the nickel alloys was not deleteriously affected and

they were considered best adapted for service at low temperatures. The impact resistance of the aluminum-base alloys was not decreased; the impact resistance of the wrought magnesium-base alloys was adversely affected by the low temperatures, while that of the cast magnesium-base alloys was not. These last-named materials were, however, extremely brittle even at room temperature.

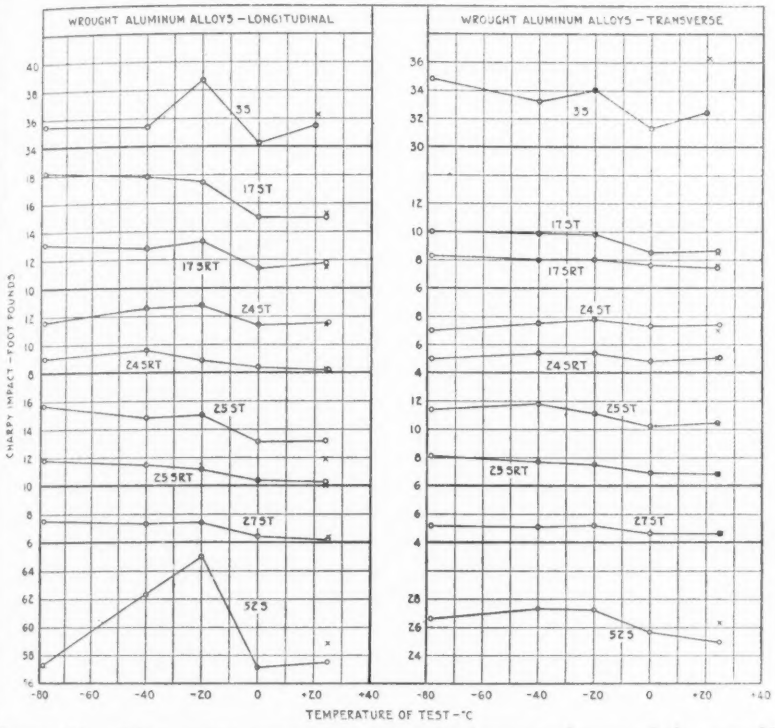

FIGURE 23.—*Effect of test temperature upon the impact resistance of the wrought aluminum alloys.*

The points indicated by the symbol "X" represent specimens which had been cooled to and held at −78° C for several hours prior to testing at room temperature.

The author is indebted to P. Devaney, National Bureau of Standards, for the construction of the special test apparatus and the machining of the hundreds of test specimens required, and to H. E. Francis, also of the National Bureau of Standards, for his help in the construction of some of the apparatus and his assistance in many of the tests.

This work was made possible through the interest and assistance of J. E. Sullivan and H. J. Huester, of the Bureau of Aeronautics, U. S. Navy Department.

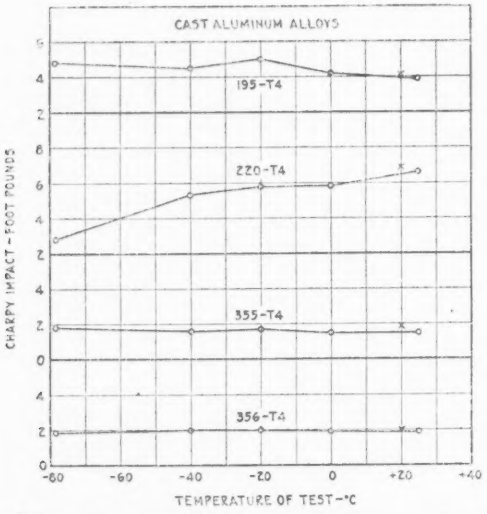

FIGURE 24.—*Effect of test temperature upon the impact resistance of the cast aluminum alloys.*

The points indicated by the symbol "X" represent specimens which had been cooled to and held at −78° C for several hours prior to testing at room temperature.

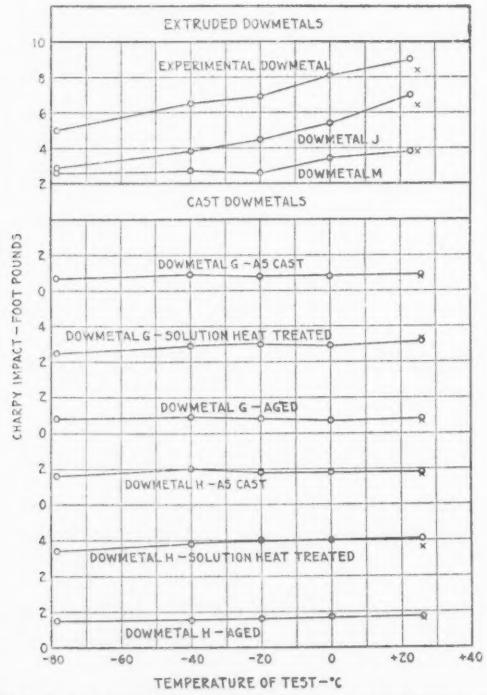

FIGURE 25.—*Effect of test temperature upon the impact resistance of the magnesium alloys.*

The points indicated by the symbol "X" represent specimens which had been cooled to and held at −78° C for several hours prior to testing at room temperature.

VII. REFERENCES

[1] D. J. McAdam, Jr. and R. W. Clyne, *The theory of impact testing: Influence of temperature, velocity of deformation, and form and size of specimen on work of deformation*, Proc. Am. Soc. Testing Materials **38**, pt. 2, 112 (1938).
[2] H. W. Russell, *Effect of low temperatures on metals and alloys*, Am. Soc. Testing Materials and Am. Soc. Mech. Engrs. Symposium on Effect of Temperature on Metals, page 658 (1931).
[3] Robert Sergeson, *Behavior of some irons and steels under impact at low temperatures*, Trans. Am. Soc. Steel Treating **19**, 368 (1932).
[4] H. W. Russell and W. A. Welcker, Jr., *Endurance and other properties at low temperatures of some alloys for aircraft use*, NACA Tech. Note 381 (1931).
[5] J. J. Egan, W. Crafts, and A. B. Kinzel, *Low temperature impact strength of some normalized low alloy steels.* Trans. Am. Soc. Steel Treating **21**, 1136 (1933).
[6] John J. Egan, Walter Crafts, and A. B. Kinzel, *Toughness of alloy steels at low temperatures.* Metal Progress **24**, 18 (Sept. 1933).
[7] C. H. Herty, Jr., and D. L. McBride, Effect of Deoxidation on the Impact Strength of Carbon Steels at Low Temperatures, Cooperative Bulletin 67, Mining and Metallurgical Investigations (Carnegie Institute of Technology and Mining and Metallurgical Advisory Boards) (1934).
[8] R. K. Hopkins, *Impact resistance of some steels and welds at sub-zero temperatures*, J. Am. Welding Soc. **13**, 16 (Oct. 1934).
[9] D. A. Campbell, *Impact resistance of certain nickel steels at low atmospheric temperatures*, Trans. Am. Soc. Metals **23**, 761 (1935).
[10] J. B. Johnson and Ture Oberg, *Mechanical properties at $-40°$ C of metals used in aircraft construction*, Metals & Alloys **4**, 25 (March 1933).
[11] E. W. Colbeck, W. E. MacGillivray, and W. R. D. Manning, *The mechanical properties of some austenitic stainless steels at low temperatures*, Trans. Inst. Chem. Engrs. **11**, 89 (1933).
[12] Franz Bollenrath and Joan Nemes, *The behavior of various metals at low temperatures*, Metallwirtschaft, **10**, 609–625 (1931).
[13] Franz Bollenrath, *On the influence of temperature on the elastic behaviour of various wrought light metal alloys*, J. Inst. Met. **48**, pt. 2, 255 (1932).
[14] R. Greaves and J. Jones, *The effect of temperature on the behaviour of metals and alloys in the notched-bar impact test*, J. Inst. Met. **34**, pt. 2, 85 (1925).
[15] K. Mattheas, *Dynamic strength properties of some light metals*, Z. Metallkunde, **24**, 176 (1932).
[16] I. Musatti, *Dynamic properties of magnesium alloys*, Met. ital. **22**, 1052 (1930).

WASHINGTON, August 24, 1940.

U. S. Department of Commerce National Bureau of Standards

RESEARCH PAPER RP1348

Part of Journal of Research of the National Bureau of Standards, Volume 25, December 1940

A PHOTOMETRIC PROCEDURE USING BARRIER-LAYER PHOTOCELLS

By Louis E. Barbrow

ABSTRACT

A procedure is described whereby barrier-layer photocells, corrected so as to have a spectral response curve simulating the ICI luminosity curve, are used in the photometry of light sources of various colors and in the determination of the transmission factors of colored filters. The procedure involves a determination of the illumination-response curve of the cell used, a method of avoiding the difficulties incident to cell fatigue, and a means for correcting for the improper spectral sensitivity of the cell. The method of correcting for the difference between the spectral response of the cell used and the ICI luminosity curve embodies essentially the procedure recommended in 1937 by the International Committee of Weights and Measures for the photometry of light sources which differ in color. Results obtained using the recommended procedure are given.

CONTENTS

	Page
I. Introduction	703
II. Circuit	704
III. Illumination-response curves	705
IV. Fatigue characteristics	707
V. Correction for improper spectral response	707
VI. Conclusion	710

I. INTRODUCTION

Historically, the advent of new light sources has always introduced the difficult problem of measuring them photometrically. Starting back only as far as 1909, we have several outstanding examples of this situation. In 1909, candlepower values were assigned to groups of carbon-filament incandescent lamps by the national standardizing laboratories of England, France, Germany, and the United States. These were to serve as the basic standards by means of which the unit of luminous intensity was to be maintained. Later, vacuum tungsten-filament lamps and then gas-filled tungsten-filament lamps became commercially available, and the various national standardizing laboratories independently derived photometric standards of these types in terms of the basic carbon-filament standards. Because of the color differences involved in such measurements, it has been found that the various laboratories are not in agreement on the tungsten-filament standards, even though they started in substantial agreement on the carbon-filament lamps. The principal reason for this is that different photometric procedures were used by the different laboratories to overcome the color differences involved.

The International Committee of Weights and Measures in 1937 [1] agreed on a procedure to be followed in deriving photometric standards of other colors from the primary standard as follows:

(a) The photometric values of sources having a color different from the primary standard shall be determined by a procedure consistent with the luminosity curve adopted by the International Committee of Weights and Measures.[2]

(b) To assure uniformity in the procedure of passing from the new primary standard to secondary incandescent filament standards of higher efficiency there is adopted the method of blue filters interposed between the photometer and one of the light sources to be compared, thus establishing a color match.[3]

More recently mercury-vapor lamps and fluorescent lamps of various colors have come into commercial use and these have presented in an exaggerated form the same general type of problem relative to their photometry.

The object of this paper is to outline a procedure for the photometry of light sources of any color by the use of barrier-layer photocells. The procedure embodies in general that adopted by the International Committee of Weights and Measures in 1937. It involves the determination of (1) the current response of the cell used over a useful range of illumination, (2) the effect of fatigue on this response, and (3) the effect of improper spectral sensitivity and a means of correcting for it.

II. CIRCUIT

The circuit in which the barrier-layer cell should be used is a current-balancing circuit giving, in effect, zero external resistance in series with the photocell in a manner recommended by Campbell and Freeth [4] in 1934. The circuit used in the work herein described is illustrated in figure 1. B is the barrier-layer cell; G, a galvanometer of high current sensitivity; S, a suitable galvanometer shunt; K, a Kohlrausch slide wire having resistance r_2 (7 ohms); e, a 1.5-volt dry cell; r_1, a 100-ohm resistance; and r_3, a variable resistance, preferably not less than 1,000 ohms. The resistance of the leads from the barrier-layer cell to the galvanometer must be negligibly small. The current generated in the cell as the result of illumination may be balanced by setting the Kohlrausch slide wire, balance being indicated by zero deflection of the galvanometer. Under this condition, the current output of the barrier-layer cell, B, is equal to the current, i_3, in the resistance r_3 and is proportional to the potential difference between points a and b, r_3 being constant. The potential difference between a and b is nearly proportional to the resistance, r, between points a and b. The degree of approximation involved may be deduced from the following expression for the current, i_3:

$$i_3 = \frac{vy}{y(r_1+r_2) - y^2 r_2 + r_3 + \frac{r_1 r_3}{r_2}}, \tag{1}$$

in which $y = r/r_2$ and v is the voltage of the dry cell, e.

[1] Procès Verbaux, Comité International des Poids et Mesures, p. 223 (1937).

[2] This luminosity curve represents the luminosity factors adopted in 1924 by the International Commission on Illumination, and is known as the ICI luminosity factors (formerly called "visibility factors"). The data on which it is based were reported by K. S. Gibson and E. P. T. Tyndall in Scientific Papers of the Bureau of Standards, volume 19, page 131, 1923–24 (S475) and, in briefer form, in the Transactions of the Illuminating Engineering Society, volume 19, page 176, 1924. See also a comprehensive paper "Spectral Luminosity Factors," by K. S. Gibson, in the Journal of the Optical Society of America, volume 30, page 51, 1940.

[3] The blue filters used in accordance with section (b), quoted above, are calibrated by determining their spectral transmission curves and calculating the integral transmission for light from the primary standard by means of the luminosity factors.

[4] N. R. Campbell and M. K. Freeth, J. Sci. Instruments **11**, 125 (1934).

On the basis that the voltage, v, is constant, the maximum error, in assuming that i_3 is proportional to r, is $100r_1r_2/(r_2r_3+r_1r_3)$ percent in all cases where r_1 is greater than r_2. This expression for the maximum error is obtained by finding the maximum variation in the denominator of eq 1.

For values of r_3 above 7,000 ohms in the circuit described above, the maximum error possible from assuming that i_3 is proportional to r, is less than 0.1 percent, and the error decreases with increasing values of r_3, so that it may be neglected if r_3 is suitably high. In this case the current output of the barrier-layer cell, B, with zero voltage across it, is very closely proportional to the setting of the Kohlrausch slide wire, assuming, of course, that the Kohlrausch slide wire itself has been calibrated and found to be uniform. If in the

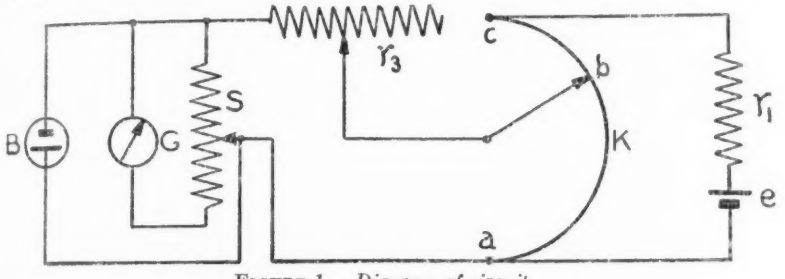

FIGURE 1.—*Diagram of circuit.*

use of this circuit, a resistance, r_3, much less than 7,000 ohms is used, corrections can be made by the use of eq 1.

III. ILLUMINATION-RESPONSE CURVES

In the present work, the barrier-layer cells studied were two Weston Photronic cells with Viscor [5] filters, designated NBS 9152 and B39. Hereafter in this paper these cells together with their Viscor filters, will be referred to simply as "cells."

In the determination of the response of these cells over a range of illuminations, a box containing ten 15-watt T-10-bulb vacuum tungsten-filament lamps, with a shutter in front of each lamp, was used. The box is illustrated in figure 2. The procedure, similar to that recommended by Atkinson, Campbell, Palmer, and Winch,[6] was as follows:

It was decided to use a range of illuminations of 0.6 to 18 foot-candles. The box was set at such a distance from the cell being tested that the illumination on the cell from one of the lamps was approximately 0.6 foot-candle. With one lamp illuminating the cell, the resistance of r_3 was set so that the reading of the index of the Kohlrausch slide wire was slightly less than 100, full scale being 1,000. The reading of the index for each lamp was recorded as shown in column 2 of table 1, the lamps in turn illuminating the cell when their shutters were opened. The shutters were then opened in groups—first, lamps 1 and 2 illuminating the cell, then lamps 1, 2, and 3, etc. The index readings are recorded in column 3 of table 1. Column 4 gives the calculated values for lamps 1; for 1 and 2; for 1, 2, and 3, etc., obtained by adding successively the values listed in column

[5] M. E. Fogle, Trans. Illum. Eng. Soc. **31**, 773 (September 1936).
[6] J. R. Atkinson, N. R. Campbell, E. H. Palmer, and G. T. Winch, Proc. Phys. Soc. (London) **50**, 934-946, (November 1938).

TABLE 1.—*Data for determining response curve of barrier-layer cell NBS 9152*

Lamp number	Kohlrausch slide wire settings		Calculated Σn	$\Delta\Sigma n$	$\Delta\Sigma n$
	Single lamp	Σn			
					Percent
1	95.6	95.6	95.6	0	0
2	98.0	194.4	193.6	.8	.4
3	90.1	285.3	283.7	1.6	.5
4	92.2	377.8	375.9	1.9	.5
5	98.0	476.1	473.9	2.2	.4
6	91.6	568.2	565.5	2.7	.4
7	86.1	654.7	651.6	3.1	.4
8	97.3	751.8	748.9	2.9	.3
9	96.4	848.1	845.3	2.8	.3
10	95.2	942.8	940.5	2.3	.2

2. The differences between the values in columns 3 and 4 are the errors in the response of the cell at the various illuminations relative to the reading at 0.6 foot-candle. These errors are listed in column

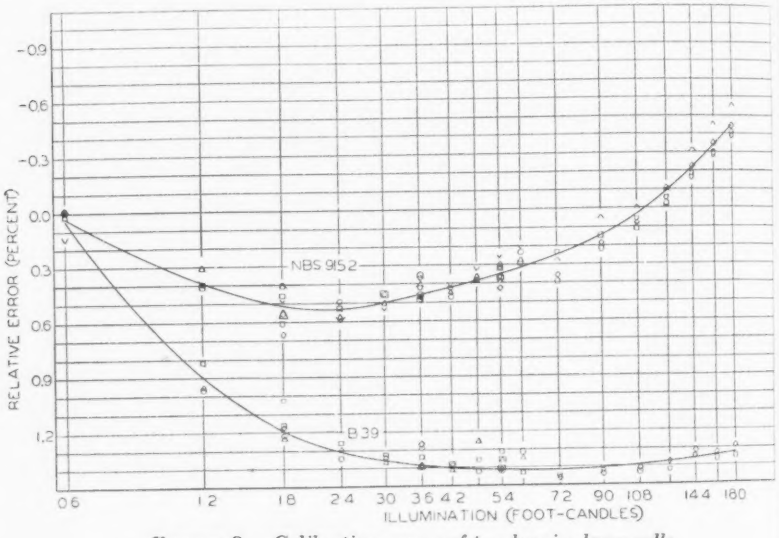

FIGURE 3.—*Calibration curves of two barrier-layer cells.*

5, the percentage errors in column 6. The above procedure gave data on the cell from 0.6 to 6 foot-candles. The lamp box was then moved closer to the cell, so that the illumination on the cell from one lamp was approximately 1.8 foot-candles. The procedure was repeated, and data on the cell were obtained for the range 1.8 to 18 foot-candles. The illumination-response curves obtained for the two cells are shown in figure 3. The data given in table 1 for cell NBS 9152 are designated by open circles in figure 3. Other similar series of data, taken over a period of 6 months, are designated by the other

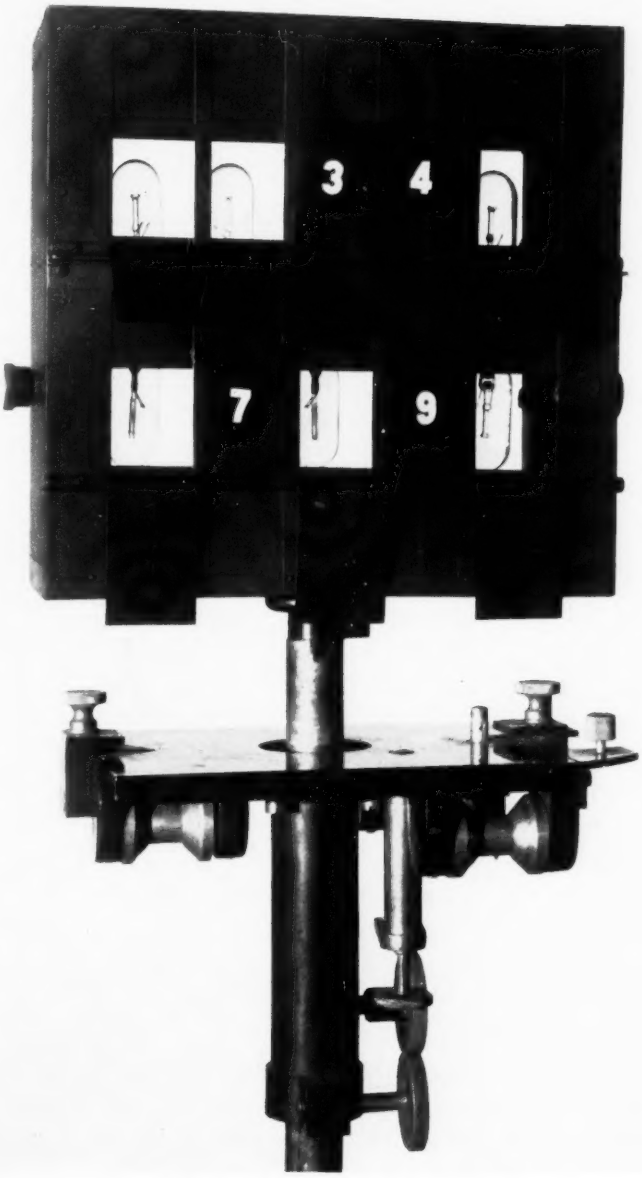

FIGURE 2.—*Lamp box and carriage.*

The shutters of lamps 3, 4, 7, and 9 are shown closed.

symbols in figure 3. The data designated by the symbols V and Λ were obtained with a blue-glass filter in front of the barrier-layer cell. This filter is one which is used with vacuum tungsten-filament lamps to color-match them with gas-filled tungsten-filament lamps. It will be noted that the response curve of the cell for lamps of the color temperature of gas-filled lamps is within experimental error, the same as the curve for vacuum lamps.

IV. FATIGUE CHARACTERISTICS

Barrier-layer cells cannot be used in precision photometry without a knowledge of their fatigue characteristics. In fact, without such knowledge the derivation, with sufficient accuracy, of curves such as those shown in figure 3 is not possible. A study of cells NBS 9152 and B39 showed that they had fatigue curves of the type shown in figure 4(A), where current is plotted against time under constant illumination. The current from the cell first rises, becomes approxi-

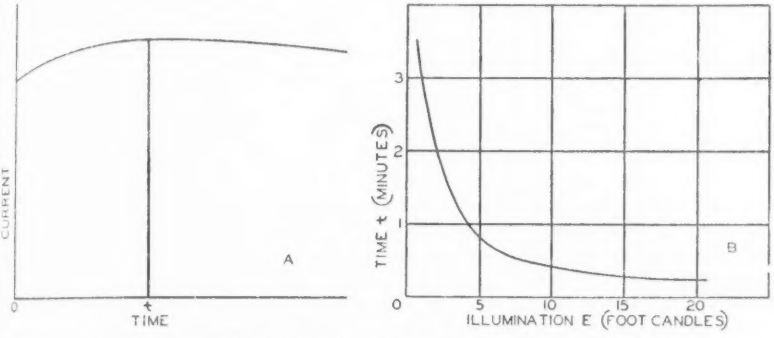

FIGURE 4.—*Fatigue characteristics of barrier-layer cells used.*

A, fatigue curve; *B*, curve of illumination against time, *t*, for obtaining maximum current.

mately constant, and then decreases. Reproducible results with these cells can be obtained by always measuring the current at time, t, when the current is a maximum. The time, t, is a function of the illumination E, as shown approximately in figure 4(B), for the two cells in question. This curve indicates, for example, that for an illumination of 0.5 foot-candle, the cells should be illuminated for about 3½ minutes before a reading is made. It was also found that the cells should not be continuously exposed to an illumination, E, for a time longer than $2t$, and also that between exposures the cells should be permitted to recover for about 1 minute for illuminations up to approximately 3 foot-candles and for about 2 minutes for higher illuminations.

V. CORRECTION FOR IMPROPER SPECTRAL RESPONSE

For best results, the photoelectric cell used should have a spectral-response curve approximating the ICI luminosity curve. A test of the spectral response of cell NBS 9152, used in this work, indicated that it had a curve similar to that described by Fogle for cells of this type. A test of the response of this cell for various spectral-energy distributions was made by measuring with it the transmission of a

group of colored filters used by Crittenden and Taylor [7] in an interlaboratory comparison in 1929. The data obtained are listed in column 4 of table 2. Column 3 of table 2 lists the transmission of the filters calculated from spectrophotometric data. These values are taken from the paper by Crittenden and Taylor. It will be noted that the agreement between the spectrophotometric values and the measured values is good (within 3 percent) except for the red filters (DR–3 and MR–3) and the amber filter (OA–3). In the case of filter DR–3, the difference is over 10 percent.

TABLE 2.—*Transmission factors of colored photometric filters for light of color temperature 2,680° K*

Filter designation	Spectral centroid	Transmission from spectrophotometric and ICI luminosity data	Measured transmission, using Weston Photronic cell with Viscor filter		Color-matching filter
			Uncorrected	Corrected	
	mμ	*Percent*	*Percent*	*Percent*	*NBS No.*
DR–3	627	12.35	13.75	12.31	3171
MR–3	616	19.7	20.8	19.0	3557
OA–3	598	38.6	41.3	38.6	3721
A–3	588	47.3	48.6	46.2	3961
BS–73	579	70.8	72.1	70.4	4306
LA–3	575	73.6	74.0	72.8	4351
BS–66	566	44.9	45.1	44.6	8481
LB–3	556	11.14	11.21	11.18	8438
DG–3	547	9.37	9.34	9.56	6340

To obviate the occurrence of errors of such magnitude in the determination of the transmission of colored filters and in the photometry of light sources which do not approximately color-match the standard lamps in terms of which they are to be measured, a "color-matching" substitution method of photometry is recommended; that is, the colored filters to be measured or the light sources to be compared are color-matched by the use of filters whose transmissions are known from spectrophotometric data.

For example, light of color temperature 2,680° K, after passing through the filters listed in column 1 of table 2, was found to approximately color-match light of color temperature 2,842° K passing through the filters listed in column 6 of table 2. These latter filters are from a large number of colored filters of known spectral transmission maintained by the photometry section of the National Bureau of Standards. The Crittenden and Taylor filters, when measured in terms of the color-matching filters, as described later, gave the results listed in column 5 of table 2. With the exception of filter MR–3, the agreement between the transmissions from spectrophotometric data (column 3), and the transmissions, as determined by the color-matching substitution method, is good.

An example of the use of the color-matching substitution method in the calibration of light sources may prove of interest. The luminous intensity of a group of "daylight" fluorescent lamps and a group of "white" fluorescent lamps was to be measured in terms of a group of gas-filled tungsten-filament standards. It was found by visual observation that the "white" fluorescent lamps approximately color-matched light of color temperature 2,842° K through blue filter 15130, and that the "daylight" fluorescent lamps were approximately

[7] E. C. Crittenden and A. H. Taylor, Trans. Illum. Eng. Soc. **26**, 153-207 (February 1929).

color-matched by light of color temperature 2,842° K through blue filters 8438, 8456, and 8331 separately. Filter 8438 was slightly too blue and filters 8456 and 8331 were not quite blue enough. The barrier-layer cell used was found to measure the transmission of filter 15130 correctly to within 0.1 percent and that of filters 8438, 8456, and 8331 low by an average of 0.6 percent. The results obtained on the "daylight" fluorescent lamps measured directly against the gas-filled tungsten standards were therefore increased by 0.6 percent; no corrections were applied to the results obtained on the "white" fluorescent lamps. Although this method of correction for color differences does not take into account the differences in spectral distribution of the sources being compared (even though a color match prevails), it is felt that the method obviates large errors except, perhaps, where extreme differences in spectral distribution remain. As photoelectric cells become obtainable which, with or without filters, more closely approximate in spectral response the ICI luminosity curve, the corrections for color differences will become progressively smaller.

The procedure outlined above was also used in the measurement of the luminous intensity of a group of vacuum tungsten-filament lamps at color temperature 2,360° K and of a group of gas-filled tungsten-filament lamps at 2,727° K, both in terms of a group of carbon-filament lamps at 2,045° K. Blue-glass filter 15130 was used as the color-matching filter in stepping from 2,045° to 2,360° K, and again in stepping from 2,360° to 2,727° K. The average candlepower of each group of lamps determined photoelectrically by the method outlined above is given in column 2 of table 3. The values assigned to the lamps by other methods are given in column 3. The value for the vacuum tungsten-filament lamps listed in column 3 was obtained by visual photometry, using the blue-glass method recommended by the International Committee of Weights and Measures. The value for the gas-filled tungsten-filament lamps listed in column 3 is an average of two values, one obtained by using the blue-glass method recommended by the International Committee of Weights and Measures and the other obtained by comparison with a black body at 2,727° K,[8] the brightness of the black body at this temperature having been calculated from that at 2,046° K by means of the luminosity factors.

TABLE 3.—*Calibration of vacuum and gas-filled incandescent lamps*

Color temperature of lamps	Candles	
	Photoelectrically	Assigned
° K		
2,360	23.63	23.83
2,727	227.5	230.2

The difference between the assigned values on these lamps and those obtained photoelectrically are of the order of 1 percent, and can probably be accounted for on the basis of the spectral difference between the radiant energy of higher color temperature and that of lower

[8] H. T. Wensel, Wm. F. Roeser, L. E. Barbrow, and F. R. Caldwell, J. Research NBS 13, 161–168 (1934) RP 699.

color temperature as transmitted by the blue filter, even though a color match exists.

VI. CONCLUSION

It is felt that the procedure outlined in this paper is applicable to photoelectric photometry generally. Obviously, the curves and data given in this paper do not necessarily apply to barrier-layer cells other than those tested, even if they are of the same type. If the characteristics of the particular photoelectric cell used are determined, and if corrections for color differences are made as recommended above, it is felt that the photometric results obtained will be more consistent and possibly more accurate than those obtained by any direct visual procedure. The accuracy obtainable by following the method proposed will increase as photoelectric cells and correcting filters become available which more closely approximate the ICI luminosity curve.

WASHINGTON, August 19, 1940.

U. S. DEPARTMENT OF COMMERCE NATIONAL BUREAU OF STANDARDS

RESEARCH PAPER RP1349

Part of Journal of Research of the National Bureau of Standards, Volume 25, December 1940

SOME PROPERTIES OF THE PORE SYSTEM IN BRICKS AND THEIR RELATION TO FROST ACTION

By Ray T. Stull and Paul V. Johnson

ABSTRACT

In the study of certain properties of the pore system in bricks and their relation to frost action, the following determinations were made on seven series of bricks: Percentage of porosity; variation in porosity within a brick; permeability to air and water; the flow of air through two members in series; mean effective capillary radius and the number of capillaries in an ideal structure, which would have the same permeability value as that determined experimentally for the brick; saturation coefficient by 48 hours' immersion; increase in saturation coefficient with repeated freezing and thawing; and resistance of the bricks to failure by repeated freezing and thawing. The data are presented in 14 tables.

CONTENTS

	Page
I. Introduction	712
II. Materials and properties studied	713
1. Selection of specimens	713
2. Properties determined	713
III. Methods and apparatus	713
1. Preparation of the specimens	713
2. Porosity	714
(a) Definition of porosity	714
(b) Bulk volume	714
(c) Solid volume	714
(d) Porosity of different sections of a brick	716
3. Permeability	716
(a) Definition of permeability	716
(b) Apparatus for determining air permeability	716
(1) Air transmission of two members in series	717
(c) Apparatus for determining water permeability	718
4. Determining mean effective radius and number of capillaries	719
5. Freezing and thawing tests	719
(a) Procedure	719
(b) Saturation coefficient	719
(c) Increase in saturation coefficient with repeated freezing and thawing	720
IV. Results and discussion	720
1. Variation in porosity within a brick	720
2. Permeability to air and water	721
3. Flow of air through two members in series	724
4. Effect of freezing and thawing on the saturation coefficient	724
5. Relations of porosity, permeability, effective capillary radius, number of capillaries, and saturation coefficient to the number of freezing and thawing cycles causing failure of bricks	725
V. Summary	729

I. INTRODUCTION

In a discussion of pore size and arrangement in sandstone and compacted sand, Slichter [1] shows that the form and size of the pores depend upon the grain size, shape, and degree of compactness or grain arrangement. For spherical grains of the same size, the maximum pore space results when the grains are arranged in a rectangular pattern and the minimum when the pattern is "triangular." With more or less rounded grains, well-compacted, the pores are in the form of irregular, truncated, tetrahedral voids interconnected at the truncations, or smallest cross sections, so as to form a network of irregularly shaped passages of variable cross section which function in a manner similar to that of a bundle of cylindrical capillary tubes.

The form and arrangement of the pores of kiln-fired clay products are considered similar to those of fine-grained sandstone, where the pores vary in size down to and including those of micro size. When formed from the plastic clay and dried, the internal structure consists of a compacted mass of mineral grains and, during the firing process, the pores change more or less in size, but probably change very little in general form up to some point below the vitrified condition.

The pore arrangement pictured by Slichter is essentially rectilinear and does not seem quite appropriate to the arrangement in bricks. For, when considered en masse, the arrangement appears more probably to be a three-dimensional lattice consisting of connecting voids of variable sizes and shapes, through which fluids in passing follow paths of least resistance along irregular or zigzag courses.

The size and structure of pores exercise an important influence on the life span of structural clay products when exposed to weather conditions, especially in climates of excessive moisture and severe freezing.

Freezing and thawing tests as means of judging certain weather-resisting properties of structural clay products have been recognized both in the United States and abroad by a large number of investigators, as indicated by the numerous reports appearing in the literature.[2]

The number of freezing and thawing cycles which structural clay products will undergo without showing signs of failure depends upon numerous well-recognized factors, such as:

1. Different modifications of the test procedure.
2. Kind of clay used in making the product.
3. Method of forming.
4. Heat treatment.
5. Soundness and uniformity of structure.
6. Hardness and mechanical strength.
7. Degree of moisture saturation, or "saturation coefficient."
8. Pore structure.

Certain properties associated with porous structure have an important bearing on the life of structural clay products, but they have

[1] Laws of the rectilinear flow of ground water through a soil. Annual Report, U. S. Geol. Survey V, II pt. 2, 305–17 (1897–8).

[2] Douglas E. Parsons, *Bibliography on the weathering of structural clay products*, Proc. Am. Soc. Testing Materials **31**, pt. 2, 825 (1931).

received scant attention heretofore. This investigation was undertaken to obtain data on these properties and on their relation to failure of bricks as a result of freezing and thawing.

II. MATERIALS AND PROPERTIES STUDIED

1. SELECTION OF SPECIMENS

Seven series of bricks, representing products of five different manufacturers, were selected for the investigation. The bricks, which are listed in table 1, were selected by visual inspection for their apparent freedom from defects; and they represent a wide range in porosity, difference in raw materials (clay or shale) used for making the products, and difference in method of manufacture. Two plaster-of-paris slabs were also included for comparison in tests for permeability to air.

TABLE 1.—*Bricks included in the investigation*

Series	Number of bricks	Material	Method of forming	Kiln treatment
D	10	Clay	Soft mud	Soft burn.
E	10	Shale	Stiff mud [1]	Hard burn.
F	7	Clay	do	Medium burn.
G	11	Shale	do	Soft burn.
H	10	do	do	Hard burn.
J	10	Clay	Dry press	Do.
K	10	do	do	Medium burn.

[1] All stiff-mud bricks were side-cut.

2. PROPERTIES DETERMINED

The physical properties investigated were:

1. Percentage of porosity (exclusive of sealed pores).[3]
   a. Bulk volume.
   b. Solid volume (including sealed pores).
2. Variation in porosity within a brick.
3. Permeability to air and water.
4. The flow of air through two members in series.
5. Mean effective radius and number of capillaries.
6. Saturation coefficient.
7. Effect of freezing and thawing on the saturation coefficient.
8. Resistance to failure by repeated freezing and thawing.

III. METHODS AND APPARATUS

1. PREPARATION OF THE SPECIMENS

The bricks were ground to a thickness of approximately 2 1/16 in. to remove any hard or "glaze-like" skin formed during the kiln treatment and to obtain approximately parallel faces for the permeability determinations.

[3] The sealed pores were included in the solid volume, inasmuch as they are inactive with respect to permeability and water absorption.

2. POROSITY

(a) DEFINITION OF POROSITY

The porosity [4] is defined by the difference between the bulk volume, V_b, and the solid volume, V_s, expressed as a percentage of the bulk volume according to the equation

$$V=\frac{100(V_b-V_s)}{V_b} \tag{1}$$

(b) BULK VOLUME

The bulk volume was obtained by means of a mercury volumeter in which the volume of the specimen was determined from the weight and density of the mercury displaced. The volumeter is similar in principle to one frequently used for measuring volumes of small laboratory specimens, but was modified in design to be suitable for determining volumes up to and including specimens the size and shape of a brick. The specimen holder (fig. 1) is provided with points which make contact with the brick in such a manner that the brick is immersed with two faces vertical and four at 45 degrees to horizontal in order to prevent entrapping air.

Before the specimen is introduced, the system is balanced by adding sufficient counterweight to immerse the holder and maintain it with the balancing mark contacting the surface of the mercury. The holder with its supporting frame is then raised, the specimen inserted, and sufficient weight added to the pan to immerse the specimen with the balancing mark again contacting the surface of the mercury.

The sensitivity of the mercury volumeter is of a high order, inasmuch as the addition of 0.1 g, after the system is balanced, sinks the balancing mark below the surface of the mercury.

The bulk volume of the brick was calculated from the equation

$$V_b=\frac{(G+g)}{D}, \tag{2}$$

where V_b is the bulk volume (cm^3), G is the weight (grams) added to the pan, g is the weight (grams) of the specimen in air, D is the density (grams per cubic centimeter) of mercury at the temperature of the determination.

(c) SOLID VOLUME

The solid volume was determined by means of a gas-expansion volumenometer. After consideration of various types recommended by different investigators, a volumenometer was constructed which operates on the principle of a porosimeter described by McGee.[5] It is simple in design, requires no vacuum pump, and is rapid in operation. In the design of the volumenometer (fig. 2), a number of refinements

[4] Two methods generally employed for the determination of porosity are: (1) Saturating the specimen with a liquid and expressing the porosity in percentage of the ratio of the volume of liquid absorbed to the bulk volume of the specimen; (2) using the gas-expansion method for determination of the solid volume and expressing the porosity as the difference between bulk and solid volumes in percentage of the bulk volume. The porosity values obtained by the liquid-saturation method may be appreciably lower than those obtained by the gas-expansion method, because of inability of the liquid to completely fill the open pores, more especially those of microscopic size. Washburn and Bunting (see *Porosity; VI. Determination of porosity by the method of gas expansion*, J. Am. Ceram. Soc. **5**, No. 2 (1922), table IX, p. 127) have shown that the porosity obtained by the water-saturation method for a stoneware clay fired to cone 10 was 0.8 percent less than that obtained by the gas-expansion method, and for a red-burning clay fired to cone 03 the porosity was 5.4 percent less than that obtained by the gas-expansion method. The gas-expansion method appears to be preferable and, therefore, was used in this investigation for the porosity determinations.

[5] *Several gas expansion porosimeters*, J. Am. Ceram. Soc. **9**, No. 12, 817 (1926).

were introduced to facilitate operation and to make possible readings of a comparatively high degree of accuracy. The volume of the specimen chamber, including that of the connecting tube up to the mark B, was determined by means of four chromium-plated steel standardizing blocks [6] whose combined volume is 1,042.1 cm^3. The volume of the chamber (representing the average of 20 determinations) is 1,451.8 cm^3, and the volume of the expansion bulb (between marks B and D) is 244.0 cm^3.

The manometer is made of 8-mm-bore glass tubing which gives menisci of sufficiently flattened surfaces so that good check readings are obtainable. The scale for reading the mercury height, h, is graduated in millimeters on a mirror by means of which readings can be made (with the aid of a reading glass) to approximately ± 0.1 mm. A chain counterbalance, G (fig. 2), is provided for ease of operation in raising and lowering the mercury bulb, and the supporting clamp for holding the mercury bulb is provided with a vernier for adjusting the mercury height at the leveling marks.

With the stopcock open to atmospheric pressure, H (mm Hg), the mercury bulb is raised until the two menisci are at the level B (fig. 2). The stopcock is then closed and the mercury bulb is lowered until the meniscus on the right is at the level D. The initial volume of the chamber, A, minus the volume of solids in the brick ($1451.8-V_s$) is thereby increased by the volume (244.0 cm^3) of the expansion bulb, C, while the pressure is decreased by h (mm Hg, corrected to correspond to H). Since the product of pressure and volume is constant,

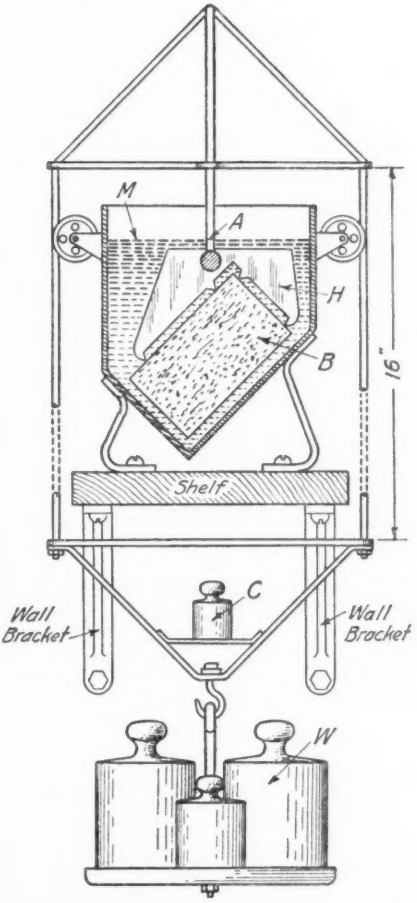

FIGURE 1.—*Sectional view of mercury volumeter for determination of bulk volume.*

A, balancing mark; *M*, mercury; *H*, specimen holder *B*, specimen; *C*, counterweight; *W*, balancing weight.

$$H(1451.8-V_s)=(H-h)(1451.8-V_s+244.0)$$

or

$$V_s=1695.8-244.0\frac{H}{h}. \quad (3)$$

[6] The chromium-plated blocks and the air-expansion bulb were calibrated for volume by the National Bureau of Standards, Division of Weights and Measures.

(d) POROSITY OF DIFFERENT SECTIONS OF A BRICK

The porosity as determined according to eq 1 represents the mean porosity of a brick as a unit. The porosity, however, differs at various points within a brick, which may be due to uneven distribution of moisture in preparing the clay for forming, the manner of forming, variable pressure during forming, or to uneven temperature of burning. In order to show the amount of variation within a specimen, porosity determinations were made on sections cut from each of five bricks. These included soft-burned, medium-burned and hard-burned, stiff-mud bricks and medium-burned and hard-burned dry-press bricks. Each brick was sawed into nine equal sections (fig. 3).

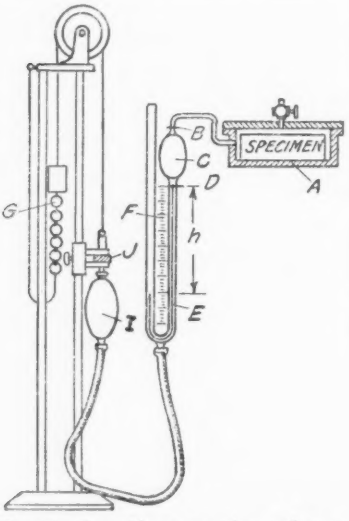

FIGURE 2.—*Air expansion volumenometer for determination of solid volume.*

A, specimen chamber; *B* and *L*, leveling marks; *C*, expansion bulb; *E*, manometer; *F*, mirror graduated scale; *G*, counterbalance; *I*, mercury bulb; *J*, leveling vernier.

3. PERMEABILITY

(a) DEFINITION OF PERMEABILITY

Permeability as used in this report is defined as the volume of fluid in cubic centimeters transmitted per second through each square centimeter of the surface of a plate of the material 1 cm thick when the difference in pressure between the two faces of the plate is 1 g/cm^2; that is, it is the rate of flow through a 1-cm cube, with unit pressure difference across the cube. It is defined by the equation

$$f \text{ or } f' = QT/AP, \tag{4}$$

where

Q=number of cubic centimeters of fluid passing per second through the brick.

P=pressure difference across the brick in grams per square centimeter.

A=average cross-sectional area in square centimeters over which flow takes place.

T=thickness of the brick, in centimeters, through which transmission of the fluid occurs.

For air, the permeability is designated by f, and that for water by f'.

(b) APPARATUS FOR DETERMINING AIR PERMEABILITY

The permeameter for determination of air permeability is similar to that described by Ketcham, Westman, and Hursh.[7] As a precautionary measure to prevent possible obstruction to flow, the clamps which were used for holding the specimen against the felt seal were replaced by a weight (fig. 4) resting on a platform, the four legs of

[7] The Measurement of the Permeability of Ceramic Bodies, Univ. of Ill. Eng. Exp. Sta. Bull. No. 50, p. 14–21 (Aug. 17, 1926).

which were pointed at the lower ends for making contact with the brick. The weight also insures a constant load on the felt seal. A kerosene manometer, *F*, was added for measuring those pressure drops across the specimen which were too high for measurement by means of the inclined manometer, *E*.

Air maintained at a constant pressure by the pressure regulator, *H* (fig. 4), is forced through a capillary flowmeter in series with the specimen and is discharged at atmospheric pressure. The calibrated manometer, *G*, of the flowmeter indicates the rate of flow through the specimen at a pressure difference shown by the manometer *F* (or *E*).

The capillary flowmeter was provided with four interchangeable capillaries of different bores for determination of rates of flow over a wide range of permeability. The capillaries were calibrated for air flow in cubic centimeters per second by means of the "standardizing flowmeter" designed by F. T. Carson.[8] The calibrations of the capillaries were made over pressures within safe limits below those causing turbulent flow.

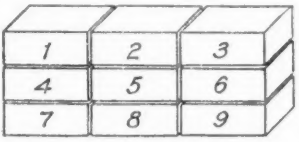

FIGURE 3.—*Method of sectioning brick for determination of variation in porosity.*

(1) *Air transmission of two members in series.* When the air permeabilities of two different bricks are f_1 and f_2, respectively, and their respective thicknesses T_1 and T_2, then the air transmission, or "air conductance," of the two bricks in series may be calculated by an equation analogous to that used for determining the electrical conductance of two conductors in series. In brick 1, the air transmission is the air flow in cubic centimeters per second per square centimeter with pressure difference of 1 g/cm^2, or f_1/T_1. Likewise, in brick 2, the air transmission is f_2/T_2.

When two electrical conductors are joined in series, the conductance through the whole is the product of the two conductances, C_1 and C_2, divided by their sum—that is, $(C_1C_2)/(C_1+C_2)$. By analogy, we write f_1/T_1 instead of C_1 and f_2/T_2 instead of C_2, giving the equation

$$F=\frac{f_1f_2}{f_1T_2+f_2T_1}, \tag{5}$$

where F is the air transmission through the two bricks in cubic centimeters per second per square centimeter for a pressure difference of 1 g/cm.[2]

As a means of determining the agreement between calculated and experimental results for obtaining the air transmission, F, for units composed of different combinations of two members in series, tests were made using five different members to form the units, each member having an area of 8 1/16 by 3 3/4 in. and of different thicknesses. Two of the members were cut from a red dry-press brick, one from a buff dry-press brick, and two were plaster-of-paris slabs. The permeabilities were first determined separately for each member, and those for the different combinations were then determined by means of the assembly shown in figure 5, representing a cross-sectional view of the permeameter box and two members in series forming a unit.

[8] *A sensitive instrument for measuring the air permeability of paper and other sheet materials*, BS J. Research 12, 578 (1934) RP681.

(c) APPARATUS FOR DETERMINING WATER PERMEABILITY

The permeameter designed for the determination of water permeability is shown schematically in figure 6. This apparatus is also suitable for measuring air permeability when the water is emptied from tank *D* and air driers *Z* are connected. The specimen, *A*, is sealed in the permeameter box, *B*, by means of a rectangular rubber tube, *C*, inflated to a pressure [9] of 70 lb/in².

For water permeability determinations, the tank, *D*, is filled with water and air pressure applied to produce flow of water through the specimen. The number of cubic centimeters of water flowing through the specimen per second is obtained by determining the number of cubic centimeters of air required for its displacement.

The pressure regulator, *E*, consisting of two cylinders connected to a 40-gal tank, *F*, is provided with a small and sensitive cut-off valve, *G*, actuated by a float operating in kerosene. With the valve, *H*, closed, air is admitted to the accumulator, *I*, through two pressure reducers, *J* and *K*. Valves *L* and *M* are closed and *N*, *O*, *P*, and *R* are opened. The pressure is allowed to build up in the pressure regulator and tank, *F*, until the desired working pressure as indicated by the pressure gage, *S*, is obtained. Valves *R* of the regulator and *P* of the by-pass are then closed, allowing the air to pass through the capillary, *T*, of the flowmeter and into the water tank. The air pressure is then regulated by the pressure reducer, *K*, so that approximately two bubbles of air per second escape through water in the glass indicator, *U*. After the pressure has been properly adjusted, it remains substantially constant and the system is allowed to stand until the arms of the manometer, *V*, come to rest at the same level. *H* is then opened to allow water to flow through the specimen.

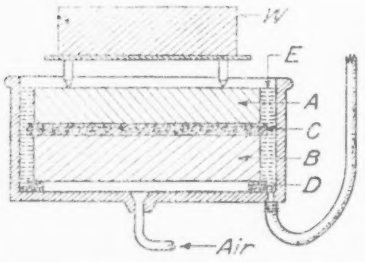

FIGURE 5.—*Method of sealing specimens for determination of the air conductance of a unit composed of two members in series.*

A and *B*, two members composing the unit; *C*, felt sealing pad; *D*, felt sealing gasket; *E*, mercury seal; *W*, sealing weight.

The capillary of the flowmeter was calibrated in cubic centimeters per second of air flow by means of the standardizing flowmeter.[10] The gage, *W*, is provided with a millimeter scale to indicate the height of water in the tank above the water level above the specimen.

Two manometers are provided for determining the drop in pressure across the specimen. These are a kerosene manometer, *X*, for determining flow pressures up to 120 g/cm², (equivalent to about 9 cm of mercury) and a mercury manometer, *Y*, for pressures up to 1,615 g/cm². The flow pressure is the sum of the pressure obtained by means of the manometer reading and the pressure of the waterhead as indicated by the water gage, *W*.

[9] Air-permeability determinations, when made on several specimens with the mercury seal and also with the inflated rubber seal, checked at a sealing air pressure of about 70 lb/in². The walls of the sealing tube were very thick, which required a pressure of 70 lb/in.² to produce the same sealing effect as that of the mercury.

[10] See footnote 8, p. 717.

Research Paper 1349
Journal of Research of the National Bureau of Standards

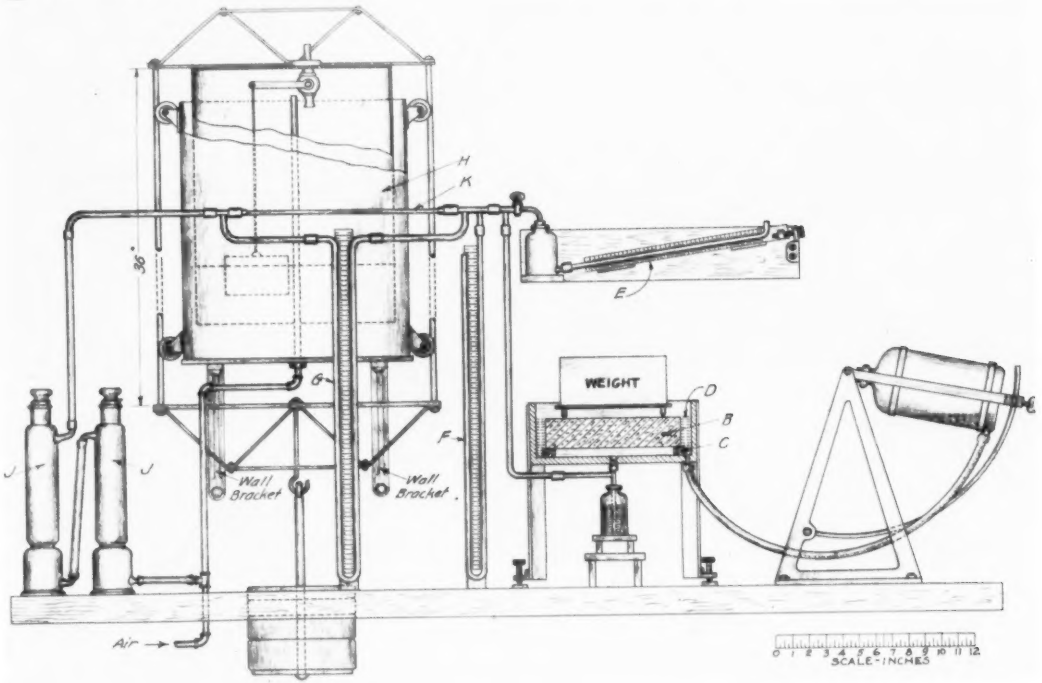

FIGURE 4.—*Air permeameter.*

B, specimen; *C*, felt seal; *D*, mercury seal; *E*, inclined manometer; *F*, kerosene manometer for determination of pressure drop across the specimen; *G*, flowmeter manometer; *H*, combination accumulator and pressure regulator; *J,J*, drying towers; *K*, interchangeable flowmeter capillary.

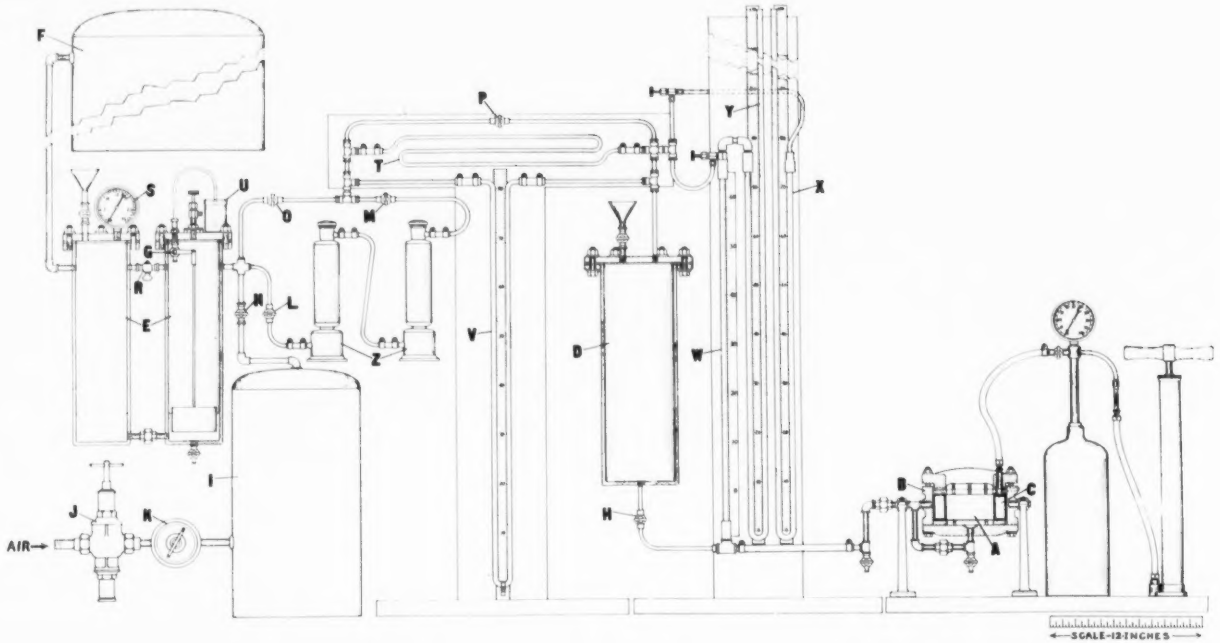

FIGURE 6.—*Water permeameter.*

Described on p. 718

4. DETERMINING MEAN EFFECTIVE RADIUS AND NUMBER OF CAPILLARIES

The volume rate of discharge of a gas passing through a porous earthy material is proportional to the pressure difference between the parallel planes between which the gas travels. The behavior is, therefore, analogous to the flow through a long cylindrical capillary passage which can be described by the Poiseuille equation.

Although the Poiseuille equation cannot be applied to the actual brick, one can, however, visualize an imaginary brick, the pore system of which is made up of N identical, parallel, uniformly distributed, cylindrical capillary passages with a radius r, and length T, which has the same air permeability as the actual brick. To this imaginary brick, one can apply the Poiseuille equation and develop expressions for r and N which serve a useful purpose in correlation with the experimental data, even though the calculated r values are probably somewhat too small and the N values too large, since the lengths of the actual air passages must be greater than T in the actual brick. The equations for evaluating r and N are substantially the same as those employed by Clews and Green.[11] When determined on the basis of a unit cube (1 cm^3) these equations are:

$$r=0.012(f/V)^{1/2} \tag{6}$$

$$N=21.7(V^2/f) \tag{7}$$

where

r=mean effective capillary radius in centimeters.
N=number of capillaries of radius r, per square centimeter of surface.
f=air permeability (as defined by eq 4).
$V=100(\pi r^2 N)$, the percentage of porosity. (8)

5. FREEZING AND THAWING TESTS

(a) PROCEDURE

Inasmuch as the method employed in making the freezing and thawing tests has a bearing on the number of freezing and thawing cycles required to cause failure of the bricks, a method was adopted which would give comparable results and reduce the time element to a minimum.

The bricks were first partially saturated by immersion for 48 hours in water at room temperature, after which each cycle consisted in freezing the bricks standing on edge in ¼ in. of water, then thawing by immersion for 4 hours in water at room temperature. No opportunity was allowed for the bricks to dry between cycles, and only six cycles per week were completed, since the bricks were allowed to remain in the freezing chamber over Sundays.

(b) SATURATION COEFFICIENT

The percentage volume of water, W, absorbed by the brick at each step in the above process is determined by removing the brick from the water, blotting the surface with a towel, and determining the weight of water absorbed, then converting the weight into percentage

[11] F. H. Clews and A. J. Green, *The permeability of refractory materials to gases, Part I.* Trans. Eng. Ceram. Soc. 32, 317 (1932-3).

FIGURE 6.—*Water permeameter.*
Described on p. 718.

by volume of the bulk volume of the brick. The saturation coefficient, S, is then defined by the equation

$$S=W/V, \tag{9}$$

in which W is the volume in percent of water absorbed and V has the same significance as in the previous equations. The saturation coefficient obtained by partial saturation of the brick by 48 hours' immersion at room temperature is herein termed the "initial" saturation coefficient and denoted by S_1.

(c) INCREASE IN SATURATION COEFFICIENT WITH REPEATED FREEZING AND THAWING

Since the volume of water absorbed increases with successive thawings by immersion in water, the saturation coefficients of the bricks at failure were determined on the basis of their original pore volumes for comparison with their respective initial saturation coefficients. Also, as a means of determining the rate of this increase, the saturation coefficients of the members of series *D* and *E* were determined for each freezing cycle after the bricks had thawed and attained room temperature.

IV. RESULTS AND DISCUSSION

1. VARIATION IN POROSITY WITHIN A BRICK

The percentage porosities obtained on the different sections of bricks *F5*, *G8*, *H9*, *J10*, and *K3* are given in tables 2 and 3. The data obtained on the sections indicate that there is no definite correlation among the specimens as to location of sections of highest, medium, and lowest porosities. The difference between the average porosity obtained on the basis of the total bulk and solid volumes of the sections for each brick, and the original porosity determined before cutting may be due to materials lost in the cutting. The spread in the variation of the porosities for the bricks ranged from 11.6 percent in *J10* to 48.4 percent in *G8*.

Obviously, the tendency of a brick is to fail at its weakest point when subjected to freezing and thawing tests. Therefore, variation in porosity evidently exercises an influence on the resistance to frost action inasmuch as permeability, saturation coefficient, and the values calculated for the effective size and the number of capillaries are partly dependent on porosity.

TABLE 2.—*Variation in porosity, V, in different sections of the bricks*

Section number [1]	Brick number				
	F5	*G8*	*H9*	*J10*	*K3*
1	28.2	17.3	13.1	24.6	31.9
2	28.6	20.6	14.6	24.7	30.0
3	29.4	21.6	13.8	24.3	33.7
4	31.6	22.2	12.1	23.5	31.1
5	31.6	22.4	11.6	23.2	28.6
6	31.3	27.7	13.6	24.9	27.6
7	27.8	20.6	11.9	24.9	30.0
8	27.1	20.8	12.9	26.0	28.8
9	27.0	20.8	11.7	24.8	28.2
Average V	29.2	21.6	12.8	24.5	30.0
Original V	29.6	20.6	12.5	24.8	30.0
Spread [2]	15.9	48.4	23.4	11.6	20.3

[1] See figure 3.
[2] Percentage difference between maximum and minimum porosities of the different bricks.

TABLE 3.—*Ranking position of porosities of the corner, middle, and center sections*

Sections	Brick number				
	F5	*G8*	*H9*	*J10*	*K3*
Average, 4 corners	Low	Low	Medium	Medium	High.
Average, 4 middles	Medium	High	High	High	Medium.
Center	High	Medium	Low	Low	Low.

2. PERMEABILITY TO AIR AND WATER

The movement of air through the bricks conformed to the laws of capillary flow in all cases except for brick *H2*, in which the permeability decreased with increase in pressure difference, conforming neither to capillary flow nor to flow through orifices, but apparently affected by a combination of the two. However, constant water permeability values were not obtained, inasmuch as consecutive determinations under continuous flow showed an increase in permeability with time of flow for some bricks, while for others permeability decreased with time of flow.

The water permeabilities determined consecutively over a period of time for the different members [12] of series *F*, *G*, *H*, *J*, and *K* are presented in table 4, arranged in sequence of their *r* values. The first reading of the manometers for obtaining the initial permeability was made after the brick became thoroughly wetted and covered with a uniform layer of approximately 2 mm of water, which required about 5 to 25 minutes for bricks ranging from high to low permeabilities, respectively. The permeabilities given in the table represent data obtained from readings made hourly after the first reading for all bricks except those of series *J* and *K*, where the readings were made at 20-minute intervals.

Table 4 shows that the specimens exhibit change in water permeability with time. Increase in water permeability with time of flow occurs with all members of series *F* and *G* except *G2*, and decrease with time for *G2* and all members of series *H*, *J*, and *K* with the possible exception of *H5*, the permeability of which is substantially constant.

Bartell,[13] in reporting his results on the water permeability of porcelain disks, attributes the decline in water permeability to progressive clogging by small particles mechanically broken off and carried into the pores by movement of the water. Muskat [14] considers that:

> "One very common cause of the plugging of a porous medium upon continuous flow of a liquid, as water, through it, is the evolution of air or gas dissolved in the liquid. The gas becomes entrapped in the pores of the medium in the form of small bubbles and may decrease the resultant permeability of the liquid to a small fraction of its original value."

Since the tests herein reported were made with nondeaired water at room temperatures, Muskat's explanation appears logical for those bricks of diminishing permeability.

[12] No water permeabilities were determined for series *D* and *E* nor for bricks *F1*, *H2*, and *H7*.

[13] F. E. Bartell, *The permeability of porcelain and copper ferrocyanide membranes*, J. Phys. Chem. **15**, 664 (1911).

[14] M. Muskat, The flow of homogeneous fluids through porous media, p. 90 (McGraw-Hill Book Co., Inc., New York, N. Y., 1937).

TABLE 4.—*Relation of mean effective capillary radius, r, to the water permeability, f', of bricks*

Brick number	Reading					
	1st $f' \times 10^7$	2d $f' \times 10^7$	3d $f' \times 10^7$	4th $f' \times 10^7$	5th $f' \times 10^7$	r
						Microns
F3	47	50	57	64	66	0.95
F5	49	53	62	67	75	.96
G7	70	98	122	139		1.27
F4	58	68	69	87	88	1.29
G4	75	97	121	141	171	1.33
G1	100	134	153	173	186	1.46
G10	72	82	88	102	106	1.49
F6	70	71	79	81	84	1.54
G11	72	85	98	116	129	1.55
G5	75	84	98	107	125	1.63
F2	70	74	80		81	1.65
G9	106	128	164	194		1.69
G8	97	133	165	179		1.75
G6	83	90	100	113	121	1.76
H5	78	75	77	79	78	1.82
G3	163	212	255	276	281	1.89
F7	110	107	124	122	129	1.98
G2	258	225	207	214	218	2.36
H4	140	89	82	80	79	2.66
H3	175	134	133	123	122	2.81
H8	209	162	131	128	119	2.97
K5	951	902	863	845	869	3.00
H6	193	181	178	168		3.05
K2	1,160	1,060	1,060	1,040	1,030	3.14
K4	1,040	969	948	943	938	3.16
K8	1,100	1,030	1,020	1,010	1,020	3.21
K3	1,010	927	909	894	881	3.23
K7	1,140	1,060	1,030	1,060	1,010	3.25
K6	1,150	1,060	1,060	1,040	1,050	3.30
H1	219	173	169	164		3.46
K9	1,410	1,330	1,280	1,270	1,280	3.48
K10	1,320	1,250	1,200	1,190	1,190	3.50
H9	294	240	215	201	220	3.50
H10	238	190	178	167	158	3.51
K1	1,620	1,570	1,590	1,570	1,590	3.52
J7	1,280	1,170	1,170	1,140	1,110	3.88
J3	2,120	1,880	1,800	1,740	1,710	3.94
J6	1,540	1,400	1,380	1,310	1,300	3.97
J8	1,550	1,470	1,450	1,420	1,380	4.00
J9	1,560	1,470	1,440	1,450	1,440	4.05
J2	1,610	1,550	1,500	1,490	1,470	4.17
J4	1,840	1,620	1,570	1,590	1,520	4.26
J10	1,710	1,600	1,520	1,500	1,470	4.32
J5	2,110	1,890	1,810	1,830	1,790	4.38
J1	2,110	2,040	1,980	1,900	1,920	4.49

Increase in water permeability with time, however, occurred with bricks of the *F* and *G* series (except *G2*), and data of this nature have not been previously recorded to the authors' knowledge. The *r* values of these bricks in which permeability increased are smaller than those in which permeability decreased under continuous flow; therefore, it would seem that clogging of the pores by small particles or by air would be more pronounced and cause a decrease rather than an increase in permeability. Progressive solution of the walls of the capillaries with consequent increase in their cross sections would explain such behavior, but the specimens are not of such a nature that solution would be probable.

The average size of r appears to effect a separation between increase and decrease in the rate of water permeability. With the exception of specimen *H5* (where permeability is about constant), all bricks having r's less than 2 microns (table 4) gave increase in water permeabilities with time. Conversely, all bricks having r's greater than 2 microns exhibited decrease in permeability.

According to Poiseuille's equation, the ratio of the permeability of one fluid to that of another is inversely proportional to their respective viscosities. Therefore, when n' and n are the respective viscosities of water and air, f the permeability of air, and f' that of water, then

$$n'/n=f/f'=a, \text{ and } (f/f')/a=1. \tag{10}$$

Since the water permeability of a brick is continuously changing under continuous flow, its value is very indefinite. Mills[15] noted the lack of agreement between the air and water permeabilities of bricks and states that this is probably explained by the "heterogeneous nature of the products and, as a consequence, the interrupting effects of surface tension."

As a means of determining the relation between the ratio of the air to the initial water permeabilities and r, the f/f' and also the $(f/f')/a$ values (where $a=55.5$) were determined for the average air permeabilities and the average initial water permeabilities for each of the *F*, *G*, *H*, *J*, and *K* series. The results are shown in table 5, arranged in sequence of their respective r values. The data, though confined to rather narrow limits, indicate that f/f' is decreasing toward the value 55.5 and $(f/f')/55.5$ toward unity as r is increasing.

TABLE 5.—*Relation between the ratio of air to water permeability and the capillary radius*

Series	Number of bricks	f/f'	$(f/f')/55.5$	r
F	6	572	10.3	1.37
G	11	481	8.7	1.64
H	10	410	7.4	2.97
K	10	184	3.3	3.28
J	10	169	3.0	4.13

From the data reported by Mills [16] on air and water permeabilities of 12 miscellaneous bricks, the $(f/f')/55.5$ values were determined. They show a range from 27.4 to 0.8. The latter value indicates that the water permeability determined for one brick was greater than that of its air permeability.

The data for the water permeabilities, however, were calculated by Mills from the readings made "when the flow had reached a steady rate" and, therefore, they do not represent initial permeabilities.

As pointed out by Muskat,[17] air dissolved in water produces erratic results in water-permeability tests. Whether the data here reported

[15] E. O. Mills, *The permeability to air and to water of some building bricks*, Trans. Eng. Ceram. Soc. **33**, 210 (1933–4).
[16] See footnote 15.
[17] See footnote 14, p. 721.

represent the actual water permeabilities of the bricks or whether they are affected by uncontrolled factors in the test method remains to be determined.

3. FLOW OF AIR THROUGH TWO MEMBERS IN SERIES

The permeabilities determined separately for the members are given in table 6. The permeabilities of the units calculated according to eq 5 and those determined experimentally are given in table 7, where it is seen that the differences between the experimental and calculated permeabilities (column 4, table 7), which may be charged to experimental error and resistance to flow through the felt pad, C (fig. 5) range from 0 to 0.49 percent. These differences are so small as to be negligible.

TABLE 6.—*Thickness and permeability of the members composing the units*

Member	Kind	Thickness, T	Air permeability, f
		cm	
1	Section of red brick	1.59	0.03139
2	do	2.96	.03358
3	Section of buff brick	2.59	.01304
4	Plaster slab	3.56	.01048
5	do	0.95	.00668

TABLE 7.—*Comparison of the calculated and measured air transmission values of different units composed of two members in series*

Members forming units [1]	F Calculated	F Determined	Difference
			Percent
1 and 2	0.00719	0.00718	0.14
1 and 3	.00404	.00402	.49
1 and 5	.00518	.00517	.19
2 and 5	.00434	.00432	.46
1 and 4	.00256	.00256	0
3 and 5	.00293	.00292	.10

[1] See table 6.

4. EFFECT OF FREEZING AND THAWING ON THE SATURATION COEFFICIENT

The saturation coefficients determined after each cycle of freezing and thawing for the members of the D and E series, when plotted against the corresponding cycles of freezing and thawing up to 60 cycles, or until the bricks failed, produced graphs which are typical of that shown in figure 7 for brick *D9*. The curve can be represented fairly well by an equation of a hyperbola which, within the limits of the data, may be expressed by the empirical equation

$$S=a-\frac{K}{b+C}, \tag{11}$$

where S is the saturation coefficient, C the cycle of freezing and thawing, and a, b, and K are constants which are different for each brick.

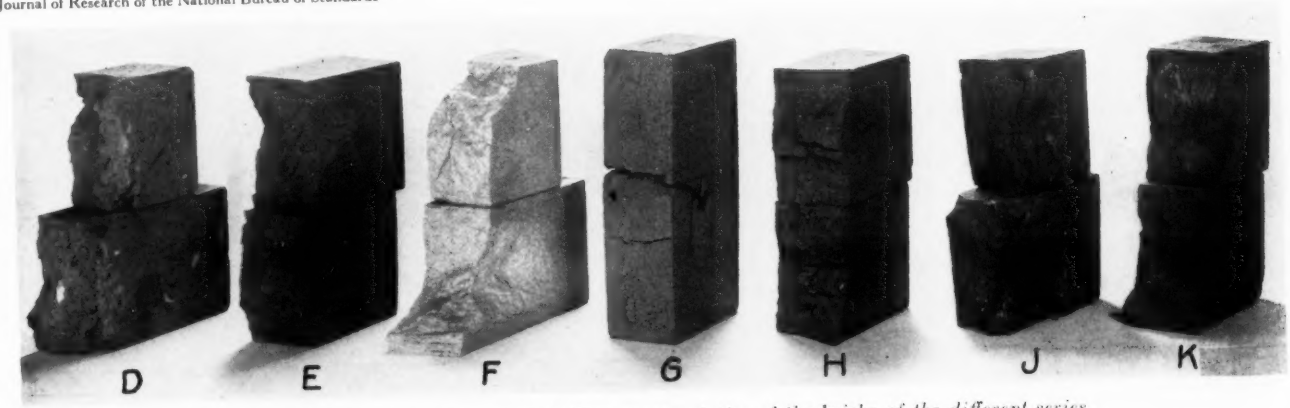

FIGURE 8.—*Typical fractures at failure representative of the bricks of the different series.*

The approximate values of the constants representing the curve for *D9* are: $a=1.35$, $b=160$, and $K=105$.

Although the extrapolation of a curve outside of the field covered by the data may not be justifiable, it is often helpful in understanding the significance of certain constants obtained from the data. Asymptote a represents the upper limiting value of S, attainable if the brick were to withstand an infinite number of freezing and thawing cycles. Bricks which attained S values greater than unity at failure are seen in the soft-burned bricks of the *G* series (column 7, table 11) and in the hard-burned bricks *J4* and *J7* (column 7, table 12). These bricks were distinctly laminated (see fig. 8), the laminations evidently functioning as laminar capillaries, inasmuch as their V, f, r, N, and S_1 values appear to be about normal. The gradual widening of the laminations during successive freezing and thawing evidently was

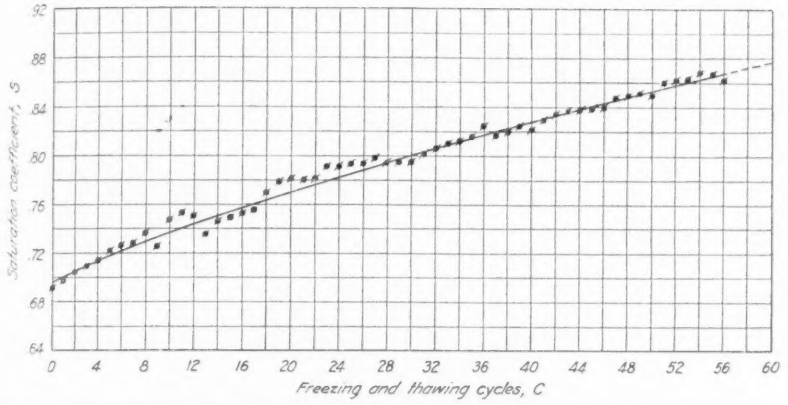

FIGURE 7.—*Relation between freezing and thawing cycles and saturation coefficient of brick D9.*

responsible for their ability to contain more water at failure than their initial pore volumes.

5. RELATIONS OF POROSITY, PERMEABILITY, EFFECTIVE CAPILLARY RADIUS, NUMBER OF CAPILLARIES, AND SATURATION COEFFICIENT TO THE NUMBER OF FREEZING AND THAWING CYCLES CAUSING FAILURE OF BRICKS

In bricks made of the same clay which are substantially free from defects, it is well known that hardness and mechanical strength increase and porosity decreases with increase in burning temperature, within the temperature ranges of commercially operated kilns. The data on various properties of the several series of bricks presented in tables 8 to 14 suggest some relation within each of the series between porosity and the other properties. There is some evidence that as porosity decreases in each series there is an increase in r, f, and C and a decrease in S_1 and N, although in some cases the correlation seems poor—notably in the *H*, *J*, and *K* series. This is, however, more apparent than real because of insufficient spread of the data for each of the three series from which satisfactory correlations can be made. Although the C values of the *H* series show considerable spread, there is very

little difference in the values of V among the different members, indicating that the bricks had received about the same heat treatment during the firing process.

TABLE 8.—*Data on series D*

Specimen number	Porosity, V	Air permeability, $f\times10^5$	Capillary radius, r	Number of capillaries, $N\times10^{-4}$	Saturation coefficient 48 hours' immersion, S_1	Saturation coefficient at failure, S	Freezing-thawing cycles at failure, C
	Percent		*Microns*				
D4	41.8	204	0.85	1,850	0.753	0.768	2
D6	41.9	214	.87	1,780	.769	.765	2
D10	40.7	335	1.10	1,070	.748	.785	4
D2	39.5	290	1.04	1,170	.737	.818	27
D7	36.2	453	1.36	628	.683	.834	36
D3	36.5	461	1.36	640	.715	.870	36
D8	37.2	404	1.26	743	.685	.824	37
D6	37.6	366	1.20	837	.700	.856	39
D9	38.4	537	1.43	594	.690	.862	56
Average	38.9	363	1.16	1,030	0.720	0.820	27

TABLE 9.—*Data on series E*

Specimen number	Porosity, V	Air permeability, $f\times10^5$	Capillary radius, r	Number of capillaries, $N\times10^{-4}$	Saturation coefficient 48 hours' immersion, S_1	Saturation coefficient at failure, S	Freezing-thawing cycles at failure, C
	Percent		*Microns*				
E3	18.2	44.9	0.60	1,160	0.721	0.870	80
E2	19.3	61.9	.69	1,300	.751	.908	83
E1	19.4	60.6	.68	1,340	.767	.923	86
E5	13.8	39.1	.65	1,050	.630	.771	92
E6	12.9	48.2	.74	751	.590	.762	103
E7	13.4	47.6	.72	820	.613	.769	105
E4	15.3	62.5	.77	814	.669	.861	107
E8	10.6	49.4	.83	495	.533	.898	454
E9	10.6	81.7	1.07	295	.524	----------	(1)
E10	8.0	67.6	1.11	206	.440	----------	(1)
Average [2]	15.4	51.8	.71	966	.659	.845	139

[1] Bricks *E9* and *E10* were still sound after 680 cycles.
[2] *E9* and *E10* excluded.

TABLE 10.—*Data on series F*

Specimen number	Porosity, V	Air permeability, $f\times10^5$	Capillary radius, r	Number of capillaries, $N\times10^{-4}$	Saturation coefficient 48 hours' immersion, S_1	Saturation coefficient at failure, S	Freezing-thawing cycles at failure, C
	Percent		*Microns*				
F7	27.0	721	1.98	231	0.837	0.944	15
F3	30.2	186	0.95	1,090	.810	.852	38
F4	31.0	353	1.29	613	.834	.976	41
F6	24.6	399	1.54	333	.747	.906	51
F2	24.8	461	1.65	307	.743	.835	52
F1	19.2	344	1.62	237	.654	.838	55
F5 [1]	29.6	188	.96	1,050	.816	----------	----------
Average [2]	26.1	411	1.50	468	.771	.892	42

[1] Used for determination of variation in porosity.
[2] *F5* excluded.

TABLE 11.—*Data on series G and H*

Specimen number	Porosity, V	Air permeability, $f\times10^6$	Capillary radius, r	Number of capillaries, $N\times10^{-4}$	Saturation coefficient 48 hours' immersion, S_1	Saturation coefficient at failure, S	Freezing-thawing cycles at failure, C
	Percent		*Microns*				
G9	29.2	550	1.66	335	0.877	1.035	45
G11	26.1	427	1.55	347	.860	1.054	52
G5	22.5	409	1.63	268	.845	1.045	54
G2	25.5	970	2.36	145	.852	0.993	54
G3	24.2	593	1.89	215	.900	1.151	55
G6	23.5	495	1.76	242	.838	1.016	57
G10	27.8	416	1.49	395	.829	1.067	61
G7	28.6	313	1.27	568	.869	1.005	64
G4	28.7	346	1.33	515	.880	1.023	64
G1	25.9	376	1.46	386	.870	1.128	90
G8 [1]	20.6	428	1.75	215	.809	----	----
Average [2]	26.2	489	1.64	341	.862	1.052	60
H5	12.3	277	1.82	117	.552	.899	63
H4	13.3	637	2.66	60	.592	.910	80
H8	13.6	813	2.97	49	.623	.921	88
H3	13.7	737	2.81	55	.591	.896	92
H6	12.5	793	3.05	43	.617	.794	93
H10	12.4	1,040	3.51	32	.605	.986	184
H1	12.3	1,010	3.46	33	.580	.798	247
H2	11.8	----	----	----	.550	.841	310
H7	12.2	1,460	4.19	22	.593	.932	314
H9 [1]	12.5	1,040	3.50	35	.588	----	----
Average [2]	12.8	846	3.06	51	.594	.892	145

[1] Used for determination of variation in porosity.
[2] *G8*, *H2*, and *H9* excluded.

TABLE 12.—*Data on series J and K*

Specimen number	Porosity, V	Air permeability, $f\times10^6$	Capillary radius, r	Number of capillaries, $N\times10^{-4}$	Saturation coefficient 48 hours' immersion, S_1	Saturation coefficient at failure, S	Freezing-thawing cycles at failure, C
	Percent		*Microns*				
J3	25.6	2,700	3.94	52.6	0.804	0.945	61
J7	24.5	2,510	3.88	51.8	.760	1.014	63
J1	26.7	3,660	4.49	42.2	.775	.927	63
J6	24.9	2,660	3.97	50.4	.764	.958	67
J8	25.5	2,780	4.00	50.6	.772	.975	93
J9	25.2	2,820	4.05	48.9	.763	.996	101
J4	24.7	3,050	4.26	43.3	.756	1.005	107
J2	24.5	2,900	4.17	45.0	.757	.993	108
J5	25.4	3,320	4.38	42.2	.756	.972	120
J10 [1]	24.8	3,160	4.32	42.2	.753	----	----
Average [2]	25.2	2,930	4.13	47.4	.767	.976	87
K5	29.2	1,800	3.00	103.0	.811	.943	38
K4	28.7	1,960	3.16	91.3	.807	.979	38
K7	29.6	2,130	3.25	89.3	.804	.946	44
K8	30.2	2,120	3.21	93.6	.812	.932	45
K2	30.1	2,020	3.14	97.2	.819	.945	47
K6	28.9	2,140	3.30	84.3	.802	.955	48
K9	31.0	2,560	3.48	81.4	.804	.948	57
K10	29.6	2,460	3.50	77.2	.801	.942	58
K1	30.7	2,590	3.52	78.6	.819	.926	60
K3 [1]	30.0	2,130	3.23	91.8	.817	----	----
Average [2]	29.8	2,200	3.28	88.4	.809	.946	48

[1] Used for determination of variation in porosity.
[2] *J10* and *K3* excluded.

TABLE 13.—*Effect of higher burning temperature of series H over that of series G on the average values of V, f, r, N, S_1, and C*

Burn	Increase			Decrease		
	$f\times10^8$	r	C	V	$N\times10^{-4}$	S_1
		Microns				
Soft, *G*	489	1.64	60	26.2	341	0.862
Hard, *H*	846	3.06	145	12.8	51	.594
Difference	357	1.42	85	13.4	290	0.268
Difference (%)	73.0	86.6	141.7	51.2	85.0	31.1

TABLE 14.—*Effect of higher burning temperature of series J over that of series K on the average values of V, f, r, N, S_1, and C*

Burn	Increase			Decrease		
	$f\times10^8$	r	C	V	$N\times10^{-4}$	S_1
		Microns				
Medium, *K*	2,200	3.28	48	29.8	88.4	0.809
Hard, *J*	2,930	4.13	87	25.2	47.4	.767
Difference	730	0.85	39	4.6	41.0	0.042
Difference (%)	33.2	25.9	81.2	15.3	46.4	5.2

The bricks of both the *J* and *K* series were made of the same kind of clay by the dry-press process and fired in the same kiln. The harder burned bricks of series *J* were selected from near the top courses of the setting of a down-draft kiln in the higher temperature zone, and the softer burned ones of series *K* from near the bottom of the setting in the lower temperature zone.

Bricks of the other five series were selected from lots such as are delivered to the builder. The bricks of each series may have come from different locations in the kiln and, therefore they would have been subjected to different temperatures. Therefore, the data would show greater spread than is shown by either the *H*, *J*, or *K* series.

Bricks of the *G* and *H* series were made of shale by the stiff-mud process at the same plant. They had been graded for the market, the harder bricks of the *H* series coming from the top portion of the kiln and the softer ones of series *G* from the bottom.

Comparing average values of series *G* with those of series *H* (table 13) and those of series *K* with those of series *J* (table 14), it is seen that harder burning has resulted in material reductions in the porosity, number of capillaries, and saturation coefficient, and increases in the air permeability, capillary radius, and cycles of freezing and thawing to cause failure.

The above findings on porosity, air permeability, effective capillary radius, and number of capillaries are in accord with those given in the reports of the following investigators.

Watkins and Butterworth [18] determined the total porosity and the microporosity of a clay fired at four different temperatures from 750° to 1,105° C and report the following results with increase in the firing temperature: "The microporosity decreases much more rapidly than

[18] C. M. Watkins and B. Butterworth, *The absorption of water by clay building brick and some related properties*, Trans. Eng. Ceram. Soc. **33**, 473 (1933–4).

the total porosity at high temperatures. In other words, although the total pore volume is decreasing, the size of the individual pores tends to increase."

Clews and Green [19] in a report on the determination of the air permeability of a number of fire clays fired at eight different temperatures from 200° to 1,400° C, show that " . . . . . the firing procedure involves a continuous increase in pore size, with corresponding but not necessarily proportional decrease in the number of the pores up to the temperature approaching the finishing." Table I of their report shows that the permeability to air increases with increase in firing temperature from 200° to 1,250° C for four groups of fire clays. In one case the increase in the permeability ranged from 0.00097 to 0.0460.

The decrease in porosity and number of capillaries indicates that some pores were filled or sealed and thus were inactive regarding permeability and absorption. The increase in permeability, together with the decrease in number of pores, indicates that the pores eliminated were mostly the smaller pores, or micropores, which were the interstitial cavities formed by the microparticles. These particles are composed mainly of mixtures of minute mineral fragments. From such particles glasses form at lower temperatures than from coarser ones and the reaction proceeds more rapidly for the finer particles; hence the number of small pores is materially reduced.

The increase in permeability with increase in burning temperature, in spite of a decrease in the number of pores, may be due to enlargement of the connecting pore openings because of partial fusion and to a receding of the angular edges of the openings between adjacent pores. The effective capillary radius, r, is increased and the number of capillaries, N, decreased, because f increases and V decreases with increase in burning temperature. (See eq 6 and 7).

The bricks in each series as selected appear to be representative of the range in variation of grades as marketed. Among such bricks there is not only insufficient spread of the data, but uncontrollable factors also, such as laminations and variable porosity, which are contributing factors tending to lower the C values. These are some of the handicaps encountered when dealing with bricks of commercial grade. In the majority of cases, however, the general trend of the data given in tables 8 to 14, inclusive, indicates that the number of cycles of freezing and thawing at failure of bricks increases when the permeability and mean effective capillary radius increase and when the porosity, number of capillaries, and saturation coefficient decrease.

V. SUMMARY

1. Variation in porosity of individual bricks is one measure of their lack of uniform structure and may be a contributing factor affecting their resistance to frost action.

2. There is no definite correlation as to location of lowest, medium, and highest porosities of the sections among the bricks tested. The spread of the differences between maximum and minimum percentage porosities of the different sections of the individual bricks ranged from 11.6 to 48.42 percent.

[19] F. H. Clews and A. T. Green, *The permeability of refractory materials to gases. Part IV. The influence of the firing process on the permeability to air of fire-clay materials*, Trans. Eng. Ceram. Soc., **33**, 485 (1933-4).

3. When the air permeabilities of two bricks are f_1 and f_2, respectively, and their respective thicknesses, T_1 and T_2, then the air transmission, or air conductance, F, of the two bricks in series may be calculated by the equation

$$F=\frac{f_1 f_2}{f_1 T_2+f_2 T_1}.$$

The differences between the calculated and experimental values for F were so small as to be negligible.

4. The average values of the data for the bricks of series G and H and also series K and J indicate that the mean effective capillary radius, the permeability, and number of cycles of freezing and thawing at failure of the bricks increase and the number of capillaries, pore volume, and initial saturation coefficient decrease, as the burning temperature of the bricks is increased.

5. Decrease in pore volume and number of pores as the burning temperature is increased indicates that some of the pores have become filled or sealed and, therefore, inactive regarding permeability and absorption. Increase in mean effective capillary radius and permeability, accompanied by a decrease in the number of pores, indicates that the pores rendered inactive were chiefly the smaller ones originally occurring as microcavities formed by the microparticles. Increase in permeability with the firing temperature must, therefore, result from an enlargement of the larger connecting pore openings, which may be due to partial fusion and receding of the angular edges of the openings between adjacent pores.

6. The air permeabilities were constant with respect to time of flow whereas the water permeabilities varied, increasing for those bricks whose mean effective capillary radii were less than 2 microns and decreasing for those whose radii were greater than 2 microns.

7. The saturation coefficients increased with increase in the number of freezing and thawing cycles, and the graph representing the plot of the two variables can be represented fairly well by an equation of a hyperbola of the form

$$S=a-\frac{K}{b+C},$$

where C is the cycle number of freezing and thawing, S the corresponding saturation coefficient, and a, b, and K are constants for a definite brick but different for different bricks. The constant a indicates that there is an upper limiting value of S for a brick, under the assumption that the brick would withstand (theoretically) an infinite number of freezing and thawing cycles.

8. Repeated freezing, and thawing by immersion, of some bricks may increase their saturation coefficients to values greater than unity, thus indicating that they contain larger volumes of water than their original pore volumes.

9. In bricks substantially free from defects, the general trend of the data indicates that the number of cycles of freezing and thawing to cause failure increases when the air permeability and mean effective capillary radius increase, and when the saturation coefficient, porosity and number of capillaries decrease.

WASHINGTON, September 13, 1940.

U. S. DEPARTMENT OF COMMERCE NATIONAL BUREAU OF STANDARDS

RESEARCH PAPER RP1350

Part of Journal of Research of the National Bureau of Standards, Volume 25, December 1940

STANDARD ELECTRODE POTENTIAL OF SODIUM[1]

By Edgar Reynolds Smith and John Keenan Taylor[2]

ABSTRACT

From measurements of the cell Na(s); NaI (in dimethylamine); Na(0.0651% amalgam) and the cell Na(0.0651% amalgam); NaCl(0.05 or 0.1 *m*), AgCl(s); Ag(s), the standard electrode potential Na(s); Na^+ over the temperature range of 5° to 40° C was obtained with the aid of values of the standard electrode potential of the silver-silver chloride electrode, previously determined by Harned and Ehlers, and of the activity coefficients of solutions of sodium chloride, previously determined at 25° C by Brown and MacInnes. The activity coefficients were corrected to the other temperatures by the use of data on heats of dilution determined by Gulbransen and Robinson. The final results were expressed by the equation

$$E^\circ = 2.71324 + 0.0007532(t-25) + 0.000000688(t-25)^2.$$

Values of changes in free energy, entropy, and heat content accompanying the reactions corresponding to various combinations of the cells were calculated.

CONTENTS

		Page
I.	Introduction	731
II.	Units and standards	732
III.	Materials	736
IV.	Apparatus and procedure	737
V.	Results and discussion	741
VI.	References	746

I. INTRODUCTION

The reaction of the alkali metals with water disturbs the equilibrium conditions necessary for direct measurements of their electrode potentials. An indirect method which overcomes this difficulty depends on the possibility of measuring (a) the potential of a dilute amalgam of the alkali metal with respect to an aqueous solution of its ions and a reference electrode, and (b) the difference in potential between the same amalgam and the pure metal when both are immersed in a nonaqueous conducting solution containing ions of the alkali metal. The nonaqueous solvent must not react with the alkali metal and must dissolve the alkali salt sufficiently to form an electrolytic solution. The success of the amalgam electrode in aqueous solution depends on the lowering of the activity of the metal

[1] Presented before the Division of Physical and Inorganic Chemistry at the 100th Meeting of the American Chemical Society, Detroit, Mich., September 9 to 13, 1940.

[2] This paper contains material from a thesis submitted to the University of Maryland by John Keenan Taylor in partial fulfillment of the requirements for the degree of Doctor of Philosophy. The interest and advice of Prof. M. M. Haring are gratefully acknowledged.

and on the high hydrogen overvoltage of mercury, which inhibits the reaction between the alkali metal and water. The standard electrode potentials of all the alkali metals have been measured by this indirect method. However, these measurements have usually involved the introduction of one or more of the uncertainties caused by the use of liquid junctions, of solutions for which the activities can only be approximated, and of unreliable reference electrodes.

The standard electrode potential of sodium in use at present depends primarily on the value at 25° C obtained 30 years ago by Lewis and Kraus [12] [3] for the nonaqueous cell.

Na(s); NaI(in ethylamine); Na(0.2062% amalgam),

which they combined with a measurement on the aqueous cell

Na(0.2062% amalgam); NaOH(0.2 *N*)|NaCl(0.2 *N*)|
KCl(0.2 *N*)|KCl(1 *N*), HgCl(s); Hg(l).

The calculation of the electrode potential from the emf of this aqueous cell involves corrections for three liquid junctions, the activity of 0.2 *N* sodium hydroxide, and the reference potential of the normal calomel electrode. Lewis and Randall [13] recalculated these corrections and obtained 2.7126 v for the standard electrode potential of sodium with respect to the hydrogen electrode. A more recent recalculation by MacInnes [15], in which the measurement of Lewis and Kraus on the nonaqueous cell is combined with an interpolated value for the cell

Na(0.2062% amalgam); NaCl(0.1005 *m*), HgCl(s); Hg(l),

from the work of Allmand and Polack [1], gives 2.7139 v at 25° C. However, Allmand and Polack place a reproducibility of only 0.001 v on their original measurements, and an interpolation of their results is possibly less precise.

Because of the importance of accurate values of the standard electrode potentials over a range of temperatures for thermodynamic and analytic calculations, a redetermination of some of the older values appears desirable. This paper gives the results of a redetermination of the standard electrode potential of sodium, in which liquid junctions were eliminated and a reliable reference electrode was used. As in the pioneer work of Lewis and Kraus, a nonaqueous and an aqueous cell were used. Dimethylamine, instead of ethylamine, was used as the solvent in the nonaqueous cell because Bent and Swift, Jr. [2], have shown that dimethylamine reacts with sodium much less readily than does ethylamine. The two cells may be represented by

Na(s); NaI(in dimethylamine); Na(amalgam)

and

Na(amalgam); NaCl (0.05 or 0.1 *m*), AgCl(s); Ag(s).

II. UNITS AND STANDARDS

According to computations to be published shortly by C. S. Cragoe, of this Bureau, the value of RT_0 is 2271.16 abs j mole^{-1}. The value of T_0, the temperature of the ice point, is taken as 273.16° K [24], and

[3] Figures in brackets indicate the literature references at the end of this paper.

the value of R is therefore 8.3144 abs j deg^{-1} mole—. To obtain the value of R in international joules, the conversion factor of 1.00020 was accepted from the critical examination by Wensel [24], thus giving R=8.3127 int j deg^{-1} mole^{-1}.

Wensel has also discussed the value of the faraday obtained from the silver and the iodine coulometers. The full precision of the mean value is given by $F=9.650\times10^4$ int coulombs.

In chemical thermodynamics, quantities of energy are often expressed in calories, even though these quantities are measured precisely in electrical units. Unfortunately, the term "calorie" by itself is not definite, since it may mean the heat capacity of water at some temperature or it may signify a unit defined arbitrarily in joules independently of the properties of water. The use of the calorie as a unit of energy thus requires the statement of a conversion factor which depends, for example, upon whether the calorie recommended by the International Union of Chemistry in 1934 [19] as 4.1833 int j, the International Steam Table calorie of 3600/860 abs j, or some other calorie is used. It would seem better to propose that the calorie be abandoned as a unit of energy and to work towards a gradual attainment of that end. In this paper the results are reported in international joules and the calorie is used only in calculations involving measurements reported in calories by other workers.

The primary reference electrode, with respect to which the values of standard electrode potentials are conventionally given, is the standard hydrogen electrode; but for the actual measurements it is usually necessary to employ a secondary reference electrode. For many determinations the silver-silver chloride electrode is an excellent secondary standard. The conditions under which it is constant and reproducible have been investigated [22, 23], and its value with respect to the standard hydrogen electrode has been particularly well studied over a range of temperatures (0° to 60° C) by Harned and Ehlers [6]. A recent recalculation of their results [5] yielded values which were neither seriously nor consistently different from the original figures. For our measurements, the values of Harned and Ehlers as expressed by their equation

$$E^\circ=-0.22239+6.4552\times10^{-4}(t-25)+3.284\times10^{-6}(t-25)^2 -9.948\times10^{-9}(t-25)^3$$

were adopted and are given in table 1.

TABLE 1.—*Reference values of the standard electrode potential E° of the silver-silver chloride electrode and of the mean activity coefficient f_m of sodium chloride*

t	E°	f_m(0.05 m)	f_m(0.01 m)
° C	*int v*		
5	−0.23391	0.8244	0.7808
10	−.23130	.8239	.7805
15	−.22851	.8233	.7800
20	−.22554	.8224	.7792
25	−.22239	.8214	.7782
30	−.21908	.8202	.7770
35	−.21562	.8189	.7756
40	−.21200	.8175	.7740

The sign of an electrode potential may be taken as that of the hypothetical cell

$$\text{electrode; solution } \|H^+(a=1); H_2(1 \text{ atm}),$$

considered as positive when the electrode acts spontaneously as the anode and the hydrogen electrode as the cathode. The double vertical lines indicate that liquid junctions or their effects have been eliminated. The numerical value of a standard electrode potential depends on the scale of concentration employed [14]. It is convenient and customary in work on electrode potentials to follow the convention popularized by G. N. Lewis [13] —to express concentrations in terms of formula weights of solute per 1,000 g of solvent. If the subscript m denotes this molal concentration and the subscript c denotes concentration per 1,000 cm³ of solution, the difference between the values of a standard electrode potential on the two scales is given by $E^\circ_m - E^\circ_c = -(RT/NF)\ln d_o$, where d_o is the density of the pure solvent at the given temperature and pressure. This equation may be derived in the following way.

By definition, activity is given by the equation $F = F^\circ + RT \ln a$. For a given mass, expressed on the two different scales of concentration, F is the same while F° and a are different. Thus

$$F = \begin{cases} F^\circ_m + RT \ln a_m \\ F^\circ_c + RT \ln a_c \end{cases}$$

Since F°_m and F°_c are both constants, it follows from the properties of the logarithm that the ratio a_m/a_c = constant. The constant may be evaluated by the following method.

Consider a solution of density d having a concentration expressed as c moles of solute of molecular weight M per 1,000 cm³ of solution, corresponding to a molality of m moles per 1,000 g of solvent of density d_o. From the definition of these scales of concentration, their ratio may be expressed by the equation

$$\frac{c}{m} = d - \frac{Mc}{1{,}000}, \tag{1}$$

and since $a_c = f_c c$ and $a_m = f_m m$, where f_c and f_m are the corresponding activity coefficients,

$$\frac{f_m a_c}{f_c a_m} = d - \frac{Mc}{1{,}000} \tag{2}$$

In aqueous solutions the infinitely dilute solution is chosen as the standard state, so that the activity coefficients approach unity as the concentration approaches zero. Thus eq 2 reduces to

$$\frac{a_c}{a_m} = d_o \tag{3}$$

when m and c become zero, since the density of the solution becomes that of the pure solvent, and this limiting case thus serves for the evaluation of the constant.

The expression for the emf of an electrode as a function of the activity on the two scales is

$$E = E_m^\circ - \frac{RT}{NF} \ln a_m = E_c^\circ - \frac{RT}{NF} \ln a_c,$$

from which

$$E_m^\circ - E_c^\circ = -\frac{RT}{NF} \ln \frac{a_c}{a_m}. \tag{4}$$

Since the standard electrode potentials on the two scales are constants independent of any actual molalities or concentrations, the activity ratio in eq 4 must have the same value at a given temperature for all corresponding molalities and concentrations, including infinite dilution, and the value of this ratio is fixed by eq 3. Equation 4 may now be written

$$E_m^\circ - E_c^\circ = -\frac{RT}{NF} \ln d_\circ, \tag{5}$$

to obtain the difference between the standard electrode potentials on the two scales. For aqueous solutions this difference amounts to zero at 4°, 0.08 mv at 25°, and 0.33 mv at 50° C.

A simple relationship between the activity coefficients on the two scales, namely,

$$\frac{f_m}{f_c} = \frac{c}{d_\circ m} \tag{6}$$

results when the activities a_m and a_c are replaced in eq 3 by their equivalent expressions $f_m m$ and $f_c c$, respectively.

The activity coefficient of sodium chloride at 25° C has been determined precisely by Brown and MacInnes [3, 16]. Their values at this temperature for the molalities of 0.05 and 0.1 used in this work were taken as standard, and the values needed for the other temperatures at the same molalities were calculated with the aid of the excellent data obtained by Robinson and Gulbransen [4, 20] on the relative partial molal heat contents of solutions of sodium chloride. From their data, the relative partial molal heat content $\overline{L}_2$ of the sodium chloride was expressed in calories as a linear function of the temperature by the equations

$$\overline{L}_2 = 93.97 + 3.256(t-25) \text{ for } 0.05m, \text{ and}$$
$$\overline{L}_2 = 100.09 + 4.542(t-25) \text{ for } 0.1\ m.$$

The difference between the logarithm of the activity coefficient at a particular temperature and at 25° C was then computed by integration of the equation

$$\frac{d \ln f_m}{dT} = \frac{-\overline{L}_2}{2RT^2},$$

in which f_m is the mean activity coefficient on the molality scale. The reference values of Brown and MacInnes, given on the volume concentration scale at 25° C, were converted to the molality scale

by eq 6 and then corrected to the other temperatures. The mean activity coefficients thus computed are given in columns 3 and 4 of table 1.

III. MATERIALS

The mercury used in the preparation of the amalgam was virgin mercury purified by washing with nitric acid, distilling in a Hulett still [7], distilling under a vacuum, and filtering through a fritted glass filter.

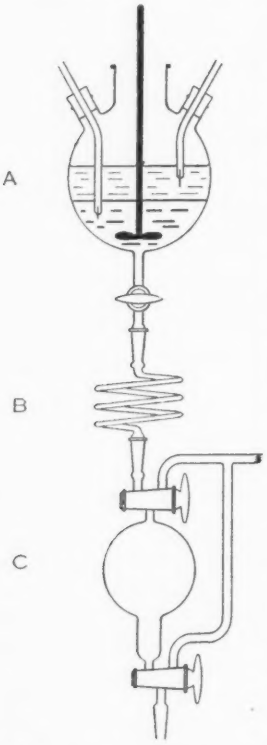

FIGURE 1.—*Apparatus for the preparation of sodium amalgam.*

A, electrolysis vessel; *B*, flexible glass spiral; *C*, amalgam storage vessel.

The amalgam was made electrolytically in a roundbottom 1-liter flask having two sidearms for the electrodes, and at the bottom an outlet tube with a stopcock and a ground joint of standard taper, as shown in figure 1. Approximately 200 ml of mercury was put in the flask, *A*, and covered with 400 ml of a 5-percent solution of sodium hydroxide, which was tested and found to conform to the specifications of the American Chemical Society for the reagent grade of this material [8]. One of the platinum electrodes dipped into the mercury and the other into the solution. The mercury was stirred mechanically during the electrolysis, which was continued until a plot of current and time indicated that the desired approximate concentration had been attained. When its preparation was completed, the amalgam was transferred to the reservoir, *C*. To relieve strain during the transfer, a flexible spiral of glass tubing, *B*, was inserted between the flask and the reservoir. The reservoir and spiral were evacuated before the amalgam was transferred. Dry nitrogen free from oxygen was then placed, at a pressure of about 20 cm above atmospheric, over the amalgam. The amalgam had substantially the same appearance as pure mercury and this appearance was retained throughout the investigation. For analysis, portions of the amalgam were decomposed by water, on a steam bath to hasten the rate of reaction. The resulting solutions of sodium hydroxide were separated from the mercury, treated with an excess of standardized sulfuric acid, boiled to remove carbon dioxide, and the excess acid was titrated with standard alkali using bromthymol blue as the indicator. The analyses, which are more informational than fundamental for the investigation since the concentration of the amalgam is not involved in the final electrode potential, showed that the amalgam contained 0.06514 $\pm$0.00006 percent by weight of sodium.

The sodium used for one electrode of the nonaqueous cell was a commercial product which was found by test to conform to the specifications of the American Chemical Society for the reagent grade

of this material [10]. A sample was converted to sodium chloride and tested for potassium [9]. Within the sensitivity of the test (0.01 percent), no potassium was found. A spectrographic examination of a sample indicated only traces of impurities.

The dimethylamine for the solvent in the nonaqueous cell was prepared from dimethylamine hydrochloride of cp grade and sodium hydroxide of reagent grade.

The sodium iodide for the electrolyte in the nonaqueous cell was of reagent grade, recrystallized, heated to incipient fusion, and stored in a desiccator until used.

The sodium chloride for the electrolyte in the aqueous cell was of reagent grade, further purified by two precipitations with gaseous hydrogen chloride, followed by recrystallization from redistilled water and fusion in a platinum dish. A sample was shown by test [9] to contain less than 0.01 percent of potassium.

The aqueous solutions were prepared to have the desired concentrations on the molal basis (formula weights of salt per 1,000 g of water) by weighing the dry salt and the added redistilled water. All weights were corrected for air buoyancy.

The nitrogen used for an inert atmosphere was freed from oxygen and other undesirable gases by passage over hot reduced copper and through columns containing dilute alkali and dilute acid. That which was used in contact with the amalgam and in the preliminary sweeping out of the cell was dried with anhydrous magnesium perchlorate, and that used to eliminate oxygen from the solution was bubbled through a solution of the same concentration.

The silver-silver chloride electrodes were of the thermal-electrolytic type and were equilibrated [22, 23] in the cell for at least 2 days before use. Two of these electrodes were used in the aqueous cell and their differences in emf were always less than 0.01 mv.

IV. APPARATUS AND PROCEDURE

The nonaqueous cell, *H*, and the apparatus for filling it are represented in figure 2. The auxiliary apparatus consisted of a still, *A*, a drying tube, *B*, filled with Drierite (anhydrous calcium sulfate), a drying tube, *C*, filled with Hydralo (anhydrous aluminum oxide), and an amine reservoir, *D*. At *E* was placed a magnetic hammer by means of which the capillary inner seal, *I*, could be broken when desired. The bottom of one limb of the cell was fitted with a standard-taper joint to accommodate the amalgam reservoir; and the other limb was fitted with a capillary tube sealed to a bulb, from which the sodium for one electrode was later filtered into the cell through the capillary. The horizontal connecting arm of the two limbs was provided with a pocket and a tube through which the electrolyte, sodium iodide, was placed in the cell. A tube for introducing the solvent was also provided. Platinum wires for contact with the electrodes were sealed in soft glass tubes, which in turn were joined to the cell by means of graded soft glass to Pyrex seals.

One hundred grams of dimethylamine hydrochloride was placed in the still pot, and a solution containing sodium hydroxide in excess of the amount necessary to liberate the free amine was added by means of the funnel inlet. The still pot was gently heated, and cold water

was circulated through the condenser. Tube *G* was open to the atmosphere at this time. Dimethylamine distilled into the receiver, *D*, which had been filled partially with shavings of metallic sodium and immersed in a cooling bath containing solid carbon dioxide in a mixture of carbon tetrachloride and chloroform. When distillation was completed, the receiver was sealed off at *F*. Tube *G* was then connected to a vacuum system and the source of pure dry nitrogen. Residual air in the receiver was removed by alternate evacuation and admission of nitrogen, after which the receiver was sealed at *G* under

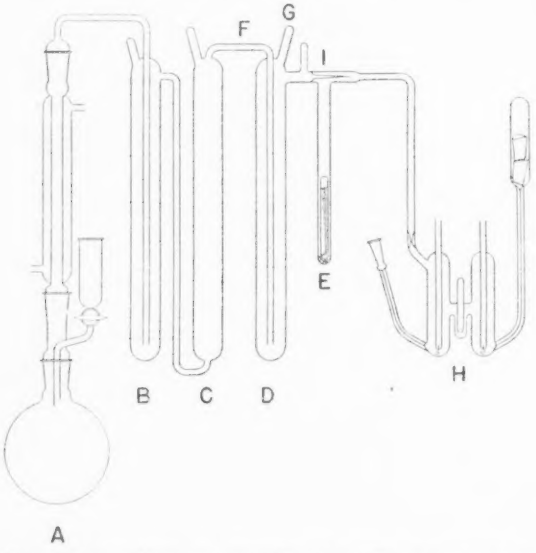

FIGURE 2.—*Nonaqueous cell and auxiliary apparatus.*

A, distilling assembly; *B*, drying tube containing Drierite; *C*, drying tube containing Hydralo; *D*, amine storage vessel; *E*, magnetic hammer; *H*, nonaqueous cell in position for filling; *I*, capillary inner-seal valve.

the vapor pressure of the dimethylamine at the temperature of the cooling bath. The liquid amine was thus stored over sodium until needed.

The amalgam reservoir was next connected to the cell by means of the standard-taper joint, sodium was placed in the bulb provided for it, and the sodium iodide was added. The apparatus was evacuated, a sufficient quantity of amalgam was introduced, and the side arm leading to the amalgam reservoir was sealed off close to its limb of the cell. The bulb containing the sodium was heated and the liquid metal flowed through the capillary to the other cell limb and, at the same time, was filtered from oxide crust. This side arm was then sealed off. After this, the cell was surrounded by the cooling bath, the capillary inner seal, *I*, was broken, and dimethylamine was distilled into the cell. When sufficient amine had been introduced, the cell was sealed off from the filling apparatus.

The main requirements upon which the design of the aqueous cell was based are (1) an easily renewable amalgam electrode to present a reproducible and unpolarized surface for each measurement; (2) a

means for removal of used amalgam to prevent continuous reaction with the solution; (3) a means for renewal of the electrolyte to eliminate solution which has reacted with amalgam; and (4) the exclusion of oxygen.

The design adopted for the aqueous cell is shown in figure 3. The cell proper, *G*, consisted of a longer limb for the capillary amalgam electrode and a shorter one for the silver-silver chloride electrodes.

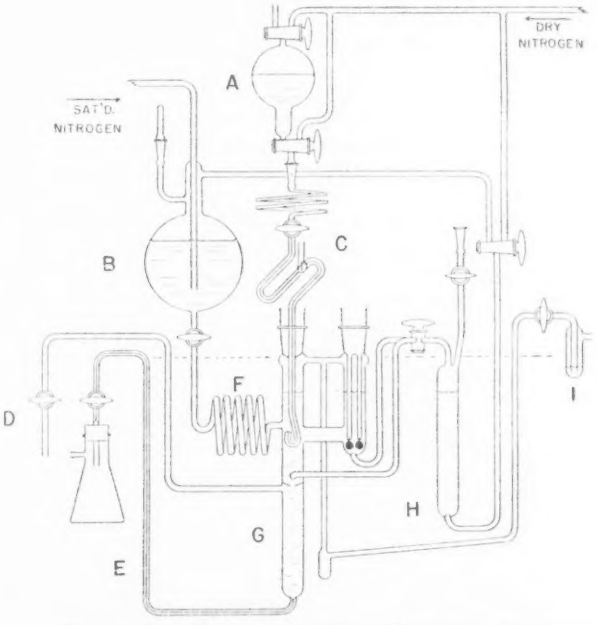

FIGURE 3.—*Aqueous cell and auxiliary apparatus.*

A, amalgam storage vessel; *B*, solution reservoir; *C*, capillary amalgam electrode; *D*, solution outlet tube; *E*, amalgam removal tube; *F*, solution inlet tube; *G*, aqueous cell; *H*, nitrogen gas saturator; *I*, nitrogen outlet. The dotted line shows the depth of immersion in the constant temperature bath.

The electrode tubes were sealed to ground joints of standard taper. The apparatus was made of Pyrex glass except for graded soft glass to Pyrex seals [4] on the two silver-silver chloride electrode tubes, which facilitated sealing in the platinum wires to hold these electrodes. Each limb contained a gas-bubbling tube so that nitrogen could be passed through either at will. The gas outlet, *I*, common to both limbs, was provided with a sump to prevent condensed water vapor from returning to the cell when measurements were made at temperatures above that of the laboratory. The longer limb had a funnel-shaped partition just below the bubble tube. A small orifice in this partition permitted drops of used amalgam to fall to the bottom and hindered back-diffusion of amalgam decomposition products. An outlet tube, *D*, just below this partition, for removing solution, and a capillary tube, *E*, for withdrawing used amalgam from the bottom, were sealed to the amalgam limb.

[4] One of the intermediate glasses in these graded seals was found to be attacked by solutions of sodium chloride. The amount of decomposition was great enough to cause mechanical failure in a relatively short time and, for this reason, the graded seals were placed above the level of the solution in the cell.

The capillary amalgam electrode was given an S-turn, *C*, because with a straight capillary tube a break and consequent gap in the column of amalgam sometimes occurred at the contact wire. The upward flow of amalgam past the contact wire eliminated this annoyance. To insure further against a break in the column of amalgam and to avoid preliminary contact and reaction of the amalgam with the solution, the capillary was first filled, by suction, with pure mercury up to and through the stopcock bore, before it was placed in the cell. To facilitate alinement with the amalgam reservoir, *A*, and to take up changes in strain, a flexible glass spiral was sealed between the stopcock and ground joint of the amalgam electrode.

The solution reservoir, *B*, consisted of a round-bottomed flask having a capacity of 1 liter, to which were sealed inlet and outlet tubes for nitrogen, a tube for filling with solution, and a spiral, *F*, connecting it to the cell. The reservoir was supported above the cell at the temperature of the laboratory. The function of the spiral was to bring the solution to the temperature of the thermostat before it entered the cell. Nitrogen, saturated with water vapor at room temperature, was passed through the reservoir to displace oxygen from the solution, on through the saturator, *H*, which was immersed in the thermostat and filled with some of the same solution, and then through the cell to the outlet, *I*. Before filling the cell and saturator, dry nitrogen was passed through them overnight and during this time a ground-glass plug took the place of the silver-silver chloride electrode tube. After the cell and saturator were filled with the oxygen-free solution, the silver-silver chloride electrodes were inserted and nitrogen was bubbled through for at least 2 days, to insure complete equilibrium of these electrodes with the solution [22, 23] before measurements were made. The next step was to connect the amalgam reservoir with the capillary electrode, evacuate the flexible spiral, and fill it with amalgam.

When a sufficient amount of amalgam had been passed through the capillary to displace the pure mercury, reproducible potential differences were obtained. During the measurements, fresh solution was passed through the amalgam limb of the cell at a rate of about 2 ml per minute. With this rate of flow, no significant differences were observed in the potentials of successive drops of amalgam, which would result if any appreciable change in composition of the solution were caused by reaction with the amalgam. To make sure of this, the amalgam limb was occasionally drained and refilled with fresh solution without causing any appreciable change in emf.

To bring the measured emf within the range of the potentiometer, an unsaturated Weston standard cell was connected in opposition to the aqueous cell, and the difference in emf was observed. This unsaturated standard cell was kept in an insulated box, and its emf was determined before and after each series of measurements.

Stationary and flowing amalgams were tried and the former proved to be more satisfactory. A fresh drop of amalgam was produced on the electrode tip and emf readings were made. The readings quickly reached a maximum which was within less than 0.1 mv of the initial value, then varied only a few hundredths of a millivolt from this value for a longer period of about 1 minute, after which a slow but definite decrease in emf occurred. Each fresh droplet behaved in the same manner, and the maximum reading of each was recorded.

The emf reported at each temperature is the average of at least 10 such readings, with an average deviation of about ±0.02 mv. After each series of measurements was completed, the solution level was lowered so that the capillary tip was out of the electrolyte but the silver-silver chloride electrodes were still immersed in the solution. This was done to minimize reaction with the amalgam during the periods between observations. The old electrolyte was drained and fresh was run in before each new series of measurements.

Both the aqueous and nonaqueous cells were immersed in an oil thermostat which was equipped with a cooling unit for maintaining temperatures below that of the room to a constancy of ±0.03° C. For temperatures above that of the room, the constancy was better than ±0.01° C. The temperatures were read with a Beckmann thermometer, the setting of which was checked at each temperature with a platinum resistance thermometer.

The measurements of electromotive force were made with a calibrated Rubicon type *B* potentiometer, and a pair of saturated Weston standard cells which were kindly made, calibrated, and supplied by G. W. Vinal and L. H. Brickwedde, of the Electrical Division of this Bureau. These cells were housed in a temperature-control box especially designed for saturated standard cells [18]. The galvanometer employed was a Leeds & Northrup Type *R* instrument which had a resistance of 495 ohms and a current sensitivity of 0.000092 (μa/mm)/m.

On any one day, measurements were made at only one temperature. The first measurements were made at 25° C and, as soon as these were completed, the temperature of the bath was lowered to approximately 20° C. On the following day the temperature was adjusted closely to 20° C. Thus the temperature was within a few tenths of a degree of the desired value for at least 18 hours, and within a few hundredths for at least 2 hours, before observations were started. This procedure was continued for successive 5-degree intervals down to 5° C. Following the measurements at 5° C the temperature was brought back to 25° C in one step for a test of reproducibility and hysteresis. The reproducibility was within a few hundredths of a millivolt, and no hysteresis effects were observed. The temperature was then raised in 5-degree steps up to 40° C and brought back in one step from 40° to 25° C. This procedure was applied to both the nonaqueous and the aqueous cells. Two concentrations of the solution of sodium chloride, 0.05 and 0.1 *m*, and one concentration of the amalgam, 0.0651 percent by weight of sodium, were used.

V. RESULTS AND DISCUSSION

Nonaqueous cell.

The measured values of the emf of the nonaqueous cell,

Na(s); NaI (in dimethylamine); Na(0.0651% amalgam),

at the different temperatures are given in column 2 of table 2. The results can be expressed by the equation

$$E=0.88578+0.00008390\ (t-25)+0.000000762\ (t-25)^2,$$

with average and greatest deviations of 0.02 and 0.06 mv, respectively.

The values of $\Delta\overline{F}$ in the third column were calculated from this equation and the relationship $\Delta\overline{F}=-FE$, in which $\Delta\overline{F}$ is the change in partial molal free energy accompanying the cell reaction and F is the faraday. The values of $\Delta\overline{S}$, the change in partial molal entropy, given in the fourth column were obtained from the relationship $\Delta\overline{S}=FdE/dT$, in which $dE/dT=0.0008390+0.000001524\,(t-25)$. The values of $\Delta\overline{H}$, the change in partial molal heat content, listed in the fifth column were calculated from the equation $\Delta\overline{H}=\Delta\overline{F}+T\Delta\overline{S}$. Bent and Swift, Jr., [2] have measured similar cells and have given equations for computing $\Delta\overline{F}$ and $\Delta\overline{H}$ for different mole fractions of sodium in sodium amalgam, at different temperatures between 5° and 25° C. The values of $\Delta\overline{F}$ computed from their equations agree with ours to 0.06 percent in the comparable range of 5° to 25° C. The values of $\Delta\overline{S}$, which depend on the temperature coefficient of emf, differ by 5 to 6 percent, and the values of $\Delta\overline{H}$ differ by about 0.2 percent. Considering the small magnitude of $\Delta\overline{S}$ and that the comparison is made with interpolated data, the agreement appears adequate.

TABLE 2.—*Cell:* Na(s); NaI *in* $(CH_3)_2NH$; Na (*0.0651% amalgam*)
Reaction: Na(s) = Na(*0.0651% amalgam*)

t	E	$\Delta\overline{F}$	$\Delta\overline{S}$	$\Delta\overline{H}$
°C	*int v*	*int j/mole*	*int j/mole deg*	*int j/mole*
5	0.88442	−85343	5.16	−83909
10	.88467	−85372	5.89	−83703
15	.88500	−85403	6.63	−83494
20	.88537	−85438	7.36	−83280
25	.88577	−85477	8.10	−83063
30	.88626	−85517	8.83	−82840
35	.88667	−85566	9.57	−82617
40	.88720	−85615	10.30	−82389

The effect of pressure on the emf of the nonaqueous cell was calculated to be approximately 0.008 mv per atmosphere by the equation $dE/dP=-\Delta\overline{V}/F$, in which $\Delta\overline{V}$ is the difference between the partial molal volume of sodium in the amalgam and of pure sodium. The partial molal volume of sodium in the amalgam was estimated from the data of Maey [17]. The pressure within the cell at the different temperatures was calculated from determinations by Simon and Huter [21] of the vapor pressure of dimethylamine. The calculated corrections ranged from less than 0.01 mv to a maximum of only 0.02 mv and were not applied to the data.

Aqueous cells.

The results with the aqueous cells are given in table 3. The $E°$ values were obtained by adding to the E values the terms

$$(RT/F)\ln(f_m m),$$

in which f_m is the activity coefficient on the molal scale, given in table 1. As a test of the reliability of the observations, the ratios of the activity coefficients were calculated by the equation $F\Delta E=2RT\ln(2f_{0.1}/f_{0.05})$, in which ΔE is the difference between

the emf of the two aqueous cells and corresponds to the transfer $NaCl(0.1m) = NaCl(0.05m)$. The calculated ratios were compared with the ratios of the values given in table 1, which were used in the computations of $E°$. Over the entire temperature range the greatest difference found between these two sets of ratios was 4 parts and the average difference was 2 parts in 1,000. This agreement is satisfactory, since the differences in emf were obtained indirectly as the differences between quantities nearly 100 times as large. However, these differences in emf are not of sufficient accuracy to justify their use for calculations of the changes in entropy and heat content accompanying the transfer of sodium chloride between the two concentrations.

TABLE 3.—*Cell:* **Na (0.0651% *amalgam*); NaCl (0.05 *or* 0.1 *m*), AgCl(s); Ag(s)**
Reaction: **Na (0.0651% *amalgam*) + AgCl(s) = NaCl(0.05 *or* 0.1 *m*) + Ag(s)**

t	E $m=0.05$	$\frac{2RT}{F}\ln(0.05f_m)$	$E°$ $m=0.05$	E $m=0.1$	$\frac{2RT}{F}\ln(0.1\,f_m)$	$E°$ $m=0.1$	Avg. $E°$
°C	*int v*	*int v*	*int v*	*int v*	*int v*	*int v*	*int v*
5	2.20084	−0.15282	2.04802	2.17009	−0.12220	2.04789	2.04796
10	2.20440	−.15560	2.04880	2.17304	−.12442	2.04862	2.04871
15	2.20775	−.15838	2.04937	2.17586	−.12665	2.04921	2.04929
20	2.21086	−.16118	2.04968	2.17850	−.12890	2.04960	2.04964
25	2.21382	−.16399	2.04983	2.18105	−.13116	2.04989	2.04986
30	2.21669	−.16682	2.04987	2.18337	−.13344	2.04993	2.04990
35	2.21943	−.16965	2.04978	2.18548	−.13574	2.04974	2.04976
40	2.22196	−.17250	2.04946	2.18757	−.13805	2.04952	2.04949

Combinations of cells.—By adding to each E given in table 3, the E of the nonaqueous cell at the same temperature, as given in table 2, the emf of the cell

$$Na(s);\ NaCl\ (0.05\ or\ 0.1\ m),\ AgCl(s);\ Ag(s)$$

is obtained for each temperature and may be expressed by the following equations.

For $m=0.05$,

$$E=3.09964+0.0006699(t-25)-0.00000240(t-25)^2$$

with average and greatest deviations of 0.02 and 0.05 mv.

For $m=0.1$,

$$E=3.06679+0.0005671(t-25)-0.00000241(t-25)^2$$

with average and greatest deviations of 0.03 and 0.07 mv.

A rather severe test of the data may be made by taking the second derivatives of these equations to calculate the difference between the molal heat capacities of the products and reactants of the cell reaction

$$Na(s)+AgCl(s)=NaCl(0.05\ or\ 0.1\ m)+Ag(s)$$

by means of the relationship $\Delta\overline{C}_p=TFd^2E/dT^2$. The value thus found may be compared with the algebraic sum of the molal heat capacities directly observed, since

$$\Delta\overline{C}_p=\overline{C}_p(Ag+\overline{C}_p(NaCl,\ 0.05\ or\ 0.1\ m)-\overline{C}_p(Na)-\overline{C}_p(AgCl)$$

At 25° C and $m=0.05$, for example, $\Delta\overline{C}_p$ is calculated from the equation involving the second derivatives of E to be -138 int j as compared with -133 for the sum of the separately measured quantities. A more interesting comparison is that of the value calculated for $\overline{C}_p$(NaCl, 0.05 or 0.1 m) with its value obtained from measurements of heats of dilution. Thus, from the values of $\overline{C}_p$ for silver (25.3), sodium (28.4), and silver chloride (52.6), listed in International Critical Tables [11], and our result of -138 int j for $\Delta\overline{C}_p$, the partial molal heat capacity of 0.05 m sodium chloride is calculated to be -82.3 int j or -19.7 cal. Gulbransen and Robinson [4], from measurements on the heats of dilution of solutions of sodium chloride, expressed its partial molal heat capacity in calories by the equation $\overline{C}_p=-21.9+15.8\ m^{\frac{1}{2}}$, which yields -18.4 calories for 0.05 m with a probable error which they estimate to be not more than 15 percent. The agreement at 0.1 m is not quite as close, the difference being 2.9 cal, but is satisfactory for a comparison which involves a second derivative and data on specific heats from various sources.

For the cell

$$\mathrm{Na(s);\ NaCl}\ (f_m m=1),\ \mathrm{AgCl\ (s);\ Ag\ (s)}$$

the value of $E°$ at each temperature was obtained by adding to each average $E°$ for the aqueous cell, given in the last column of table 3, the corresponding E for the nonaqueous cell given in table 2. The results, which are given in table 4, may be expressed by the equation

$$E°=2.93564+0.0001096(t-25)-0.00000268(t-25)^2,$$

which shows an average deviation of 0.02 mv and a greatest deviation of 0.04 mv from the tabulated results. Table 4 also includes the change in partial molal free energy, entropy, and heat content accompanying the cell reaction, calculated with the aid of the equation and its first derivative.

TABLE 4.—*Cell:* Na(s); NaCl($f_m m=1$), AgCl(s); Ag(s)
Reaction: Na(s)+AgCl(s)=NaCl($f_m m=1$)+Ag(s)

t	$E°$	$\Delta F°$	$\Delta S°$	$\Delta H°$
°C	*int v*	*int j/mole*	*int j/mole deg*	*int j/mole*
5	2.93238	−282975	20.9	−277156
10	2.93338	−283072	18.3	−277879
15	2.93429	−283158	15.8	−278619
20	2.93501	−283229	13.2	−279369
25	2.93563	−283289	10.6	−280134
30	2.93616	−283336	8.0	−280914
35	2.93643	−283369	5.4	−281702
40	2.93669	−283390	2.8	−282507

The standard electrode potential of sodium.—The emf of the hypothetical cell

$$\mathrm{Na(s);\ Na^+}(f_m m=1)\|\mathrm{H^+}(f_m m=1);\ \mathrm{H_2(1\ atm)}$$

may be found by adding the standard electrode potential of the silver-silver chloride electrode, given in table 1, to the electrode potential of the cell

$$\mathrm{Na(s);\ NaCl}(f_m m=1),\ \mathrm{AgCl(s);\ Ag(s)}$$

given in table 4, at each temperature. The $E°$ value thus obtained at each temperature is the standard electrode potential of sodium. These final results are shown in table 5 together with the value of $E°$, $\Delta F°$, $\Delta S°$, and $\Delta H°$ calculated from the equation

$$E°=2.71324+0.0007532(t-25)+0.000000688(t-25).^2$$

This equation expresses the tabulated values of the standard potential of sodium in the temperature range of 5° to 40° C, with an average deviation of 0.02 and a greatest deviation of 0.05 mv. The smoothed values of $E°$, calculated from the equation and given in column 3 of table 5, are recommended as "best" values for the standard electrode potential.

TABLE 5.—*The standard electrode potential of the sodium electrode*

t	$E°$ from measurements	$E°$ from equation	$\Delta F°$	$\Delta S°$	$\Delta H°$
°C	*int v*	*int v*	*int j/mole*	*int j/mole deg*	*int j/mole*
5	2.69847	2.69846	−260401	70.0	−240921
10	2.70208	2.70206	−260749	70.7	−240732
15	2.70578	2.70578	−261108	71.4	−240545
20	2.70947	2.70949	−261466	72.0	−240353
25	2.71324	2.71324	−261828	72.7	−240155
30	2.71708	2.71703	−262193	73.4	−239956
35	2.72082	2.72084	−262561	74.0	−239754
40	2.72469	2.72466	−262930	74.7	−239543

The accuracy of the final results depends on a number of factors. Leaving out of consideration, for the moment, the reference silver-silver chloride electrode, the most critical of these factors and the calculated influence of their estimated uncertainties are:

(1) The activity coefficients of sodium chloride, including their corrections to the different temperatures (0.03 mv).

(2) Accuracy and constancy of temperatures (0.01 mv).

(3) Polarization of the amalgam electrode in the aqueous solution (0.02 mv).

(4) Calibrations of potentiometer and standard cells (0.02 mv).

(5) The concentrations of the aqueous solutions (0.005 mv).

(6) Accidental errors (0.01 mv).

(7) Neglect of pressure corrections (0.00 to 0.02 mv).

The square root of the sum of the squares of these errors gives 0.04 to 0.05 mv for an estimate of the over-all accuracy of the measurements. The reference values of the silver-silver chloride electrode are probably good to about the same amount, so that the values obtained for the standard electrode potential of the sodium electrode are considered to be correct to within 0.1 mv.

VI. REFERENCES

[1] A. J. Allmand and W. G. Pollack, J. Chem. Soc. **115,** 1020 (1919).
[2] H. E. Bent and E. Swift, Jr., J. Am. Chem. Soc. **58,** 2216 (1936).
[3] A. S. Brown and D. A. MacInnes, J. Am. Chem. Soc. **57,** 1356 (1935).
[4] E. A. Gulbransen and A. L. Robinson, J. Am. Chem. Soc. **56,** 2637 (1934).
[5] W. J. Hamer, J. O. Burton, and S. F. Acree, J. Research NBS **24,** 269 (1940) RP1284.
[6] H. S. Harned and R. W. Ehlers, J. Am. Chem. Soc. **55,** 2183 (1933).
[7] G. A. Hulett, Phys. Rev. **33,** 312 (1911).
[8] Ind. Eng. Chem. **17,** 756 (1925); **18,** 636 (1926).
[9] Ind. Eng. Chem. **20,** 979 (1928).
[10] Ind. Eng. Chem. Anal. Ed. **2,** 351 (1930).
[11] Int. Crit. Tables **5,** 85–97 (1929).
[12] G. N. Lewis and C. A. Kraus, J. Am. Chem. Soc. **32,** 1459 (1910).
[13] G. N. Lewis and M. Randall, Thermodynamics, p. 33 and 416 (McGraw-Hill Book Co., Inc., New York, N. Y., 1923).
[14] A. Macfarlane and O. Gatty, Phil. Mag. [7] **13,** 283, 291 (1932).
[15] D. A. MacInnes, Principles of Electrochemistry, p. 197 (Reinhold Publishing Corporation, New York, N. Y., 1939).
[16] D. A. MacInnes and A. S. Brown, Chem. Rev. **18,** 335 (1936).
[17] E. Maey, Z. physik. Chem. **29,** 119 (1899).
[18] E. F. Mueller and H. F. Stimson, J. Research NBS **13,** 699 (1934) RP 739.
[19] Premier Rapport de la Commission Permanente de Thermochimie, International Union of Chemistry, p. 3 (1934).
[20] A. L. Robinson, J. Am. Chem. Soc. **54,** 1311 (1932).
[21] A. Simon and J. Huter, Z. Elektrochem. **41,** 28 (1935).
[22] E. R. Smith and J. K. Taylor, J. Research NBS **20,** 837 (1938) RP 1108.
[23] J. K. Taylor and E. R. Smith, J. Research NBS **22,** 307 (1939) RP 1183.
[24] H. T. Wensel, J. Research NBS. **22,** 375 (1939) RP 1189.

WASHINGTON, September 20, 1940.

U. S. DEPARTMENT OF COMMERCE NATIONAL BUREAU OF STANDARDS

RESEARCH PAPER RP1351

Part of Journal of Research of the National Bureau of Standards, Volume 25, December 1940

PREPARATION OF BENZOIC ACID OF HIGH PURITY

By Frank W. Schwab and Edward Wichers

ABSTRACT

A comparative study was made of methods for preparing benzoic acid of a purity not less than 99.99 mole percent. The methods studied were fractional distillation in vacuum, recrystallization from water and from purified benzene, fractional freezing, oxidation of purified toluene with subsequent recrystallization from water, and hydrolysis of purified benzoyl chloride. The best preparations were obtained by repeated crystallization from benzene, by hydrolysis of benzoyl chloride, and by fractional freezing. They had a purity of 99.999 mole percent as determined by the freezing range and by specific heat measurements. The freezing point of benzoic acid is tentatively given as 122.36 ±0.01° C.

CONTENTS

	Page
I. Introduction	747
II. Criteria of purity	748
1. Vaporizing and condensing behavior	748
2. Crystallizing and melting behavior	749
III. Stability of benzoic acid	750
IV. Methods of preparation	752
1. From parent substances by selected reactions	752
(a) Oxidation of toluene	752
(b) Hydrolysis of purified benzoyl chloride	752
2. By purification of a commercial product	752
(a) Distillation	752
(b) Fractional freezing	753
(c) Crystallization from solvents	753
V. Results and discussion	756

I. INTRODUCTION

Many properties of substances are determined by comparative rather than by absolute methods. The accuracy of comparative methods depends on the precision of the measurements and on the accuracy with which the properties of the standard substance used for comparison are known. As methods of making comparative measurements improve, an increasing demand is made on the accuracy with which the properties of the standard substance are determined. A high degree of accuracy in the original determination of the properties of this reference substance requires not only a high degree of uniformity of composition but also a close approach to ideal purity.

Benzoic acid is commonly used as a standard substance for calorimetry and acidimetry, and "standard samples" of this substance have been issued by the National Bureau of Standards for many years. Morey[1] made a study of the suitability of benzoic acid as a primary standard in acidimetry and alkalimetry. He found that it could be titrated with a standard alkali to a high degree of accuracy

[1] George W. Morey, J. Am. Chem. Soc. **34**, 1027 (1912).

and that this method afforded a rapid and accurate means of comparing the purity of various preparations. Morey purified commercial benzoic acid by recrystallizing it from solvents and fractionally subliming it in a vacuum.[2] Weaver[3] purified the acid in a manner similar to that used by Morey. Each fused the acid prior to titration. This treatment was designed to remove water that was absorbed during contact with air.

When a redetermination of the heat of combustion of benzoic acid was recently undertaken by the Heat Measurements Section of this Bureau, with an anticipated precision of 0.01 percent, it became desirable to prepare benzoic acid which would have a purity of at least 99.99 mole percent.

II. CRITERIA OF PURITY

Criteria of purity for a nearly pure organic substance should be independent of known properties of the substance. Physical properties are usually not known with sufficient accuracy to permit estimation of purity by comparison even though the identities of the compounds under consideration and of some of the impurities in it are known. Independent criteria which are generally used depend on (1) vaporizing or condensing behavior and (2) freezing or melting behavior. If, like benzoic acid, the substance is a moderately strong acid, its acid value is also a useful index of purity and is often so used. The acidimetric method as commonly applied is not suitable, however, for determining differences in purity smaller than 0.01 percent.

1. VAPORIZING AND CONDENSING BEHAVIOR

The behavior on evaporation or condensation as a criterion of purity[4] is suitable only for substances that do not decompose significantly, and is generally utilized by measuring the boiling range under constant pressure or by determining the initial and final vapor pressures during an isothermal vaporization or condensation. The method is most sensitive when the substance is distilled in an efficient fractionating column. The boiling points under the same external pressure, or the difference in vapor pressure at the same temperature, of the first and last fractions may then be compared.

It is known that benzoic acid undergoes measurable decomposition at temperatures 50° to 100° C below its normal boiling point (about 250° C). The identity of some of the products of decomposition is not known, but in the course of the present work it was found that one of the reactions at these temperatures is the slow formation of benzoic anhydride and water. Although the concentrations of anhydride and of water are probably small under equilibrium conditions at 130° C or somewhat higher temperatures, transformation of the acid to these products is rapid enough so that distillation in an efficient fractionating column for the desired separation is not practicable. It is obvious, therefore, that this method cannot be readily applied under conditions most suitable for obtaining the highest sensitivity.

[2] George W. Morey, J. Am. Chem. Soc. **34**, 550 (1912).
[3] E. R. Weaver, J. Am. Chem. Soc. **35**, 1309 (1913).
[4] E. W. Washburn, *The problem of establishing the identity and purity of a hydrocarbon obtained from petroleum*, J. Ind. Eng. Chem. **22**, 985 (1930). Also see Martin Shepherd, *A critical test for the purity of gases*, BS J. Research **12**, 185 (1934) RP 643. For a further discussion of this subject see W. Swiętosławski, Ebulliometry (Chemical Publishing Co., New York, N. Y., 1937).

2. CRYSTALLIZING AND MELTING BEHAVIOR

In the work described in this paper the purity of benzoic acid was determined from its behavior during freezing or melting. The test based on the freezing behavior is customarily applied by determining the cooling curve through the entire freezing range. White [5] has discussed the theoretical aspects of this method and the assumptions involved.

In adapting this method to the present problem, the authors [6] found numerous sources of error which limited its accuracy but which could be largely eliminated by comparing the freezing range of the substance with that of the same substance after adding a known concentration of a properly chosen "impurity." By so doing it was found possible to use any selected interval of the freezing range and, with appropriately refined technique, to determine concentrations of impurity of 0.01 mole percent or less. Since the completion of the work just cited, the technique has been further perfected.[7] It was found that for preparations containing up to about 0.30 mole percent of impurity the uncertainty of the determination is not greater than 0.01 mole percent. The purity of highly pure samples was determined to 0.001 mole percent or better by making several observations on a given preparation. It was possible, for example, to distinguish between two preparations estimated, respectively, as 99.999_2 and 99.999_4 mole percent pure. The accuracy of the method is limited in part by the very slow formation of benzoic anhydride when the liquid to be frozen is thoroughly dried.

Another sensitive test of purity is based on the variation in the heat capacity of a substance at temperatures slightly below its melting point. This test involves a determination of the first part of the melting range by calorimetric rather than by thermometric means. Any departure from a linear variation of heat capacity with respect to temperature is ascribed to absorption of heat associated with melting. Several of the preparations described in this paper were so examined by R. S. Jessup, of the Heat Measurements Section of this Bureau, in accordance with a procedure described by Dickinson and Osborne.[8]

It will be noted from table 2 that the estimates of purity of several preparations which are based on the calorimetric method are in close agreement with those based on the measurement of the freezing range. The samples used for the calorimetric measurements were prepared before the slow formation of benzoic anhydride during drying had been observed. It is possible, therefore, that some of these samples were somewhat "overdried" and hence less pure than the corresponding ones used later for the measurement of the freezing ranges. The calorimetric method, although inherently more sensitive than the thermometric method is more time-consuming.

---

[5] Walter P. White, J. Phys. Chem. **24**, 393 (1920).

[6] F. W. Schwab and Edward Wichers, Precise Measurement of the Freezing Range as a Means of Determining the Purity of a Substance. This paper appears as a chapter in Temperature, Its Measurement and Control in Science and Industry, (Reinhold Publishing Co., New York, N. Y., 1940).

[7] All the results reported in this paper were obtained by freezing the substance at twice the initial rate employed in the earlier work. This was done by doubling the difference in temperature between the freezing substance and the cooling bath. The desired part of the freezing range was observed in about 60 minutes, and better conditions were obtained at the beginning of freezing.

[8] H. C. Dickinson and N. S. Osborne, Bul. BS **12**, 49 (1915) S248. See also Evald L. Skau, J. chim. phys. **31**, 366 (1934), for a quantitative treatment of this subject.

In the remainder of this paper all references to "purity" and "content of impurity" are based on determinations of the freezing range.

III. STABILITY OF BENZOIC ACID

Before it was possible to reach a conclusion as to the relative merits of various methods of purification, and of various tests of purity, it was necessary to investigate the stability of benzoic acid at temperatures above its melting point. Three samples of material currently issued by the Bureau as Standard Sample 39e (containing 0.017 mole percent of impurity) were heated in sealed glass tubes (Pyrex) at 200° C for 72 hours. One was filled with air and a second with oxygen, each under a pressure of 1 atmosphere, and a third was evacuated. After this treatment the first contained 0.046; the second, 0.047; and the third, 0.025 mole percent of impurity, as estimated from the freezing behavior. The color of the sample heated in the evacuated tube was pale yellow; that of the sample heated under air, light brown; and that of the sample heated under oxygen, slightly darker brown. From these results it appears that of the slight amount of decomposition which occurs below 200° C more is to be attributed to oxidation than to dissociation of the acid into benzoic anhydride and water.

It was concluded that any treatment of the acid involving heating at temperatures not over 135° C for relatively short periods was not likely to cause significant deterioration. More exact information about the formation of anhydride was obtained in another way. During the process of repeatedly measuring the freezing range of a very pure sample of benzoic acid, the acid was dried before freezing and stirred while freezing by passing through it air which had been dried by phosphorus pentoxide. The dried air was passed at a constant rate through the molten benzoic acid, which was maintained at a temperature of about 130° C, for measured intervals between successive freezings. A progressive but slow decrease in purity was observed. After freezing the sample five times, the total change was 0.005 mole percent. Since benzoic anhydride is a possible product of this treatment, it seemed reasonable that an increase in the partial pressure of the water in the air would reverse the reaction. It was found that a partial pressure of water in the air equal to 0.5 mm Hg (corresponding to 0.005 mole percent dissolved in the acid) [9] was sufficient to do this, and by this treatment the content of impurity was reduced from 0.005 to 0.001 mole percent.

In another series of experiments a known quantity of benzoic anhydride (0.764 mole percent) was added to the benzoic acid. The concentration of water in the liquid acid was controlled by passing through it air saturated with water at selected temperatures. The rate of hydrolysis at 130° C was measured by maintaining a known concentration of water during a measured interval of time, then removing the excess of water from the liquid by passing through it air

[9] The relation between the amount of water dissolved in benzoic acid and the partial pressure of water in the air with which the acid is in equilibrium was determined approximately by observing the depression of the freezing point of the acid when frozen successively in equilibrium with dry air and with air containing 4.6 and 17.8 mm of water vapor. The indicated partial pressures of water were established by saturating air with water at 0° C and at 20.0° to 20.3° C, respectively. At these partial pressures the observed depressions of the freezing temperature were 0.04° and 0.15° C, which correspond to 0.05 and 0.20 mole percent of dissolved water.

dried over phosphorus pentoxide and observing the change in freezing temperature. The results in table 1 show that the reaction may be represented by the equation

$$(C_6H_5CO)_2O+H_2O \rightleftharpoons 2C_6H_5COOH.$$

TABLE 1.—*Rate of hydrolysis of benzoic anhydride*

[Temperature=130° C]

Minutes	Mole percent of a	Mole percent of x	$a-x$	$\frac{a}{a-x}$	$\log\frac{a}{a-x}$	k
Concentration of water =0.31 mole percent						
390	0.73	0.27	0.46	1.6	0.1959	0.0012
240	.46	.17	.30	1.6	.1931	.0019
180	.30	.05	.24	1.2	.0864	.0011
120	.24	.04	.21	1.2	.0756	.0015
300	.18	.06	.12	1.5	.1614	.0012
Concentration of water=0.05 mole percent						
165	0.21	0.02	0.19	1.1	0.0374	0.0005
180	.19	.01	.18	1.1	.0253	.0003

Since the concentration of water is held constant and the rate of the reverse reaction is negligible in comparison with the rate of hydrolysis, the reaction is of the first order. The velocity constant for this reaction, for a given concentration of water in the liquid, may be calculated from the equation

$$k=\frac{1}{t}\ln\frac{a}{a-x},$$

in which

a=mole percent of benzoic anhydride at the beginning,
x=mole percent of benzoic anhydride changed to resultants,
t=time in minutes,
k=velocity constant.

No attempt was made to measure the rate of hydrolysis accurately. However, the results show that the rate of reaction is dependent on the concentrations of water and of anhydride. After the last observation 0.18 mole percent of anhydride remained. Several milliliters of water was then added to the acid, and the mixture again heated to 130° C. The excess water was removed by washing with dry air. After this treatment, the purity of the acid was 99.996 mole percent, which indicates that substantially complete hydrolysis of the anhydride had taken place. Since the acid was kept at about 130° C for 50 hours before and 30 hours during this course of treatment, its final purity shows that, except for the formation of anhydride, benzoic acid is remarkably stable at temperatures not much above its melting point. As previously noted, the formation of the anhydride occurs only when the acid is in contact with very dry air.

IV. METHODS OF PREPARATION

Two general courses were followed in the preparation of pure benzoic acid. One was to prepare the acid from carefully purified parent substances by selected reactions. The other was to start with a relatively pure acid (Standard Sample 39e) and purify it by the best available processes.

1. FROM PARENT SUBSTANCES BY SELECTED REACTIONS

(a) OXIDATION OF TOLUENE

One of the reactions chosen was the oxidation of toluene which had been purified by distillation until its boiling point was constant to within 0.01° C. This was done to insure the elimination of impurities, such as xylenes, which would yield derivatives difficult to separate from the benzoic acid. The toluene was treated with potassium permanganate in a nearly neutral solution. The partial oxidation of organic substances is difficult to control, and in the oxidation of toluene evidence was obtained of the formation of aliphatic acids and also of some tarry material. After four crystallizations from water the product was 99.980 mole percent pure. It was, therefore, less pure than Standard Sample 39e (99.983 mole percent). Because of these difficulties this method was abandoned as a means of providing benzoic acid of high purity, although some modification of the procedure might have yielded a better product.

(b) HYDROLYSIS OF PURIFIED BENZOYL CHLORIDE

A reaction which proved to yield highly pure benzoic acid was the hydrolysis of carefully distilled benzoyl chloride.[10] Two lots of benzoyl chloride were used in this work. A portion of lot 1 was hydrolyzed in the vapor phase at about 100° C. Benzoyl chloride was brought into the reaction chamber by passing a stream of nitrogen through the liquid at the desired rate. An excess of water vapor was simultaneously passed into the reaction chamber, which served to continuously wash benzoic acid from it and thus to minimize the possibility of secondary reactions. Hydrolysis of a second portion of lot 1, in the liquid phase, proceeded very rapidly when the substance was treated with an excess of water and heated to about 115° C. Each product was crystallized seven times from water. The purity of each was 99.996 mole percent. Since vapor-phase hydrolysis is slow and since there was no measurable difference in the purity of the products obtained, a portion of benzoyl chloride from lot 2 was hydrolyzed in the liquid phase. The product was not recrystallized from water; hydrogen chloride and water were removed by passing dry air through the liquid. The product so obtained was 99.999 mole percent pure.

2. BY PURIFICATION OF A COMMERCIAL PRODUCT

(a) DISTILLATION

An unsuccessful attempt was made to purify Standard Sample 39e by fractional distillation in an evacuated bulb in which the distillate collected as liquid (at about 123° C). One-fifth of the distillate was

[10] Commercial benzoyl chloride was distilled under the supervision of F. D. Rossini. The substance was twice distilled in a 30-plate bubble-cap still under 215-mm pressure to minimize the possibility of thermal decomposition. The still was charged twice with 2,500 ml of benzoyl chloride, and each time about 1,200 ml was collected as the middle fraction. The combined middle portions, lot 1, were redistilled and about 1,500 ml collected, rejecting about equal quantities of the first and last fractions. This 1,500 ml (lot 2) distilled at about 150° C, with a range not greater than 0.2° C, the limit of sensitivity of the thermometer.

then distilled into a second receiver in the same way. A comparison of the freezing ranges of these three fractions showed no improvement in purity in the middle fraction and a slight decrease in the end fractions. Evidently the impurities in the original material did not differ enough in vapor pressure from benzoic acid to be removable by a simple process of distillation. In view of the difficulties of operating an efficient rectifying column at low pressures, above the melting point of the acid (122.4° C), this method was abandoned.

E. R. Weaver of this Bureau has suggested that sublimation in a partial vacuum would be more successful than distillation, provided the temperature of condensation (in the solid phase) were properly regulated and the vapor space ventilated so that the vapor phase would never become saturated with any of the impurities. In view of the success of other methods of purification this procedure was not tried.

(b) FRACTIONAL FREEZING

Fractional crystallization can be accomplished either with or without the use of a solvent. The latter method, fractional freezing, was suggested by the use of the freezing range as a criterion of purity. This method was first applied by allowing the molten acid to freeze rather slowly in a Dewar flask (method 1). Solid and liquid were kept thoroughly mixed. When the substance was one-half to two-thirds frozen, the remaining liquid was drawn off by suction. The solid portion was then remelted and the process repeated. The increase in purity which resulted from the use of this method was somewhat slower than was expected. This indicated that a satisfactory approximation to equilibrium freezing was not realized or that the crystals could not be properly drained. The head fraction had an estimated purity of 99.998 mole percent.

A different method of fractional freezing (method 2), used by R. S. Jessup, of the Heat Measurements Section, was more successful. He lowered a glass tube containing the molten material (39e) very slowly from a heating coil. Freezing began at the bottom of the cell and progressed upward until the whole mass was frozen. The portion remaining liquid was stirred constantly. About 50 grams was frozen in 6 hours. The glass tube was cut so that the last portion of the solid to freeze (one-third to one-fourth) was discarded. The process was then repeated with the remainder. Purification by this method was more effective than by the first method of fractional freezing. The purity of the best preparation exceeded 99.999 percent. The substance was allowed to freeze very slowly and nearly ideal conditions for separation were evidently obtained.

(c) CRYSTALLIZATION FROM SOLVENTS

In recrystallizing benzoic acid from solvents, ethyl alcohol, which is sometimes recommended for this purpose, was found unsuitable because ethyl benzoate is readily formed. Water and benzene are satisfactory, with a slight apparent advantage in favor of the benzene in the rate of purification by successive batch recrystallizations. The benzene was carefully purified by distillation in a highly efficient rectifying column. In each case the solvent was saturated with benzoic acid at about 100° C, the solution cooled in the usual way to about 15° C, and the recrystallized acid separated on a fritted

glass funnel. One hundred grams of a saturated aqueous solution contains 0.25 g of benzoic acid at 15° C and 5.9 g at 100° C; 100 g of a saturated solution in benzene contains about 7 g of benzoic acid at 15° C and about 78 g at 100° C.[11]

Benzene is a more convenient solvent but not as readily available in high purity as water. The results in table 2 show that purification under the conditions which were maintained in these experiments was more efficient from benzene than from water.

After favorable experience with batch recrystallization, an apparatus was built for continuous recrystallization combined with extraction.[12] The apparatus, shown in figure 1, was essentially an elongated U-tube occupying the full height of the laboratory (about 10 feet), with a condenser connecting the upper ends of the two arms. An enlarged part near the bottom of the larger arm of the U served as a container for the solid benzoic acid. A fritted glass disk, sealed in place near the bottom of this container, supported the crystals. The funnel-shaped part of the apparatus below the disk was designed to minimize channeling. The solvent (benzene was used in the work here described) was introduced by suction into the small arm through the solvent inlet and circulated by gravity. The solvent was saturated at room temperature by dissolving benzoic acid from the bottom of the crystalline mass supported on the fritted disk. Light tapping caused the remainder of the crystalline mass to settle as this process went on. Solvent was added until the saturated solution reached the desired level in the boiler. The liquid level in the two arms was not the same because of the difference in density of pure solvent and saturated solution; however, the arms above the boiler were long enough to compensate for this difference. An electric heating element served to warm the boiler, from which nearly pure solvent distilled through a water-cooled condenser into the opposite arm of the apparatus. Evaporation was allowed to proceed at a regular rate while crystals separated in or just below the boiler. The crystals fell slowly through about 180 cm of the saturated solution and settled on the mass of solid already retained on the fritted disk. During this process the crystals were purified by washing and exchange (reaction) in a solution that was less concentrated with respect to the more soluble fraction than the solution in the boiler from which they separated. An inlet near the top of the container for the solid permitted the passage of a slow current of air up through the extractor arm, which was necessary to keep the crystals agitated and to prevent clogging. The air was saturated with benzene at room temperature to prevent loss of solvent by evaporation. When the apparatus was operated at atmospheric pressure, satisfactory separation of crystals did not occur. It was found by trial to operate properly under a pressure of 215 mm. A receiver was connected with the boiler by a tube which was fitted to the extractor arm through a ground joint. Each time after the entire charge of benzoic acid had been dissolved and recrystallized in the apparatus (at the end of each cycle), a portion of solution was removed from the boiler; and thus a

[11] Atherton Seidell, Solubilities of Inorganic and Organic Compounds, ed. 2, p. 133–135 (D. Van Nostrand Co., New York, N. Y., 1919).

[12] F. W. Rose, Jr., of the American Petroleum Institute Project 6 at the National Bureau of Standards, made many helpful suggestions in the design and application of this method, which is an adaptation to solid material of the Fenske reflux extractor. (M. R. Cannon and M. R. Fenske, Ind. Eng. Chem. 28, 1035 (1936).

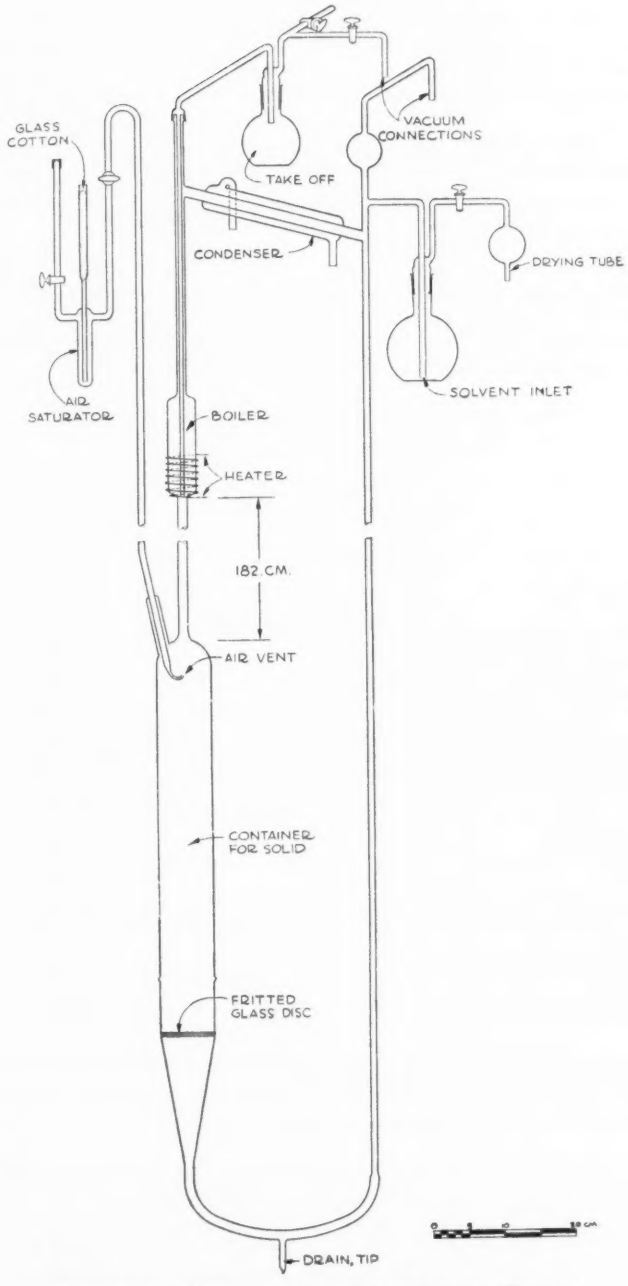

FIGURE 1.—*Apparatus for continuous recrystallization.*

charge could be divided into as many fractions as desired, varying from the most soluble to the least soluble portions of the material. Each fraction was cooled to 15° C, and the crystals which formed were filtered from the mother liquor. Separation per unit crystallization was not as good in this apparatus as that obtained by batch crystallization. This was probably caused, in part, at least, by channeling and diffusion, which prevented ideal separation.

V. RESULTS AND DISCUSSION

The estimates of purity of the preparations discussed in the foregoing paragraphs, together with others obtained in the course of this work, are collected in table 2. For a number of these, the purity was estimated both from the freezing range and from measurements of the apparent specific heat of the solid near its melting point.

TABLE 2.—*Purity of various preparations of benzoic acid*

Preparation	Purity (mole percent)	
	From freezing range	From specific-heat measurements
Standard Sample 39f	99.977	
Standard Sample 39e:		
Untreated	99.983	99.98_9
Recrystallized 4 times from water	[a] 99.99_0	
Recrystallized 8 times from water	99.995	
Recrystallized 4 times from benzene	[a] 99.99_2	
Recrystallized 8 times from benzene	99.999	99.99_9
Recrystallized from benzene in extractor:		
(a) First cycle	99.942	
(b) Composite 3d to 8th cycles	99.995	
(c) Composite 9th, 10th, 11th cycles	99.996	
(d) Composite 13th and 14th cycles	99.998	
After fractionally freezing three times by method 1:		
(a) Head fraction	99.998	99.99_5
(b) Tail fraction	[a] 99.95_0	
After fractionally freezing by method 2:		
(a) Once frozen		99.99_6
(b) Twice frozen	99.999	99.99_9
Heated at 200° C for 72 hours:		
(a) In air	99.954	
(b) In a vacuum	99.976	
(c) In oxygen	99.953	
Hydrolysis of benzoyl chloride:		
Fraction 1: [b]		
(a) Vapor-phase hydrolysis	99.996	
(b) Liquid-phase hydrolysis	[a] 99.99_8	
Fraction 2: [c]		
(a) Liquid-phase hydrolysis	99.999	
Oxidation of purified toluene [d]	99.980	

[a] These values were obtained by an earlier method and are not as accurate as the other results.
[b] Original product was recrystallized from water 7 times.
[c] Original product was not recrystallized; hydrogen chloride and water were removed by passing dry air through the liquid.
[d] Original product was recrystallized from water 4 times.

It will be seen that the best preparations obtained by crystallization from benzene, by hydrolysis of benzoyl chloride, and by fractional freezing are of substantially equal purity, as estimated from the freezing range, and that any of the three methods can be used to prepare benzoic acid of sufficiently high purity to meet very exacting requirements. In using the substance two circumstances must always be

taken into account. One is that it is notably hygroscopic in the liquid phase and the other that formation of anhydride occurs, very slowly, at temperatures near the melting point of the acid if the atmosphere in contact with it is very dry (much drier than is ever encountered without intentional and thorough drying).

A valid objection may be raised to the use of the freezing (or melting) behavior as a criterion of purity for a substance purified by fractional freezing. Quite apart from the fact that the freezing range of the substance purified by fractional freezing was substantially equal to those of the best preparations obtained by crystallization from benzene and by hydrolysis of benzoyl chloride, the temperature at any given stage of freezing was identical for the three preparations, within the reproducibility of the measurements (about 0.002° C).[13] This is independent evidence that these three preparations were identical in composition, and hence were pure substances rather than mixtures of the rare type that has a constant freezing point.

A brief comment on the freezing point of benzoic acid may be desirable. Estimation of purity from the freezing range is based entirely on sufficiently precise measurement of *differences* in temperature, rather than on any exact knowledge of the actual temperatures of freezing. Since the freezing point of benzoic acid was not of direct interest in the work reported in this paper, the resistance thermometer and bridge were not kept under calibration in a manner to permit recording absolute freezing temperatures to 0.001° C, although differences in temperature of about 0.0001° C during freezing were regarded as significant. Further, the measurement of a freezing range involves the withdrawal of heat at a rate rapid enough to cause the observed temperature to differ somewhat from the true temperature of equilibrium between the liquid and solid phases. These considerations limit the accuracy with which the freezing point of benzoic acid can be reported on the basis of the work with which this paper is concerned. The value tentatively assigned is 122.36 $\pm$0.01° C.

WASHINGTON, September 27, 1940.

[13] The average deviation was 0.002° C and the range was 0.005° C. The freezing temperature of the product obtained by fractional freezing fell between that of the other two.

U. S. DEPARTMENT OF COMMERCE NATIONAL BUREAU OF STANDARDS

RESEARCH PAPER RP1352

Part of Journal of Research of the National Bureau of Standards, Volume 25, December 1940

EFFECT OF COMPOSITION AND OTHER FACTORS ON THE SPECIFIC REFRACTION AND DISPERSION OF GLASSES

By John C. Young and Alfred N. Finn

ABSTRACT

Seven of the better known specific-refraction ratios were examined for their comparative applicability to glass. It is shown by a comprehensive statistical treatment of available data (including many new data) that, of these ratios, only the Gladstone-Dale possesses to a satisfactory degree each of the following desirable features: (1) It varies linearly with chemical composition and with the square of the wave number of the incident light; (2) for a given composition and wavelength of light, it is substantially the same for both the vitreous and crystalline states; and (3) for the vitreous state, it is independent of thermal history. Gladstone-Dale factors for 47 oxides as constituents of glass (and corresponding factors derived from nonglassy substances) are given. These factors are shown to be related to the periodicity of the elements. Specific dispersion factors, useful for computing the dispersion index, or ν-value, of a glass are given for 32 oxides.

CONTENTS

	Page
I. Introduction	759
II. Source material	761
III. Correlation of the data	761
1. Chemical composition	761
2. Heat treatment	766
3. Vitreous and crystalline states	767
(a) Oxides	767
(b) Elements	769
4. Wavelength of light	771
IV. Relation of the Gladstone-Dale ratio to the periodic arrangement of the elements	772
V. Relation of dispersion to specific refraction and to composition	777
VI. Summary	781
VII. References	781

I. INTRODUCTION

Many attempts have been made to link the refractive index and density of a substance in such a way that the proposed relationship, frequently called specific-refraction or specific-refractive power, would possess, among other features, the following: (1) It would be constant for a given substance and wavelength of light when certain other conditions are varied; (2) it would bear an additive relationship to the chemical composition of a substance and vary linearly with some simple function of the wavelength of light. A great deal has been written on the subject in its application to gases and liquids since Gladstone and Dale developed their well-known theorem [1].[1] Larsen and Berman [2] determined the Gladstone-Dale ratio for hundreds

[1] Numbers in brackets indicate the literature references at the end of this paper.

of minerals and calculated factors for the constituent oxides. But in the field of glass technology, despite the apparent wealth of data, similar work has been confined to a very few of the commoner oxides. Morey and Merwin [3] calculated specific-refraction factors for soda-lime-silica glasses, using the Gladstone-Dale and other proposed formulas. More recently Wulff and Majumdar [4] applied the Lorentz-Lorenz formula to a few soda–boric-oxide glasses, while Biltz and Weibke [5], using principally the data of others, calculated Gladstone-Dale factors for Na_2O, K_2O, CaO, B_2O_3, and SiO_2. Randall and Gee [6] utilized the Lorentz-Lorenz ratio in connection with atomic size for calculating the refractive index of glasses containing PbO in addition to the oxides just enumerated. Still more recently, Kordes [7] studied the variation in the Lorentz-Lorenz ratio of glasses with composition; he obtained some data on glasses in the binary systems PbO-B_2O_3, ZnO-B_2O_3, CdO-B_2O_3, PbO-SiO_2, and PbO-P_2O_5, and expressed his results by some rather complicated empirical equations.

The results of none of these investigations, however, have a general application, owing to the limited fields of composition studied. It was the purpose of the present research, therefore, to determine, by a comprehensive statistical study of all available data, how a number of the proposed specific-refraction relationships apply, under a variety of conditions, to glass and glass-forming materials.

The specific refraction (R) type ratios considered are:

$\frac{n-1}{D}$	Gladstone-Dale [1]
$\frac{n^2-1}{n^2+2}\cdot\frac{1}{D}$	Lorentz-Lorenz [8, 9]
$\frac{\log n}{D}$	Lichtenecker [10]
$\frac{n^2-1}{n+0.4}\cdot\frac{1}{D}$	Eykman [11]
$\frac{n^2-1}{D}$	Newton [12]
$\frac{\sqrt{n}-1}{D}$	Johst [13]
$\frac{n-1}{nD}$	Edwards [14]

In these formulas, n and D are refractive index and density, respectively. Unless otherwise stated, n is for sodium light.

The variables considered, which might influence the various specific refraction ratios of a glass or oxide, are changes in (1) chemical composition, (2) heat treatment, (3) vitreous and crystalline states, and (4) wavelength of light.

No data are presented here on the effect of temperature on the different type ratios. It is a well-established fact [40] that, whereas

the density of a glass decreases continuously with rising temperature, there is usually a corresponding decrease in the refractive index only in the rapid-expansion range. Therefore, for most glasses, none of the type ratios could remain constant or vary linearly with increasing temperatures, except possibly for certain limited temperature ranges.

II. SOURCE MATERIAL

The data on glass herein considered were collected from many sources, references to which are given at the end of this paper. References not specifically mentioned in the text are indicated in tables 2 and 8, under the heading "Source of glass data."

The symbol "*s*" in tables 2 and 8 refers to unpublished data on certain of the more unusual oxides incorporated in glasses made especially for this study. For each of these glasses, one of the special oxides was added to a parent glass having the composition 71.5 percent of SiO_2, 18.3 percent of Na_2O, and 10.2 percent of CaO (weight percentages), the amount added varying with the different glasses of a given series up to the maximum percentage indicated. All of these glasses were made from materials of known composition, but only the glasses containing Rb_2O, Cs_2O, ThO_2, and ZrO_2 were analyzed.

The symbol "*u*" in the tables refers to unpublished data obtained at this Bureau on a wide variety of glasses containing only the more common oxides. Nearly all of these glasses were analyzed.

The symbol "*g*" in the tables refers to some data on natural glasses, the compositions of which are given by Washington [37], and the corresponding densities and refractive indices by George [38].

The data on crystalline and liquid compounds are taken almost exclusively from the International Critical Tables [36].

III. CORRELATION OF THE DATA

1. CHEMICAL COMPOSITION

To determine the relative degree of linearity of the relationship between chemical composition and the various type ratios, two series of binary glasses were first studied, a series of 51 soda-silica, and a series of 35 potash-silica glasses, whose densities (but not the corresponding refractive indices) and compositions have been reported recently by this Bureau [15]. Figure 1 shows the results obtained by plotting the specific refractions of the glasses in each series, as computed from the seven type formulas previously mentioned, against the composition (silica content) of the glasses. The individual specific refraction values, R, for these two series of glasses, together with those of 60 additional glasses containing all three of these constituents (Na_2O, K_2O and SiO_2) [15], were used to determine, by a least squares solution, the unknown constants of the equation.

$$R=1/100(r_A p_A+r_B p_B+r_E p_E), \qquad [1]$$

for each of the type ratios (except the Newton and the Edwards). The p's are the weight percentages of silica, A; soda, B; and potash, E, respectively, and the r's are constants which may be considered as the

specific refraction factors of the respective oxides. In each solution the respective factor for silica, r_A, was considered as "known", and was obtained from the most probable values of the refractive index

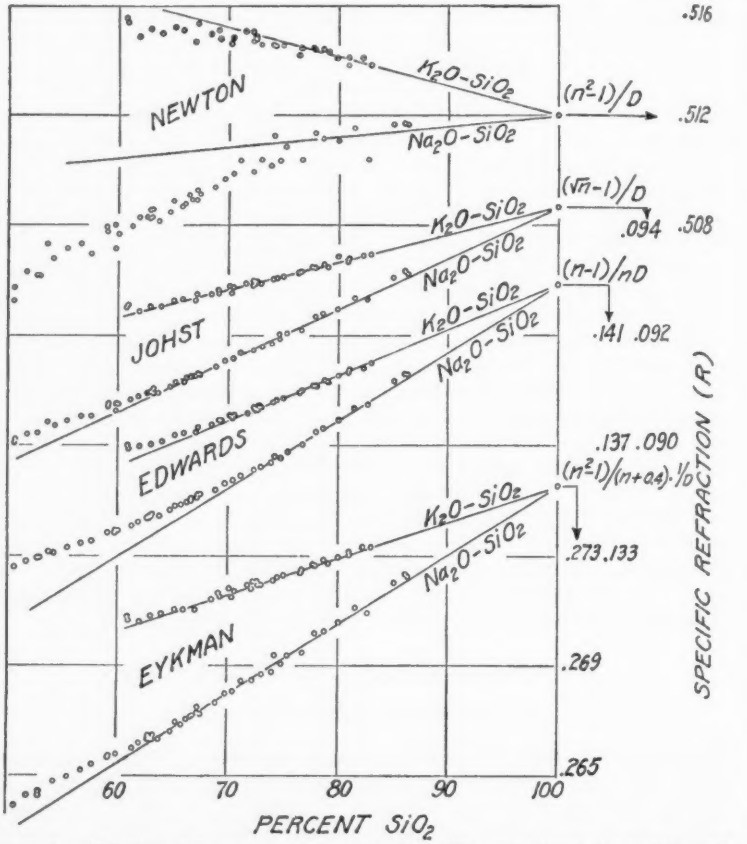

FIGURE 1.—*Relation between specific refraction (R), calculated from the various formulas and compositions, for a series of soda-silica and a series of potash-silica glasses made at the National Bureau of Standards* [15].

and of the density of vitreous silica [18], that is, 1.4585 and 2.2026, respectively. The results of these calculations are shown in table 1.

TABLE 1.—*Values of constants for eq 1, and average deviation between observed and calculated specific refractions (R) for 146 soda-potash-silica glasses*

Type ratio (R)	r_A	r_B	r_a	Average percentage deviation from observed R's	Average deviation in terms of n_D
Gladstone-Dale	0.20815	0.19365	0.20185	0.045	0.00025
Lorentz-Lorenz	.12400	.11025	.11585	.092	.0006
Lichtenecker	.07444	.06584	.06894	.100	.0007
Eykman	.27537	.25123	.26267	.065	.0004
Johst	.09430	.08533	.08931	.070	.0007

It is evident from table 1 that the average percentage deviation for the Gladstone-Dale ratio is about two-thirds that for the Eykman, and about half those for the Lorentz-Lorenz, Lichtenecker, and Johst

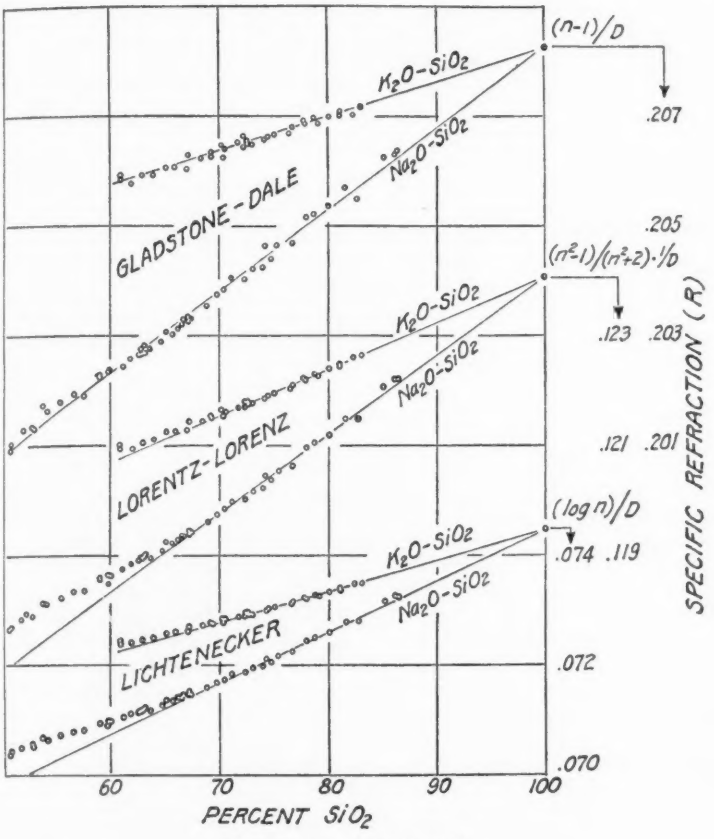

FIGURE 1.—(Continued)

ratios. Moreover, the deviations for the latter four type ratios appear to be highly systematic (as shown in part by fig. 1),[2] while the "average deviation in terms of n_D" is sufficiently small to be comparable to the experimental error in refractive index (about 0.0002) for the Gladstone-Dale ratio only. Although the average percentage deviations shown in table 1 are somewhat less than those found by Morey and Merwin for a series of soda-lime-silica glasses (they did not consider the Johst ratio), the values of the constants for the soda-silica glasses, and the relative "goodness of fit" of the straight lines for the various type formulas, are in good agreement with the findings of those investigators.

[2] The straight lines were drawn in figure 1 merely to show visually the departure of the plotted points from linearity and have no connection with the constants given above.

No similar computations were made for the Newton and the Edwards type ratios for, while there may be some justification for fitting straight lines to the points of the potash-silica data, an inspection of the respective graphs for the soda-silica glasses shows rather decisively that these ratios are not linear with composition. Indeed, it is worth noting that the plots for the Edwards ratio bear a striking resemblance to those recently presented by this Bureau, illustrating for the same binary systems the relation between specific volume and composition [15]. The percentage change in specific refraction per unit silica content, however, is less for the Newton ratio than for any of the other ratios studied.

From these preliminary data, therefore, it appears that only the Gladstone-Dale ratio affords a fit sufficiently close to a linear relationship to justify its application to glasses of a wide variety of compositions. Accordingly, with the foregoing constants serving as a basis, the Gladstone-Dale specific refraction factors, r, for many other oxides as constituents of glasses, were calculated statistically from the available data to fit the following general expression (simply an extension of equation 1):

$$R=1/100(r_A p_A+r_B p_B+ \ldots .). \quad (2)$$

The values of the factors thus determined for the different oxides are given in table 2, column 4. Many of these factors were evaluated from a composite body of data drawn from more than one source. Preliminary study had shown that, regardless of what oxides were present in the different glasses or what the thermal histories of the glasses were, data from different sources did not yield significantly different values of the Gladstone-Dale factor for a particular oxide. The completed equation, therefore, appears to hold for glasses of greatly differing compositions and also for pure vitreous silica and germania, whose specific refraction values are known from measurements on the oxides themselves.

TABLE 2.—*Specific refraction factors of some oxides as occurring in glasses and crystals*

Oxide	Glass			Crystal			Source of glass data [b]
	Number of glasses containing oxide	Maximum percentage [a]	r (Gladstone-Dale)	Number of compounds containing oxide	r (Gladstone-Dale)	r (Lorenz-Lorentz)	
1	2	3	4	5	6	7	8
H_2O	3	9	0.344	128	0.345	0.231	g
Li_2O	11	26	.308	8	.293	----------	u
Na_2O	111	50	.1937	24	.197	.156	u [15]
K_2O	95	40	.2019	21	.204	.193	u [15]
Rb_2O	3	55	.133	13	.134	.099	u
Cs_2O	2	60	.124	13	.130	.086	u
Tl_2O	5	55	.148	7	.120	----------	u [31]
$(NH_4)_2O$	----------	----------	----------	14	.542	----------	----------
BeO	44	16	.236	5	.232	----------	[24, 25]
MgO	26	40	.212	34	.217	.126	u [33]
CaO	46	56	.2270	36	.228	.136	[3, 16, 17]
ZnO	28	65	.150	12	.156	.095	u [7, 21, 34]
SrO	4	63	.154	3	.151	----------	u [32]

See footnotes at end of table.

TABLE 2.—*Specific refraction factors of some oxides as occurring in glasses and crystals*—Continued

Oxide	Glass			Crystal			Source of glass data [b]
	Number of glasses containing oxide	Maximum percentage [a]	r (Gladstone-Dale)	Number of compounds containing oxide	r (Gladstone-Dale)	r (Lorentz-Lorenz)	
1	2	3	4	5	6	7	8
CdO	7	71	.126	4	.115		*u* [7]
BaO	18	49	.126	9	.129	.076	*u* [30, 34]
PbO	44	82	.134	8	.139		[7, 30, 34]
NiO				9	.152	.151	
CoO				8	.151	.156	
CuO				6	.19		
MnO				17	.197	.142	
FeO	3	11	.190	21	.198	.114	*g*
HgO				[c] 1	.112		
B_2O_3	45	100	.236	7	.208		[7, 21, 34]
Al_2O_3	61	37	.2070	64	.204	.116	[20, 33]
Sc_2O_3				1	.23		
Ga_2O_3	3	11	.153	4	.158		*s*
Y_2O_3	3	12	.172	5	.151		*s*
In_2O_3	3	17	.138	2	.14		*s*
La_2O_3	3	20	.146		[d](.149)		*s*
Ce_2O_3				3	.143		
Pr_2O_3	3	15	.143	1	.14		*s*
Nd_2O_3	8	10	.138	1	.14		*s*
Sm_2O_3	4	15	.130	1	.13		*s*
Gd_2O_3	2	15	.124				*s*
Ho_2O_3	2	10	.157				*s*
Er_2O_3	3	15	.120				*s*
Cr_2O_3				4	.233		
As_2O_3				10	.179		
Fe_2O_3	3	30	.265	14	.262	.170	*s*
Bi_2O_3	11	53	.147	5	.168		[26]
Sb_2O_3	4	20	.169	3	.22		[26, 34]
CO_2				8	.217		
SiO_2	[c] 1	100	.2082	69	.208	.108	[18]
TiO_2	8	10	.300	7	.371		*s* [23]
GeO_2	5	100	.167	2	.166		[28, 29]
ZrO_2	8	18	.209	[c] 1	.213		*s*
SnO_2	2	10	.15$_9$	[c] 1	.148		*s*
ThO_2	5	20	.113	[c] 1	.120		*s*
CeO_2	8	6	.16$_9$				*s*
UO_2				3	.121		
N_2O_5				7	.231		
P_2O_5	12	71	.202	25	.196	.037	[7, 34]
V_2O_5	3	3	.35	3	.38		*s*
As_2O_5				15	.173		
Cb_2O_5	3	16	.230	1	.23		*s*
Sb_2O_5	1	18	.16		[d](.152)		*u*
Ta_2O_5	3	17	.134		[d](.133)		*s*
Cl_2O_5				3	.218		
Br_2O_5				3	.175		
I_2O_5					[d](.177)		
SO_3				65	.177	.057	
CrO_3				6	.307		
SeO_3				21	.161	.063	
MoO_3	2	3	.21	5	.22		*s*
WO_3	4	10	.142	3	.13		*s*
UO_3	2	3	.12	6	.12		*s*
Mn_2O_7				1	.22		
OsO_4				[c] 1	.13		

[a] Figures in this column indicate for each oxide the maximum percentage reported in the literature referred to in column 8; validity of the factor is not necessarily confined to such maximum.

[b] Numbers in brackets indicate references at the end of this paper; *s* indicates unpublished data on special glasses made at this Bureau (see section II); *u* indicates other unpublished data obtained at this Bureau; *g* indicates data from natural glasses [37, 38]; all crystal data are from International Critical Tables.

[c] Pure oxide.

[d] From Larsen and Berman [2].

The most discordant data are those involving B_2O_3; the various measurements on the pure oxide give an average value for r of about 0.250, whereas the value obtained from glasses containing B_2O_3 as a constituent is 0.236. The latter value may be more nearly correct than the former, because the difficulties of obtaining anhydrous glasses containing B_2O_3 seem to increase with increasing percentages of B_2O_3, and any water present would tend to increase the specific refraction, since the factor r, for water is 0.345. Similarly, the effect of water on glasses containing P_2O_5 may lead to discordant results; the factor determined for P_2O_5 in glass is about 0.202, whereas from Kordes' data [7] on some PbO-P_2O_5 glasses, the specific-refraction-composition graph curves upward with increasing P_2O_5 content, attaining the value 0.225 for a pure P_2O_5 glass. Kordes admitted that his reported densities on the glasses of high P_2O_5 content were probably too low, and for that reason they were not included in the present calculations. Concerning certain other elements as, for instance Fe, Tl, and Sb, there is reason for believing that some amount of such elements may be present in glass in states of oxidation other than that reported. Our own vanadium glasses, for example, although calculated to contain V_2O_5, had the greenish color characteristic of V_2O_3.

2. HEAT TREATMENT

There appear to be very few published data on the effect of heat treatment of glass on the resulting specific refraction. The most extensive sets of data, involving a wide variation in heat treatment, are those of Morey and Merwin on soda-lime-silica glasses [3], and of Tool and Tilton on various optical glasses [19].[3] Statistical analysis of the former data shows that, in contrast to the differences in density of about 0.27 percent, on the average, between the "annealed" and the "unannealed," glasses the corresponding differences in specific refraction vary from 0.15 percent for the Edwards ratio, to only 0.04 percent for the Newton, and 0.03 percent for the Gladstone-Dale ratios. The latter percentage difference is within the stated precision of the respective measurements, and the percentage differences for the individual glasses are not noticeably related to composition. Similar evidence is afforded by the data of Tool and Tilton on optical glasses, as well as by some observations made by the authors on a plate glass (unpublished data), and also by Wulff and Majumdar's data on a soda-boric oxide glass [4]. A résumé of all these data is given in table 3, from which it may be concluded that the Gladstone-Dale and the Newton ratios show, about equally, the least variation with differing heat treatments, whereas the Edwards ratio shows the greatest.

[3] The data in the latter paper consisted not of a report of the actual measurements, but of a set of coefficients derived from such measurements, whereby the refractive indices and densities corresponding to the different heat treatments may be calculated for the various glasses if the index and density corresponding to some one similar heat treatment are known. When these factors were published they were said to be subject to revision as additional data were obtained. The values given in table 3 of the current report are based on the latest (but unpublished) factors. In each case the heat treatment applied consisted in chilling the glass from a given temperature after approximate equilibrium had been attained.

TABLE 3.—*Effect of heat treatment on specific refractions (R) of various glasses*

	Optical glasses [19]					
	Medium flint	Light crown	Light barium crown	Borosilicate crown	Dense flint	Dense barium crown
Range of annealing temperatures [1] (°C)	360 to 440	460 to 540	480 to 560	460 to 540	360 to 440	560 to 620
n_D for highest annealing temperature used [1]	1.5891	1.5196	1.5725	1.5165	1.6548	1.6215
Density for highest annealing temperature used [1]	3.3428	2.4932	3.1503	2.5242	3.9218	3.6911
Percentage increase for each 100 degree *C* decrease in annealing temperature:						
n_D	0.16	0.20	0.38	0.32	0.23	0.37
Density	.47	.64	.96	1.02	.66	1.24
Gladstone-Dale	−.03	−.06	−.18	−.09	−.08	−.28
Lorentz-Lorenz	−.13	−.17	−.33	−.26	−.32	−.48
R Lichtenecker	−.13	−.17	−.33	−.27	−.21	−.48
Newton	+.07	+.05	−.01	+.08	+.06	+.05
Eykman	−.07	−.11	−.24	−.17	−.13	−.40
Johst	−.08	−.12	−.26	−.19	−.15	−.38
Edwards	−.20	−.26	−.47	−.41	−.32	−.65

	Plate glass		Soda-boric oxide glass [4] [2]		Soda-lime-silica glasses [3] [2]	
	A Chilled from 660°C	*B* Cooled 5°C per hour through "annealing range"	*A* "Quickly cooled"	*B* "Slowly cooled"	*A* "Unannealed"	*B* "Annealed"
n_D	1.5189	1.5205	1.4797	1.4841	----------	----------
Density	2.4997	2.5072	1.9690	1.9876	----------	----------
Percentage increase of *B* over *A*: n_D	0.11		0.30		0.07	
Density	.30		.95		.27	
Gladstone-Dale	−.01		−.02		−.03	
Lorentz-Lorenz	−.04		−.15		−.13	
R Lichtenecker	−.04		−.19		−.09	
Newton	+.07		+.16		+.04	
Eykman	−.02		−.08		−.07	
Johst	−.02		−.12		−.08	
Edwards	−.10		−.32		−.15	

[1] Measurements of n_D and density made after sample was cooled quickly from annealing temperature. See text footnote 3.
[2] The composition of this glass is given as 93.2% of B_2O_3 and 6.8% of Na_2O.
[3] Figures under this heading represent averages based on the entire series of glasses.

3. VITREOUS AND CRYSTALLINE STATES

(a) OXIDES

Assuming a linear relationship with composition, as in section III–1, the Gladstone-Dale ratios for 60 oxides were calculated from the data on about 400 crystalline oxides and compounds reported in the International Critical Tables. The compounds considered were only those consisting of two or more of the oxides listed in table 2, and for convenience will be referred to as "oxide-compounds." The refractive index used for each compound was the mean index for the crystal (that is $(2\omega+\epsilon)/3$ or $(\alpha+\beta+\gamma)/3$), but in general the data were not used for crystals whose birefringence exceeded 0.04 in refractive index.

The data on more than 200 of these compounds, containing one or more of 20 of the commoner oxides, were treated separately from the main body of data, and the individual factors, r, for these oxides determined simultaneously by the method of least squares. The number of compounds containing each oxide varied from 8 for CoO to 128 for H_2O. The available experimental data on the pure oxides were included, but they were not weighted differently from the data on the compounds containing these oxides. The factor for each of the oxides not included in this solution was determined from the average contribution of that oxide to the specific refractions of all the compounds containing only that oxide in addition to other oxides whose factors were already evaluated.

The results obtained are given in table 2, column 6. The agreement between these values and those reported by Larsen and Berman [2] is very good, whereas the average deviation between calculated and observed specific refractions (about 2.5 percent) appears to be somewhat lower than theirs. The number of significant figures given in table 2 for the different oxide factors varies from two to four, and represents a rough estimate of the precision of the factors; each factor is thought to be precise within two or three units in the last decimal given. Although most of the factors are given to three decimals, it is difficult to estimate the accuracy of any one of these factors since the accuracy depends, among other things (and in some cases in an unknown manner), upon (1) the reliability of the physical measurements, (2) the amount of birefringence of an individual compound, (3) the percentage of the oxide in the compound, and (4) the number of compounds used in evaluating the factor. Each of these items varies considerably from one compound to another.

Although, as indicated in section III–1, the relation between composition and the Lorentz-Lorenz ratio does not appear to be linear for glasses, a computation similar to that just outlined for the Gladstone-Dale factors was made nevertheless to determine the Lorentz-Lorenz factors for each of the original 20 constituent oxides. This computation entailed merely the substitution of the appropriate Lorentz-Lorenz values in the left-hand members of the 20 normal equations previously set up for the Gladstone-Dale ratio, and performing the necessary numerical operations. The factors thus found for these oxides are given in table 2, column 7. It was found, however, that the average deviation between the observed and the calculated values for the Lorentz-Lorenz ratio was over 7 percent, which is almost three times that for the Gladstone-Dale ratio. Moreover, in most cases the Lorentz-Lorenz oxide-factors obtained by solving the normal equations are considerably different from the corresponding values for the pure oxides—a further evidence that the Lorentz-Lorenz specific-refraction–composition relationship is not linear. The foregoing calculations for the Lorentz-Lorenz factors were made principally because this type ratio is widely favored for a variety of purposes, and for certain limited applications has some theoretical foundation, but no similar computations for the other type ratios were attempted.

It should be noted from table 2 that in most cases the Gladstone-Dale factor, r, for an oxide in a crystalline compound, is not markedly different from that of the same oxide as a constituent of glass. A partial explanation for most of the large discrepancies found has already been indicated in section III–1. Concerning observations on the pure oxides, refractive index and density data for both the crystalline and vitreous state appear to be limited to those on SiO_2, and these data are accordingly reported in table 4, together with the corresponding values for all the type ratios studied. Table 4 indicates that the Gladstone-Dale ratio is substantially the same for both vitreous SiO_2 and the various modifications of crystalline SiO_2. Moreover, as between quartz and vitreous silica, the order of placement (by percentage difference) of the various type ratios is about the same as that found for heat treatment of glasses—least for the Gladstone-Dale ratio, greatest for the Edwards. It might be mentioned in passing that this correspondence is not surprising, since the different states might be regarded in a sense as the outcome of different "heat treatments."

TABLE 4.—*Specific refractions of vitreous and crystalline* SiO_2

	n_D	Density	Specific refraction (R)						
			Gladstone-Dale	Lorentz-Lorenz	Lichtenecker	Newton	Eykman	Johst	Edwards
(*A*) Vitreous silica	1.4585	2.203	0.2081	0.1240	0.0744	0.5117	0.2753	0.0943	0.1427
(*B*) Tridymite	1.470	2.26	.2080	.1234	.0740	.5137	.2747	.0940	.1415
(*C*) Cristobalite	1.486	2.32	.2094	.1238	.0741	.5208	.2761	.0944	.1410
(*D*) Quartz	1.547	2.651	.2064	.1197	.0715	.5257	.2700	.0920	.1334
Percentage increase of (*D*) over (*A*)	6.0	20.5	−0.8	−3.5	−3.9	+2.7	−2.0	−2.5	−6.5

(b) ELEMENTS

Thus far the oxide has been taken as the basic unit for a glass or compound. Assuming that the specific refraction (Gladstone-Dale) of a compound is an additive function of the specific refractions of its constituent elements, the atomic refraction, mr', for each of the various elements was evaluated statistically to fit the formula,

$$MR = n_a m_a r_a' + n_b m_b r_b' + \ldots . \qquad (3)$$

For each compound, M and R are the molecular weight and specific refraction, respectively, and m, n, and r' are the atomic weight, number of atoms, and specific refraction factor ("element-factor") of each of the elements a, b, etc., occurring in the compound. The data used were derived from about 300 miscellaneous crystalline and liquid compounds, including halides and metal-organic compounds, listed in the International Critical Tables, and for convenience will be referred to as "miscellaneous compounds"; but none of those described above as "oxide compounds" was included. The values of atomic refraction, mr', thus found are given in table 5, column 4.

TABLE 5.—*Atomic refraction factors (mr')*

Valence group	Serial number	Element A	Element B	Atomic refraction factors (mr') From miscellaneous compounds [a]	From "oxide compounds" (table 2, col. 6) O=2.50	Weighted average from all compounds [a]	From glasses (table 2, col. 4) O=2.50
1	2	3		4	5	6	7
I	1		H	1.81 (34)	1.85	1.84 (162)	1.84
	2		Li	3.4 (6)	3.1$_5$	3.25 (14)	3.35
	3		Na	4.9$_0$ (11)	4.8$_7$	4.88 (35)	4.73
	4	K		8.3 (10)	8.3$_5$	8.33 (31)	8.25
	5		Cu	14.1 (10)	12.6	13.5 (16)	
	6	Rb		11.9 (3)	11.4	11.5 (16)	11.2
	7		Ag	20 (10)		20 (10)	
	8	Cs		17.5 (3)	17.0	17.2 (16)	16.7
II	2		Be	3.2 (1)	3.3	3.3 (6)	3.40
	3		Mg	6.3 (8)	6.3$_0$	6.3$_0$ (42)	6.05
	4	Ca		10.5 (6)	10.3	10.3 (42)	10.25
	5		Zn	10.0 (3)	10.2	10.2 (15)	9.70
	6	Sr		13.6 (4)	13.1	13.4 (7)	13.5
	7		Cd	17.0 (5)	11.9	14.7 (9)	13.7
	8	Ba		16.5 (10)	17.3	16.9 (19)	16.8$_1$
	11		Hg	20 (4)	22	21 (5)	
III	2		B	4.4 (3)	3.5	3.7$_5$ (10)	4.4$_1$
	3		Al	6.9 (7)	6.6$_2$	6.6$_5$ (71)	6.80
	4	Sc			12.0	12.0 (1)	
	5		Ga		11.1	11.1 (4)	10.9
	6	Yt			13.2	13.2 (5)	15.7
	7		In		17.2	17.2 (2)	15.3
	8	La		21 (1)		21 (1)	20.0
	11		Tl		24.2	24.2 (5)	30.4
IV	2		C	4.8$_0$ (39)	4.3$_0$	4.7$_2$ (47)	
	3		Si	7.4 (4)	7.50	7.50 (73)	7.52
	4	Ti		27 (2)	24.5	25 (9)	19.0
	5		Ge	12.7 (2)	12.3	12.5 (4)	12.4$_1$
	6	Zr			21.2	21.2 (1)	20.8
	7		Sn		17.3	17.3 (1)	17.2
	8	Ce		20 (3)	20.2	20 (6)	22.2
	11		Pb	28.0 (18)	28.5	28.1 (26)	27.4
	12	Th			26.7	26.7 (1)	25.0
V	2		N	4.4$_0$ (16)	6.2	4.9$_5$ (23)	
	3		P	7.9 (10)	7.6$_5$	7.7$_3$ (35)	8.1
	4	V		31 (1)	28$_6$	29$_2$ (4)	25.4
	5		As	14.9 (4)	13.7	13.9 (29)	
	6	Cb			24.5	24.5 (1)	24.5
	7		Sb		[b] 19.3	[b] 19.3	19.5
	10	Ta			[b] 24.2	[b] 24.2	23.4
	11		Bi		35.5	35.5 (5)	30.5
VI	2		O^{2-}	2.50 (38)		2.50 (38)	
	3		S	8.8 (19)	6.7$_0$	7.2$_3$ (83)	
			S^{2-}	29.5 (14)		29.5 (14)	
	4	Cr		20 (1)	22	22 (11)	
	5		Se		13.1	13.1 (21)	
	6	Mo			24	24 (5)	23.1
	10	W			23.7	23.7 (3)	25.2
	12	U			27.4	27.4 (9)	26.9
VII	2		F^-	0.5$_0$ (15)		0.5$_0$ (15)	
	3		Cl		10.1	10.1 (3)	
			Cl^-	10.0 (31)		10.0 (31)	
	4	Mn		12 (2)	11.7	11.7 (20)	
	5		Br		14.7	14.7 (3)	
			Br^-	15.7 (18)		15.7 (19)	
	7		I		[b] 23.3	[b] 23.3	
			I^-	24.0 (10)		24.0 (10)	

[a] Numbers in parentheses after factor indicate number of compounds used in evaluating that factor.
[b] From oxide values given by Larsen and Berman [2].

TABLE 5.—*Atomic refraction factors (mr')*—Continued

Valence group	Serial number	Element A	Element B	Atomic refraction factors (mr') From miscellaneous compounds	From "oxide compounds" (table 2, col. 6) O=2.50	Weighted average from all compounds	From glasses (table 2, col. 4) O=2.50
1	2	3		4	5	6	7
VIII	4	.....	Fe^{2+}	.....	11.7	11.7 (21)	11.1
	4	.....	Fe^{3+}	18.1 (3)	17.4	17.5 (17)	17.4
	4	.....	Co	9.3 (2)	8.8	9.2 (10)	.....
	4	.....	Ni	10.3 (2)	8.9	9.2 (11)	.....
	10	.....	Os	.....	22	22 (1)	.....
	10	.....	Pt	25 (2)	.....	25 (2)	.....
Rare earths	.....	.....	Pr	20 (1)	20	20 (2)	19.9
	.....	.....	Nd	20 (1)	20	20 (2)	19.8
	.....	.....	Sm	19 (1)	19	19 (2)	19.0
	.....	.....	Eu	21 (1)	.....	21 (1)	.....
	.....	.....	Gd	19 (1)	.....	19 (1)	18.8
	.....	.....	Dy	18 (1)	.....	18 (1)	.....
	.....	.....	Ho	.....	.....	.....	25.7
	.....	.....	Er	23 (1)	.....	23 (1)	19.7

The condition that the various element factors do not change for different valencies was, of course, implicitly assumed in deriving these values. Since it has long been known that such an assumption is not valid for every type of material, a careful comparison of the observed and computed specific refractions of the individual compounds was made for the purpose of revealing any systematic deviations which might reasonably be ascribed to valency. Some tendency toward systematic deviation between observed and computed specific refractions was found for compounds containing long-series elements (*A*-subgroups) of the periodic system, but the results of the search were not on the whole conclusive, considering the probable accuracy of the observations. On the other hand, a rather close agreement was found between the atomic refraction factors, *mr'*, as evaluated for eq 3 and those calculated directly from the oxide factors previously determined (either glassy or crystalline), by applying, in every case, the value 2.5 for the atomic refraction of oxygen. For this comparison see table 5. It should be stated, however, that of the many compounds involved in the determination of the atomic refraction factors, less than 10 percent contained elements of the *A*-subgroups (long-series elements), so that the computations are heavily weighted in favor of the *B*-subgroups (short-series elements). Therefore, granting that the factors might vary with the different valencies, the data available are too few for demonstrating such a difference by the present method.

4. WAVELENGTH OF LIGHT

All specific-refraction values considered up to this point have been based on the refractive index for sodium light only, but the methods of analysis used may be extended to include data involving other

wavelengths. The most complete data available on a glass-forming material for correlating specific refraction with wavelength, λ, are those on the refractive index of vitreous silica for various wavelengths from 0.1855 to 0.7948 micron [18]. A plot of R against the square of the wave number, $1/\lambda^2$, (a modified application of the Cauchy dispersion formula) gives, within very narrow limits of error (expressible as ± 0.0001 in refractive index), a straight line from about 0.3000 to 0.7000 micron for each of the seven type ratios. For many of the soda-lime-silica and soda-potash-silica glasses made at this Bureau, the refractive indices have been measured (but not yet published) for the four wavelengths 0.4358, 0.5461, 0.5893, and 0.6708 micron. The Gladstone-Dale ratio for each of these wavelengths was accordingly correlated with composition, following the same system of computation used in section III–1, and the four factors, r's, thus obtained for each of the oxides, Na_2O, CaO, and K_2O, as constituents, were plotted as functions of $1/\lambda^2$. As in the case of the R for vitreous silica, these factors were found also to be linear functions of $1/\lambda^2$ within the limits of the data, that is, for each oxide, $r=\alpha+\beta\ (1/\lambda^2)$, λ being expressed in microns. Table 6 gives the values thus obtained for the constants (α's and β's) for all four oxides in the expression

$$R=(\alpha_A+\beta_A.1/\lambda^2)p_A+(\alpha_B+\beta_B.1/\lambda^2)p_B+\ \ldots \qquad (4)$$

For the same reason stated in section III–1, no attempt was made to obtain similar values of α and β for the other type ratios.

TABLE 6.—*Values of constants for eq 4*

Constants	SiO_2	Na_2O	K_2O	CaO
α	0.20355	0.18610	0.19540	0.21715
β	.001595	.00262	.00222	.00257

IV. RELATION OF THE GLADSTONE-DALE RATIO TO THE PERIODIC ARRANGEMENT OF THE ELEMENTS

Larsen and Berman [2], in their work on the specific refractions of the oxides in minerals, stated that there was a tendency for the specific-refraction values in each group to decrease as the molecular weight increases, but that there are many exceptions. It is found that the oxide factors obtained for glasses behave in a similar manner; the exceptions referred to, however, are merely apparent, and may be removed if the data are plotted as in figure 2. In this figure each of the oxide factors r, obtained from the glass data (or from crystalline materials where the former were not available) is plotted, for the different valence groups, against the "serial number" of the basic element of the oxide. The respective plots show that there is a definite downward trend of the points as the serial number increases, with the qualification, however, that the points of each group first divide themselves into two subgroups which correspond to the long-series, A, and short-series, B, classification of the elements.

Following this classification, the element factors, mr', as given in table 5, were then plotted as shown in figure 3, making separate graphs for the A and B elements. It appears from the graph that in general, the B-elements fall into a consistent periodic pattern[4]: the

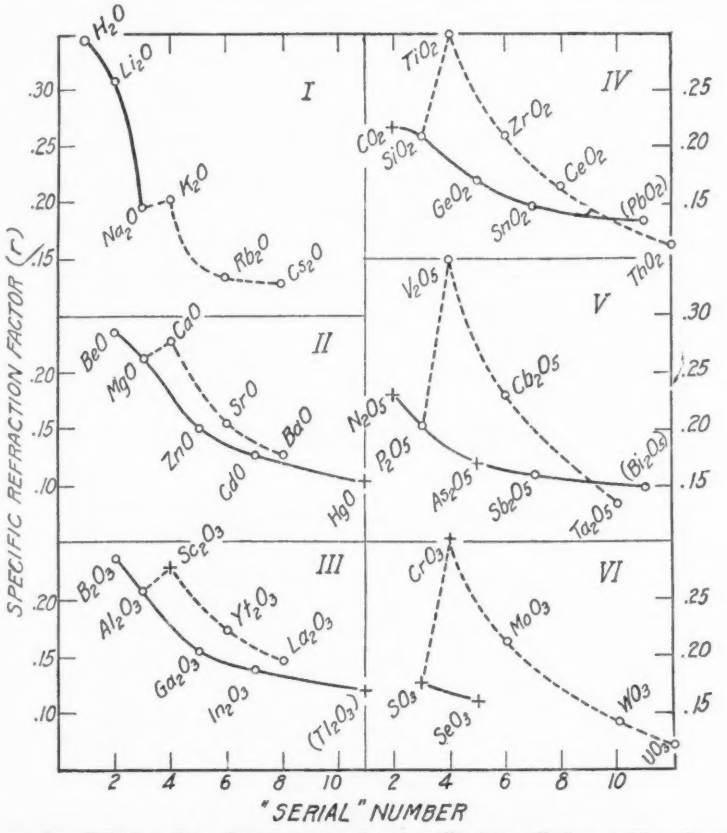

FIGURE 2.—*Relation, by valence groups, between Gladstone-Dale specific refraction factors for the oxides and the periodic arrangement of the elements.*

Factors from glasses are indicated by ○; and those from other materials by +.

points for each valence group fall on approximately a straight line passing through the origin, the slopes of the different lines increasing proportionately with the group number.
Specifically,

$$mr' = 0.280S(G+5), \tag{5}$$

in which S and G are, respectively, the serial- and valence-group number of a given element.

[4] The only values which do not appear to conform to this pattern are those for Cu, Ag, S, and Se. These values have been omitted in the plot, but there is no readily apparent reason why they should be exceptional.

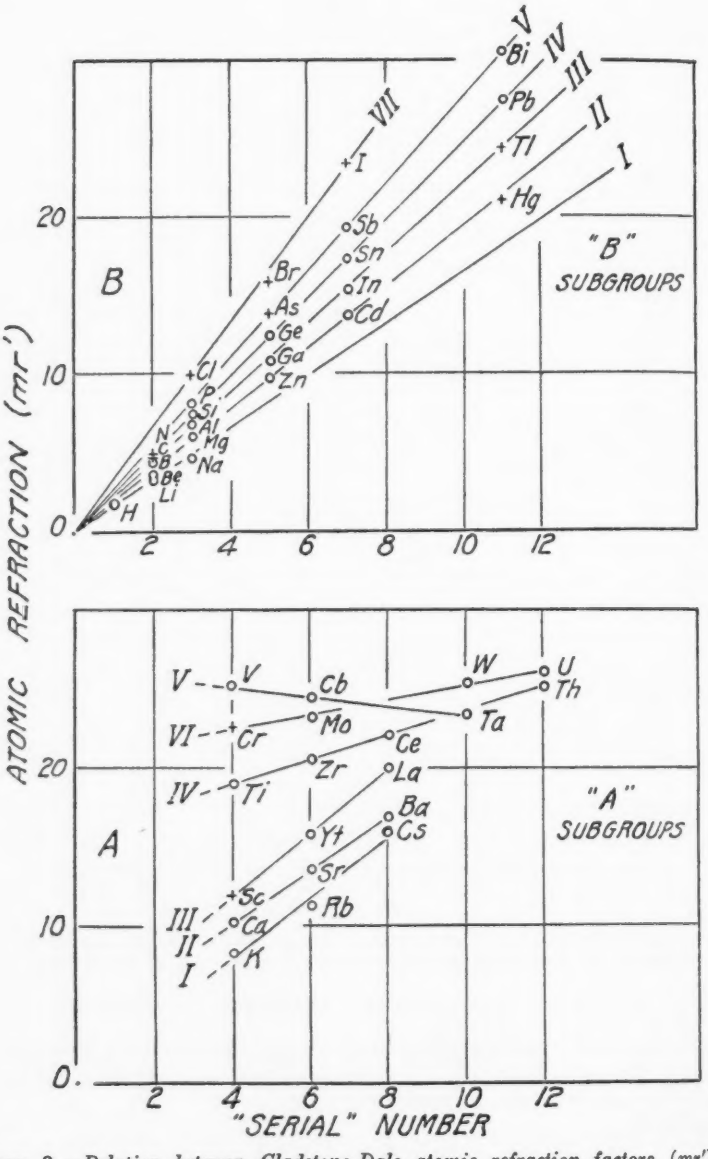

FIGURE 3.—*Relation between Gladstone-Dale atomic refraction factors (mr') of various elements and the positions of the elements in the periodic system.*

Valence groups are indicated by roman numerals. Factors from glasses are indicated by ○, and those from other materials by +.

The elements of the *A*-subgroups, on the other hand, do not give a plot similar to that for the *B*-subgroups. Neither an orderly relation between the different lines, nor the significance of the differing intercepts is easily discernible. The plotted values for these elements are shown in figure 3, graph *A*. For the rare earth elements, the value for La only is plotted, as the values for all the rare earth elements are essentially the same.

The atomic refraction factors, plotted in figure 3, were originally evaluated on the assumption that they did not vary for different combinations of the elements. Since, however, such an assumption may not be justified, it was decided to study the oxide factors themselves. So the latter factors, r, as given in table 2, were first reduced to "unit oxygen" by multiplying each r-value by the quantity M/n_0 in which M and n_0 are, respectively, the corresponding molecular weight and number of oxygen atoms for the oxide. Then for each oxide the value Mr/n_0 (which may be called "equivalent refraction") was plotted against the serial number of the basic element of the oxide, with the results shown in figure 4. For the *B*-elements, a configuration somewhat similar to that found for the mr'-values (fig. 3) results, except that the various straight lines for the different subgroups, instead of passing through the origin, have a common intercept at 2.5. That is,

$$Mr/n_0=2.5+0.560S(1+5/G). \tag{6}$$

Whether by coincidence or not, the intercept is numerically equal to the atomic refraction factor, mr', found previously for oxygen. At any rate, assuming the value 2.5 for oxygen, the values of Mr/n_0 for Tl_2O_3, PbO_2, and Bi_2O_5 were then calculated from the oxide factors previously found (table 2) for Tl_2O (from crystals), and PbO and Bi_2O_3 (from glass). The values thus calculated, when plotted in figure 4, graph *B* (points enclosed in parentheses), are found to fit n their expected places, and thus the inference concerning the value for oxygen seems justified.

From a similar plot for the *A*-elements (fig. 4, graph *A*) it is found that, although the points for each subgroup lie on a straight line, the intercept is different for each subgroup, the values ranging from about 3 for subgroup *IA* to 13 for *VA*. It might be inferred, therefore, that the atomic refraction factor for oxygen would be different for each of the subgroups of *A*-elements, and that for any subgroup the numerical value of the factor would equal, at least approximately, that of the corresponding intercept, as given by figure 4, graph *A*. Some confirmation of such an inference regarding the value, or values, thus assignable to oxygen is afforded by an independent calculation of the atomic refraction factor for oxygen from the oxide factors for different states of oxidation of a particular element. For example, from the oxide factors (from crystals) for CrO_3 and Cr_2O_3 (table 2), an oxygen factor of 8.7 is obtained.[5] From figure 4, graph *A*, the corresponding value of the intercept for subgroup VIA (Cr, Mo, W, and U) is found to be about 9.0. On the other hand, a similar calculation from the oxide factors (from crystals) of As_2O_3 and As_2O_5 gives a value of 2.2 for

[5] That is,

$$2(mr')_{Cr}+3(mr')_O=(Mr)_{Cr_2O_3}=152\times0.233$$

and

$$(mr')_{Cr}+3(mr')_O=(Mr)_{CrO_3}=100\times0.307$$

From which $(mr')_O=8.7$.

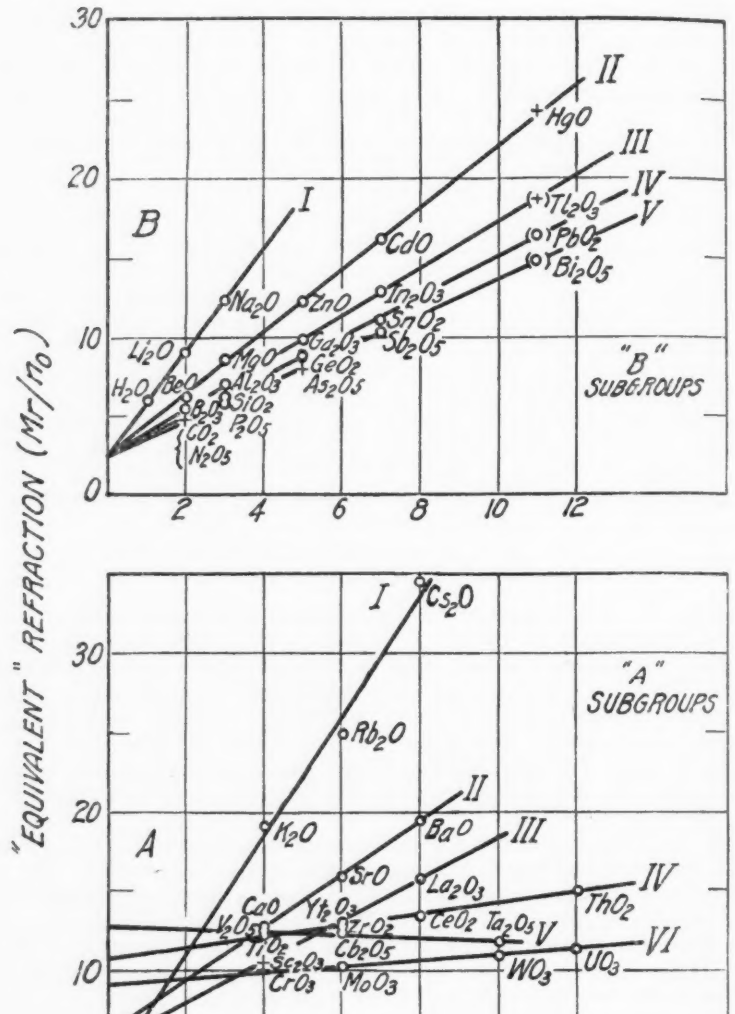

FIGURE 4.—*Relation between Gladstone-Dale "equivalent refraction" factors* (Mr/n_0) *of various oxides and the positions of the base elements in the periodic system.*

Valence groups are indicated by roman numerals. Factors from glasses are indicated by O, and those from other materials by +.

the oxygen factor, which value corresponds to the intercept 2.5 found for all the *B*-subgroups. But an elaborate check of this nature could not be made for glass, since there are as yet no appropriate data on glasses containing the several elements in their various states of oxidation.

Considering the two methods of analysis of the data, as shown by figures 3 and 4, the latter method seems definitely the better since the apparent anomalies involving the values for the *A*-elements may be attributed to a varying oxygen factor. In this connection, it should be noted that Gladstone and Dale themselves believed that the specific refraction factors of the elements were not constant under all circumstances, but that the factors were "modified by the manner of combination" of the elements. In principle, the second method here presented supports this belief, and, at least for the elements as occurring in glass, would furthermore identify oxygen as having the only variable factor, and then only when in combination with an *A*-element.

V. RELATION OF DISPERSION TO SPECIFIC REFRACTION AND TO COMPOSITION

The most important properties of an optical glass are its refractive indices for various wavelengths of light; so important, in fact, that a particular glass is, for most practical purposes, "defined" when its refractive index for the *D*-line (n_D) and ν-value ($\nu \equiv (n_D-1)/(n_F-n_C)$) are specified. The latter quantity is sometimes called optical constringence, or dispersive index. But neither the refractive index nor ν-value has been found to be a linear or, apparently, even a simple function of composition for glasses in general.[6] It, is, therefore, not surprising that accurate quantitative information concerning a relationship between either refractive index or ν-value and composition is confined to experimental glasses of comparatively simple composition. From a knowledge of specific refraction relationships, however, a method for calculating the ν-value of a glass from its composition may be developed, which appears to hold within practical limits of accuracy for glasses of a wide variety of compositions.

Since, as has been shown above, $(n-1)/D$ is a linear function of composition for various wavelengths of light, the quantity $(n_F-n_C)/D$, which may be called "specific dispersion," should also vary linearly with composition; that is

$$Q=1/100(q_Ap_A+q_Bp_B+\ \ldots\ .), \tag{7}$$

where Q is the specific dispersion of a glass, and the q's are numerical constants representing the specific dispersion factors for the constituent oxides A, B, etc. If, then, eq 7 can be established experimentally and the factors (q's) evaluated for a large number of oxides,

[6] For calculating ν-values of optical glasses from the compositions, Knapp [39] presents an "equation" wherein each constituent oxide is represented by eight constants.

it is comparatively simple to calculate the ν-value for a glass containing any combination of such oxides from the relationship,

$$\nu \equiv \frac{n_D - 1}{n_F - n_C} = \frac{R}{Q},$$

in which R is the specific refraction (Gladstone-Dale) of the glass for sodium light. For an oxide, x, of course, ν_x is equal simply to r_x/q_x, but for a glass

$$\nu_{\text{Glass}} = \frac{r_A p_A + r_B p_B + \ldots}{q_A p_A + q_B p_B + \ldots}, \tag{8}$$

in which the numerator and denominator (which are taken from eq 2 and 7, respectively) must be calculated separately, from the values of the respective r's and q's.

Fortunately, a large body of data exists for testing the validity of eq 7 for glasses containing the four oxides, SiO_2, Na_2O, CaO, and K_2O. Morey and Merwin have reported the refractive indices for the D line, the densities, and the partial dispersions ($n_F - n_C$) for their soda-lime-silica glasses [3], as well as for a series of potash-lime-silica glasses [35, p. 397]. The respective specific dispersion factors for the four oxides were accordingly evaluated statistically from these data with the results shown in table 7. These factors yielded very much the same individual deviations between observed and calculated partial dispersions (the latter obtained by multiplying the computed specific dispersions by the observed densities) as the departures obtained by Morey and Merwin from the isodispersion lines which they presented graphically.

TABLE 7.—*Specific dispersion factors, $q \equiv (n_f - n_c)/D$, for four oxides, calculated as constituents of glasses*

Source of data	SiO_2	Na_2O	K_2O	CaO
	$q \times 10^4$	$q \times 10^4$	$q \times 10^4$	$q \times 10^4$
Morey and Merwin [3, 35]	30.7	49.5	42.0	49.4
National Bureau of Standards [1]	30.5	50.0	42.5	49.1

[1] These values derived from eq 4; see text, section V.

The refractive indices for our own glasses were not measured for the particular spectral lines F and C, but since $1/\lambda_F^2 - 1/\lambda_C^2 = 1.91$, the specific dispersion factors which would correspond to those from Morey and Merwin's data are easily obtained for our glasses from the relation $q = 1.91\beta$, the four β's having the values given in table 6. The latter conversion depends, of course, on eq 4. The factors thus obtained, together with those obtained from the data of Morey and Merwin, are given in table 7, and it is evident that the agreement between the two sets of factors is very good.

Equation 7 was then extended to include data on glasses of a wide variety of compositions. Table 8 gives the specific dispersion factors, q, evaluated statistically from available data, as well as the dispersive indices calculated from the relation $\nu_x = r_x/q_x$, for all of the oxides commonly used in making optical glass, and for several other oxides not so used at present.

TABLE 8.—*"Specific aispersion" factors (q) and ν-values (=r/q) of some oxides as constituents of glasses*

Oxide	r (from table 2)	$q\times10^4$	ν $(=r/q)$	Number of glasses containing oxide	Maximum percent [a]	Source of data [b]
Li_2O	0.308	70	44	8	26	*u*
Na_2O	.1937	49.5	39.2	138	45	[3]
K_2O	.2019	42.0	48.1	49	38	[35, p. 397]
Rb_2O	.133	26	51	3	55	*u*
Cs_2O	.124	22	56	2	60	*u*
Tl_2O	.148	120	12.3	4	55	[31]
BeO	.236	30	78	16	16	[24]
MgO	.212	45.0	47.1	13	40	[33]
CaO	.2270	49.4	46.0	148	56	[3]
ZnO	.150	42.0	35.7	38	60	[21, 34]
SrO	.154	32	48	9	67	[32]
BaO	.126	26.8	47.0	35	48	[34]
PbO	.134	[d] 66.0	[d] 20.3	70	90	[34, 35, p. 374]
B_2O_3	.236	[c] 40	[c] 59	40	100	[34]
Al_2O_3	.2070	42	49	19	52	[34, 35, p. 393]
Ga_2O_3	.153	39	39	3	12	*s*
Yt_2O_3	.172	41	42	3	11	*s*
In_2O_3	.138	36	38	3	17	*s*
La_2O_3	.146	33	44	3	20	*s*
As_2O_3	.179	37	47	20	2	[34]
Sb_2O_3	.160	70	23	2	20	[34]
Bi_2O_3	.147	79	19	5	45	[26]
SiO_2	.2082	30.5	68.2	1	100	[18]
TiO_2	.300	170	17.7	5	50	[35, p. 393]
GeO_2	.167	40.1	41.6	1	100	[29]
ZrO_2	.209	69	30.3	8	18	*s*
SnO_2	.150	45	33	2	10	*s*
ThO_2	.113	33	34	5	20	*s*
P_2O_5	.202	25.3	80	6	71	[34]
Cb_2O_5	.230	100	23	3	16	*s*
Ta_2O_5	.134	50	27	3	17	*s*
WO_3	.142	58	24	4	10	*s*

[a] Figures in this column indicate for each oxide the maximum percentage for which dispersion data are reported in the literature referred to; validity of the q-factor is not necessarily limited to this maximum.

[b] Figures in brackets indicate references at end of paper; *s* indicates unpublished data on special glasses made at this Bureau (see section II); *u* indicates other unpublished data obtained at this Bureau.

[c] This is the value for 100 percent only; for any percentage of B_2O_3, $q\times10^4=0.20\times(100+\%\ B_2O_3)$.

[d] This value holds only through the range 0 to 60 percent of PbO; for higher percentages, $q\times10^4=0.047\times(\%[PbO-60)^2+66.0$.

The q-factor for each of the oxides studied, except for PbO and B_2O_3, appears to be constant for any concentration of the oxide. The factor for PbO is constant only for percentages of PbO up to 60, and increases rapidly with the higher percentages. The factor for B_2O_3, on the other hand, varies proportionally with the percentage of B_2O_3 throughout the entire range 0 to 100 percent. The expressions for the q-factors for these two oxides are given in footnotes *d* and *c*, respectively, of table 8, and appear to hold accurately [7] for glasses containing any amount of these oxides, as well as for pure vitreous B_2O_3 [35, p. 370].

In general, the substitution of the respective r- and q-factors in eq 8 yields ν-values whose average deviation from the observed values is about 1 percent (approximately ±0.5 in ν-value). The more accurate the observed data, the better the agreement. For instance, for 62 analyzed optical glasses of numerous types, whose

[7] An apparent exception is Pyrex (a heat-resisting glass of the borosilicate type), for which the computed ν-value is about 4 percent higher than reported values. This discrepancy, however, may result from inadequate data rather than from any inaccuracy in the factors.

ν-values have been determined with care, the average difference between observed and calculated ν-values is only about ± 0.3, which difference is comparable to the experimental error of observations made by the Pulfrich method. For glasses containing some of the more unusual oxides, however (such as Cs_2O, Ga_2O_3, Cb_2O_5, etc.), the precision of eq 8 appears to be much lower than that stated above, as the factors for such oxides are in most cases based on few glasses or on low concentrations of these oxides.

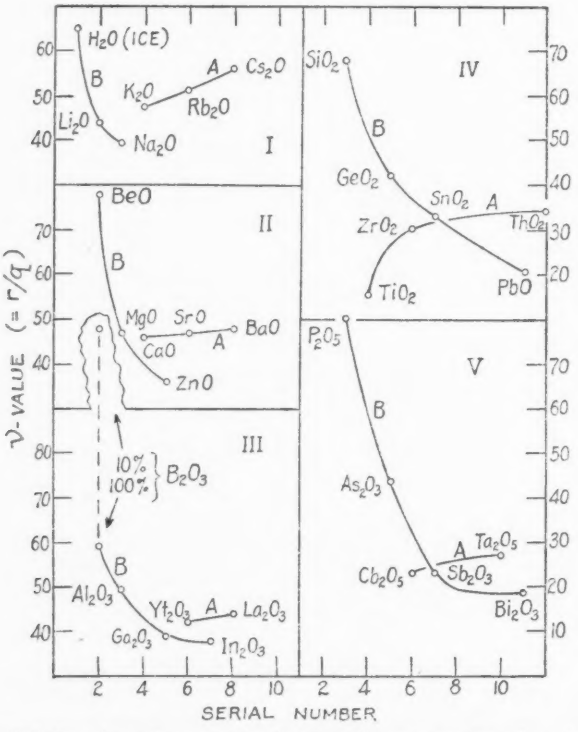

FIGURE 5.—*Relation, by valence groups, between the computed ν-values for the oxides in glasses and the periodic arrangement of the elements.*

It is worth noting that the hypothetical ν-values for BeO and P_2O_5, calculated from their r- and q-factors to be 78 and 80, respectively, are the highest of any of the oxides studied. Moreover, the similarly calculated ν-value for B_2O_3 is greater than 79 for amounts of B_2O_3 up to 50 percent. The factors for these three oxides should, therefore, be most useful in designing glasses of very low dispersions.

An attempt was made to determine how the ν-values for the oxides vary with the positions of the respective elements in the periodic system. The data do not appear to be extensive enough at present to justify a quantitative correlation, such as that made for the Gladstone-Dale specific refraction factors, but qualitatively, from an inspection of figure 5, a very striking trend may be observed: the ν-values for the oxides divide themselves sharply into the *A*- and *B*-subgroupings, corresponding to those shown above for the Gladstone-Dale factors.

With increasing serial number the ν-values in the A-subgroups increase, whereas those in the B-subgroups decrease. In general, with increasing group number the converse is true.

VI. SUMMARY

The study of the tables and figures here presented indicates that, for glass and glass-forming materials, only the Gladstone-Dale ratio, among the seven specific refraction ratios considered, possesses to a satisfactory degree each of the following features: (1) it varies linearly with the chemical composition of the material and with the square of the wave-number of the incident light ($1/\lambda^2$); (2) with a few exceptions it is substantially the same for both the vitreous and crystalline states for a given composition; and (3) it is practically independent of the thermal history of the material. Each of the other type ratios failed in one or more of these particulars.

It is found that factors can be assigned to each of the various elements considered, by means of which the Gladstone-Dale ratio for glasses and crystals may be calculated. These factors are shown to be related to the periodic arrangement of the elements.

Appropriate numerical factors for the Gladstone-Dale ratio for sodium light, and for the ratio $(n_F - n_C)/D$ (which may be called specific dispersion) are presented for all of the oxides commonly used in making optical glass, as well as for several other oxides not so used at present. It is shown how these two ratios may be used for obtaining a rather accurate estimate of the dispersive index, or ν-value, of any glass of known or proposed composition.

VII. REFERENCES

Many of the data taken from the following publications have been reprinted in [35]. This circumstance is indicated below by the letter "M," followed by the page number.

[1] J. H. Gladstone and T. P. Dale, Proc. Roy. Soc. (London) **12,** 448 (1863).
[2] E. S. Larsen and H. Berman, U. S. Geol. Survey Bul. 848 (1934).
[3] G. W. Morey and H. E. Merwin, J. Opt. Soc. Am. **22,** 632 (1932) M383.
[4] P. Wulff and S. K. Majumdar, Z. physik. Chem. **31** [B], 319 (1936) M228.
[5] W. Biltz and F. Weibke, Glastech. Ber. **16,** 131 (1938).
[6] J. T. Randall and N. Gee, J. Soc. Glass Tech. **15,** 41 (1931).
[7] E. Kordes, Z. anorg. allgem. Chem. **241,** 1 (1939).
[8] H. A. Lorentz, Wied. Ann. **9,** 641 (1880).
[9] R. Lorenz, Wied. Ann. **11,** 70 (1880).
[10] K. Lichtenecker, Physik. Z. **27,** 115 (1926).
[11] J. F. Eykmann, Rec. Pays-Bas **14,** 185 (1895); **15,** 52 (1896).
[12] Sir Isaac Newton, Optics, book 2, pt. 3; (also P. S. Marquis de Laplace, Mécanique Céleste [4] **10,** 237 (1805).
[13] W. Johst, Wied. Ann. **20,** 47 (1883).
[14] W. F. Edwards, Am. Chem. J. **16,** 625 (1894); **17,** 473 (1895).
[15] J. C. Young, C. A. Faick, A. N. Finn, and F. W. Glaze, J. Research NBS **22,** 453 (1939) RP1197.
[16] C. A. Faick and A. N. Finn, BS J. Research **6,** 993 (1931) RP320. Also J. Am. Ceram. Soc. **14,** 518 (1931) M237.
[17] F. W. Glaze, J. C. Young, and A. N. Finn, BS J. Research **9,** 799 (1932) RP507, M237.
[18] R. B. Sosman, The Properties of Silica (Reinhold Publishing Corporation, New York, N. Y., 1927) M371.
[19] A. Q. Tool and L. W. Tilton, Misc. Pub. NBS 102, 24 (1929).

[20] C. A. Faick, J. C. Young, D. Hubbard, and A. N. Finn, J. Research NBS **14,** 133 (1935) RP762, M238.
[21] S. English and W. E. S. Turner, J. Soc. Glass Tech. **7,** 155 (1923), M232 and 382.
[22] S. English, W. E. S. Turner, and F. Winks, J. Soc. Glass Tech. **12,** 287 (1928), M234 and 383.
[23] A. R. Sheen and W. E. S. Turner, J. Soc. Glass Tech. **8,** 187 (1924), M231 and 382.
[24] C. F. Lai and A. Silverman, J. Am. Ceram. Soc. **13,** 393 (1930), M240.
[25] C. A. Becker, Sprechsaal **67,** 139 (1934), M241.
[26] E. R. Riegel and D. E. Sharp, J. Am. Ceram. Soc. **17,** 88 (1934), M394.
[27] J. D'Ans and J. Löffler, Z. Anorg. allgem. Chem. **191,** 1 (1930).
[28] L. M. Dennis and A. W. Laubengayer, J. Am. Chem. Soc. **47,** 1945 (1925).
[29] L. M. Dennis and A. W. Laubengayer, J. Phys. Chem. **30,** 1510 (1926), M405.
[30] C. J. Peddle, J. Soc. Glass Tech. **5,** 72 (1921), M379.
[31] F. A. Bannister, Mineral. Mag. **21,** 152 (1929).
[32] P. Eskola, Am. J. Sci. **4,** 331 (1922), M375.
[33] E. S. Larsen, Am. J. Sci. **28,** 263 (1909), M392.
[34] Ordnance Dept. Doc. 2037, Superintendent of Documents, Washington, D. C. (1921).
[35] G. W. Morey, The Properties of Glass (Reinhold Publishing Corporation, New York, N. Y., 1938).
[36] International Critical Tables.
[37] H. S. Washington, U. S. Geol. Survey, Professional Papers 99 (1917).
[38] W. O. George, J. Geol. **32,** 353 (1924).
[39] O. Knapp, Sprechsaal **63,** 61 (1930).
[40] C. G. Peters, BS Sci. Pap. **20,** 635 (1926) S521.

WASHINGTON, September 11, 1940.

U. S. DEPARTMENT OF COMMERCE NATIONAL BUREAU OF STANDARDS

RESEARCH PAPER RP1353

Part of Journal of Research of the National Bureau of Standards, Volume 25, December 1940

STRENGTH AND ELONGATION OF SILK YARNS AS AFFECTED BY HUMIDITY

E. Max Schenke and Howard E. Shearer[1]

ABSTRACT

Silk hosiery yarns varying in number of threads from 2 to 9 and in number of turns of twist per inch from 5 to 36 were tested for breaking strength and breaking elongation at 70° F after various periods of exposure in relative humidities from 33 to 86 percent. The strengths of the yarns were not affected significantly by changes in relative humidity between 33 and 55 percent. The yarns were weaker above 55-percent relative humidity. The elongations of the yarns increased with an increase in relative humidity of the air. The elongation, on the average, increased 1 percent with an increase in relative humidity from 33 to 43 percent, and 1.9 percent with an increase in relative humidity from 76 to 86 percent. The average strength of all yarns was 3.41 g per denier when tested under standard conditions. This figure seems to be independent of the size of the yarn, although the strength of a given size varies with the amount of twist. Some data are given on the breaking strength and elongation of one-thread raw silk.

CONTENTS

		Page
I.	Introduction	783
II.	Material	784
III.	Test procedure	784
IV.	Test results	785
V.	Conclusion	790

I. INTRODUCTION

In a previous report [2] the authors showed that the moisture content of silk yarn is chiefly dependent upon the relative humidity of the atmosphere with which the silk is in equilibrium. The fact that this moisture affects the properties of the silk is well known to the hosiery and silk industry. For example, if the humidity is low, the silk will be harsh and brittle, resulting in the production of sleazy knitted fabric, and manufacturing difficulties will be increased by the generation of static electric charges. If the humidity is too high, the troubles are almost as great. The silk will have a tendency to stretch and become limp, resulting in the production of tight and loose loops in the fabric and in unpredictable dimensions. There is also the danger of corrosion of needles, and of loss of silk through the growth of mildew. Manufacturers, therefore, prefer to knit in an atmosphere having a relative humidity of 65 to 75 percent.

[1] Director of Research and Research Associate, respectively, at the National Bureau of Standards, representing the National Association of Hosiery Manufacturers.

[2] E. Max Schenke and Howard E. Shearer, *Moisture content of thrown silk affected by threads and twist*, Southern Knitter (Jan. 1940).

Two of the important properties of silk yarn are its strength and breaking elongation. The present work shows how these properties are affected by differences in the relative humidity of the air and the consequent differences in the moisture content of the silk.

II. MATERIAL

Preliminary data on the strength and breaking elongation were obtained on 13/15 denier, one thread, raw silk, furnished by two hosiery manufacturers. Each manufacturer furnished 4 samples of 10 skeins each.

For the main part of the work thrown silk yarns of 2 to 9 threads and a variety of twists were used as indicated in table 1.[3] Seventeen of these yarns were made from 1 bale of 1934 spring crop, nominal 13/15 denier, 87 percent of Japan silk, and 1 yarn made from China silk of the same denier.[4] After soaking in sulfonated olive oil by the open-tub method, portions of the silk were thrown into yarns of specified numbers of threads and twists. These yarns were wound on cones. One dozen cones were wound for each combination of thread and twist, and 3 cones of each thread and twist were selected from which to secure the test skeins.

TABLE 1.—*Size of thrown silk*

Number of threads	Twist per inch	Denier per thread at 65-percent relative humidity	Denier per thread, ovendry	Denier per thread of boiled-off silk, ovendry
2	25	15.4	14.1	10.4
2	36	15.7	14.3	10.5
3	20	14.9	13.7	9.9
3	30	14.9	13.7	9.9
[a] 3	30	16.1	14.8	10.9
4	10	15.2	14.0	9.9
4	18	15.7	14.4	10.4
4	36	15.8	14.5	10.4
5	6	14.7	13.5	9.8
5	15	15.3	14.1	10.1
5	20	15.9	14.7	10.5
5	36	16.2	15.0	10.7
7	10	15.0	13.8	9.6
7	15	15.7	14.5	10.3
7	36	16.9	15.6	11.5
9	6	15.1	13.9	9.9
9	15	15.4	14.2	10.2
9	36	16.8	15.5	11.3

[a] China silk.

III. TEST PROCEDURE

Five test skeins of yarn, each weighing approximately 2.5 g, were wound from different portions of each cone selected. The skeins of thrown and raw silk were kept in a small conditioning room, where the moisture condition could be maintained at any predetermined figure within ±2 percent relative humidity, and the temperature held con-

[3] The samples are from the same yarns for which humidity data have already been presented. (See footnote 2.)

[4] The "denier" of a silk yarn is the weight of a 450-m length expressed in 1/20-g units.

stant at 21° ±2° C. The conditioning equipment changed the air in the room about twice a minute. Both humidity and temperature were continuously recorded on a hygrothermograph, which was checked with a sling psychrometer each time a set of determinations was made.

The yarns were first conditioned at the lowest relative humidity (33 percent). Breaking strength and ultimate elongation tests were made approximately 6 hours after the yarns were placed in the 33-percent relative humidity atmosphere. Ten individual tests were made on single ends selected from three skeins of each yarn. These tests were repeated at approximately 24, 48, and 72 hours. Thus 40 tests were made on each combination of thread and twist at one humidity. It required about 72 hours for the silks to reach equilibrium, as indicated by their attaining constant weight.[5] After tests at one humidity had been completed, the humidity was increased and the silk again tested after the same time intervals. Tests were made at 33-, 43-, 50-, 55-, 65-, 76-, and 86-percent relative humidity. The test skeins were kept in airtight containers during the interval required to increase the relative humidity of the rooms to the next highest level.

Tests were made on a single-end[6] breaking-strength machine, operating at a jaw speed of 12 inches per minute, with an initial distance of 10 inches between jaws.

IV. TEST RESULTS

The data from the preliminary tests of the samples of single-thread raw silks submitted by two hosiery manufacturers are given in tables 2 and 3. The irregularity of the strengths (table 2) of the one-thread silk is so great that no conclusions may be drawn as to the effect of the moisture condition of the silk upon its strength. There is also considerable irregularity in the breaking elongations (table 3), but the averages of the elongations of all eight samples at each relative humidity show a definite trend for the elongation to increase as the relative humidity increases.

TABLE 2.—*Single-end breaking strength of one-thread raw silk*

Sample number	Percentage of relative humidity						
	33	43	50	55	65	76	86
	g	*g*	*g*	*g*	*g*	*g*	*g*
4653-K	52	40	55	45	44	41	36
5728-K	54	58	53	48	53	40	36
5781-K	63	43	51	53	65	56	52
5800-K	53	42	38	46	42	47	45
1-AG	52	47	51	47	34	34	32
2-AG	41	40	58	50	62	49	52
3-AG	40	46	46	50	52	42	44
4-AG	50	40	38	38	47	46	31
Average	51	45	49	47	50	45	41

[5] E. Max Schenke and Howard E. Shearer, *Moisture content of thrown silk affected by threads and twist*, Southern Knitter (Jan. 1940.)

[6] In the textile industry the term "single-end breaking strength" designates the strength of a single yarn. This is to distinguish from the older practice of applying the breaking load to a skein which consists of a large number of the individual yarns.

TABLE 3.—*Breaking elongation of one-thread raw silk*

Sample number	Percentage of relative humidity						
	33	43	50	55	65	76	86
	%	%	%	%	%	%	%
4653-K	21.4	17.2	20.1	21.5	23.0	21.1	25.8
5728-K	15.2	19.3	18.5	20.1	20.3	21.5	27.0
5781-K	17.6	19.5	20.6	21.2	24.1	25.3	26.1
5800-K	16.7	20.9	20.7	21.5	24.5	22.4	27.1
1-AG	16.8	16.9	19.5	21.7	23.6	22.7	23.8
2-AG	19.8	17.3	19.2	18.8	23.3	20.4	27.5
3-AG	18.7	20.4	18.7	20.3	24.0	22.2	24.6
4-AG	16.1	16.1	17.7	18.9	21.7	23.6	23.7
Average	17.8	18.5	19.4	20.5	23.1	22.4	25.7

Table 4 gives the strengths of the 2- to 9-thread yarns. The strengths given are the averages of the strengths observed at 6, 24, 48, and 72 hours after exposure at a particular humidity. A few tests made after 3 hours' exposure at these various relative humidities indicated that the strengths thus observed were not significantly different from the strengths after 72 hours' exposure. Apparently most of the change in strength with a change in relative humidity took place within the first 3 hours of exposure to the new humidity. There was likewise no indication that the strengths were significantly different at 6, 24, 48, or 72 hours' exposure at any one humidity. Therefore only the averages are given since no systematic variation in strength with time of exposure was found. The average of the strengths of all yarns after 72 hours' exposure at each humidity is given at the bottom of table 4.

TABLE 4.—*Average single-end breaking strength of thrown silk at various relative humidities*

Yarn No.	Number of threads	Twist per inch	Percentage of relative humidity							Average strength, all humidities
			33	43	50	55	65	76	86	
			g	g	g	g	g	g	g	g
1	2	25	101	113	107	104	102	101	85	102
2	2	36	107	104	117	116	112	99	91	106
3	3	20	161	160	153	156	156	149	133	153
4	3	30	142	157	156	155	160	150	128	150
5	[a]3	30	169	178	178	173	164	170	148	169
6	4	10	200	198	206	210	197	197	182	199
7	4	18	220	230	230	215	217	203	183	214
8	4	36	204	213	221	210	196	199	170	202
9	5	6	270	263	273	263	251	252	246	260
10	5	15	287	289	293	284	276	276	243	279
11	5	20	263	261	258	267	270	261	244	261
12	5	36	265	276	278	265	273	238	208	258
13	7	10	384	378	365	360	363	333	315	357
14	7	15	407	382	380	400	413	388	348	388
15	7	36	362	373	385	374	364	345	306	358
16	9	6	498	519	518	507	474	483	427	489
17	9	15	510	519	508	500	510	484	459	499
18	9	36	482	476	478	480	477	453	428	468
Average			280	283	284	280	277	266	241	
Average strength of yarns tested at 72 hours			280	285	283	282	274	262	240	

[a] China silk.

Figure 1 gives the strengths of each of the yarns of table 4 at each of the relative humidities, and the average strength of all 18 yarns at each relative humidity. This figure shows that with variation in

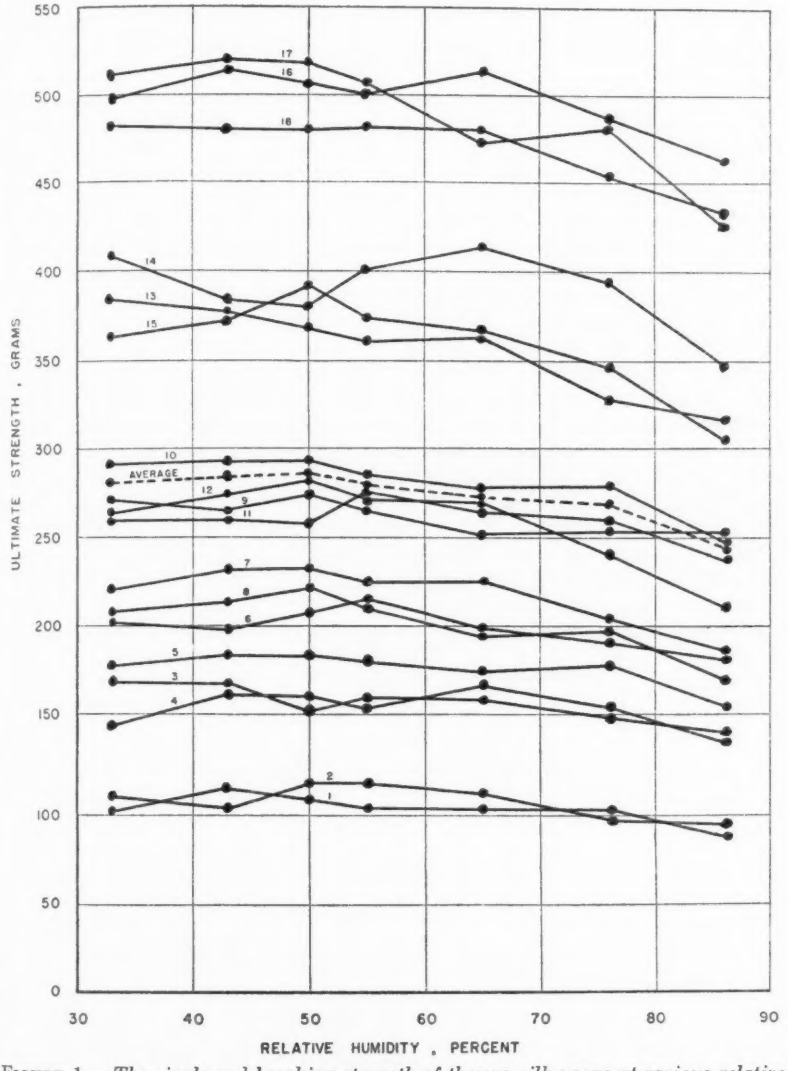

FIGURE 1.—*The single-end breaking strength of thrown silk yarns at various relative humidities.*

humidity the trend of the strength of each combination of thread and twist was the same.

The average strengths of all yarns varied little, if at all, with variation of relative humidity from 33 to 55 percent. The least and greatest average strengths within this range of humidities, 280 g at 33 and 55 percent and 284 g at 50 percent, were practically within

the experimental error of results. With increase in relative humidity beyond 55 percent, however, there is a continual decrease in strength. It should be noted that the change in strength which accompanied each change in humidity was so small that one could not expect the tests made at different times of exposure to give much information as to the rate of change of strength with the steps in humidity used in these tests.

From figure 1 and table 4 it is apparent that for yarns of each thread group there is a twist which will give the greatest strength. Thus for 4- to 9-thread yarns, the 4–18, 5–15, 7–15, and 9–15 yarns have the greatest strength for yarns with like thread count.

As with the strengths, the breaking elongations (table 5) were almost independent of the time the yarns were kept in the atmosphere at specified relative humidity before test. Therefore, the table gives averages of all 4 durations. The table also gives the average of the elongations of all yarns at 72 hours after exposure. The averages of the elongations at 72 hours are slightly higher than the averages for all durations of exposure, indicating a slight increase in elongation with time of exposure. However, only the averages for the 4 periods of exposure are given for the individual yarns since these average values are much more consistent than those at any one time of exposure. If the data for the 72-hour exposure are tabulated, there are 17 exceptions to the rule that the breaking elongation increases with relative humidity; if the tests for the 4 exposure durations are averaged, there are only 9 exceptions. For a fourfold increase in observations we would expect to decrease the deviations by 2 ($2=\sqrt{4}$), which is the ratio of the number of exceptions found.

TABLE 5.—*Average single-end breaking elongation of thrown silk at various relative humidities*

Yarn number	Number of threads	Twist per inch	Percentage of relative humidity						
			33	43	50	55	65	76	86
			%	%	%	%	%	%	%
1	2	25	13.2	15.4	15.0	15.5	17.0	18.9	20.1
2	2	36	15.9	15.1	16.7	17.4	18.5	19.4	23.0
3	3	20	14.1	15.1	15.8	16.1	18.0	19.7	20.7
4	3	30	15.6	16.5	16.4	17.5	19.8	20.6	22.0
5	*3	30	15.7	16.1	17.4	17.7	18.8	20.7	22.6
6	4	10	15.1	15.9	16.8	17.3	18.4	20.7	22.8
7	4	18	15.8	17.1	18.3	18.0	19.5	20.3	21.7
8	4	36	17.2	18.5	19.5	19.0	19.5	21.8	23.0
9	5	6	16.3	17.9	18.4	18.7	20.6	21.7	25.2
10	5	15	16.8	17.5	18.6	19.5	20.1	22.7	24.5
11	5	20	16.2	17.8	18.2	18.6	20.0	21.7	24.0
12	5	36	17.3	18.6	18.5	18.8	20.7	18.5	20.2
13	7	10	14.9	16.1	16.4	17.3	19.0	20.4	22.5
14	7	15	17.9	18.0	18.8	19.7	21.9	22.9	24.7
15	7	36	19.5	20.8	21.1	21.0	22.3	24.8	25.5
16	9	6	16.1	17.4	18.3	18.8	20.1	22.9	24.6
17	9	15	18.2	19.0	19.4	19.5	20.6	22.8	25.1
18	9	36	20.8	21.0	22.4	23.2	24.0	25.8	28.1
Average			16.5	17.5	18.2	18.6	20.0	21.5	23.4
Average elongation of yarns tested at 72 hours			16.6	17.6	18.2	18.7	20.1	21.9	23.7

* China silk.

Figure 2 gives the yarns having the highest and the lowest breaking elongation and the average breaking elongation of all 18 yarns of table 5 at each relative humidity. This figure shows that with varia-

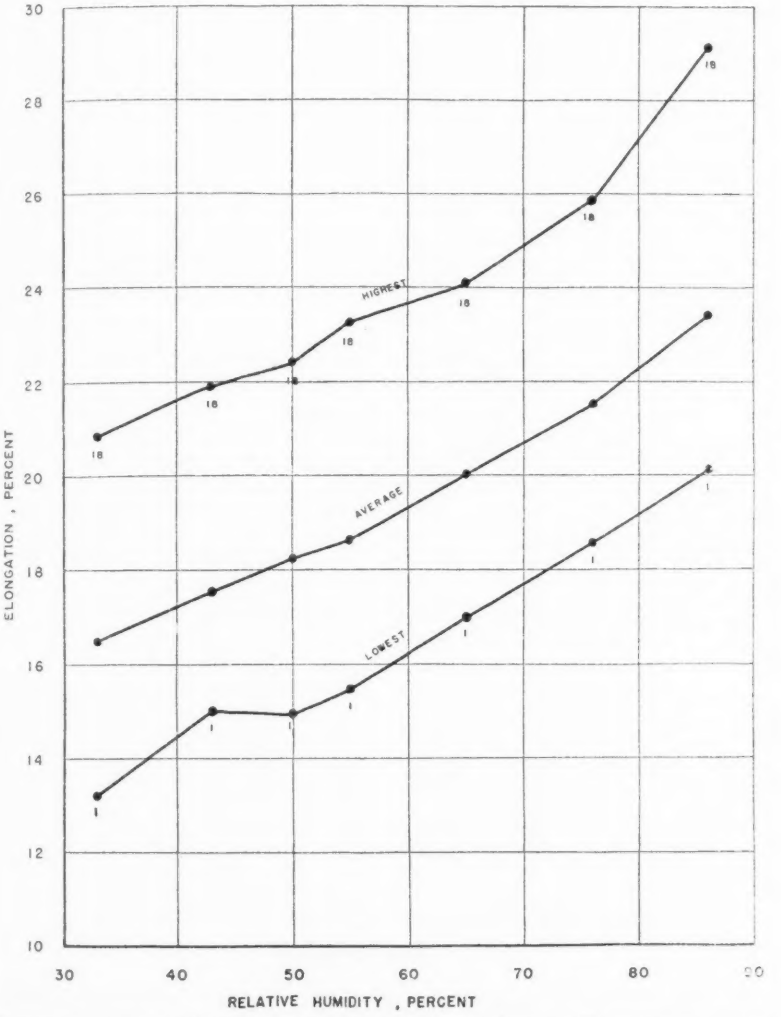

FIGURE 2.—*The single-end breaking elongation of thrown silk yarns at various relative humidities.*

tions in humidity the trend of the elongation of the combinations of thread and twist is the same.

The breaking elongation increases with the relative humidity, but the increase is larger as the relative humidity increases. Thus, from 33- to 43-percent relative humidity the elongations increased from 16.5 to 17.5 percent (a difference of 1 percent), whereas from 76- to 86-percent relative humidity the elongations increased from 21.5 to

23.4 percent, or almost twice as much difference in percent (1.9 percent).

There is a distinct trend for the breaking elongation to increase with the twist in all but the five-thread yarn. In this yarn there was no appreciable difference in the breaking elongation of the four twists.

In table 6 are given the denier of the yarns of tables 4 and 5, their breaking strength and breaking elongation at the standard condition[7] of 65-percent relative humidity, and 70° F, and the strength per denier of each yarn. These strengths varied from 3.08 to 3.76 g per denier, with an average value of 3.41 g per denier. There was no significant difference in the strength per denier of yarns containing different numbers of threads; however, there is a distinct difference in strength per denier of yarns with different numbers of twists. As with the total strengths of yarns, the strength per denier was greatest, in the 4- to 9-thread group, for the 4–18, 5–15, 7–15 and 9–15 yarns. There is a slight trend for the breaking elongation to be more for the yarns with the larger number of threads.

TABLE 6.—*Denier, breaking strength, and breaking elongation of thrown silk yarns, at 65 percent relative humidity and 70° F*

(A), from table 4; (B), from table 5.

Number of threads	Twist per inch	Denier of thrown yarn	(A) Breaking strength	(B) Breaking elongation	Breaking strength per denier
			g	%	*g*
2	25	30.8	102	17.0	3.32
2	36	31.4	112	18.5	3.67
3	20	44.7	156	18.0	3.50
3	30	44.7	160	19.8	3.58
[a] 3	30	48.3	164	18.8	3.40
4	10	60.8	197	18.4	3.24
4	18	62.8	217	19.5	3.46
4	36	63.2	190	19.5	3.10
5	6	73.5	251	20.6	3.42
5	15	76.5	276	20.1	3.61
5	20	79.5	270	20.0	3.40
5	36	81.0	273	20.7	3.37
7	10	105.0	363	19.0	3.46
7	15	109.9	413	21.9	3.76
7	36	118.3	364	22.3	3.08
9	6	135.9	474	20.1	3.49
9	15	138.6	510	20.6	3.68
9	36	151.2	417	24.0	3.15
				Average...	3.41

[a] China silk.

V. CONCLUSION

The strength of the yarns varied little, if at all, with variation in relative humidity from 33 to 55 percent. With increase in humidity beyond 55 percent the strength decreased more rapidly as the humidity increased. The strength at 86-percent relative humidity was approximately 86 percent of that at 55-percent relative humidity, while the elongation was approximately 26 percent greater. The strength per denier was independent of the number of threads in the yarns, but did vary with the number of twists.

WASHINGTON, September 28, 1940.

[7] Federal Specification CC-T-191a requires that textile tests be made at a temperature of 70° F and 65-percent relative himidity.

INDEX TO VOLUME 25

A

Page

Absolute measurement of self inductance by dual bridge, RP1310 ... 1
AC–DC transfer instrument, RP1344 ... 545
Acidic groups in cotton and wool, RP1314 ... 61
Acid-resistant enamels, RP1315 ... 71
Aging of leather, accelerated, RP1319 ... 149
Aircraft, corrosion of metals used in, RP1316 ... 75
Aircraft, metals, effect of low temperatures on properties, RP1347 ... 673
Alloys, corrosion of, RP1316 ... 75
Alloys, high-purity iron-carbon, effect of rate of heating on austenitic grain size, RP1322 ... 215
Aluminum alloys, corrosion, RP1328 ... 315
Amplifier, vacuum tube, RP1312 ... 41
Ash in textile fibers, electrodialytic estimation of, RP1314 ... 61
Austenitic grain size as affected by heating rate, RP1322 ... 215
Automatic weather observations, RP1318 ... 133

B

Barbrow, L. E., A photometric procedure using barrier-layer photocells, RP1348 ... 703
Barrier-layer photocell photometry, RP1348 ... 703
Basic groups in wool, RP1314 ... 61
Batteries, storage, RP1335 ... 417
Benzoic acid, high purity, preparation of, RP1351 ... 747
Bricks, air and water permeability, RP1349 ... 711
Bridge, dual, for the measurement of self ind uctance, RP1310 ... 1
Building stone, RP1320 ... 161
Bunting, E. N., R. F. Geller, Length changes of whiteware clays and bodies during initial heating, with supplementary data on mica, RP1311 ... 15
Burdick, Milton D., Studies on the system lime-ferric oxide-silica, RP1340 ... 475

C

Calcium oxide, ternary system with ferric oxide and silica, RP1340 ... 475
Cells, soil-corrosion, electrode potentials and polarization, RP1336 ... 421
Cement paste, relative humidity over, RP1334 ... 403
Cement, portland, nature of glass in, RP1324 ... 295
Ceramic materials, decomposition of, RP1331 ... 379
Clay, length changes during initial heating, RP1311 ... 15
Cobalt, effect in storage batteries, RP1335 ... 417
Compensator, alternating voltage, RP1312 ... 41
Concrete, relative humidity inside, RP1334 ... 403
Conrad, Carl M., Roy L. Whistler, Albert R. Martin, Pectin substance of cotton fibers in relation to growth, RP1326 ... 305
Cook, Richard K., Absolute pressure calibrations of microphones, RP1341 ... 489
Cooter, Irvin L., Frank Wenner, Chester Peterson, A vacuum-tube alternating-voltage compensator, RP1312 ... 41
Corrosion, cells, soil, electrode potentials and polarization, RP1336 ... 421
Corrosion of aluminum alloys, RP1328 ... 315
Corrosion of metals used in aircraft, RP1316 ... 75
Cotton, acidic properties of, RP1313 ... 47
Cotton, cation exchange in, RP1313 ... 47
Cotton, pectic substance in relation to growth of, RP1326 ... 305
Craig, D. Norman, George W. Vinal, Clarence L. Snyder, Note on the effects of cobalt and nickel in storage batteries, RP1335 ... 417
Cryostat for thermocouple calibration, RP1339 ... 459
Curtis, Harvey L., L. W. Hartman, A dual bridge for the measurement of self inductance in terms of resistance and time, RP1310 ... 1
Curtiss, Leon F., Integrating circuit for vapor-type Geiger-Müller counters, RP1330 ... 369

D

Page

Darnielle, Robert B., Measurement of electrode potentials and polarization in soil-corrosion cells, RP1336 ... 421
Diamond, Harry, Wilbur S. Hinman, Jr., An automatic weather station, RP1318 ... 133
——, ——, *Francis W. Dunmore, Evan G. Lapham*, An improved radio sonde and its performance, RP1329 ... 327
Diazomethane, reaction with silk and other proteins, RP1338 ... 451
Digges, Thomas G., Samuel J. Rosenberg, Effect of rate of heating through the transformation range on austenitic grain size, RP1322 ... 215
Dispersion, specific, of glasses, RP1352 ... 759
Drying conditions, effects on textiles, RP1337 ... 435
Dual bridge for the measurement of self inductance, RP1310 ... 1
Dunmore, Francis W., Harry Diamond, Wilbur S. Hinman, Jr., Evan G. Lapham, An improved radio sonde and its performance, RP1329 ... 327
Duralumin, corrosion, RP1328 ... 315

E

Effect of oxygen and moisture on the stability of leather atelevated temperatures, RP1319 ... 149
Electrode potential, of sodium, RP1350 ... 731
Electrode potentials in soil-corrosion cells, RP1336 ... 421
Electrodialytic estimation of ash, RP1314 ... 61
Electrodynamic wattmeter, standard, RP1344 ... 545
Ele ctron attachment in the ionosphere, RP1342 ... 507
Elongation of silk yarns as affected by humidity, RP1353 ... 783
Enamels, determination of thickness, RP1315 ... 71
Expansion, thermal, of clay during initial heating, RP1311 ... 15

F

Ferric oxide, ternary system with calcium oxide and silica, RP1340 ... 475
Films, thickness, of adhering, RP1332 ... 385
Finn, Alfred N., John C. Young, Effect of composition and other factors on the specific refraction and dispersion of glasses, RP1352 ... 759
Four-terminal conductors, RP1323 ... 229
Freezing range as a criterion of purity, RP1351 ... 747
Frost, action on bricks, RP1349 ... 711
Fugitt, Charles H., Arnold M. Sookne, Jacinto Steinhardt, Electrodialytic estimation of ash and of acidic and basic groups in textile fibers, RP1314 ... 61
——, *Jacinto Steinhardt, Milton Harris*, Combination of wool protein with acid and base: The effect of temperature on the titration curve, RP1343 ... 519

G

d-Galacturonic acid, preparation of, RP1325 ... 301
Gause, G. Rupert, John Tucker, Jr., Method for determining the moisture condition in hardened concrete, RP1334 ... 403
Geiger-Müller counters, RP1330 ... 369
Geller, R. F., E. N. Bunting, Length changes of whiteware clays and bodies during initial heating, with supplementary data on mica, RP1311 ... 15
Glass, composition of, and specific refraction, RP1352 ... 759
Glass, nature of, in portland cement clinker, RP1324 ... 295
Glass, specific refraction of RP1352 ... 759
Gloss measurements, RP1345 ... 581
Granite, properties of, RP1320 ... 161

H

Page

Harris, Milton, Arnold M. Sookne, Relation of cation exchange to the acidic properties of cotton, RP1313 ... 47
——, *Henry A. Rutherford, Wilbur I. Patterson,* Reaction of silk fibroin with diazomethane, RP1338 ... 451
——, *Jacinto Steinhardt, Charles H. Fugitt,* Combination of wool protein with acid and base: The effect of temperature on the titration curve, RP1343 ... 519
Harrison, William N., Leo Shartsis, Determination of thickness of acid-resistant portion of vitreous enamel coatings, RP1315 ... 71
Hartman, Charles C., Determination of nonvolatile matter and the calculation of "cut" of shellac varnish, RP1333 ... 395
Hartman, L. W., Harvey L. Curtis, A dual bridge for the measurement of self inductance in terms of resistance and time, RP1310 ... 1
Heating, effect of rate on grain size of steel, RP1322 ... 215
Hinman, Wilbur S., Jr., Harry Diamond, An automatic weather station, RP1318 ... 133
——, ——, *Francis W. Dunmore, Evan G. Lapham,* An improved radio sonde and its performance, RP1329 ... 327
Hobbs, Robert B., Effect of speed of pulling jaws on the tensile strength and stretch of leather, RP1321 ... 207
Hoffman, James I., Decomposition of rocks and ceramic materials with a small amount of sodium carbonate, RP1331 ... 379
Humidity, effect on strength and elongation of silk yarns, RP1353 ... 783
Humidity, relative, inside concrete, RP1334 ... 403
Hunter, Richard S., A multipurpose photoelectric reflectometer, RP1345 ... 581
Hygrometer, electric, applied to humidity measurements inside concrete, RP1334 ... 403
Hygrometer, electric type, in improved radio sonde, RP1329 ... 327

I

Inductance, self, a dual bridge for the measurement of, RP1310 ... 1
Inductor, supplement to, RP1312 ... 41
Insley, Herbert, Nature of the glass in portland cement clinker, RP1324 ... 295
——, *Daniel W. Kessler, William H. Sligh,* Physical, mineralogical, and durability studies on the building and monumental granites of the United States, RP1320 ... 161
Integrating circuit for Geiger-Müller counters, RP1330 ... 369
Ionosphere, recombination and electron attachment in, RP1342 ... 507

J

Johnson, Paul V., Ray T. Stull, Some properties of the pore system in bricks and their relation to frost action, RP1349 ... 711

K

Kanagy, Joseph R., Effect of oxygen and moisture on the stability of leather at elevated temperatures, RP1319 ... 149
Kessler, Daniel W., Herbert Insley, William H. Sligh, Physical, mineralogical, and durability studies on the building and monumental granites of the United States, RP1320 ... 161

L

Lapham, Evan G., Harry Diamond, Wilbur S. Hinman, Jr., Francis W. Dunmore, An improved radio sonde and its performance, RP1329 ... 327
Leather, accelerated aging of, RP1319 ... 149
Leather, effect of jaw speed on strength and stretch of, RP1321 ... 207
Lewis, Arthur B., John H. Park, Standard electrodynamic wattmeter and ac-dc transfer instrument, RP1344 ... 545
Liquid films, thickness, RP1332 ... 385
Logan, Hugh L., Electrode potential measurements as a means of studying the corrosion characteristics of wrought aluminum alloys of the duralumin type, RP1328 ... 317

M

Martin, Albert R., Roy L. Whistler, Carl M. Conrad, Pectic substance of cotton fibers in relation to growth, RP1326 ... 305
Masonry materials, RP1320 ... 161
Meggers, William F., Charlotte E. Moore, Description and analysis of the second spectrum of vanadium (V II), RP1317 ... 83
Metals, aircraft, effect of low temperatures on properties, RP1347 ... 673
Meteorological factors, automatic remote measurement of, RP1318 ... 133
Mica, effect on clay, and supplementary data, RP1311 ... 15
Microphones, absolute-pressure calibrations, RP1341 ... 489
Mohler, Fred L., Recombination and electron attachment in the *F* layers of the ionosphere, RP1342 ... 507
Moisture, effect of, on leather, RP1319 ... 149
Moore, Charlotte E., William F. Meggers, Description and analysis of the second spectrum of vanadium (V II), RP1317 ... 83
Morey, Francis C., Thickness of a liquid film adhering to a surface slowly withdrawn from the liquid, RP1332 ... 385
Mutchler, Willard, Corrosion of metals used in aircraft, RP1316 ... 75
Mutual inductance of parallel helices, RP1346 ... 619

N

Neoprene *G*, permeability to hydrogen, RP1327 ... 309
Nickel, effect in storage batteries, RP1335 ... 417

O

Ohm's law, RP1323 ... 229
Oxygen, effect of, on leather, RP1319 ... 149
Oxygen point apparatus, RP1339 ... 459

P

Parallel solenoids, mutual inductance, RP1346 ... 619
Park, John H., Arthur B. Lewis, Standard electrodynamic wattmeter and ac-dc transfer instrument, RP1344 ... 545
Patterson, Wilbur I., Henry A. Rutherford, Milton Harris, Reaction of silk fibroin with diazomethane, RP1338 ... 451
Pectic substance in cotton fibers of various ages, RP1326 ... 305
Pectin, acidic properties of, RP1313 ... 47
Pectin, preparation of *d*-galacturonic acid from, RP1325 ... 301
Permeability of bricks to water and air, RP1349 ... 711
Permeability of elastic polymers to hydrogen, RP1327 ... 309
Peterson, Chester, Irvin L. Cooter, Frank Wenner, A vacuum-tube alternating-voltage compensator, RP1312 ... 41
Photocell, barrier-layer, photometry, RP1348 ... 703
Photoelectric reflectometer, RP1345 ... 581
Photometry, using barrier-layer photocells, RP1348 ... 703
Pigman, William Ward, Improvements in the preparation of *d*-galacturonic acid, RP1325 ... 301
Polarization in soil-corrosion cells, RP1336 ... 421
Polymers, elastic, permeability to hydrogen of, RP1327 ... 309
Pore system in bricks, RP1349 ... 711
Portland cement, nature of glass in, RP1324 ... 295
Pressure, calibrations of microphones, RP1341 ... 489

R

Radio meteorograph (radio sonde), improvements and performance of, RP1329 ... 327
Radio sonde, audio modulation type, improvements and performance of, RP1329 ... 327
Radio weather station for isolated locations, RP1318 ... 133

Page

Recombination of electrons in the ionosphere, RP1342 ... 507
Recrystallization, continuous, apparatus for, RP1351 ... 747
Reflection measurement, RP1345 ... 581
Reflectometer, RP1345 ... 581
Refraction, specific, of glasses, RP1352 ... 759
Resistance comparisons, RP1323 ... 229
Robot weather station for remote locations, RP1318 ... 133
Rosenberg, Samuel J., Effect of low temperature on the properties of aircraft metals, RP1347 ... 673
——, *Thomas G. Digges*, Effect of rate of heating through the transformation range on austenitic grain size, RP1322 ... 215
Rubbers, synthetic, permeability to hydrogen, RP1327 ... 309
Rutherford, Henry A., Wilbur I. Patterson, Milton Harris, Reaction of silk fibroin with diazomethane, RP1338 ... 451

S

Sager, Theron P., Permeability of elastic polymers to hydrogen, RP1327 ... 309
Self inductance, dual bridge for the measurement of, RP1310 ... 1
Schenke, E. Max, Howard E. Shearer, Strength and elongation of silk yarns as affected by humidity, RP1353 ... 783
Schwab, Frank W., Edward Wichers, Preparation of benzoic acid of high purity, RP1351 ... 747
Scott, Russell B., Calibration of thermocouples at low temperatures, RP1339 ... 459
Shartsis, Leo, William N. Harrison, Determination of thickness of acid-resistant portion of vitreous enamel coatings, RP1315 ... 71
Shearer, Howard E., E. Max Schenke, Strength and elongation of silk yarns as affected by humidity, RP1353 ... 783
Shellac varnish, determination of nonvolatile in, RP1333 ... 395
Silica, determination of, RP1331 ... 379
Silicates, decomposition of, RP1331 ... 379
Silk, methylation of with diazomethane, RP1338 ... 451
Silk yarns, effect of humidity on strength and elongation, RP1353 ... 783
Single layer solenoids with parallel axes, RP1346 ... 619
Sligh, William H., Daniel W. Kessler, Herbert Insley, Physical, mineralogical, and durability studies on the building and monumental granites of the United States, RP1320 ... 161
Smith, Edgar Reynolds, John Keenan Taylor, Standard electrode potential of sodium, RP1350 ... 731
Snow, Chester, Mutual inductance of two helices whose axes are parallel, RP1346 ... 619
Snyder, Clarence L., George W. Vinal, D. Norman Craig, Note on the effects of cobalt and nickel in storage batteries, RP1335 ... 417
Sodium, standard electrode potential, RP1350 ... 731
Soil-corrosion cells, electrode potentials and polarization, RP1336 ... 421
Sookne, Arnold M., Charles H. Fugitt, Jacinto Steinhardt, Electrodialytic estimation of ash and of acidic and basic groups in textile fibers, RP1314 ... 61
——, *Milton Harris*, Relation of cation exchange to the acidic properties of cotton, RP1313 ... 47
Specific heat as a criterion of purity, RP1351 ... 747
Specific refraction of glasses, RP1352 ... 759
Spectrum of vanadium, RP1317 ... 83
Standard electrode potential of sodium, RP1350 ... 731
Standard electrodynamic wattmeter, RP1344 ... 545
Standard resistors, comparison of, RP1323 ... 229
Steel, effect of rate of heating on austenitic grain size, RP1322 ... 215
Steinhardt, Jacinto, Arnold M. Sookne, Charles H. Fugitt, Electrodialytic estimation of ash and of acidic and basic groups in textile fibers, RP1314 ... 61
——, *Charles H. Fugitt, Milton Harris*, Combination of wool protein with acid and base: The effect of temperature on the titration curve, RP1343 ... 519

Page

Storage batteries, effect of cobalt and nickel, RP1335 ... 417
Stratosphere, measurements by improved radio sonde, RP1329 ... 327
Stull, Ray T., Paul V. Johnson, Some properties of the pore system in bricks and their relation to frost action, RP1349 ... 711
System, silica, with calcium and ferric oxides, RP1340 ... 475

T

Taylor, John Keenan, Edgar Reynolds Smith, Standard electrode potential of sodium, RP 1350 ... 731
Temperature, effect of, on leather, RP1319 ... 149
Temperatures, low, effect on properties of aircraft metals, RP1347 ... 673
Textiles, acidic and basic groups in, RP1314 ... 61
Textiles, effects of drying conditions on, RP1337 ... 435
Thermal dilatation of clay during initial heating, RP1311 ... 15
Thermocouples at low temperatures, RP1339 ... 459
Thickness of enamel coatings, RP1315 ... 71
Titration curves, effect of temperature on, of wool with hydrochloric acid and potassium hydroxide, RP1343 ... 519
Transfer instrument, ac-dc, RP1344 ... 545
Tucker, John, Jr., G. R. Gause, Method for determining the moisture condition in hardened concrete, RP1334 ... 403
Tyrosine, methylation of, in proteins, RP1338 ... 451

U

Units of electrical resistance, RP1323 ... 229
Uronic acid, in cotton fibers of various ages, RP 1326 ... 305

V

Vacuum tube, RP1312 ... 41
Vanadium, second spectrum of, RP1317 ... 83
Varnish, shellac, calculation of "cut," RP1333 ... 395
Vinal, George W., D. Norman Craig, Clarence L. Snyder, Note on the effects of cobalt and nickel in storage batteries, RP1335 ... 417
Voltage compensator, vacuum-tube, RP1312 ... 41

W

Wattmeter, standard electrodynamic, RP1344 ... 545
Weather-exposure tests on metals used in aircraft, RP1316 ... 75
Weather instruments, automatic remote indication of, RP1318 ... 133
Weather observations in upper atmosphere by radio sonde, RP1329 ... 327
Wenner, Frank, Methods, apparatus, and procedures for the comparison of precision standard resistors, RP1323 ... 229
——, *Irvin L. Cooter, Chester Peterson*, A vacuum-tube alternating-voltage compensator, RP1312 ... 41
Whistler, Roy L., Albert R. Martin, Carl M. Conrad, Pectic substance of cotton fibers in relation to growth, RP1326 ... 305
Wichers, Edward, Frank W. Schwab, Preparation of benzoic acid of high purity, RP1351 ... 747
Wiegerink, James G., Effects of drying conditions on properties of textile yarns, RP1337 ... 435
Wool, combination of, with hydrochloric acid and potassium hydroxide as affected by temperature, RP1343 ... 519

Y

Yarns, effects of drying conditions on textile, RP1337 ... 435
Yarns, silk, effect of humidity on strength and elongation, RP1353 ... 783
Young, John C., Alfred N. Finn, Effect of composition and other factors on the specific refraction and dispersion of glasses, RP1352 ... 759

neering
brary

UNITED STATES DEPARTMENT OF COMMERCE

FEB 17 194

Journal of Research

of the

National Bureau of Standards

Vol. 25, No. 6 December 1940

CONTENTS

RP	TITLE AND AUTHOR	Page
1346.	Mutual inductance of two helices whose axes are parallel. Chester Snow....[Price 10¢]	619
1347.	Effect of low temperatures on the properties of aircraft metals. Samuel J. Rosenberg....[Price 10¢]	673
1348.	A photometric procedure using barrier-layer photocells. Louis E. Barbrow....[Price 5¢]	703
1349.	Some properties of the pore system in bricks and their relation to frost action. Ray T. Stull and Paul V. Johnson....[Price 10¢]	711
1350.	Standard electrode potential of sodium. Edgar Reynolds Smith and John Keenan Taylor....[Price 5¢]	731
1351.	Preparation of benzoic acid of high purity. Frank W. Schwab and Edward Wichers....[Price 5¢]	747
1352.	Effect of composition and other factors on the specific refraction and dispersion of glasses. John C. Young and Alfred N. Finn....[Price 5¢]	759
1353.	Strength and elongation of silk yarns as affected by humidity. E. Max Schenke and Howard E. Shearer....[Price 5¢]	783
	Index to volume 25 (July 1940 to December 1940) Research Papers (RP1310 to RP1353)...	791

The articles listed may be purchased separately (see cover page II) at the prices stated

A monthly periodical of pure and applied science published by our National Government

Journal of Research

of the

National Bureau of Standards

The July 1940 issue of the JOURNAL OF RESEARCH of the National Bureau of Standards began the twenty-fifth semiannual volume of this periodical. Fundamental researches in progress in the Bureau's laboratories are reported in this JOURNAL. If you are interested in new developments in science and technology, you should receive the JOURNAL. If you are not already a subscriber, you are invited to send in your subscription.

Technical News Bulletin

This is a monthly publication containing short articles reporting progress of work in the Bureau laboratories, abstracts of papers which appear in the JOURNAL OF RESEARCH, accounts of scientific and technical meetings in which the Bureau has taken part, a list of all publications by members of the staff, and other items within the Bureau's fields. The BULLETIN is designed primarily to give a general and timely review of the activities of the Bureau in brief form. It is a prompt and reliable source of official information. If you have not already subscribed for the BULLETIN, you are invited to do so.

ANNUAL SUBSCRIPTION	Prices	
	United States, Canada, Cuba, Mexico, Newfoundland, Republic of Panama	Other countries
JOURNAL OF RESEARCH of the National Bureau of Standards:		
12 monthly issues (2 volumes), paper covers	$3.50	$4.50
Bound volume (½ year, 1 volume), blue buckram	3.00	3.50
Technical News Bulletin, 12 monthly issues	.50	.70

Research Papers, reprinted individual articles appearing in the JOURNAL OF RESEARCH, are available from the Superintendent of Documents shortly after appearance of monthly issue of the JOURNAL.

Address orders only to
Superintendent of Documents, U. S. Government Printing Office,
Washington, D. C.